PyCAMA report generated by tropl2-proc

tropl2-proc

2025-12-12 (03:15)

1 Short Introduction

1.1 The list of parameters

You may want to keep the list given in table 1 at hand when viewing the results.

2 Definitions

The averages shown here are *unweighed* averages:

$$\overline{x} = \frac{1}{N}\sum_{i=1}^{N} x_i \tag{1}$$

with N the number of observations in the dataset.

The spread of the measurements is indicated with the variance $V(x)$, or rather the standard deviation $\sigma(x) = \sqrt{V(x)}$.

$$V(x) = \frac{1}{N-1}\sum_{i=1}^{N}(x_i - \overline{x})^2 \tag{2}$$

We also report the more robust statistics median, minimum, maximum, various percentiles and inter quartile range.

The median m is the value of parameter x for which half of the observations of x is smaller than m:

$$P(x \leq m) = P(x \geq m) = \int_{-\infty}^{m} f(x)\,\mathrm{d}x = \frac{1}{2} \tag{3}$$

with $f(x)$ the probability density function.

The median is a special case of a percentile. Instead of ½ in equation 3, other threshold values can be used. We report results for 1 %, 5 %, 10 %, 15.9 %, 25 %, 75 %, 84.1 %, 90 %, 95 % and 99 %. The inter quartile range is the difference between the 75 % and 25 % percentiles. Similarly the minimum and maximum values correspond to the 0 % and 100 % percentiles respectively.

For normally distributed parameters the mean and median are the same, while the $\mu \pm \sigma$ values and the 15.9 % and 84.1 % percentiles coincide.

To get a measure for the relation of one variable $x_{(k)}$ with another $x_{(l)}$, we calculate the covariance matrix C_{kl}.

$$C_{kl} = C(x_{(k)}, x_{(l)}) = \frac{1}{N-1}\sum_{i=1}^{N}(x_{(k),i} - \overline{x_{(k)}})(x_{(l),i} - \overline{x_{(l)}}) \tag{4}$$

Rather than a dimensionally dependent covariance, it is often easier to interpret a correlation matrix R_{kl}, a matrix of Pearson's r coefficients:

$$R_{kl} = R(x_{(k)}, x_{(l)}) = \frac{C_{kl}}{\sqrt{C_{kk}C_{ll}}} = \frac{C_{kl}}{\sqrt{V(x_k)V(x_l)}} \tag{5}$$

The diagonal elements of the covariance matrix are the variances of the elements, $V(x_{(k)}) = C_{kk}$ and obviously $R_{kk} = 1$.

Table 1: Parameterlist and basic statistics for the analysis

Variable	mean $\pm\sigma$	Count	Mode	IQR	Median	Minimum	Maximum
qa value [1]	0.740 ± 0.297	1165304	0.995	0.600	1.000	0.400	1.000
methane mixing ratio [parts per 10^9]	$(0.182 \pm 0.010) \times 10^4$	1165304	1.732×10^3	183	1.778×10^3	1.057×10^3	2.562×10^3
methane mixing ratio precision [parts per 10^9]	3.09 ± 1.78	1165304	1.30	1.99	2.79	0.666	55.8
methane mixing ratio bias corrected [parts per 10^9]	$(0.183 \pm 0.008) \times 10^4$	1165304	1.738×10^3	160	1.802×10^3	1.086×10^3	2.596×10^3
number of spectral points in retrieval [1]	798 ± 3	1165304	798	4.00	798	596	805
wavelength calibration offset SWIR [nm]	$(-1.105 \pm 0.254) \times 10^{-2}$	1165304	-1.100×10^{-2}	1.901×10^{-3}	-1.086×10^{-2}	-7.651×10^{-2}	5.085×10^{-2}
chi square SWIR [1]	$(0.126 \pm 4.871) \times 10^5$	1165304	2.350×10^3	1.018×10^4	3.796×10^3	1.567×10^3	4.983×10^8
chi square NIR [1]	$(0.519 \pm 62.563) \times 10^5$	1165304	2.250×10^3	1.105×10^4	1.319×10^4	43.4	5.938×10^9
degrees of freedom [1]	17.8 ± 0.5	1165304	17.2	0.971	17.7	17.0	20.9
number of iterations [1]	10.1 ± 1.1	1165304	10.2	0.0	10.00	10.00	30.0
fluorescence [mol s^{-1} m^{-2} nm^{-1} sr^{-1}]	$(-2.202 \pm 2.643) \times 10^{-8}$	1165304	-8.500×10^{-9}	3.314×10^{-8}	-2.599×10^{-8}	-6.336×10^{-7}	1.458×10^{-6}
land fraction [1]	0.953 ± 0.199	1165304	0.995	0.0	1.000	0.0	1.000

Table 2: Percentile ranges

Variable	1 %	5 %	10 %	15.9 %	25 %	75 %	84.1 %	90 %	95 %	99 %
qa value [1]	0.400	0.400	0.400	0.400	0.400	1.000	1.000	1.000	1.000	1.000
methane mixing ratio [parts per 10^9]	1.677×10^3	1.698×10^3	1.709×10^3	1.718×10^3	1.732×10^3	1.915×10^3	1.935×10^3	1.947×10^3	1.959×10^3	1.979×10^3
methane mixing ratio precision [parts per 10^9]	1.13	1.24	1.33	1.47	1.80	3.79	4.47	5.17	6.20	8.97
methane mixing ratio bias corrected [parts per 10^9]	1.694×10^3	1.715×10^3	1.726×10^3	1.736×10^3	1.751×10^3	1.911×10^3	1.929×10^3	1.941×10^3	1.956×10^3	1.981×10^3
number of spectral points in retrieval [1]	792	793	794	795	796	800	801	802	803	804
wavelength calibration offset SWIR [nm]	-1.702×10^{-2}	-1.413×10^{-2}	-1.329×10^{-2}	-1.267×10^{-2}	-1.196×10^{-2}	-1.006×10^{-2}	-9.678×10^{-3}	-9.284×10^{-3}	-8.548×10^{-3}	-5.448×10^{-3}
chi square SWIR [1]	1.892×10^3	2.070×10^3	2.204×10^3	2.344×10^3	2.572×10^3	1.275×10^4	2.312×10^4	3.406×10^4	4.959×10^4	7.786×10^4
chi square NIR [1]	1.263×10^3	2.140×10^3	3.164×10^3	4.503×10^3	6.808×10^3	1.786×10^4	2.022×10^4	2.192×10^4	2.409×10^4	2.865×10^4
degrees of freedom [1]	17.1	17.2	17.2	17.3	17.4	18.3	18.5	18.6	18.8	18.9
number of iterations [1]	10.00	10.00	10.00	10.00	10.00	10.00	10.00	10.00	10.00	11.0
fluorescence [mol s^{-1} m^{-2} nm^{-1} sr^{-1}]	-7.268×10^{-8}	-5.725×10^{-8}	-5.031×10^{-8}	-4.538×10^{-8}	-3.996×10^{-8}	-6.822×10^{-9}	7.350×10^{-10}	9.411×10^{-9}	2.394×10^{-8}	5.843×10^{-8}
land fraction [1]	0.0	0.776	0.993	1.000	1.000	1.000	1.000	1.000	1.000	1.000

Table 3: Parameterlist and basic statistics for the analysis for observations in the northern hemisphere

Variable	mean $\pm\sigma$	Count	IQR	Median	Minimum	Maximum	25 % percentile	75 % percentile
qa value [1]	0.795 ± 0.284	393322	0.600	1.000	0.400	1.000	0.400	1.000
methane mixing ratio [parts per 10^9]	$(0.193 \pm 0.003) \times 10^4$	393322	36.2	1.933×10^3	1.339×10^3	2.562×10^3	1.914×10^3	1.950×10^3
methane mixing ratio precision [parts per 10^9]	2.15 ± 1.50	393322	0.932	1.75	0.955	43.5	1.38	2.32
methane mixing ratio bias corrected [parts per 10^9]	$(0.193 \pm 0.003) \times 10^4$	393322	35.9	1.927×10^3	1.376×10^3	2.596×10^3	1.909×10^3	1.945×10^3
number of spectral points in retrieval [1]	798 ± 3	393322	4.00	798	779	805	796	800
wavelength calibration offset SWIR [nm]	$(-1.123 \pm 0.333) \times 10^{-2}$	393322	2.461×10^{-3}	-1.108×10^{-2}	-7.074×10^{-2}	4.610×10^{-2}	-1.249×10^{-2}	-1.003×10^{-2}
chi square SWIR [1]	$(0.245 \pm 0.280) \times 10^5$	393322	2.609×10^4	1.408×10^4	1.718×10^3	4.152×10^6	7.995×10^3	3.409×10^4
chi square NIR [1]	$(0.915 \pm 46.976) \times 10^5$	393322	6.820×10^3	5.804×10^3	43.4	4.729×10^8	3.337×10^3	1.016×10^4
degrees of freedom [1]	18.4 ± 0.4	393322	0.536	18.4	17.0	20.9	18.1	18.7
number of iterations [1]	10.2 ± 1.7	393322	0.0	10.00	10.00	30.0	10.00	10.00
fluorescence [mol s^{-1} m^{-2} nm^{-1} sr^{-1}]	$(-6.195 \pm 22.068) \times 10^{-9}$	393322	2.005×10^{-8}	-7.764×10^{-9}	-2.792×10^{-7}	7.937×10^{-7}	-1.785×10^{-8}	2.199×10^{-9}
land fraction [1]	0.963 ± 0.162	393322	1.393×10^{-3}	1.000	0.0	1.000	0.999	1.000

Table 4: Parameterlist and basic statistics for the analysis for observations in the southern hemisphere

Variable	mean $\pm\sigma$	Count	IQR	Median	Minimum	Maximum	25 % percentile	75 % percentile
qa value [1]	0.712 ± 0.300	771982	0.600	1.000	0.400	1.000	0.400	1.000
methane mixing ratio [parts per 10^9]	$(0.176 \pm 0.006) \times 10^4$	771982	58.2	1.744×10^3	1.057×10^3	2.045×10^3	1.719×10^3	1.778×10^3
methane mixing ratio precision [parts per 10^9]	3.57 ± 1.72	771982	1.69	3.27	0.666	55.8	2.56	4.25
methane mixing ratio bias corrected [parts per 10^9]	$(0.178 \pm 0.005) \times 10^4$	771982	64.8	1.766×10^3	1.086×10^3	2.469×10^3	1.737×10^3	1.802×10^3
number of spectral points in retrieval [1]	798 ± 3	771982	4.00	798	596	805	796	800
wavelength calibration offset SWIR [nm]	$(-1.095 \pm 0.201) \times 10^{-2}$	771982	1.662×10^{-3}	-1.078×10^{-2}	-7.651×10^{-2}	5.085×10^{-2}	-1.173×10^{-2}	-1.007×10^{-2}
chi square SWIR [1]	$(0.654 \pm 59.806) \times 10^4$	771982	1.579×10^3	2.839×10^3	1.567×10^3	4.983×10^8	2.363×10^3	3.942×10^3
chi square NIR [1]	$(0.317 \pm 69.166) \times 10^5$	771982	7.456×10^3	1.581×10^4	160	5.938×10^9	1.251×10^4	1.996×10^4
degrees of freedom [1]	17.6 ± 0.4	771982	0.476	17.5	17.0	20.8	17.3	17.7
number of iterations [1]	10.0 ± 0.4	771982	0.0	10.00	10.00	30.0	10.00	10.00
fluorescence [mol s^{-1} m^{-2} nm^{-1} sr^{-1}]	$(-3.009 \pm 2.477) \times 10^{-8}$	771982	2.382×10^{-8}	-3.486×10^{-8}	-6.336×10^{-7}	1.458×10^{-6}	-4.434×10^{-8}	-2.052×10^{-8}
land fraction [1]	0.949 ± 0.215	771982	0.0	1.000	0.0	1.000	1.000	1.000

Table 5: Parameterlist and basic statistics for the analysis for observations over water

Variable	mean $\pm\sigma$	Count	IQR	Median	Minimum	Maximum	25 % percentile	75 % percentile
qa value [1]	0.664 ± 0.298	38385	0.600	0.400	0.400	1.000	0.400	1.000
methane mixing ratio [parts per 10^9]	$(0.187 \pm 0.003) \times 10^4$	38385	40.7	1.869×10^3	1.421×10^3	2.000×10^3	1.847×10^3	1.888×10^3
methane mixing ratio precision [parts per 10^9]	2.95 ± 1.47	38385	0.969	2.79	0.666	32.5	2.29	3.26
methane mixing ratio bias corrected [parts per 10^9]	$(0.187 \pm 0.003) \times 10^4$	38385	40.9	1.876×10^3	1.426×10^3	2.008×10^3	1.855×10^3	1.895×10^3
number of spectral points in retrieval [1]	798 ± 3	38385	4.00	798	724	803	796	800
wavelength calibration offset SWIR [nm]	$(-1.051 \pm 0.144) \times 10^{-2}$	38385	1.258×10^{-3}	-1.033×10^{-2}	-2.963×10^{-2}	1.168×10^{-2}	-1.108×10^{-2}	-9.820×10^{-3}
chi square SWIR [1]	$(0.244 \pm 26.815) \times 10^5$	38385	3.869×10^3	5.681×10^3	1.853×10^3	4.983×10^8	4.336×10^3	8.205×10^3
chi square NIR [1]	$(0.270 \pm 0.597) \times 10^4$	38385	1.577×10^3	2.049×10^3	160	8.440×10^5	1.525×10^3	3.102×10^3
degrees of freedom [1]	18.1 ± 0.2	38385	0.200	18.1	17.0	19.1	18.0	18.2
number of iterations [1]	10.0 ± 0.6	38385	0.0	10.00	10.00	30.0	10.00	10.00
fluorescence [mol s^{-1} m^{-2} nm^{-1} sr^{-1}]	$(-4.493 \pm 18.375) \times 10^{-9}$	38385	1.676×10^{-8}	-7.598×10^{-9}	-6.336×10^{-7}	1.458×10^{-6}	-1.486×10^{-8}	1.906×10^{-9}
land fraction [1]	0.0 ± 0.00	38385	0.0	0.0	0.0	0.0	0.0	0.0

Table 6: Parameterlist and basic statistics for the analysis for observations over land

Variable	mean $\pm\sigma$	Count	IQR	Median	Minimum	Maximum	25 % percentile	75 % percentile
qa value [1]	0.738 ± 0.298	966618	0.600	1.000	0.400	1.000	0.400	1.000
methane mixing ratio [parts per 10^9]	$(0.180 \pm 0.009) \times 10^4$	966618	169	1.759×10^3	1.374×10^3	2.562×10^3	1.726×10^3	1.895×10^3
methane mixing ratio precision [parts per 10^9]	3.16 ± 1.70	966618	2.12	2.93	0.955	55.8	1.81	3.93
methane mixing ratio bias corrected [parts per 10^9]	$(0.181 \pm 0.008) \times 10^4$	966618	146	1.782×10^3	1.396×10^3	2.596×10^3	1.744×10^3	1.890×10^3
number of spectral points in retrieval [1]	798 ± 3	966618	4.00	798	779	805	796	800
wavelength calibration offset SWIR [nm]	$(-1.105 \pm 0.164) \times 10^{-2}$	966618	1.772×10^{-3}	-1.085×10^{-2}	-6.523×10^{-2}	2.918×10^{-2}	-1.188×10^{-2}	-1.011×10^{-2}
chi square SWIR [1]	$(0.123 \pm 0.219) \times 10^5$	966618	1.077×10^4	3.224×10^3	1.567×10^3	5.083×10^6	2.470×10^3	1.324×10^4
chi square NIR [1]	$(0.589 \pm 68.334) \times 10^5$	966618	8.234×10^3	1.441×10^4	381	5.938×10^9	1.060×10^4	1.883×10^4
degrees of freedom [1]	17.8 ± 0.6	966618	0.993	17.6	17.0	20.9	17.3	18.3
number of iterations [1]	10.1 ± 1.1	966618	0.0	10.00	10.00	30.0	10.00	10.00
fluorescence [mol s^{-1} m^{-2} nm^{-1} sr^{-1}]	$(-2.522 \pm 2.609) \times 10^{-8}$	966618	3.147×10^{-8}	-3.080×10^{-8}	-2.728×10^{-7}	4.348×10^{-7}	-4.200×10^{-8}	-1.052×10^{-8}
land fraction [1]	1.000 ± 0.000	966618	0.0	1.000	1.000	1.000	1.000	1.000

Table 7: Correlation matrix

Viewing zenith angle	Solar zenith angle	Latitude	Mole fraction of CH_4	Precision of mole fraction of CH_4	Bias corrected mole fraction of CH_4	Number of points in the spectrum	Spectral offset SWIR ($\lambda_{true} - \lambda_{nominal}$)	χ^2 (SWIR)	χ^2 (NIR)	Degrees of freedom	Number of iterations	Fluorescence	Land fraction
1.000	-4.344×10^{-2}	0.111	0.119	−0.150	0.106	4.959×10^{-2}	−0.383	3.253×10^{-3}	-2.612×10^{-3}	0.194	2.978×10^{-2}	0.321	4.704×10^{-3}
-4.344×10^{-2}	1.000	−0.455	−0.536	0.466	−0.515	8.319×10^{-3}	-3.262×10^{-2}	-1.934×10^{-2}	-6.741×10^{-3}	−0.631	-3.873×10^{-2}	−0.496	0.425
0.111	−0.455	1.000	0.923	−0.449	0.905	1.819×10^{-4}	-2.975×10^{-2}	1.966×10^{-2}	4.805×10^{-3}	0.792	9.806×10^{-2}	0.518	−0.117
0.119	−0.536	0.923	1.000	−0.457	0.991	-4.089×10^{-3}	-3.269×10^{-2}	2.143×10^{-2}	1.912×10^{-3}	0.863	6.764×10^{-2}	0.476	−0.112
−0.150	0.466	−0.449	−0.457	1.000	−0.374	-1.307×10^{-2}	6.554×10^{-2}	-1.805×10^{-2}	-3.905×10^{-3}	−0.463	-4.100×10^{-2}	−0.346	-7.356×10^{-2}
0.106	−0.515	0.905	0.991	−0.374	1.000	-6.771×10^{-3}	-2.432×10^{-2}	1.861×10^{-2}	9.124×10^{-4}	0.825	6.118×10^{-2}	0.450	−0.129
4.959×10^{-2}	8.319×10^{-3}	1.819×10^{-4}	-4.089×10^{-3}	-1.307×10^{-2}	-6.771×10^{-3}	1.000	-2.331×10^{-2}	5.261×10^{-4}	-6.274×10^{-4}	7.753×10^{-3}	6.288×10^{-3}	2.021×10^{-2}	1.231×10^{-2}
−0.383	-3.262×10^{-2}	-2.975×10^{-2}	-3.269×10^{-2}	6.554×10^{-2}	-2.432×10^{-2}	-2.331×10^{-2}	1.000	-6.448×10^{-4}	5.002×10^{-4}	-6.079×10^{-2}	-1.570×10^{-2}	−0.188	-4.838×10^{-2}
3.253×10^{-3}	-1.934×10^{-2}	1.966×10^{-2}	2.143×10^{-2}	-1.805×10^{-2}	1.861×10^{-2}	5.261×10^{-4}	-6.448×10^{-4}	1.000	5.490×10^{-4}	2.657×10^{-2}	4.848×10^{-3}	1.632×10^{-2}	-3.334×10^{-3}
-2.612×10^{-3}	-6.741×10^{-3}	4.805×10^{-3}	1.912×10^{-3}	-3.905×10^{-3}	9.124×10^{-4}	-6.274×10^{-4}	5.002×10^{-4}	5.490×10^{-4}	1.000	1.445×10^{-2}	1.587×10^{-2}	2.666×10^{-2}	1.746×10^{-3}
0.194	−0.631	0.792	0.863	−0.463	0.825	7.753×10^{-3}	-6.079×10^{-2}	2.657×10^{-2}	1.445×10^{-2}	1.000	3.566×10^{-2}	0.553	-9.190×10^{-2}
2.978×10^{-2}	-3.873×10^{-2}	9.806×10^{-2}	6.764×10^{-2}	-4.100×10^{-2}	6.118×10^{-2}	6.288×10^{-3}	-1.570×10^{-2}	4.848×10^{-3}	1.587×10^{-2}	3.566×10^{-2}	1.000	9.723×10^{-2}	8.925×10^{-3}
0.321	−0.496	0.518	0.476	−0.346	0.450	2.021×10^{-2}	−0.188	1.632×10^{-2}	2.666×10^{-2}	0.553	9.723×10^{-2}	1.000	−0.136
4.704×10^{-3}	0.425	−0.117	−0.112	-7.356×10^{-2}	−0.129	1.231×10^{-2}	-4.838×10^{-2}	-3.334×10^{-3}	1.746×10^{-3}	-9.190×10^{-2}	8.925×10^{-3}	−0.136	1.000

Table 8: Covariance matrix

Viewing zenith angle	Solar zenith angle	Latitude	Mole fraction of CH_4	Precision of mole fraction of CH_4	Bias corrected mole fraction of CH_4	Number of points in the spectrum	Spectral offset SWIR ($\lambda_{true} - \lambda_{nominal}$)	χ^2 (SWIR)	χ^2 (NIR)	Degrees of freedom	Number of iterations	Fluorescence	Land fraction
251	-9.48	87.8	179	-4.23	143	2.19	-1.539×10^{-2}	2.513×10^{4}	-2.591×10^{5}	1.66	0.503	1.347×10^{-7}	1.483×10^{-2}
-9.48	189	-311	-702	11.4	-602	0.320	-1.139×10^{-3}	-1.297×10^{5}	-5.805×10^{5}	-4.68	-0.568	-1.803×10^{-7}	1.16
87.8	-311	2.476×10^{3}	4.367×10^{3}	-39.7	3.825×10^{3}	2.527×10^{-2}	-3.755×10^{-3}	4.765×10^{5}	1.496×10^{6}	21.2	5.20	6.811×10^{-7}	-1.16
179	-702	4.367×10^{3}	9.047×10^{3}	-77.3	8.005×10^{3}	-1.09	-7.888×10^{-3}	9.928×10^{5}	1.138×10^{6}	44.2	6.85	1.198×10^{-6}	-2.12
-4.23	11.4	-39.7	-77.3	3.17	-56.5	-6.494×10^{-2}	2.959×10^{-4}	-1.565×10^{4}	-4.347×10^{4}	-0.444	-7.772×10^{-2}	-1.625×10^{-8}	-2.603×10^{-2}
143	-602	3.825×10^{3}	8.005×10^{3}	-56.5	7.209×10^{3}	-1.60	-5.237×10^{-3}	7.699×10^{5}	4.847×10^{5}	37.7	5.53	1.010×10^{-6}	-2.17
2.19	0.320	2.527×10^{-2}	-1.09	-6.494×10^{-2}	-1.60	7.79	-1.651×10^{-4}	715	-1.096×10^{4}	1.167×10^{-2}	1.870×10^{-2}	1.491×10^{-9}	6.833×10^{-3}
-1.539×10^{-2}	-1.139×10^{-3}	-3.755×10^{-3}	-7.888×10^{-3}	2.959×10^{-4}	-5.237×10^{-3}	-1.651×10^{-4}	6.436×10^{-6}	-0.797	7.94	-8.312×10^{-5}	-4.245×10^{-5}	-1.258×10^{-11}	-2.441×10^{-5}
2.513×10^{4}	-1.297×10^{5}	4.765×10^{5}	9.928×10^{5}	-1.565×10^{4}	7.699×10^{5}	715	-0.797	2.373×10^{11}	1.673×10^{9}	6.974×10^{3}	2.516×10^{3}	2.101×10^{-4}	-323
-2.591×10^{5}	-5.805×10^{5}	1.496×10^{6}	1.138×10^{6}	-4.347×10^{4}	4.847×10^{5}	-1.096×10^{4}	7.94	1.673×10^{9}	3.914×10^{13}	4.873×10^{4}	1.058×10^{5}	4.409×10^{-3}	2.173×10^{3}
1.66	-4.68	21.2	44.2	-0.444	37.7	1.167×10^{-2}	-8.312×10^{-5}	6.974×10^{3}	4.873×10^{4}	0.290	2.047×10^{-2}	7.870×10^{-9}	-9.851×10^{-3}
0.503	-0.568	5.20	6.85	-7.772×10^{-2}	5.53	1.870×10^{-2}	-4.245×10^{-5}	2.516×10^{3}	1.058×10^{5}	2.047×10^{-2}	1.14	2.738×10^{-9}	1.891×10^{-3}
1.347×10^{-7}	-1.803×10^{-7}	6.811×10^{-7}	1.198×10^{-6}	-1.625×10^{-8}	1.010×10^{-6}	1.491×10^{-9}	-1.258×10^{-11}	2.101×10^{-4}	4.409×10^{-3}	7.870×10^{-9}	2.738×10^{-9}	6.985×10^{-16}	-7.171×10^{-10}
1.483×10^{-2}	1.16	-1.16	-2.12	-2.603×10^{-2}	-2.17	6.833×10^{-3}	-2.441×10^{-5}	-323	2.173×10^{3}	-9.851×10^{-3}	1.891×10^{-3}	-7.171×10^{-10}	3.956×10^{-2}

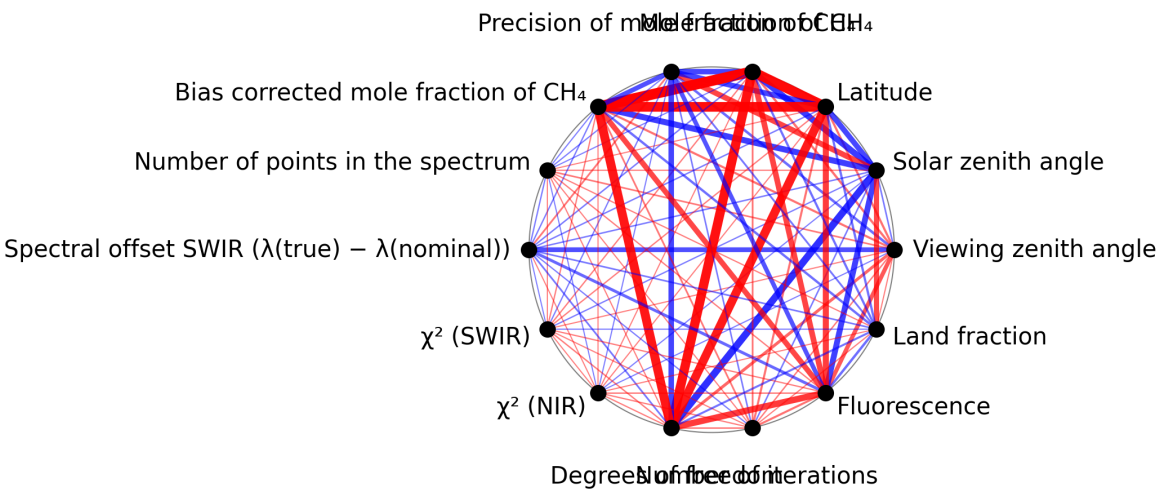

Figure 1: Map of correlation graph for 2025-11-26 to 2025-11-28.

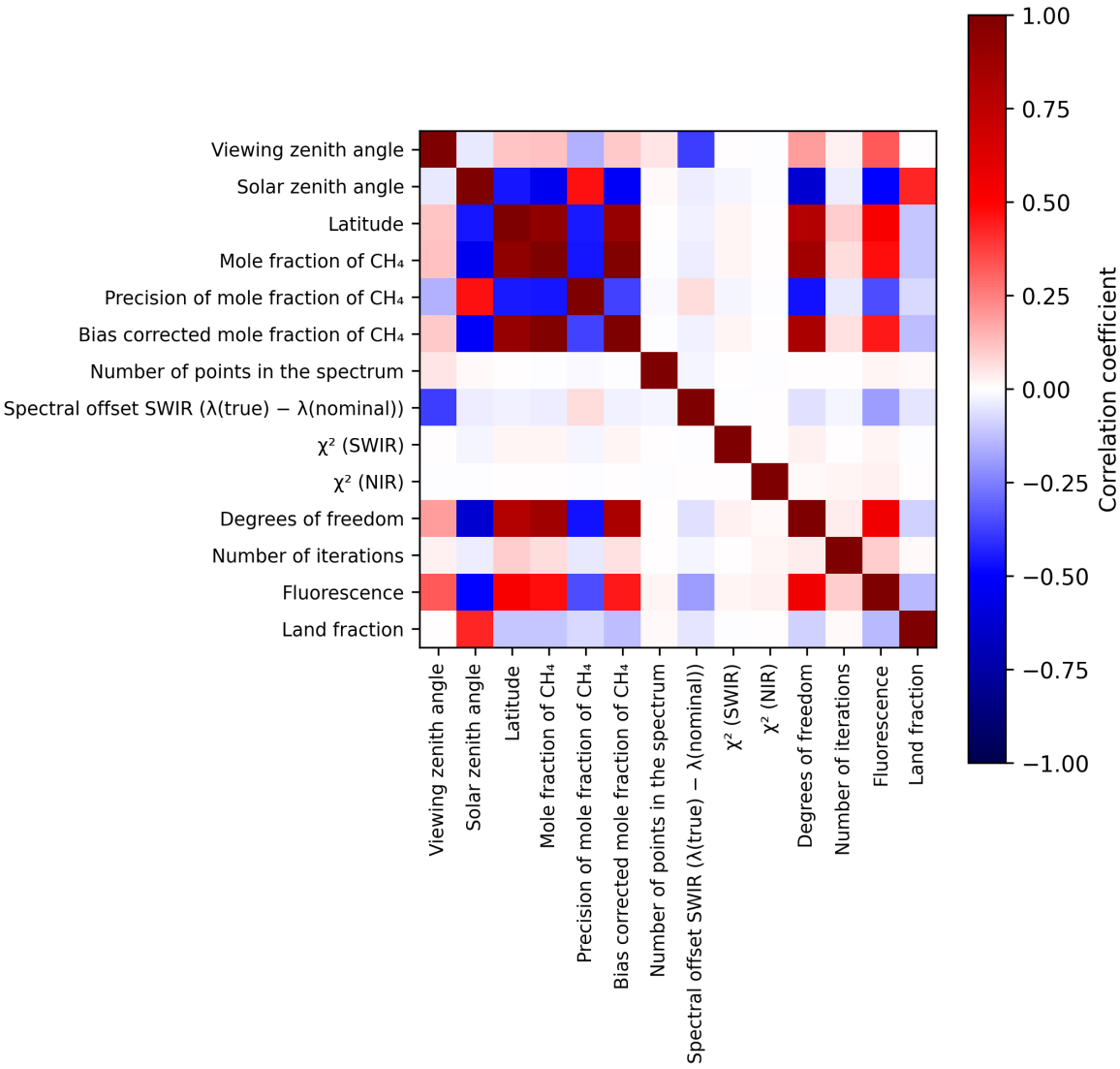

Figure 2: Map of correlation matrix for 2025-11-26 to 2025-11-28.

3 Granule outlines

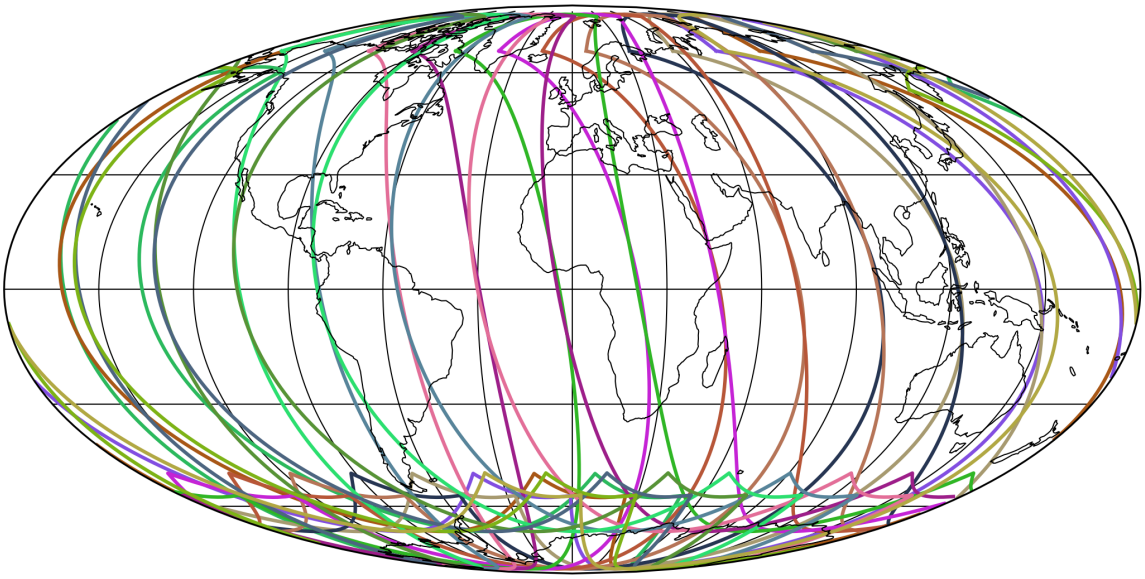

Figure 3: Outline of the granules.

4 Input data monitoring

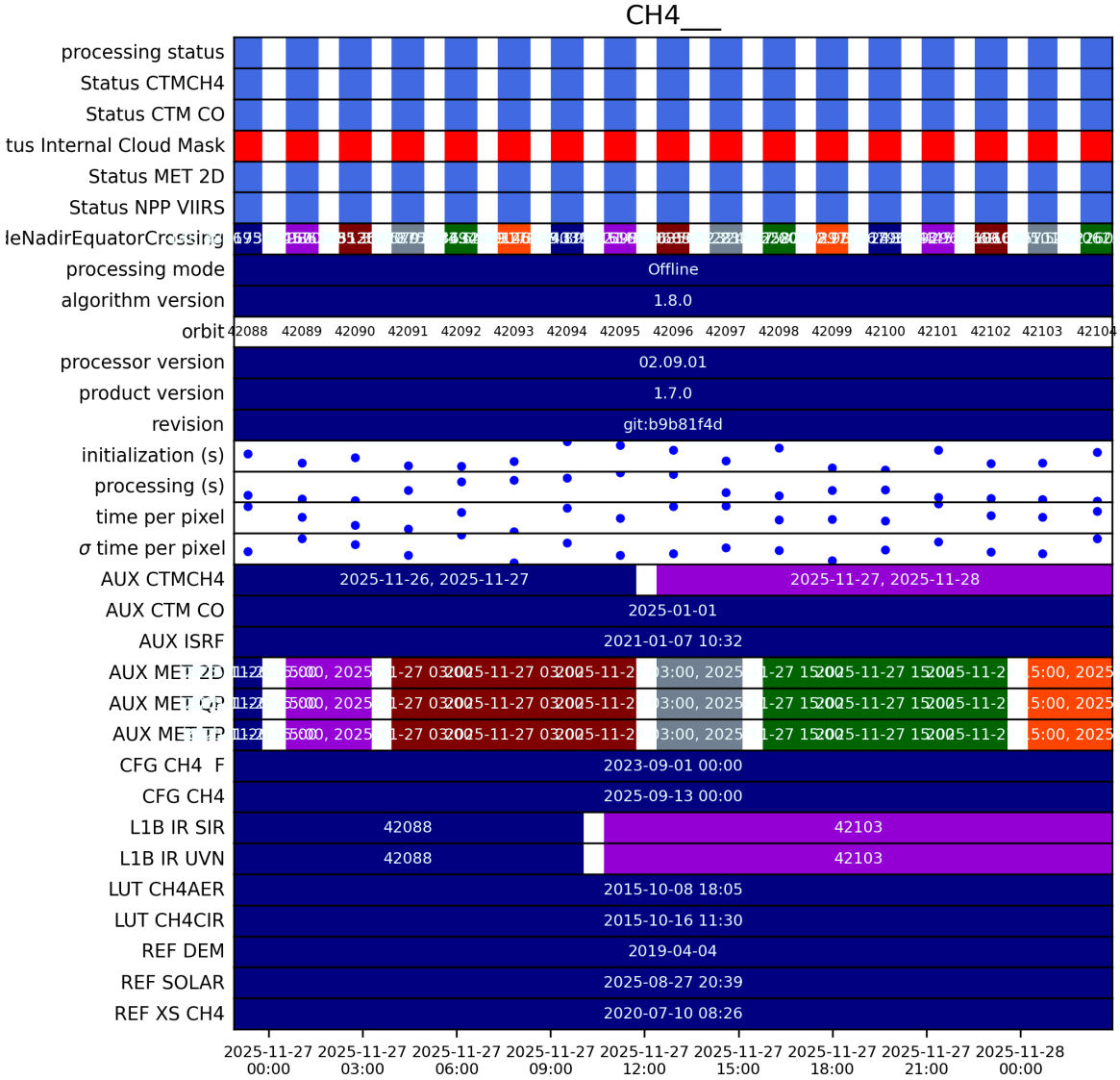

Figure 4: Input data per granule

5 Warnings and errors

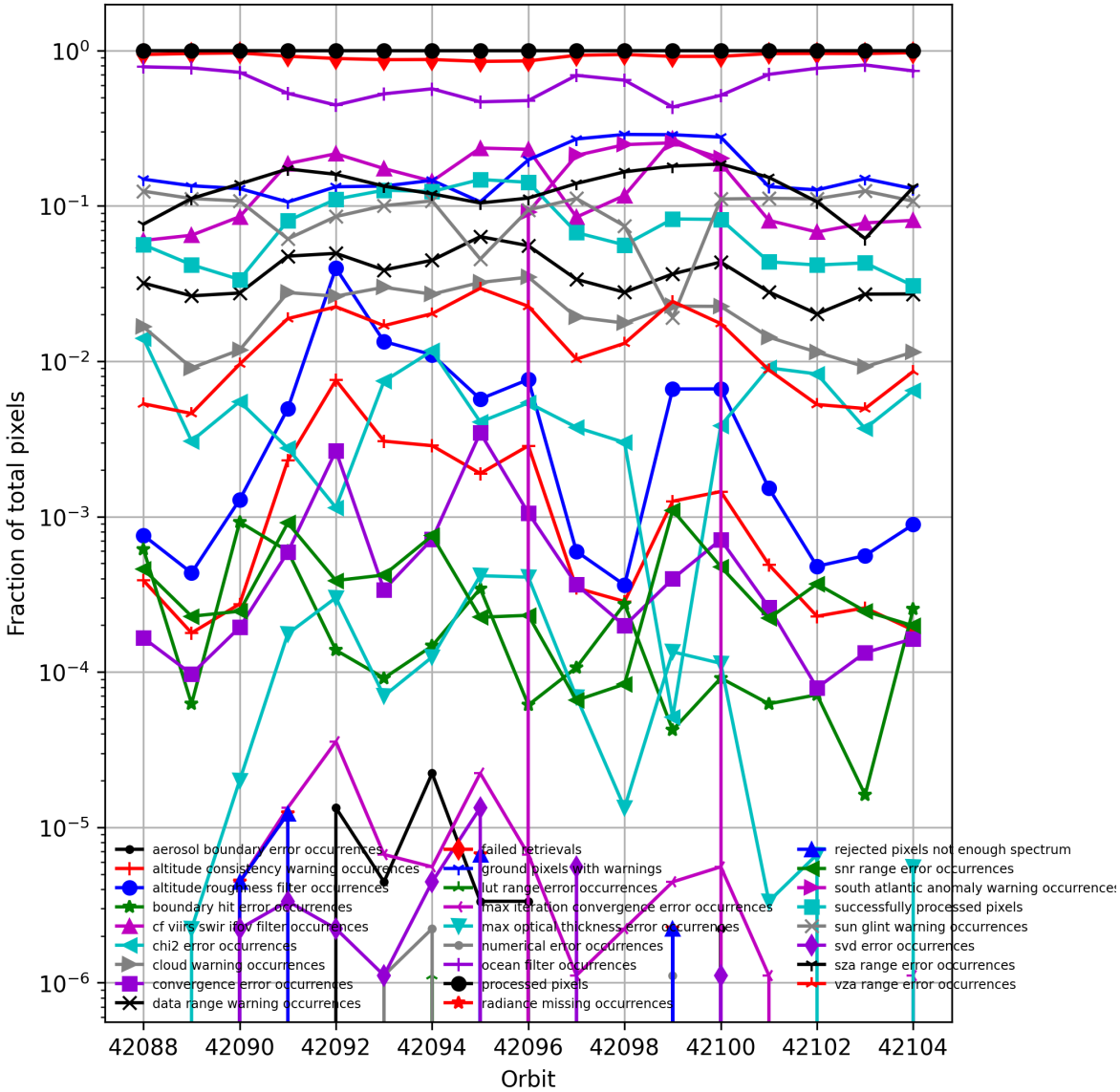

Figure 5: Fraction of pixels with specific warnings and errors during processing

6 World maps

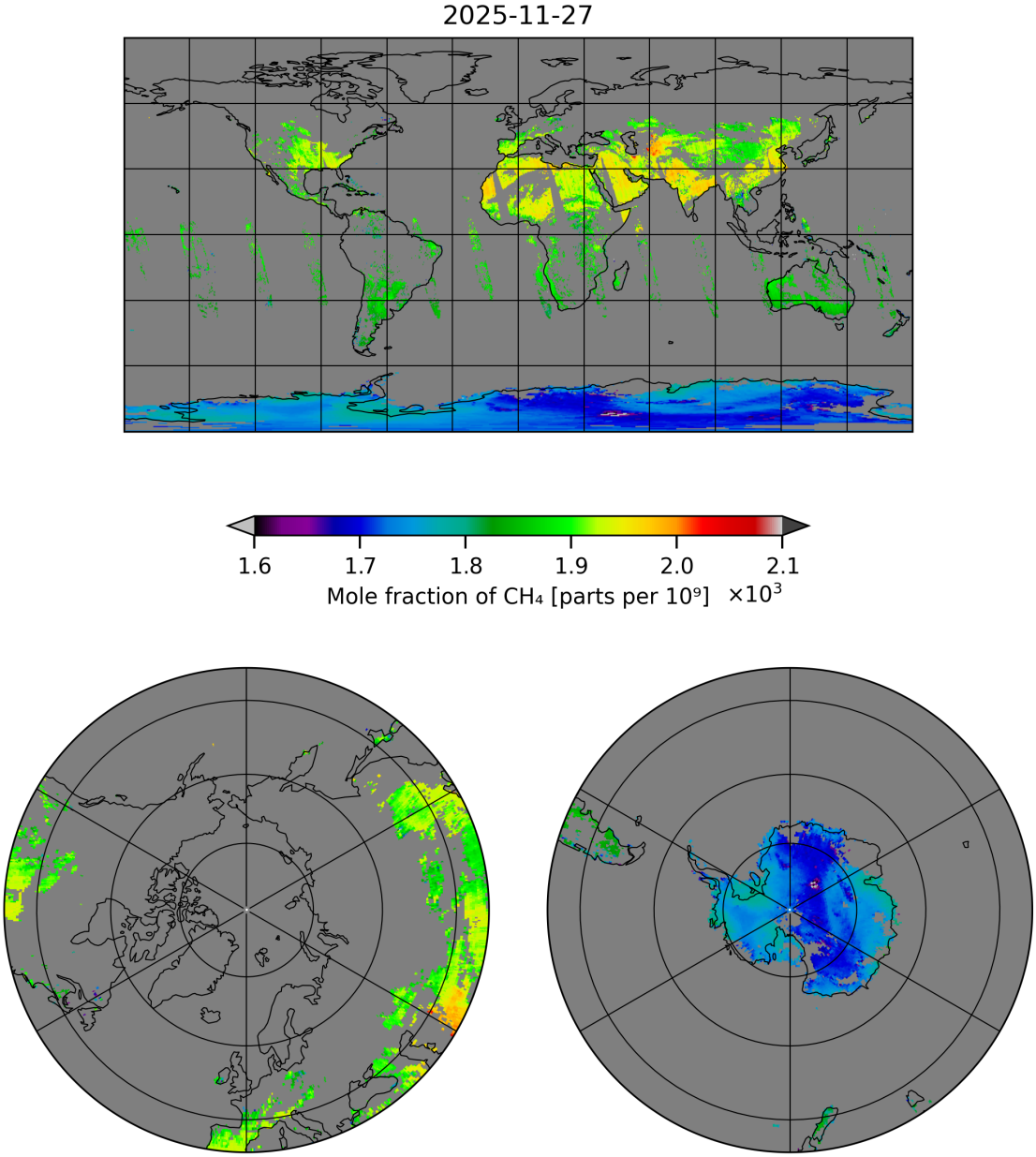

Figure 6: Map of "Mole fraction of CH_4" for 2025-11-26 to 2025-11-28

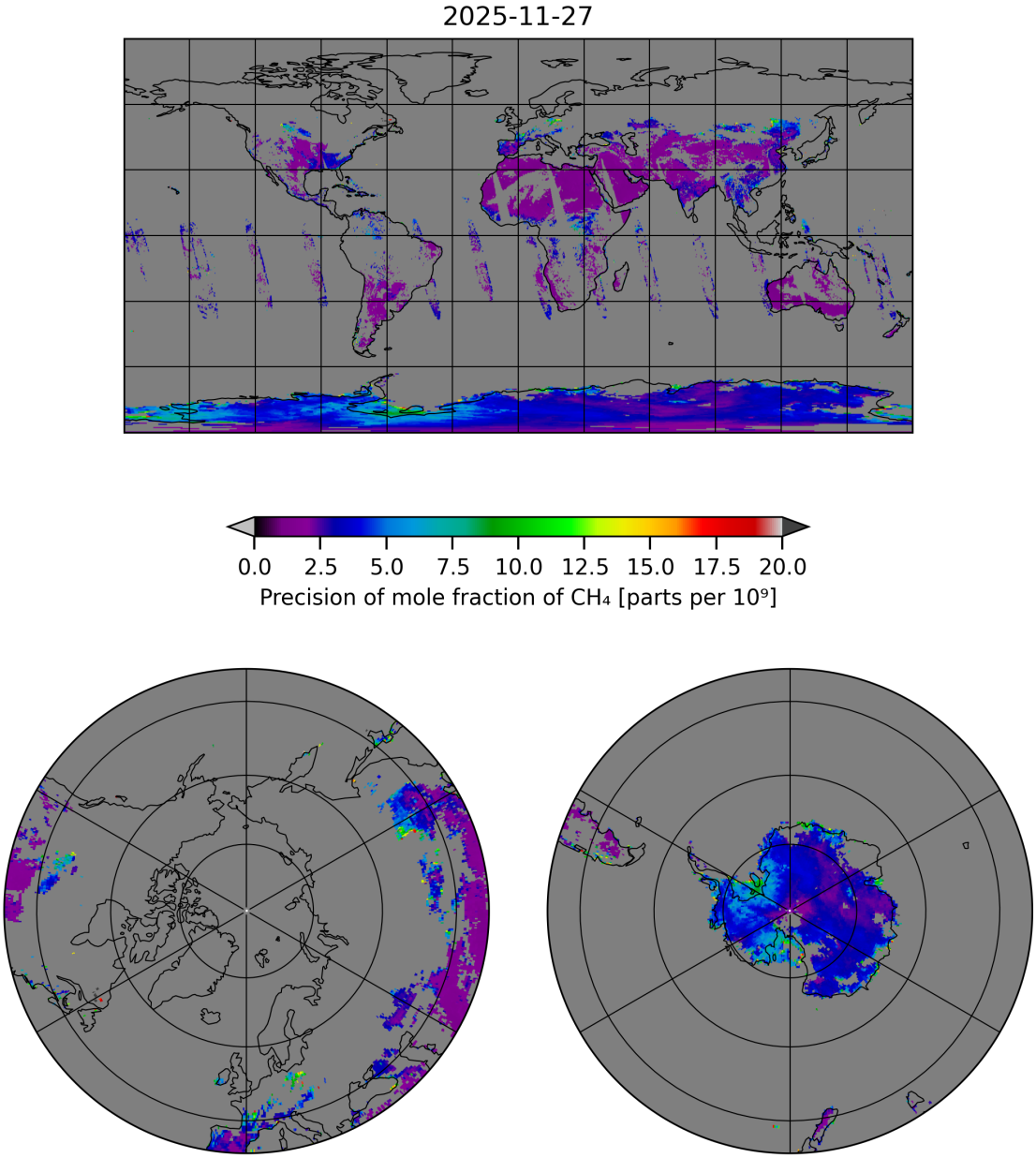

Figure 7: Map of "Precision of mole fraction of CH_4" for 2025-11-26 to 2025-11-28

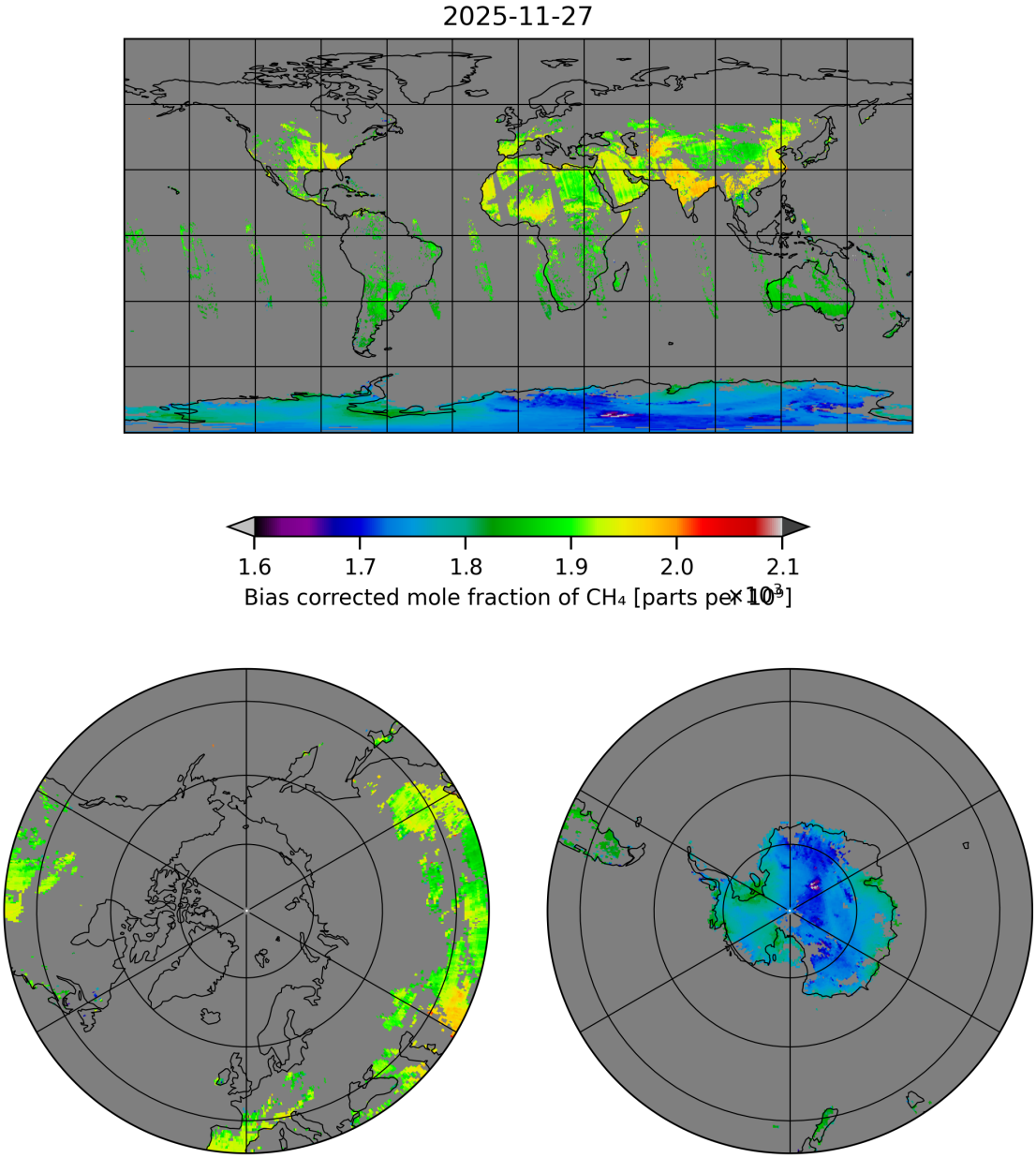

Figure 8: Map of “Bias corrected mole fraction of CH_4” for 2025-11-26 to 2025-11-28

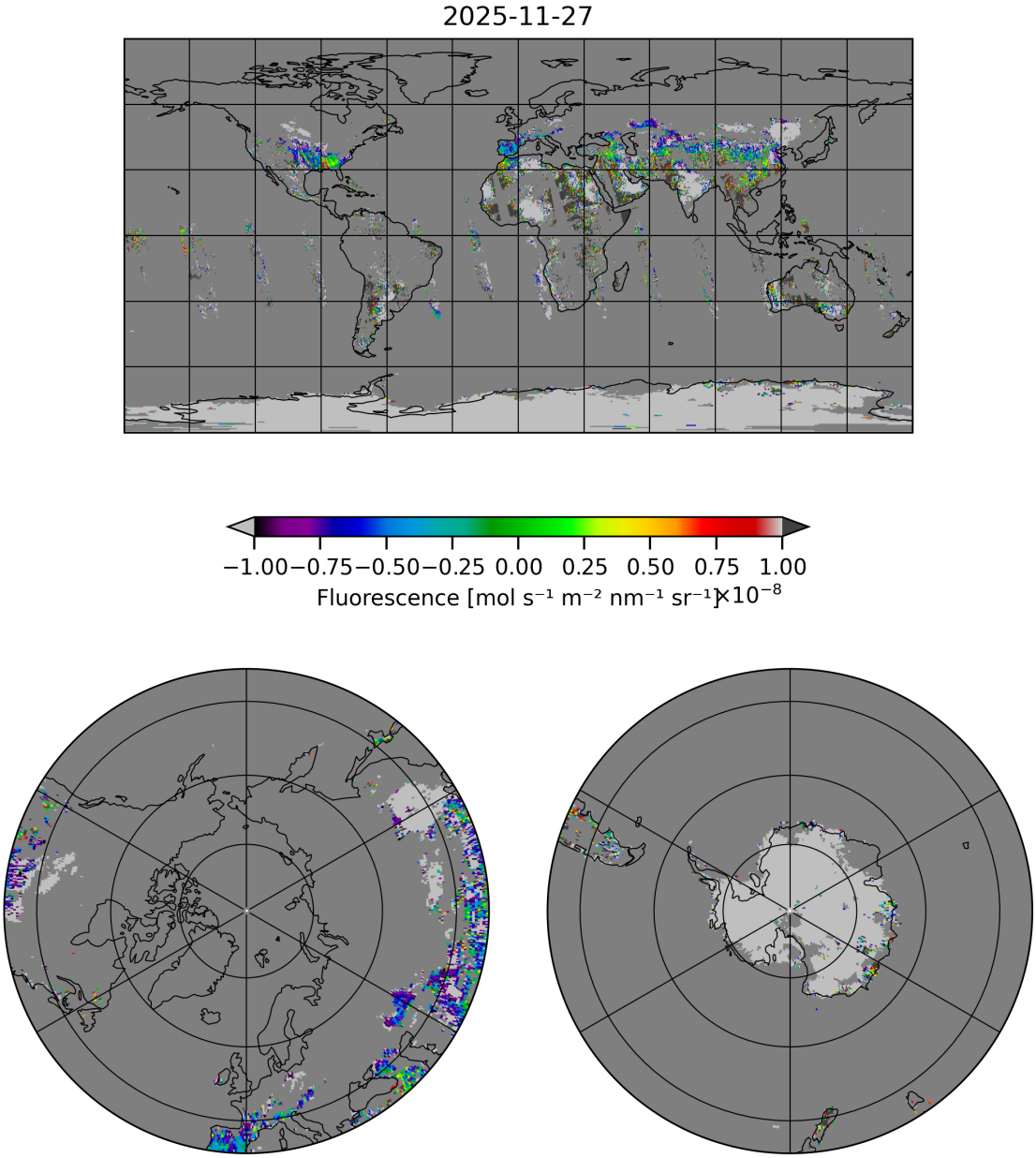

Figure 9: Map of “Fluorescence” for 2025-11-26 to 2025-11-28

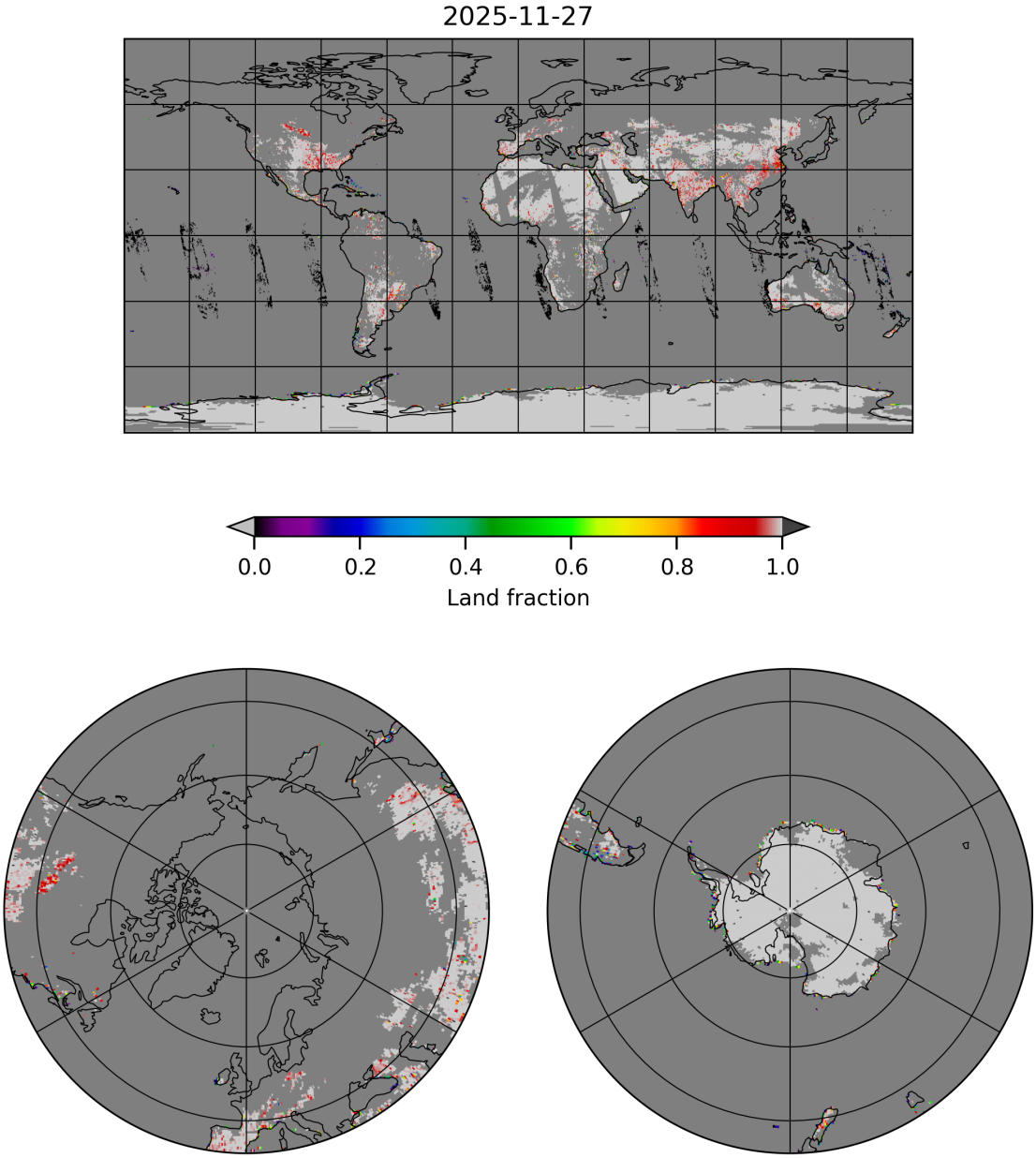

Figure 10: Map of “Land fraction” for 2025-11-26 to 2025-11-28

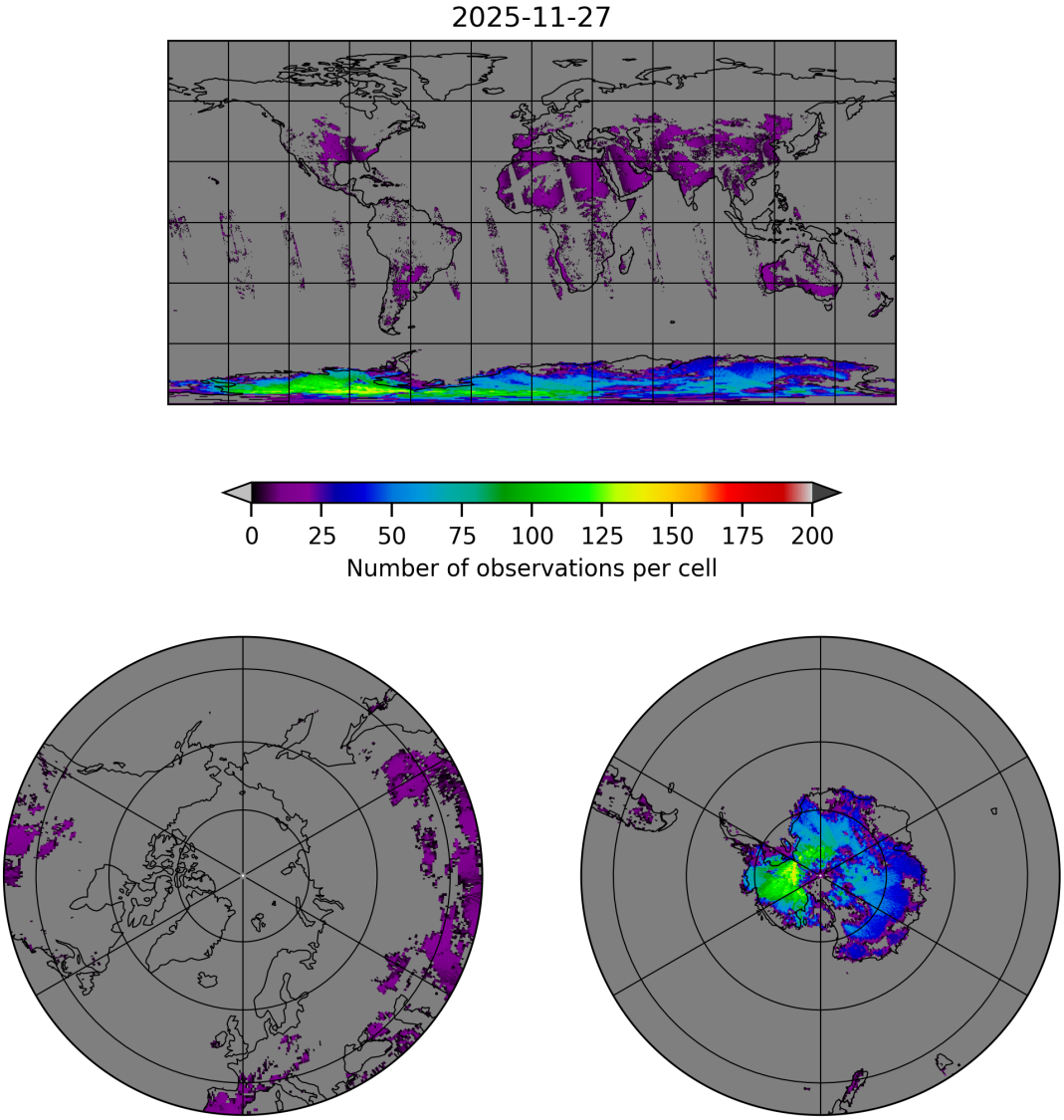

Figure 11: Map of the number of observations for 2025-11-26 to 2025-11-28

7 Zonal average

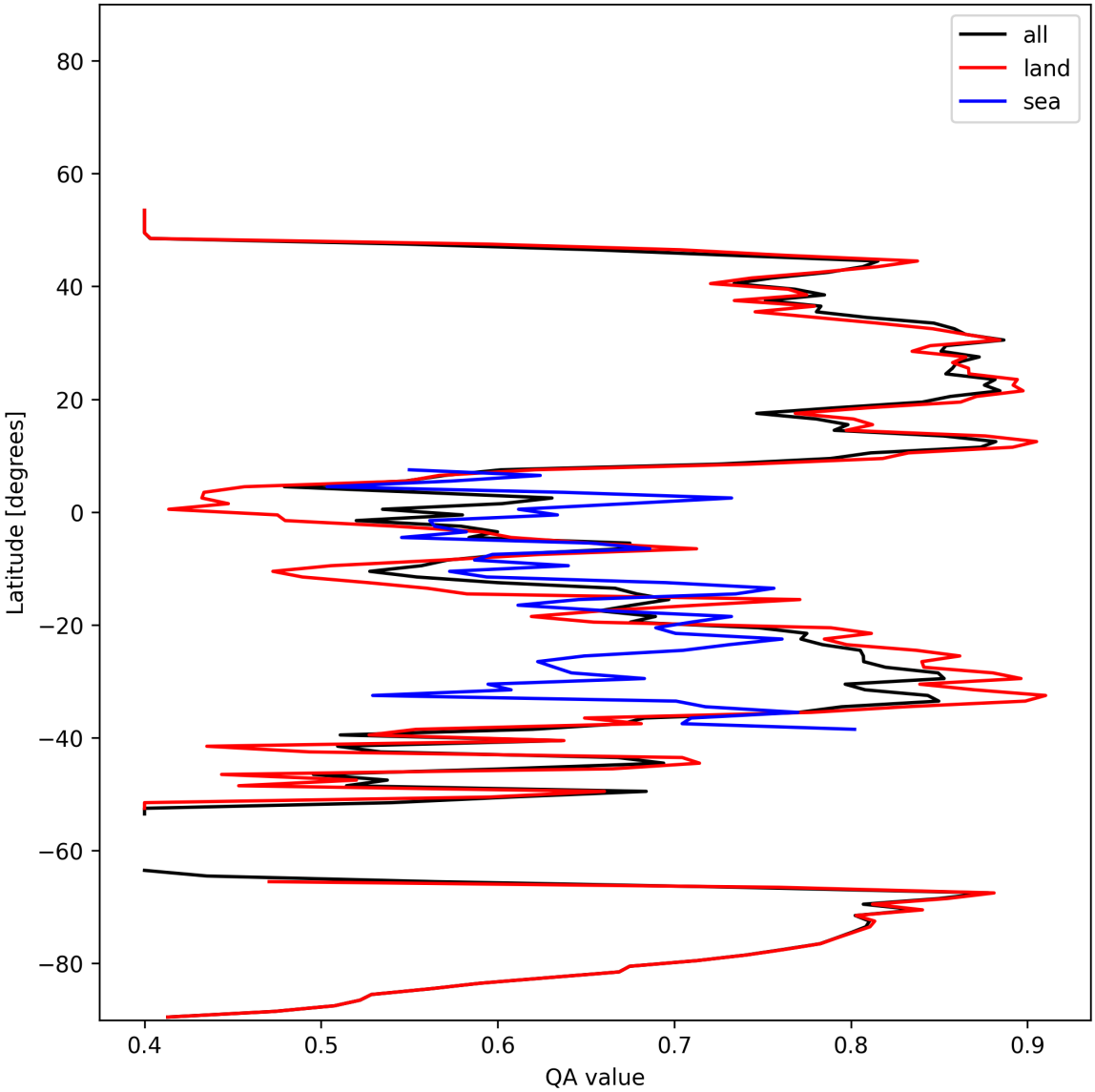

Figure 12: Zonal average of “QA value” for 2025-11-26 to 2025-11-28.

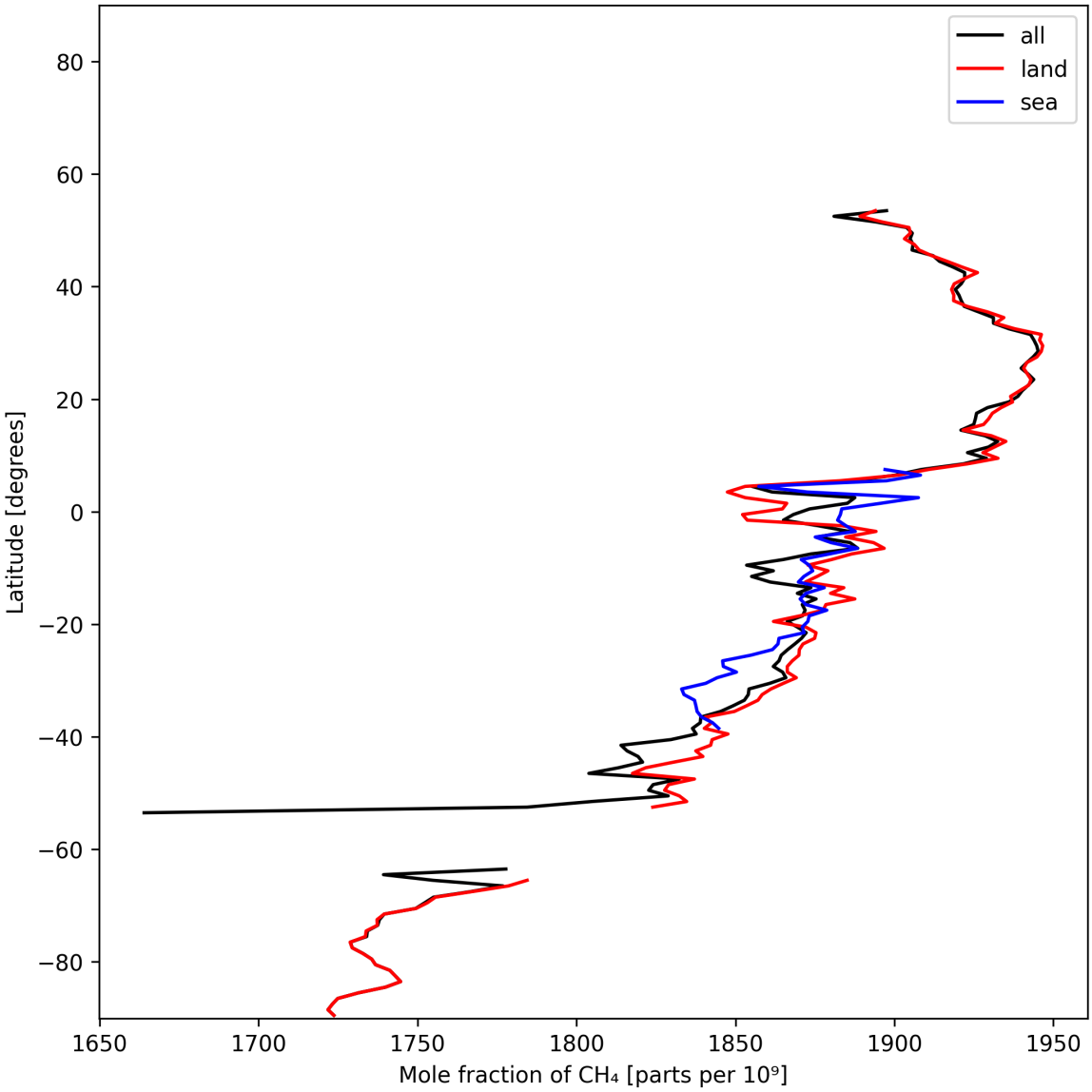

Figure 13: Zonal average of "Mole fraction of CH_4" for 2025-11-26 to 2025-11-28.

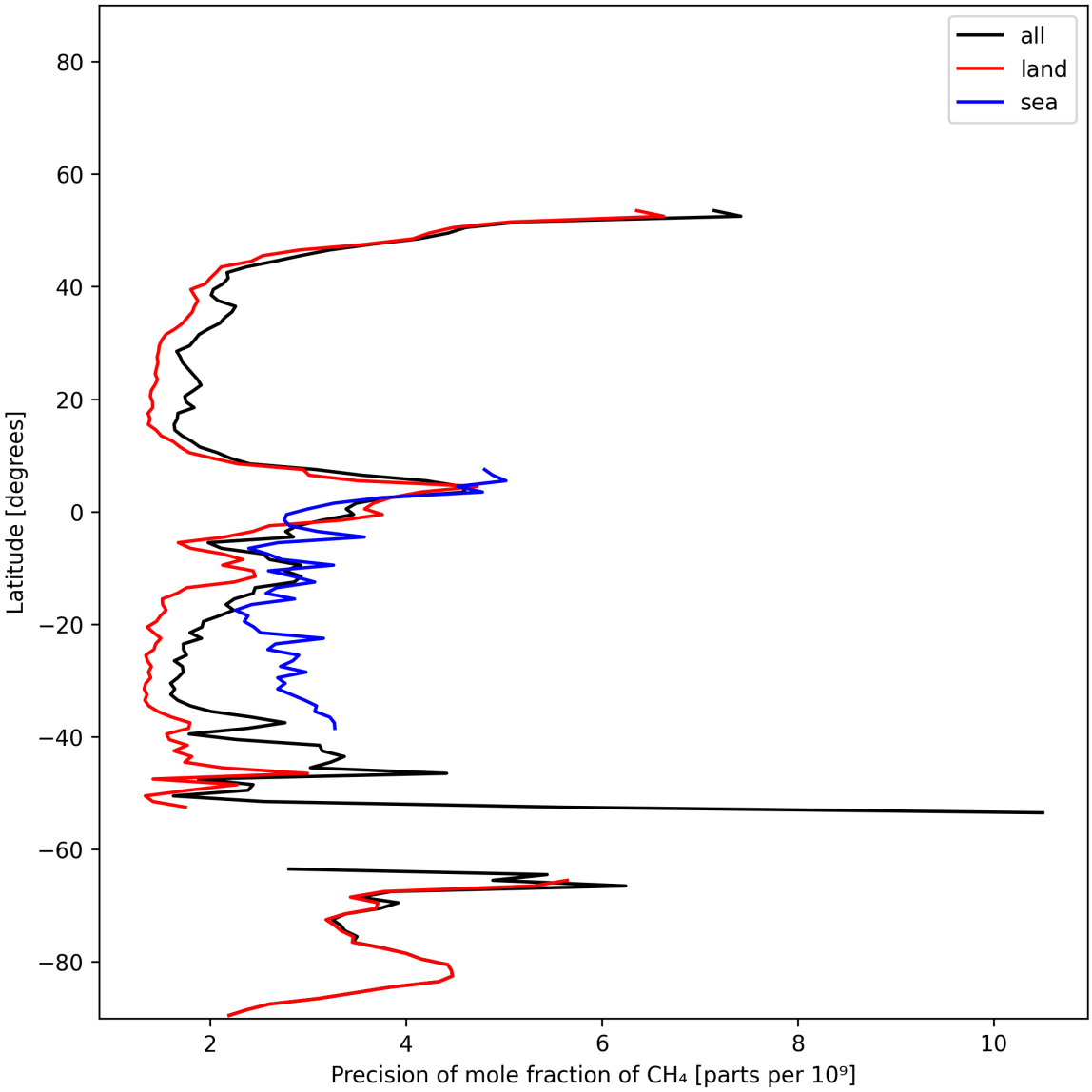

Figure 14: Zonal average of "Precision of mole fraction of CH_4" for 2025-11-26 to 2025-11-28.

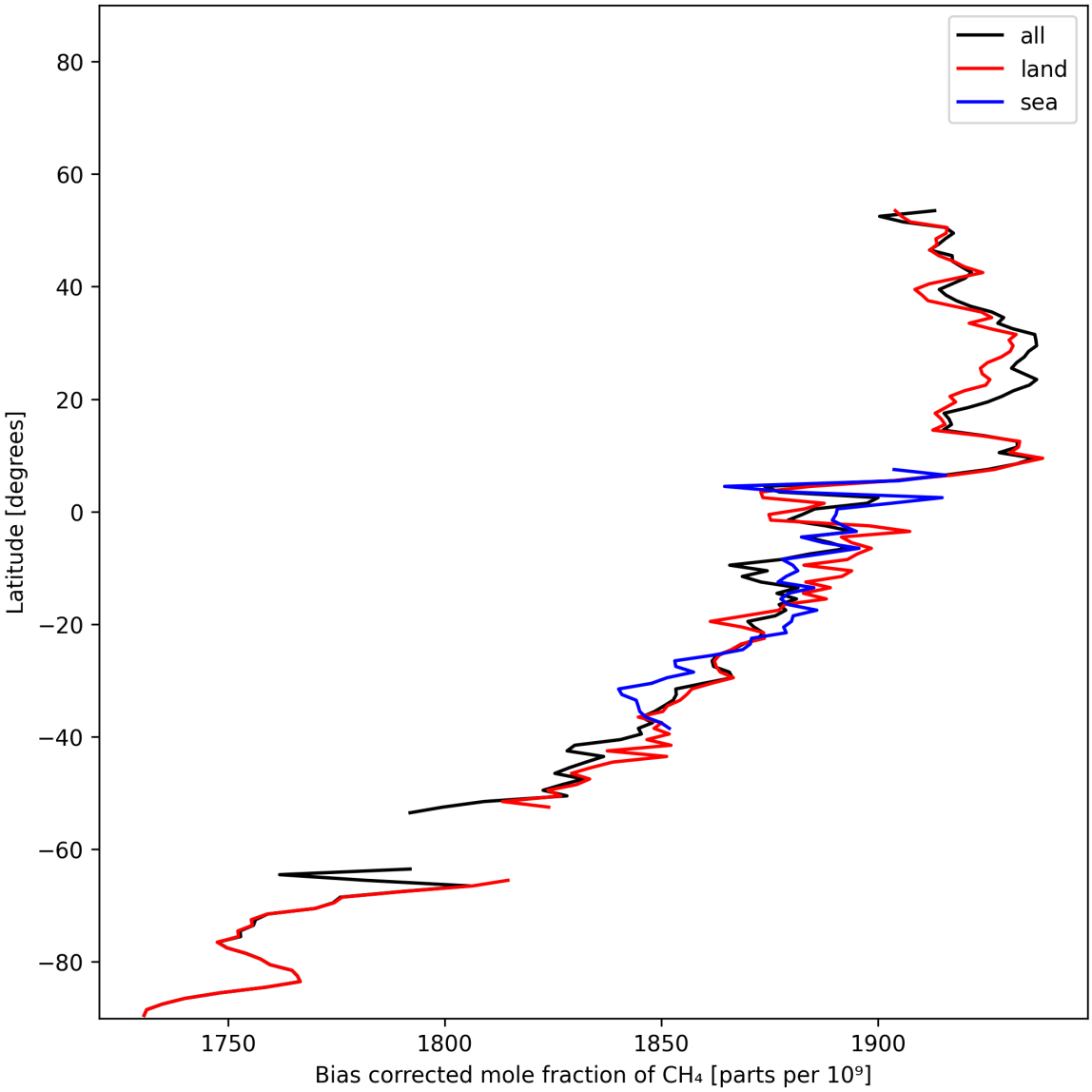

Figure 15: Zonal average of "Bias corrected mole fraction of CH_4" for 2025-11-26 to 2025-11-28.

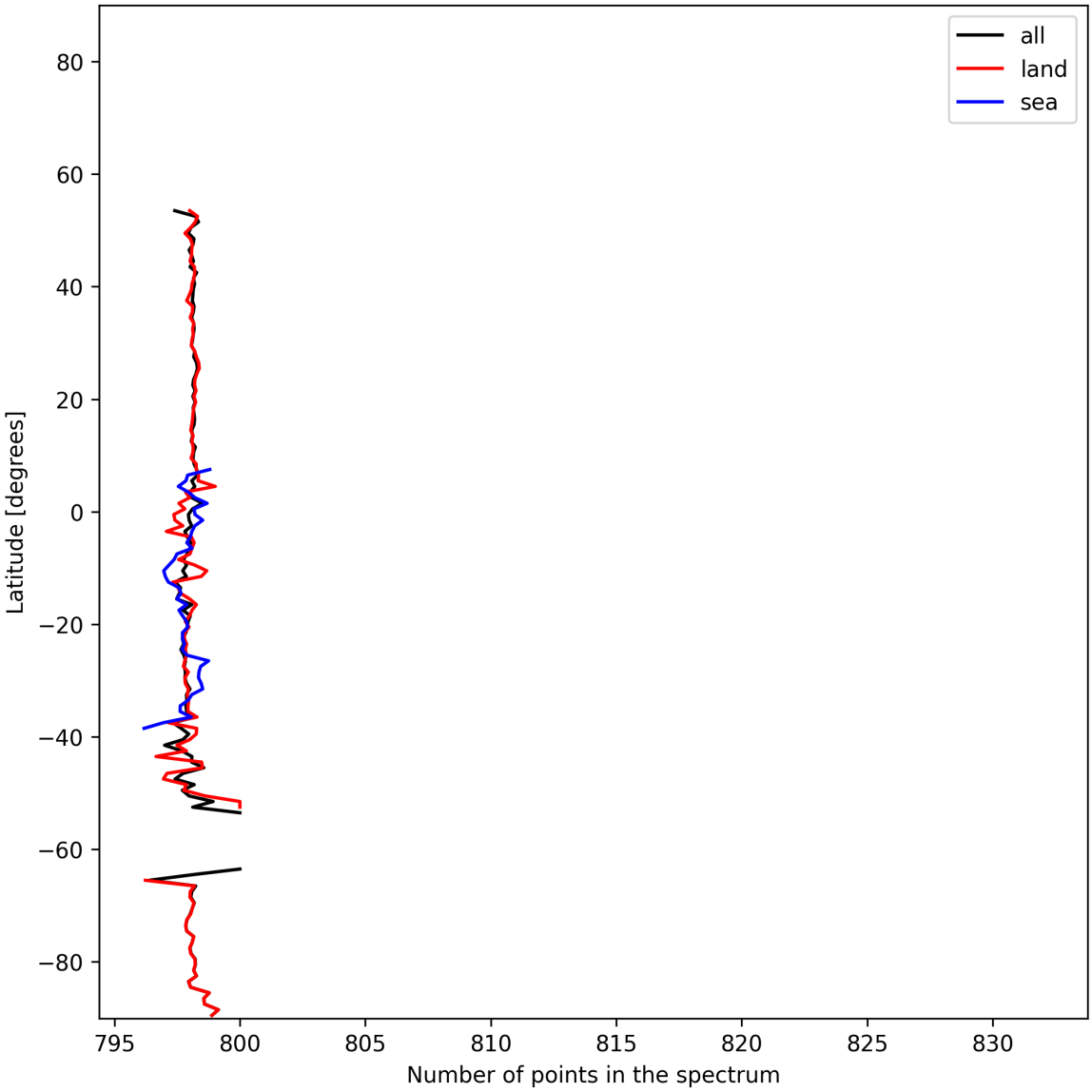

Figure 16: Zonal average of “Number of points in the spectrum” for 2025-11-26 to 2025-11-28.

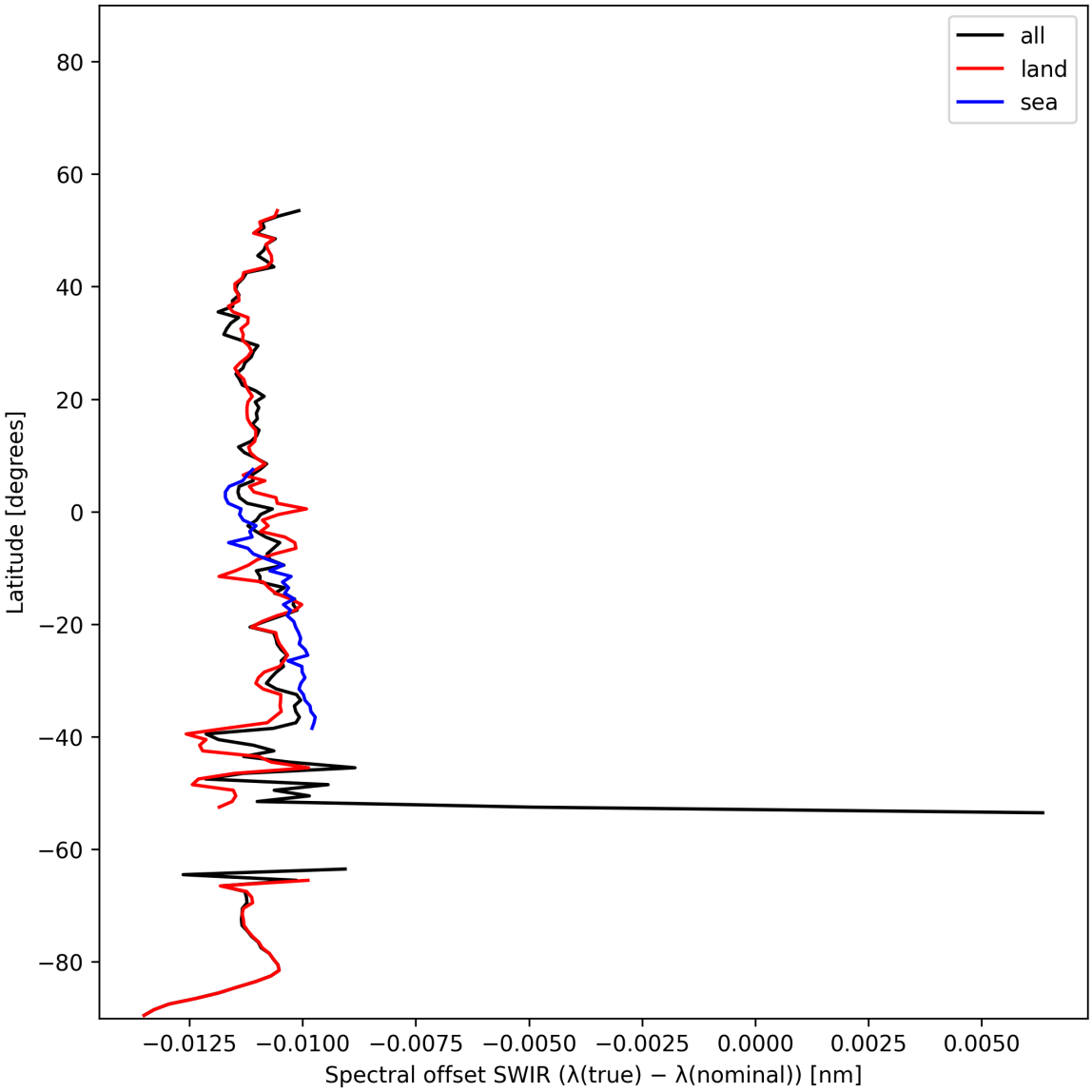

Figure 17: Zonal average of "Spectral offset SWIR ($\lambda_{\text{true}} - \lambda_{\text{nominal}}$)" for 2025-11-26 to 2025-11-28.

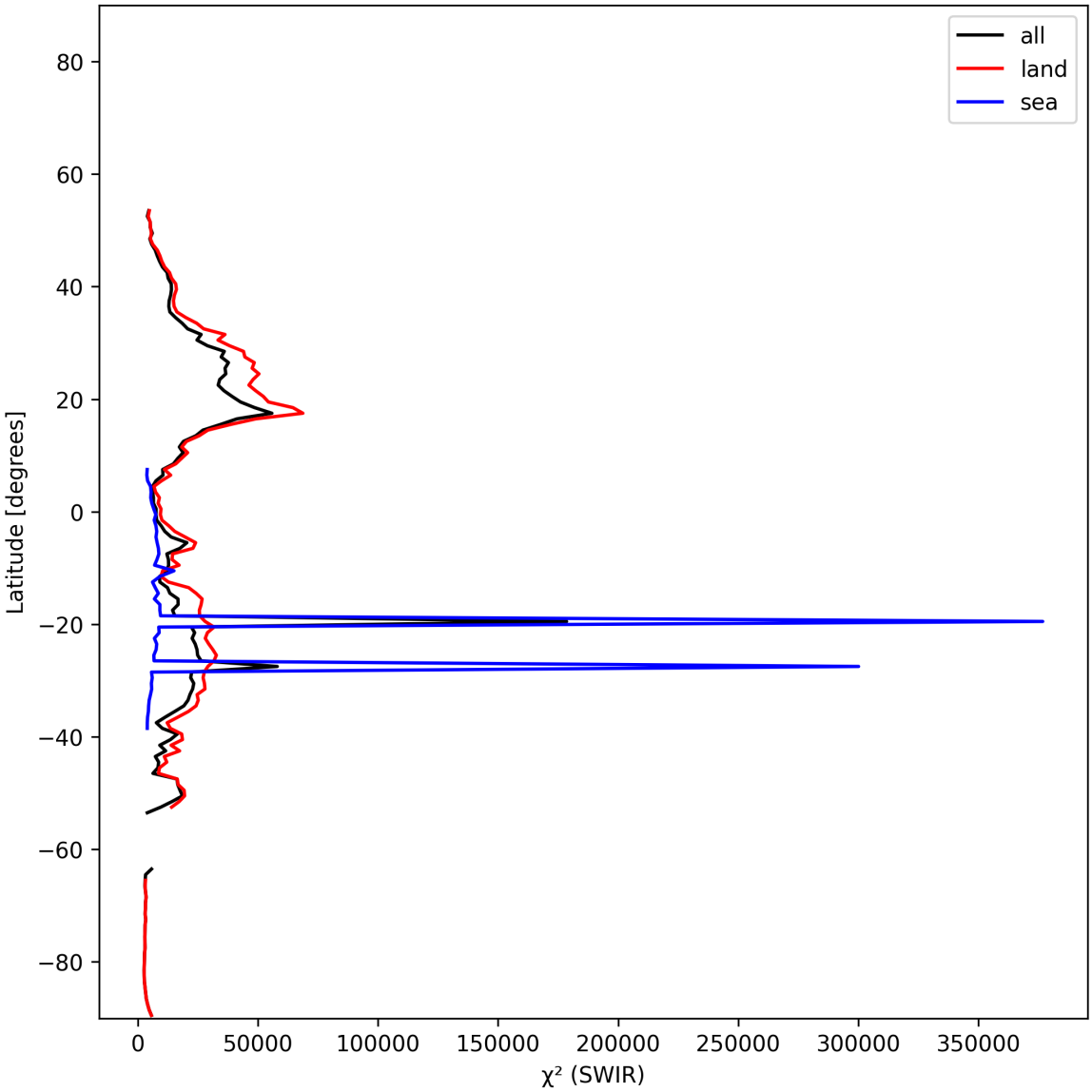

Figure 18: Zonal average of "χ^2 (SWIR)" for 2025-11-26 to 2025-11-28.

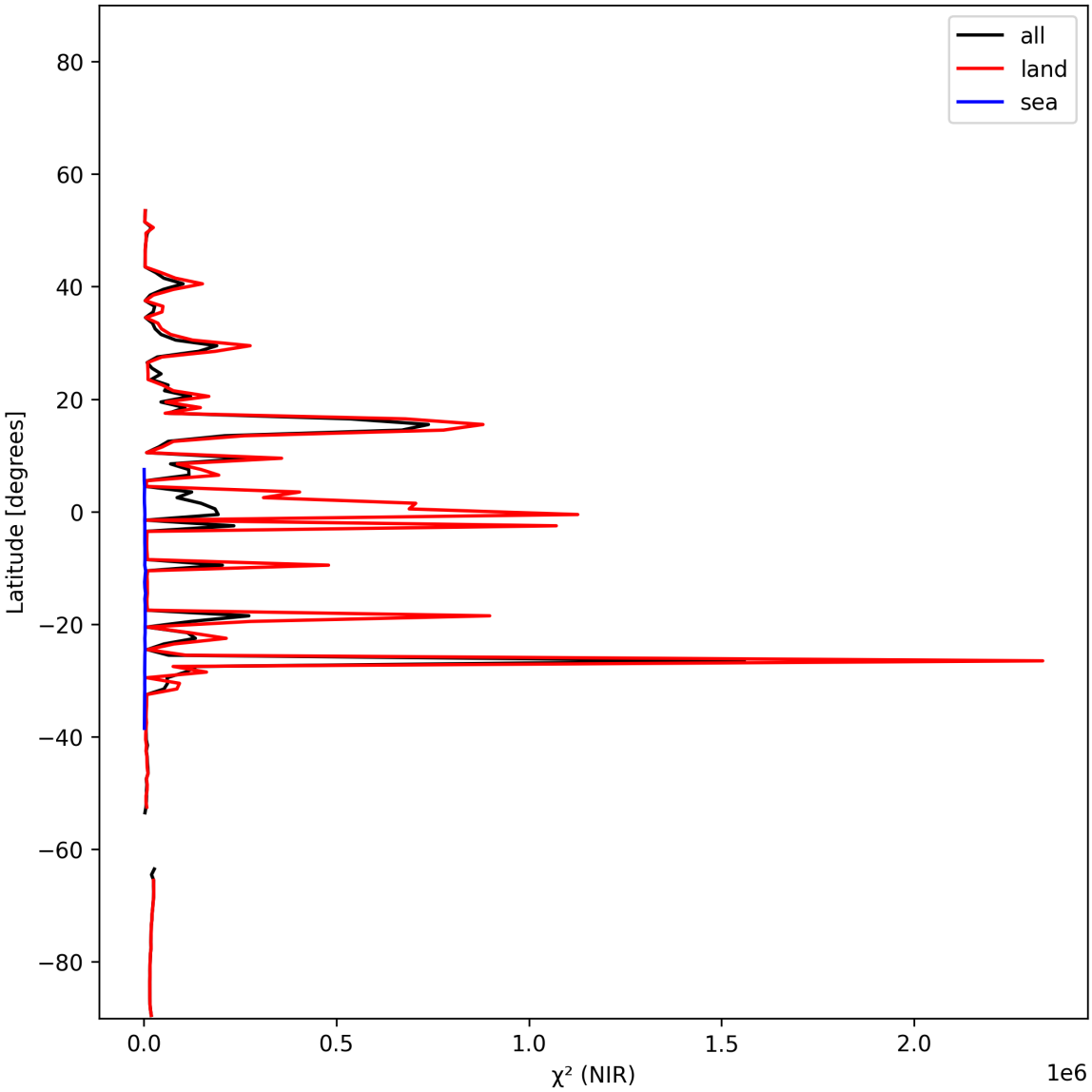

Figure 19: Zonal average of "χ^2 (NIR)" for 2025-11-26 to 2025-11-28.

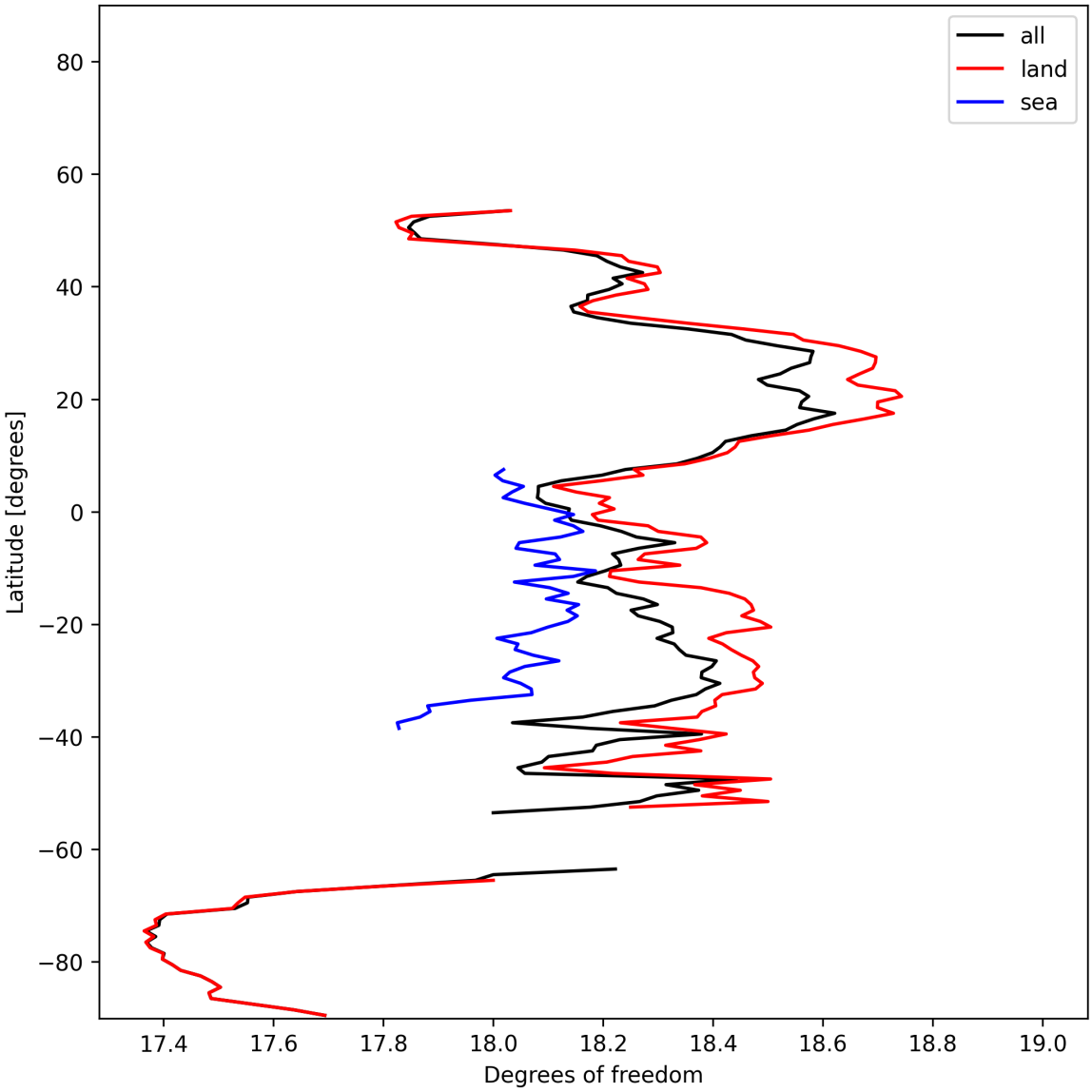

Figure 20: Zonal average of “Degrees of freedom” for 2025-11-26 to 2025-11-28.

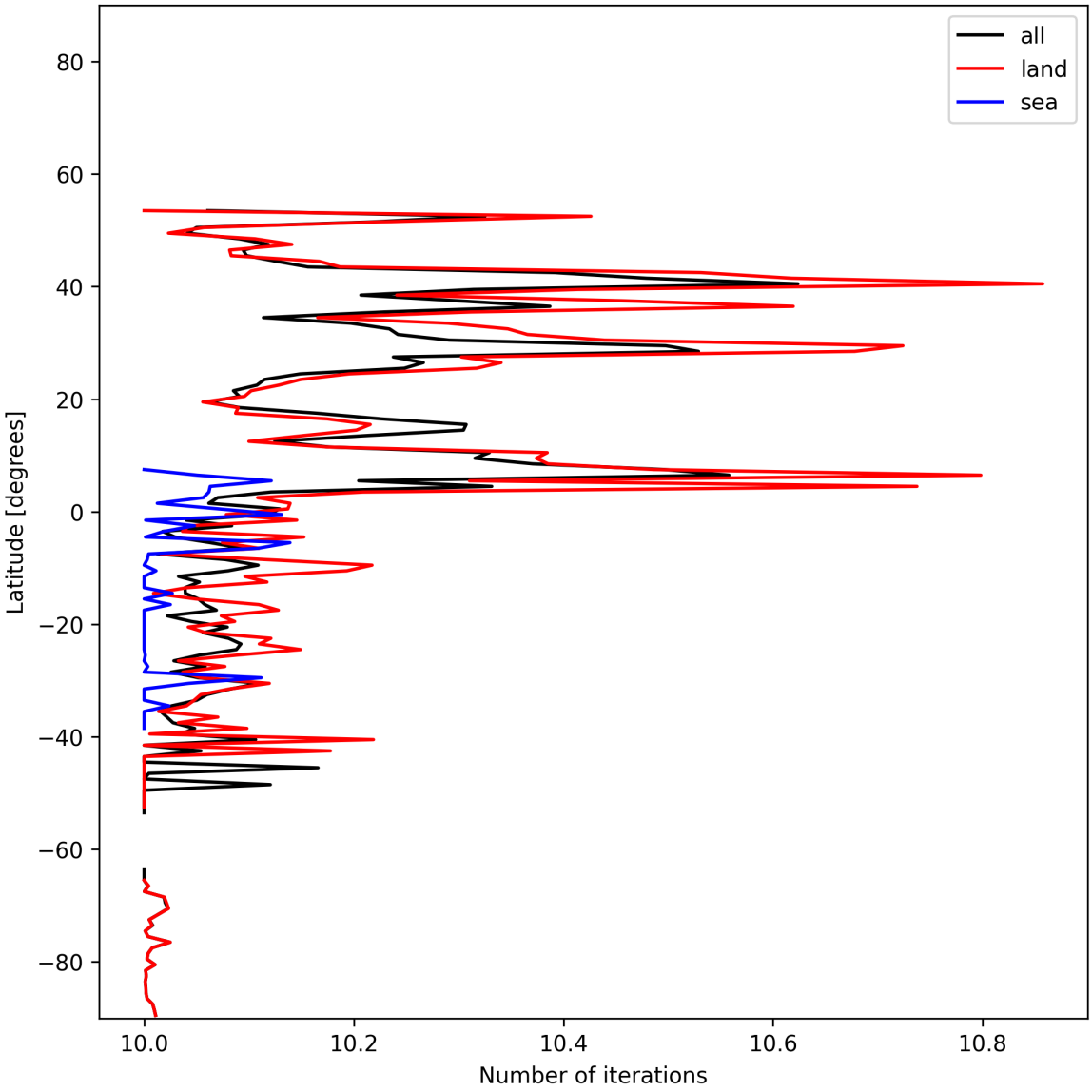

Figure 21: Zonal average of “Number of iterations” for 2025-11-26 to 2025-11-28.

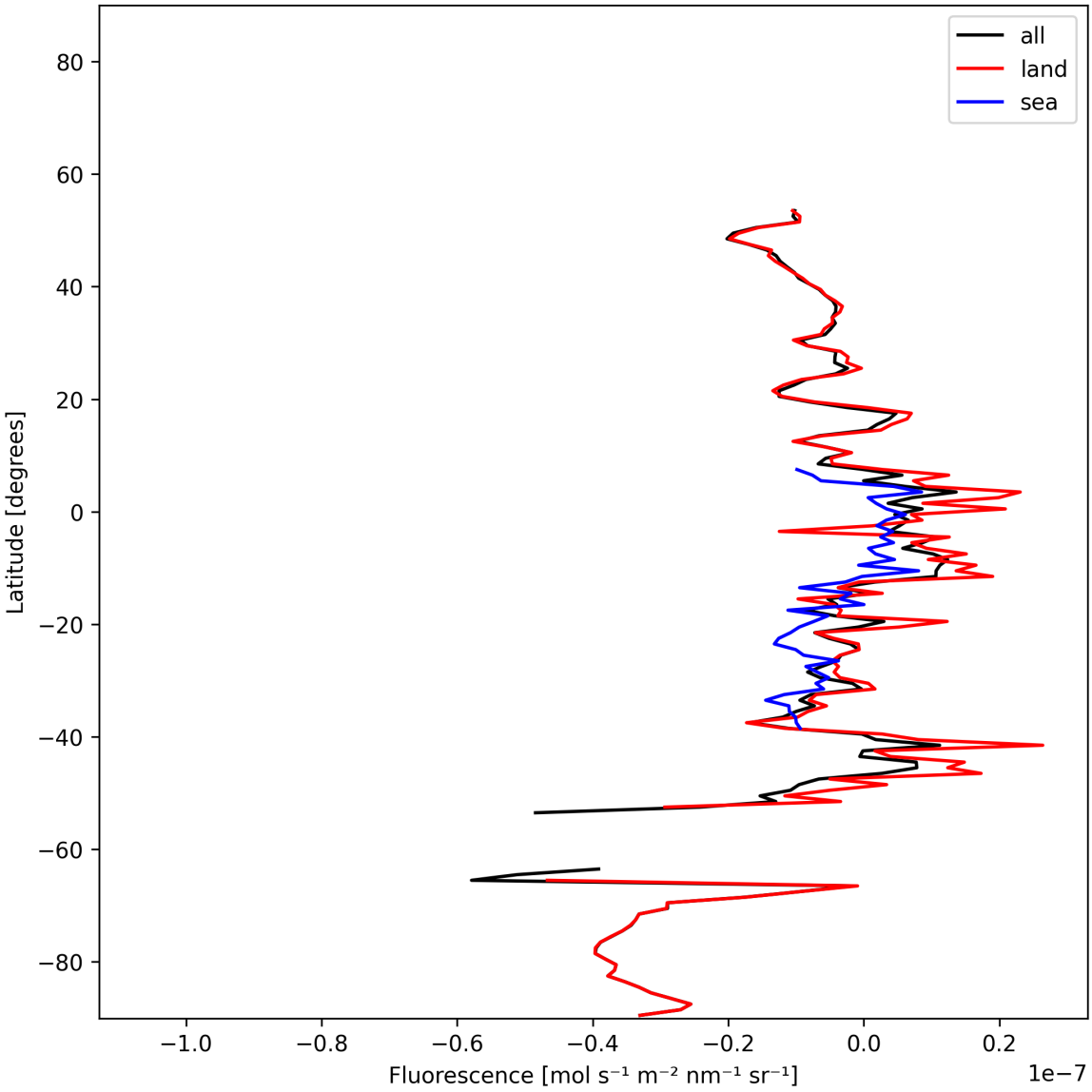

Figure 22: Zonal average of “Fluorescence” for 2025-11-26 to 2025-11-28.

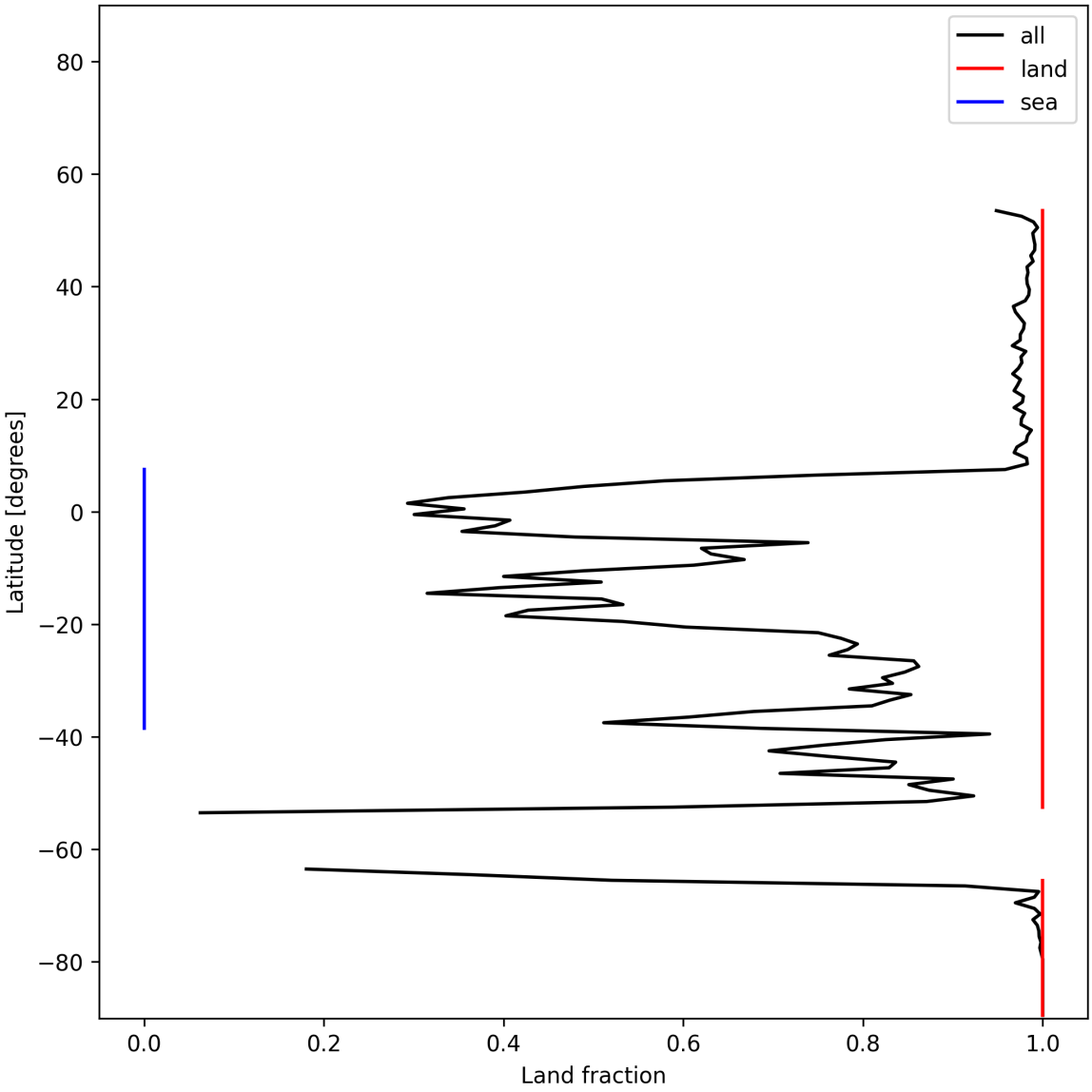

Figure 23: Zonal average of “Land fraction” for 2025-11-26 to 2025-11-28.

8 Histograms

The definitions of the parameters given in this section can be found in section 2.

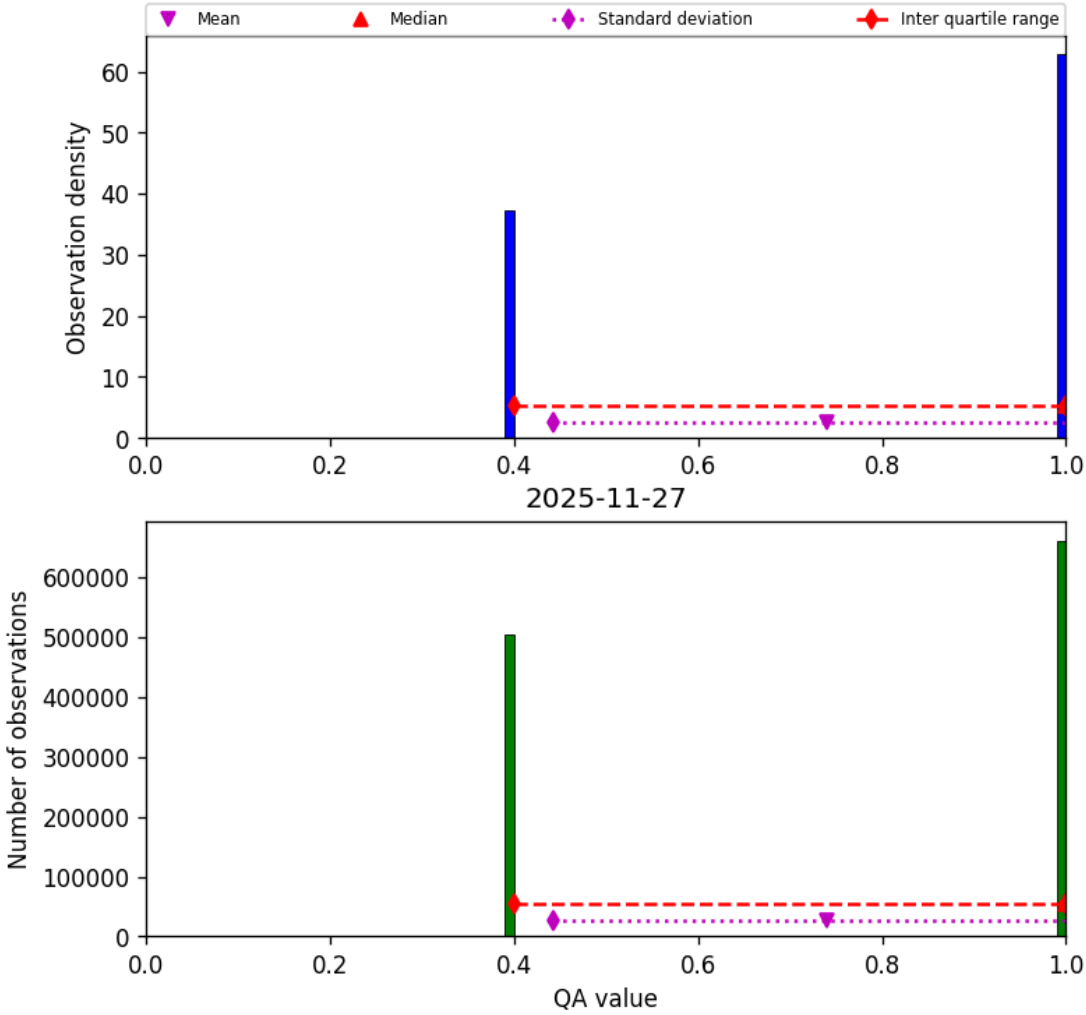

Figure 24: Histogram of “QA value” for 2025-11-26 to 2025-11-28

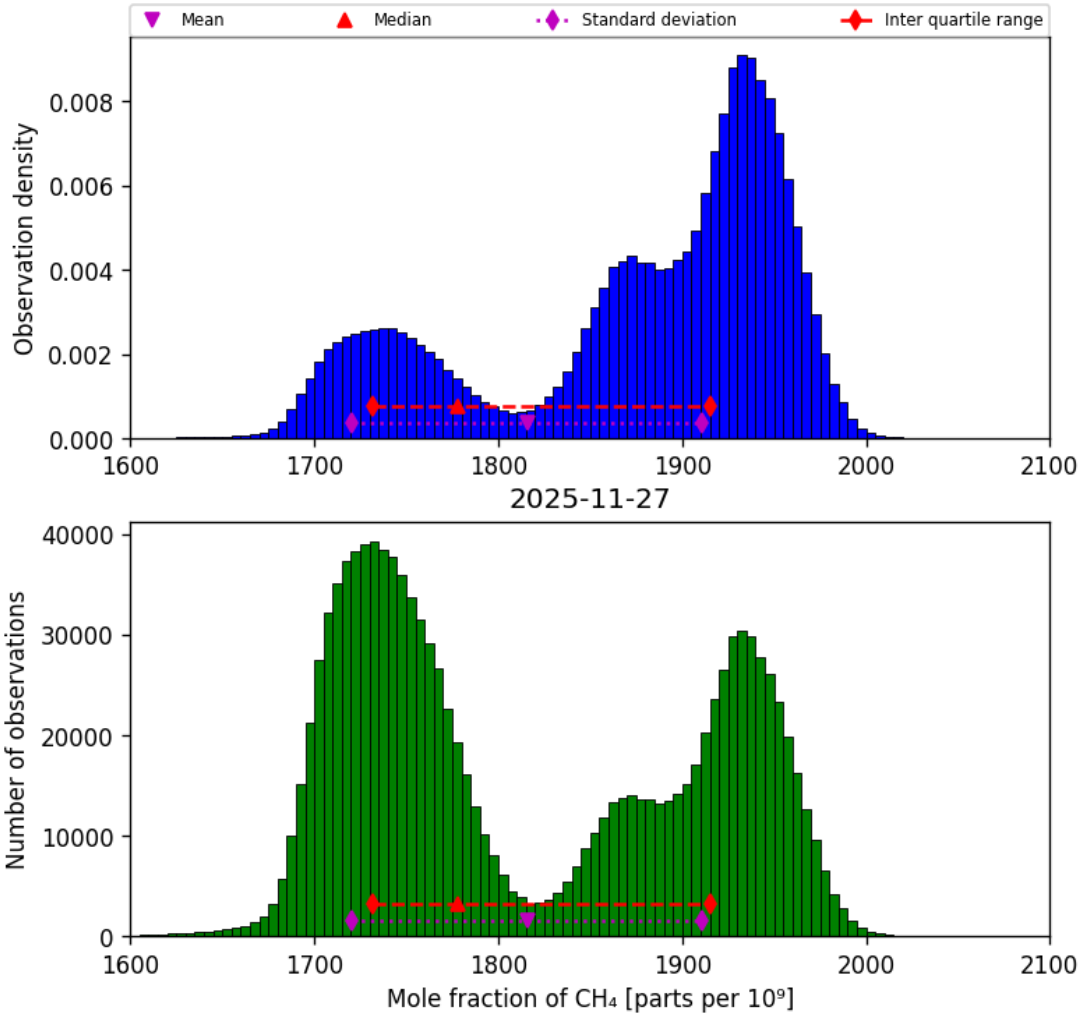

Figure 25: Histogram of "Mole fraction of CH_4" for 2025-11-26 to 2025-11-28

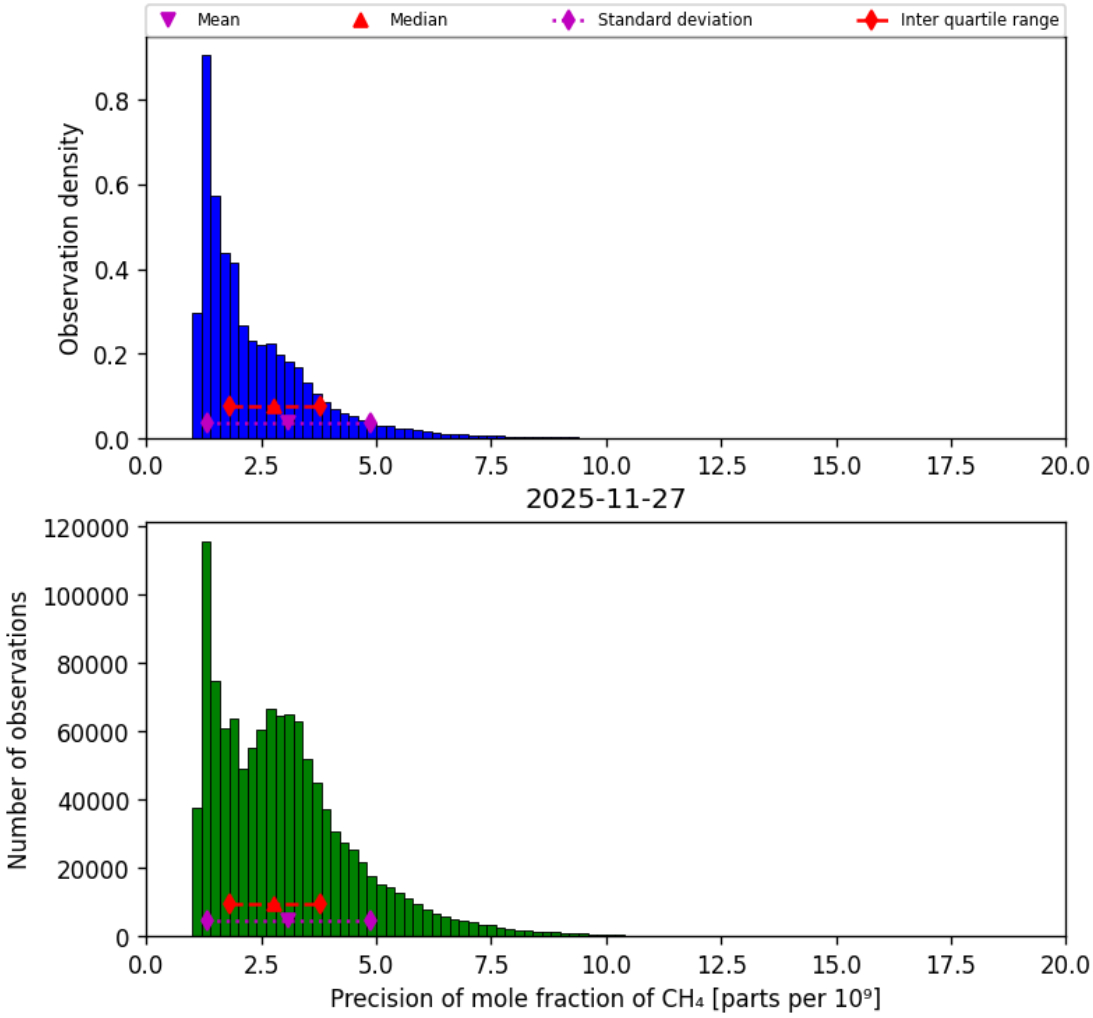

Figure 26: Histogram of "Precision of mole fraction of CH_4" for 2025-11-26 to 2025-11-28

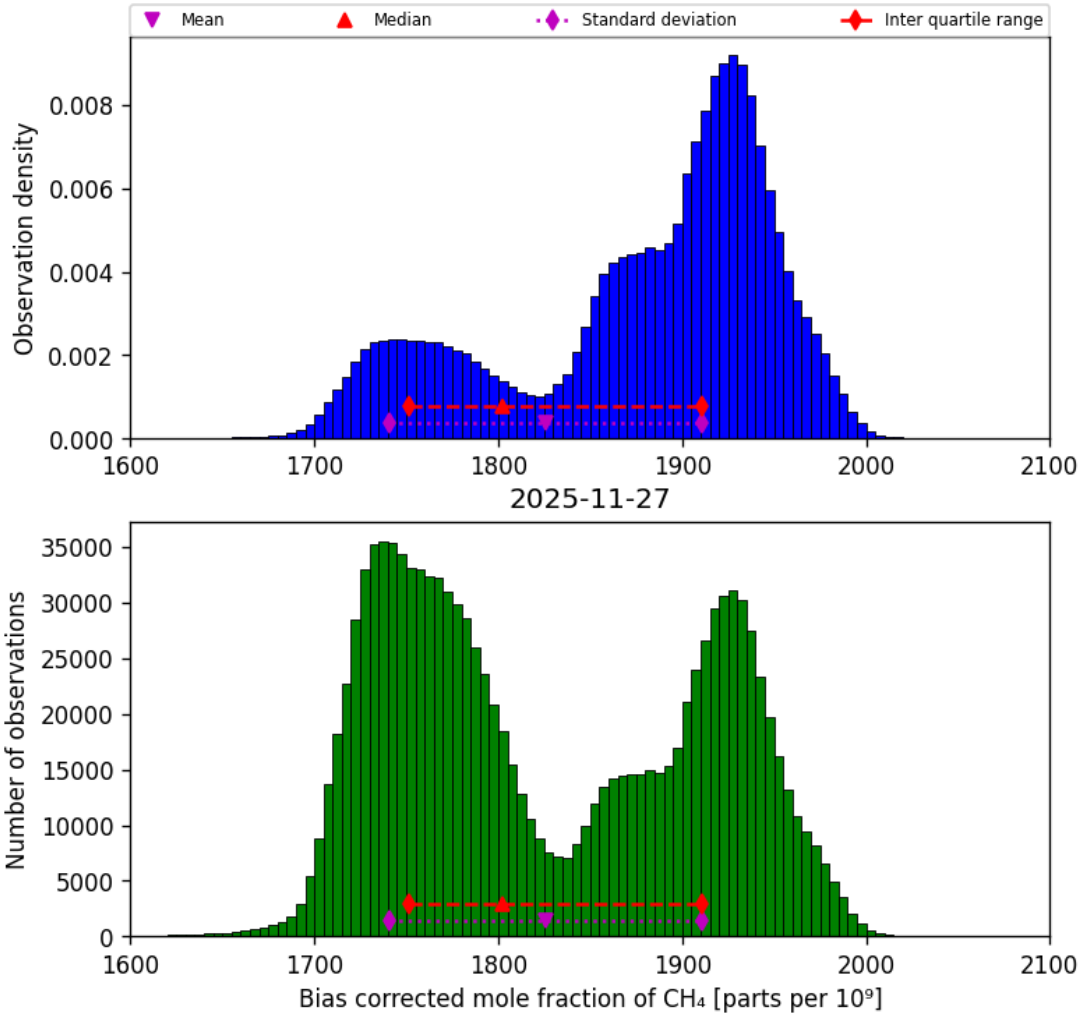

Figure 27: Histogram of "Bias corrected mole fraction of CH_4" for 2025-11-26 to 2025-11-28

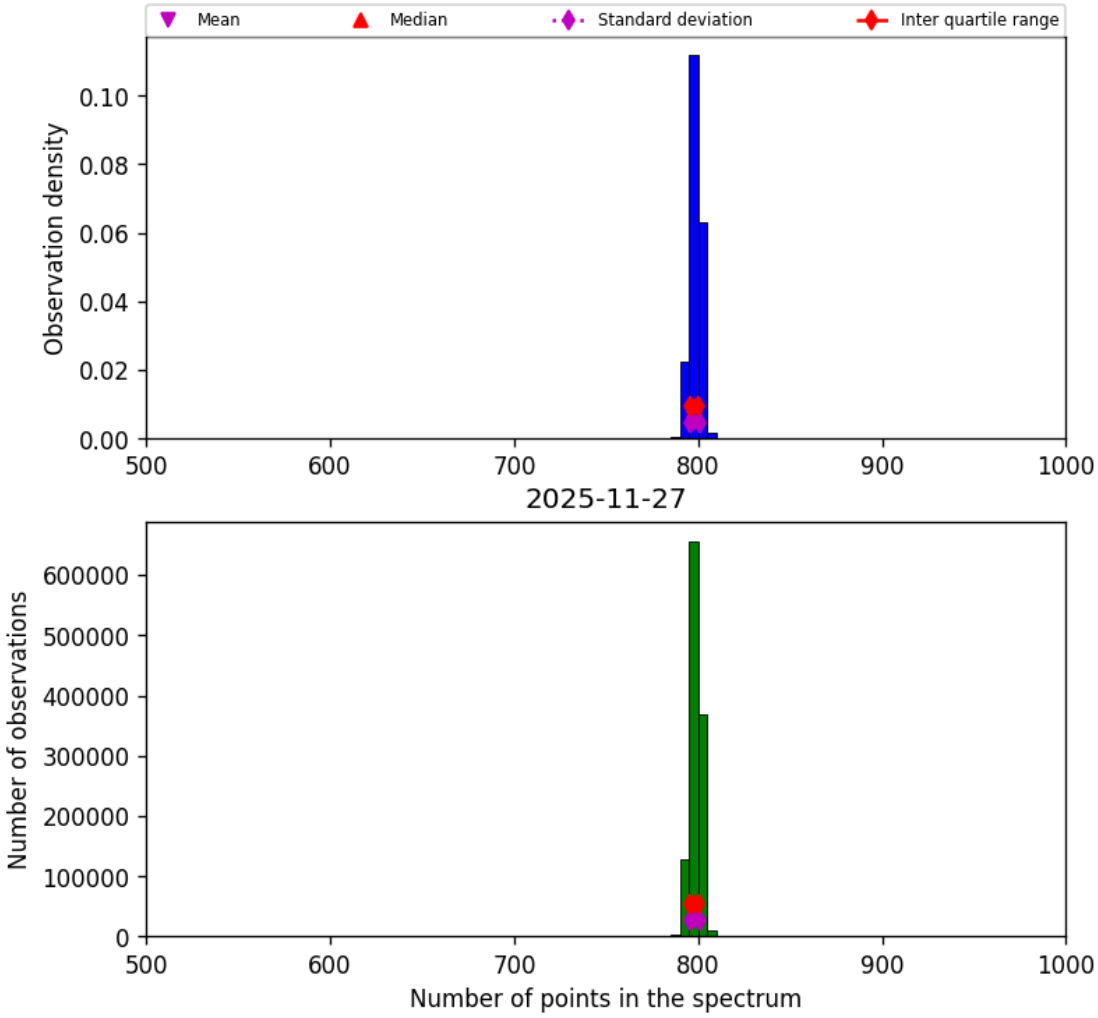

Figure 28: Histogram of “Number of points in the spectrum” for 2025-11-26 to 2025-11-28

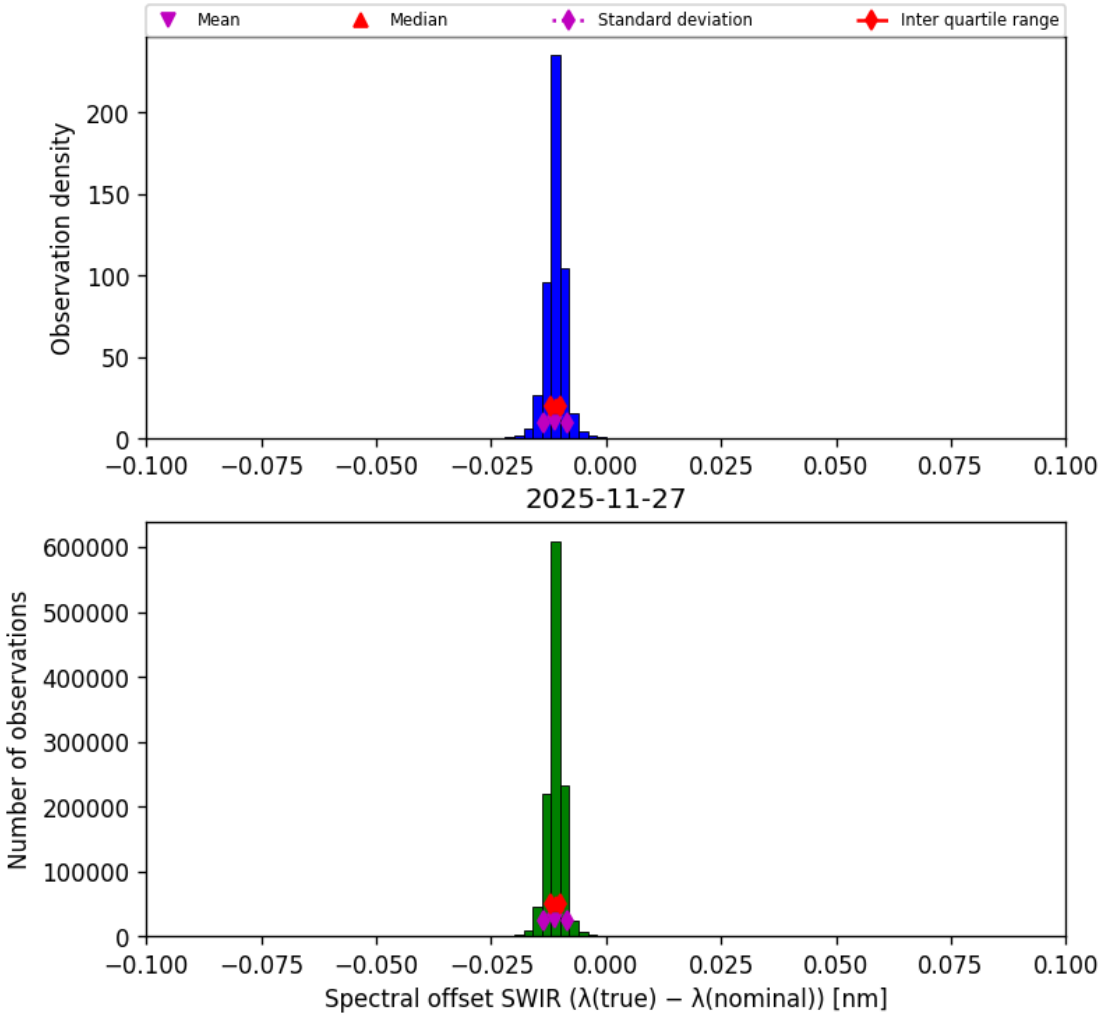

Figure 29: Histogram of "Spectral offset SWIR ($\lambda_{\text{true}} - \lambda_{\text{nominal}}$)" for 2025-11-26 to 2025-11-28

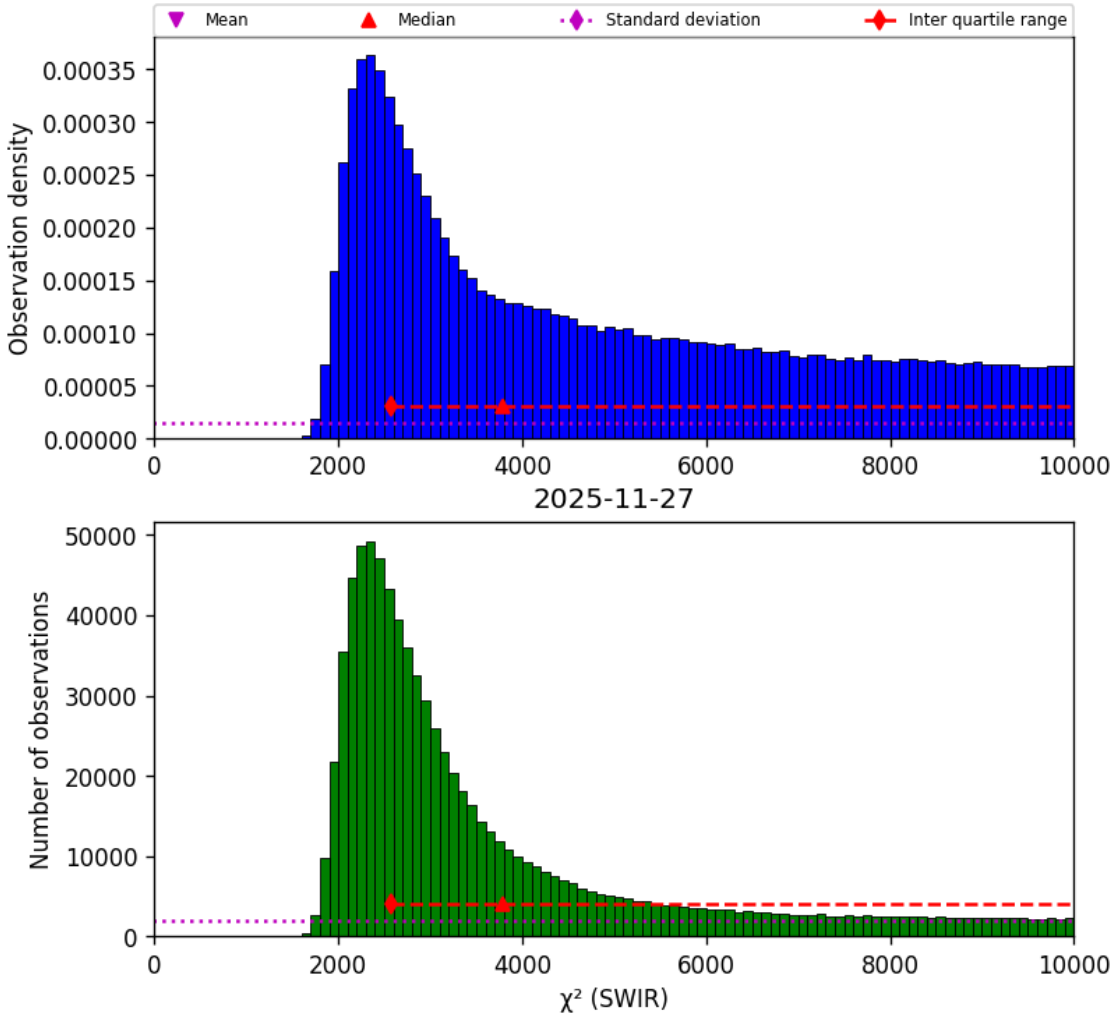

Figure 30: Histogram of "χ^2 (SWIR)" for 2025-11-26 to 2025-11-28

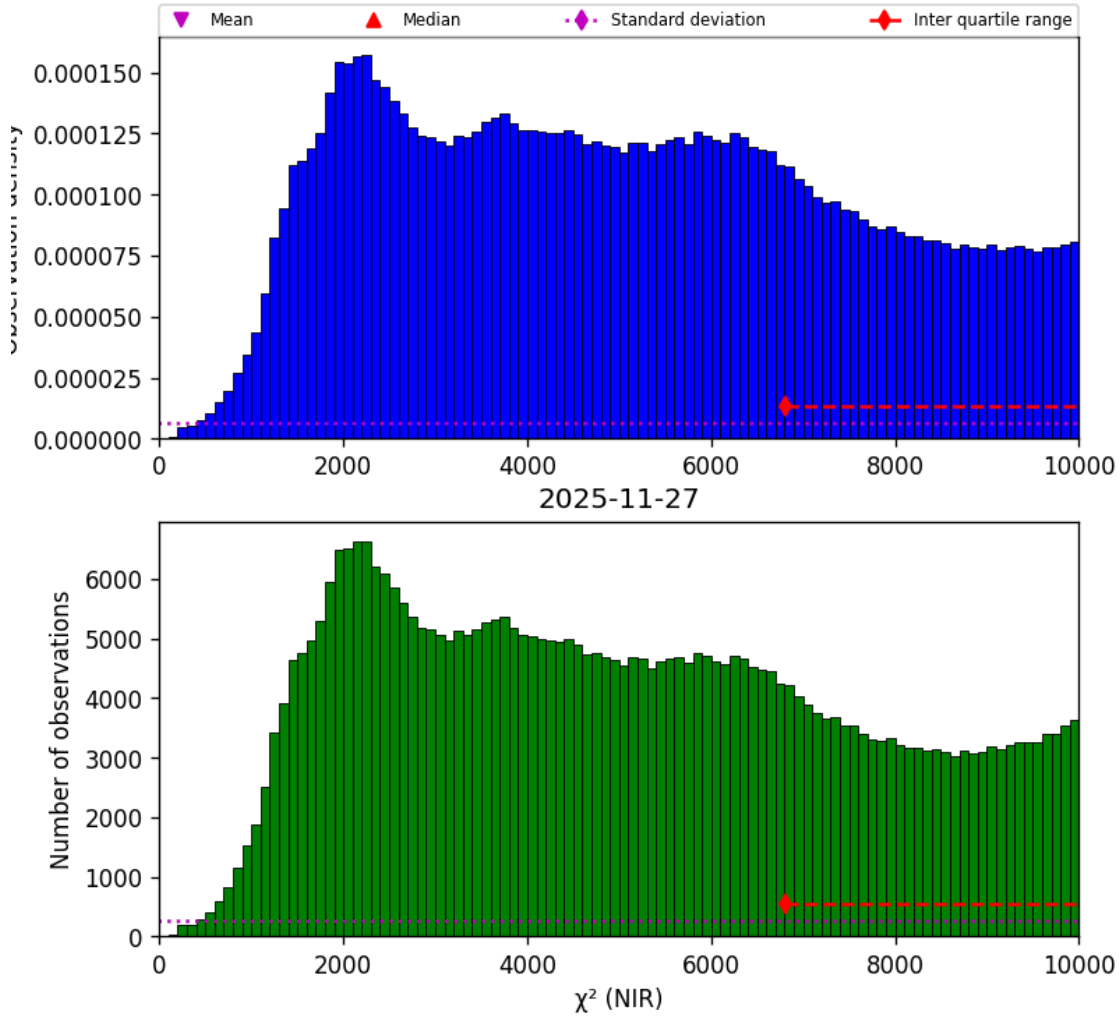

Figure 31: Histogram of "χ^2 (NIR)" for 2025-11-26 to 2025-11-28

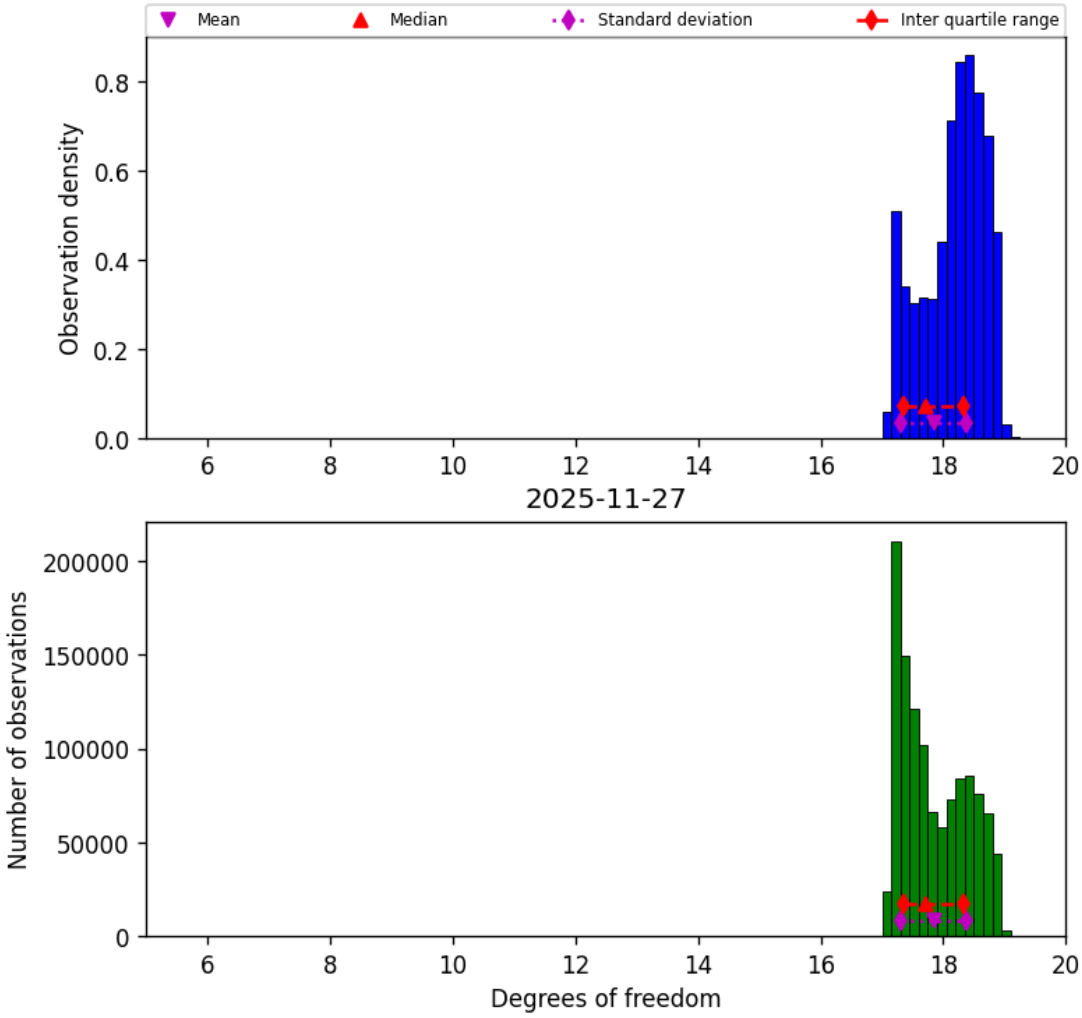

Figure 32: Histogram of “Degrees of freedom” for 2025-11-26 to 2025-11-28

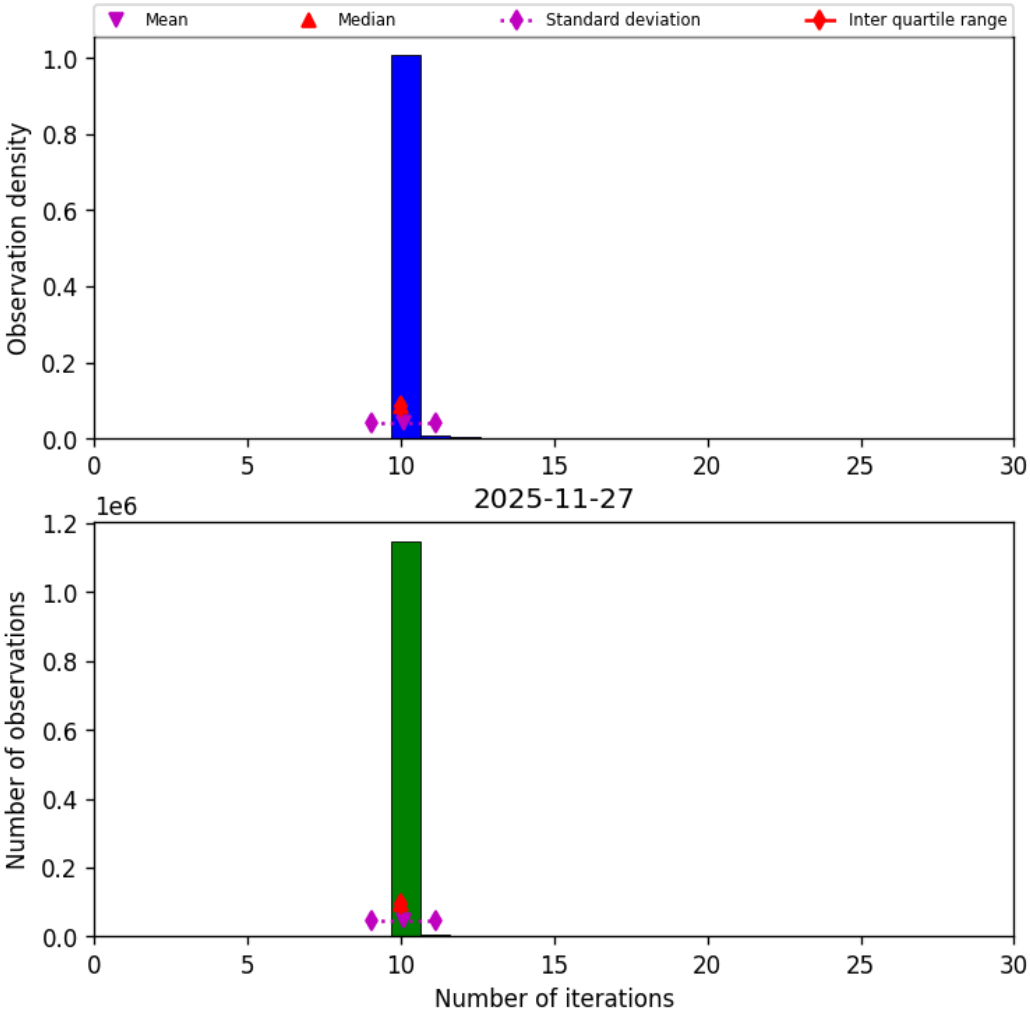

Figure 33: Histogram of “Number of iterations” for 2025-11-26 to 2025-11-28

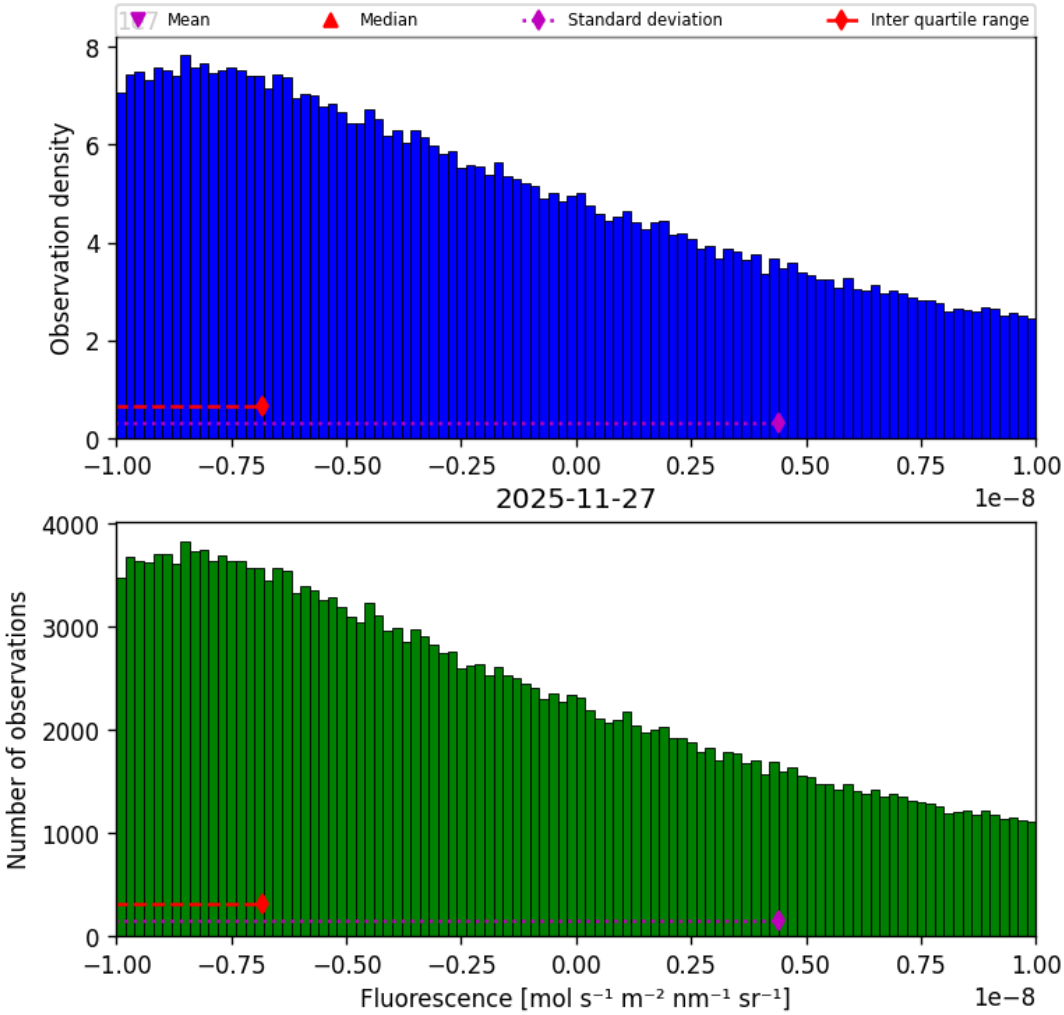

Figure 34: Histogram of “Fluorescence” for 2025-11-26 to 2025-11-28

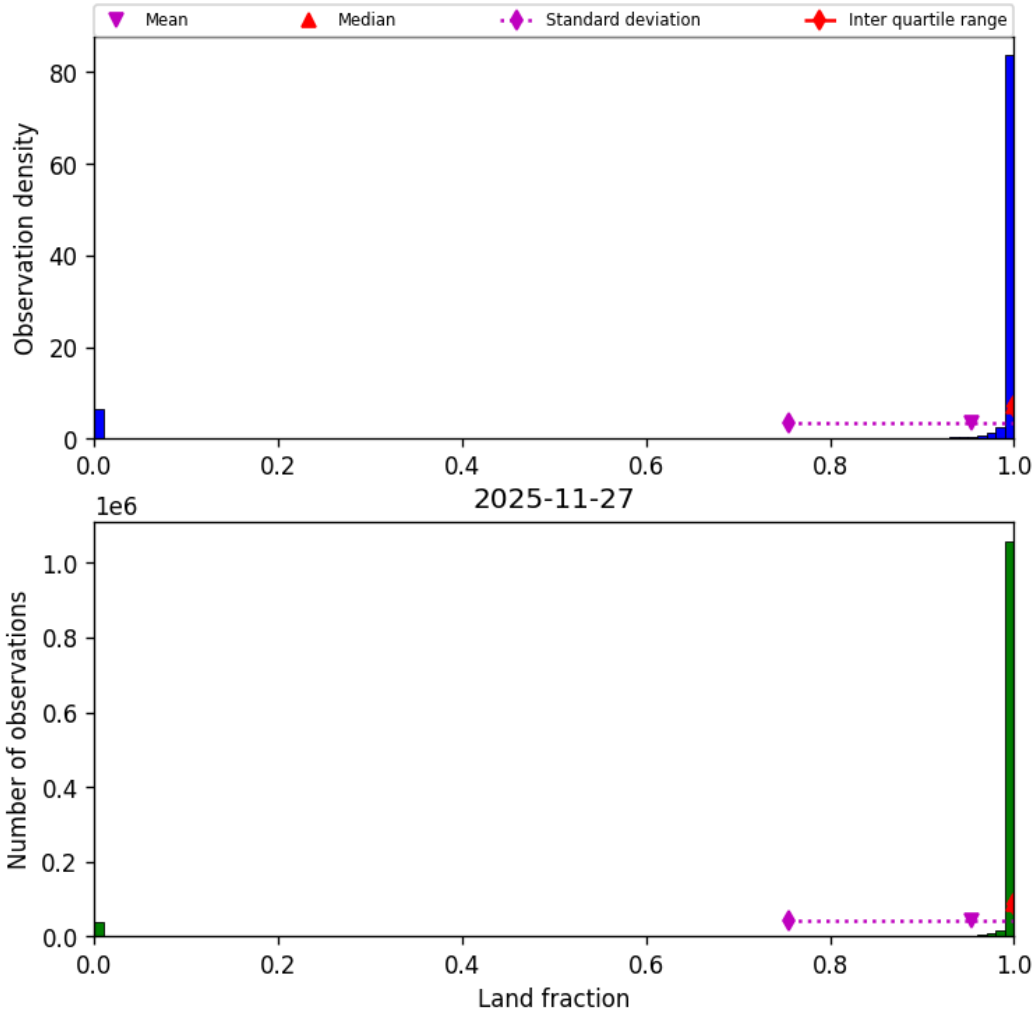

Figure 35: Histogram of “Land fraction” for 2025-11-26 to 2025-11-28

9 Along track statistics

The TROPOMI instrument uses different binned detector rows for different viewing directions. In this section statistics are presented for each of the binned rows in the instrument.

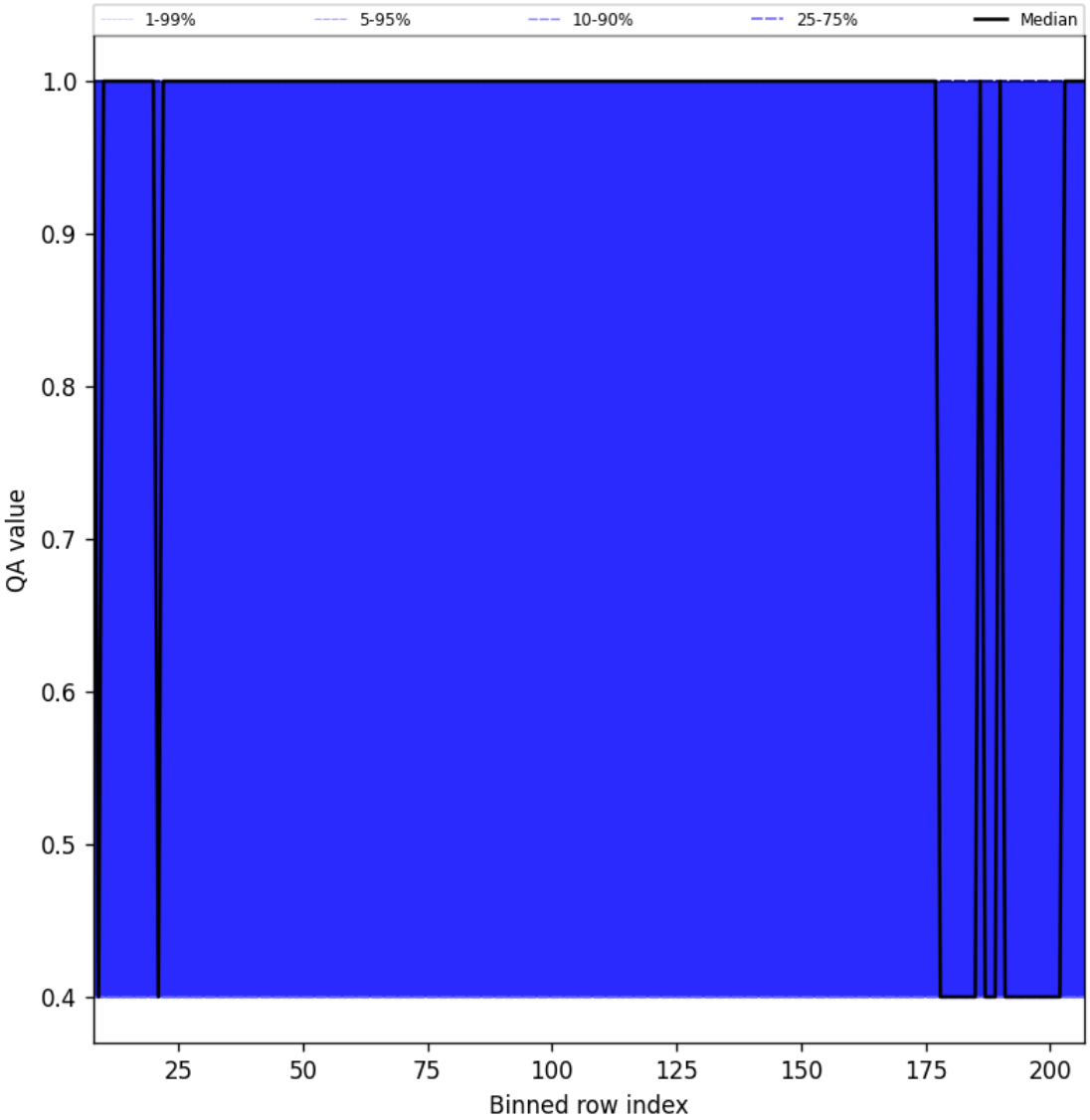

Figure 36: Along track statistics of “QA value” for 2025-11-26 to 2025-11-28

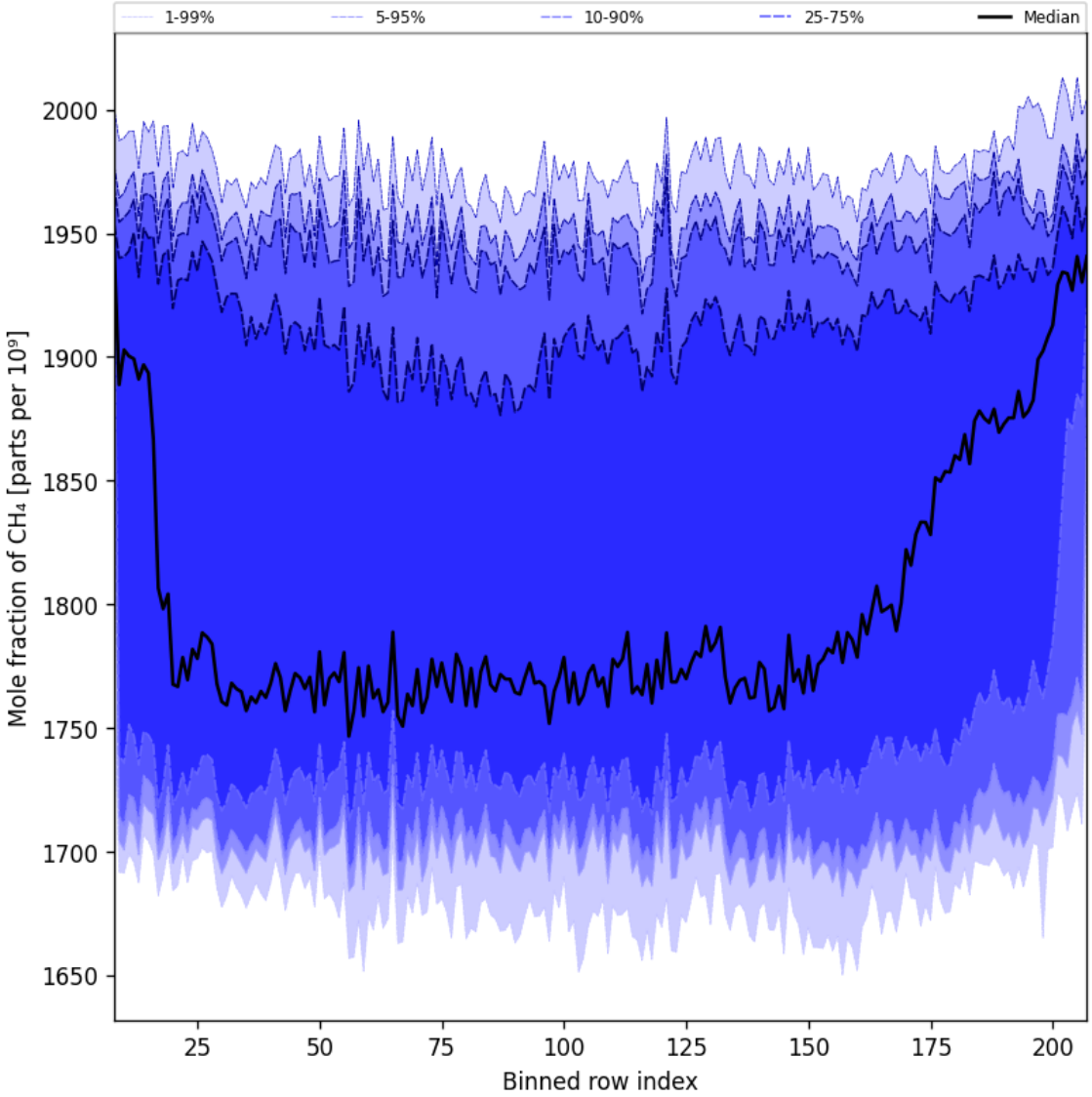

Figure 37: Along track statistics of “Mole fraction of CH_4” for 2025-11-26 to 2025-11-28

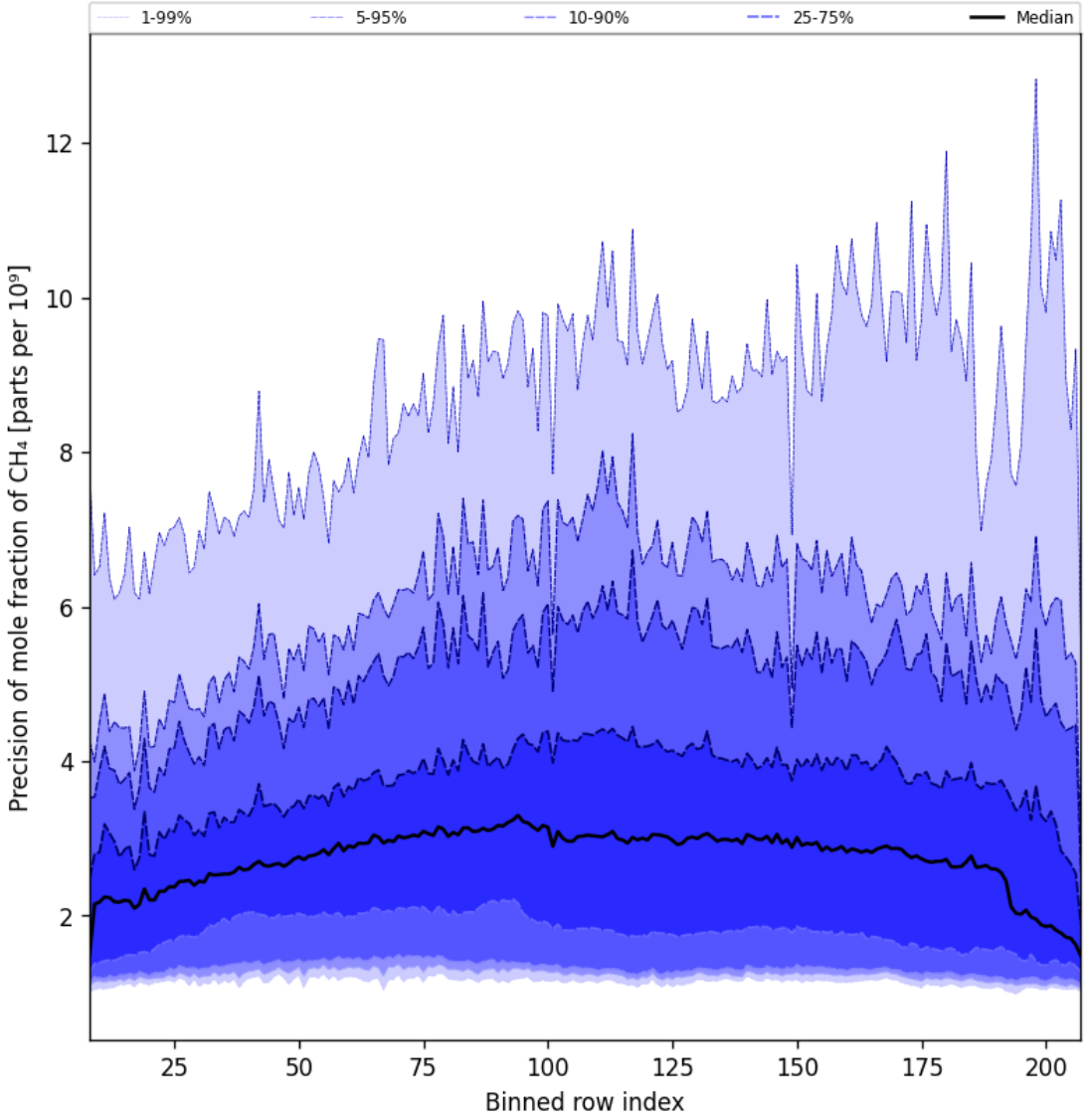

Figure 38: Along track statistics of “Precision of mole fraction of CH_4” for 2025-11-26 to 2025-11-28

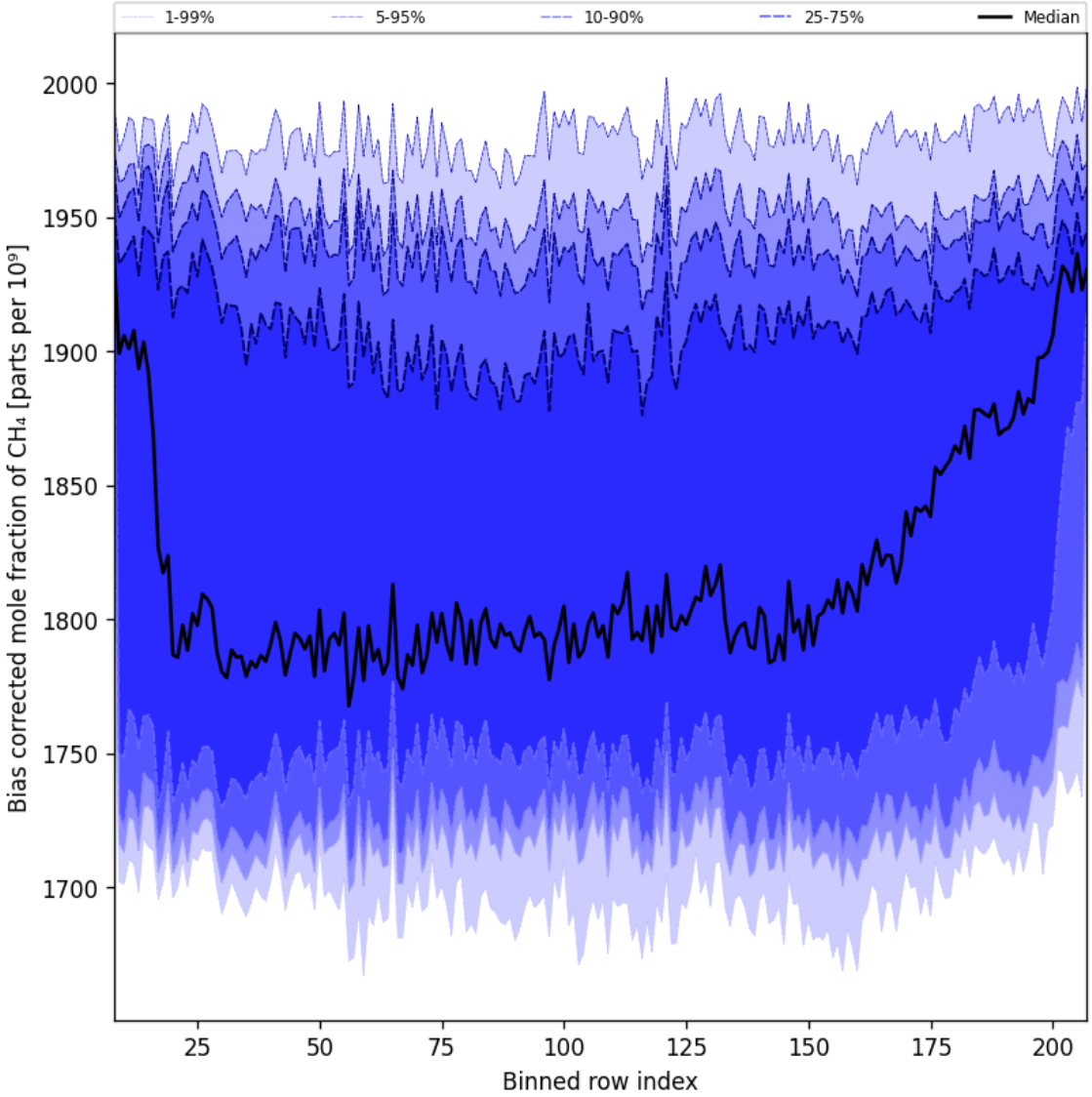

Figure 39: Along track statistics of “Bias corrected mole fraction of CH_4” for 2025-11-26 to 2025-11-28

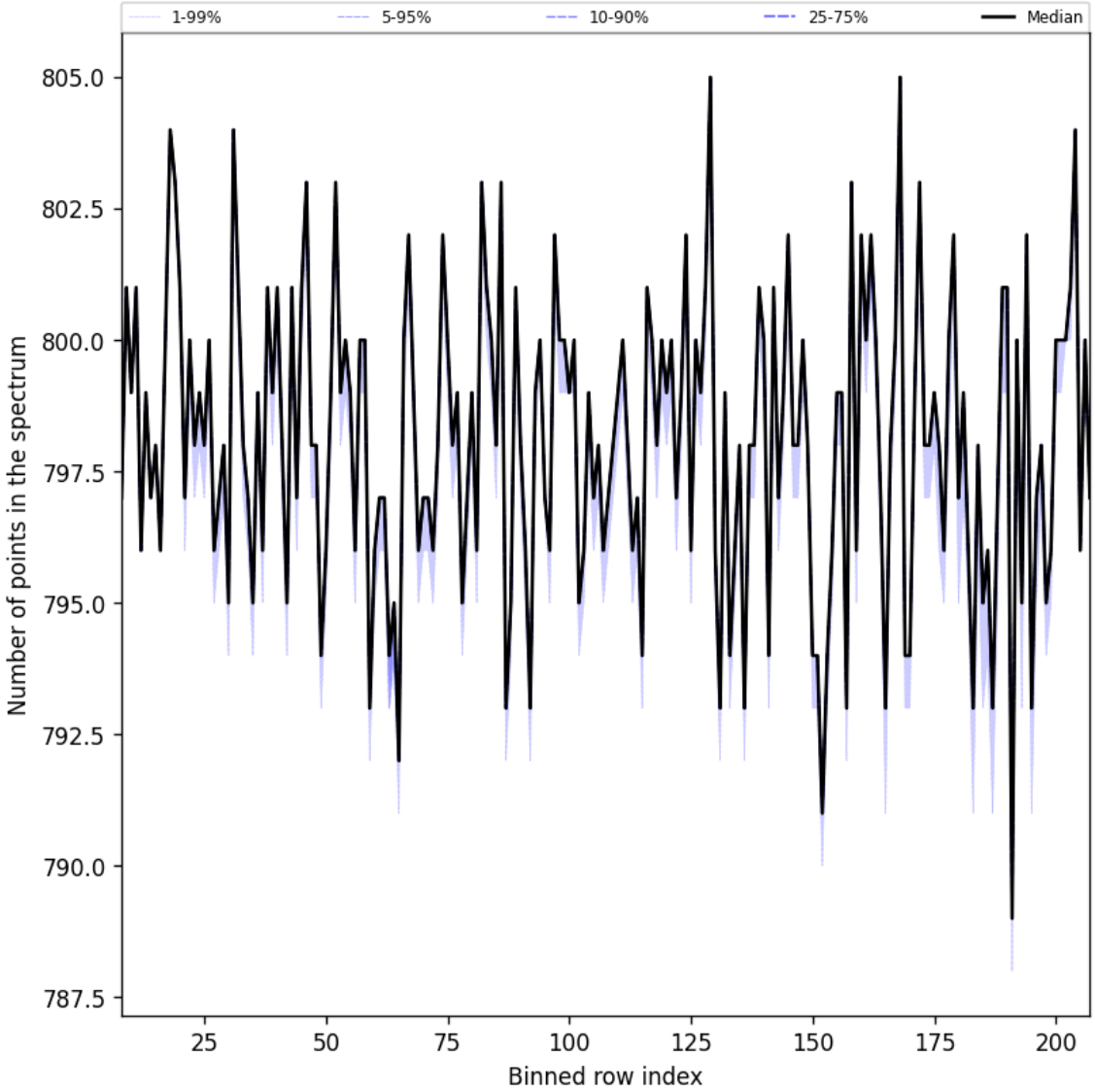

Figure 40: Along track statistics of “Number of points in the spectrum” for 2025-11-26 to 2025-11-28

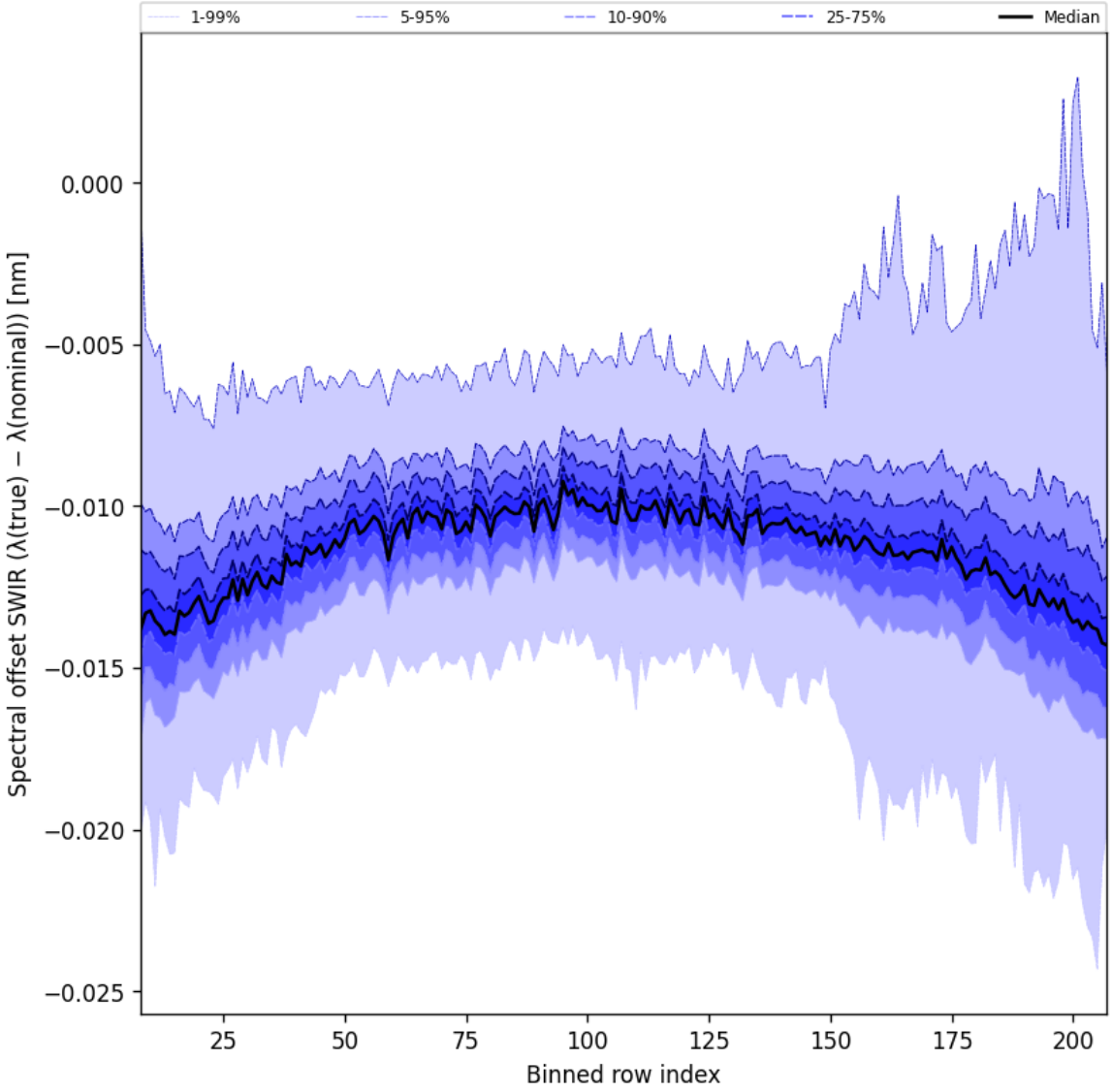

Figure 41: Along track statistics of "Spectral offset SWIR ($\lambda_{\text{true}} - \lambda_{\text{nominal}}$)" for 2025-11-26 to 2025-11-28

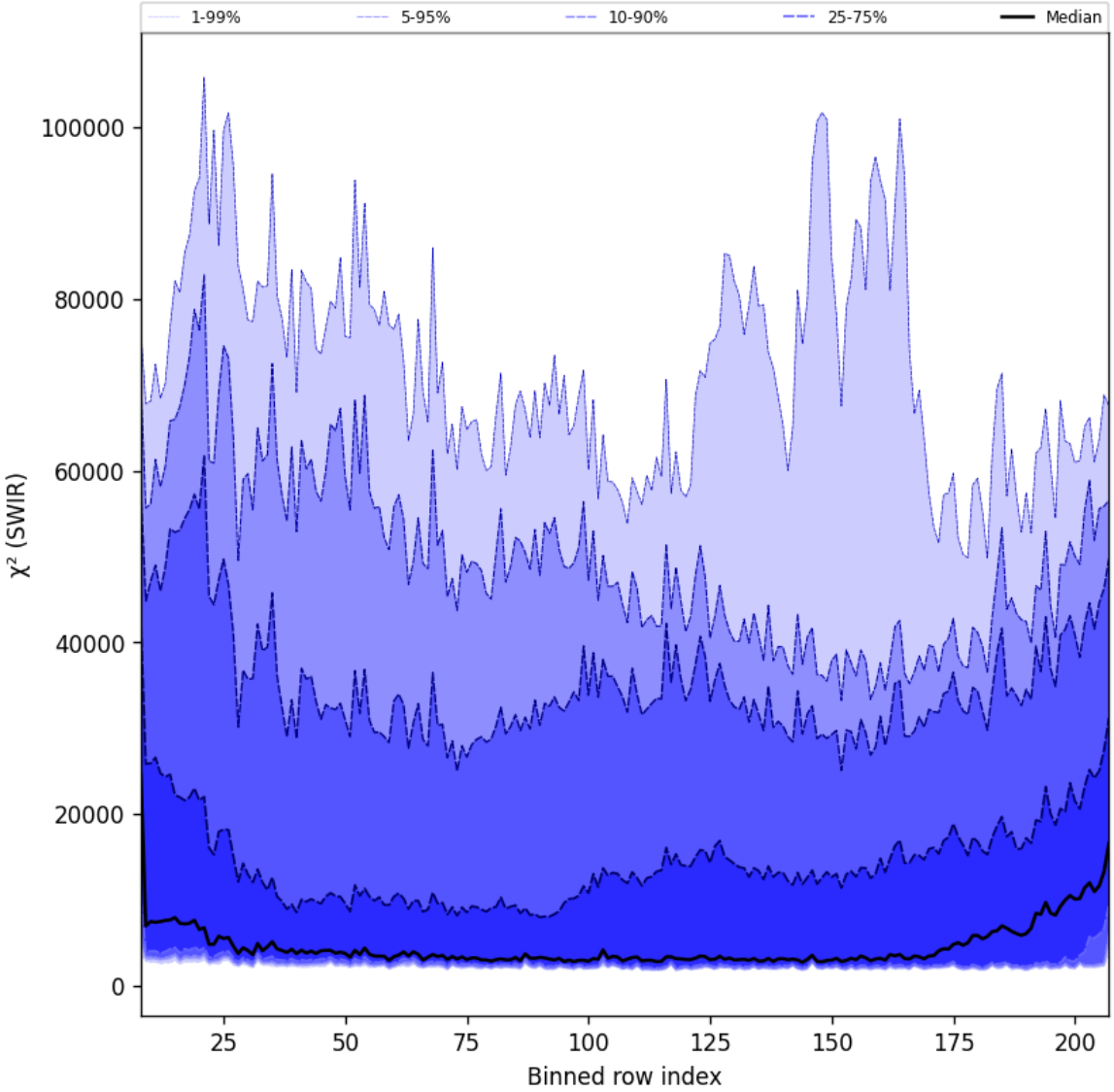

Figure 42: Along track statistics of "χ^2 (SWIR)" for 2025-11-26 to 2025-11-28

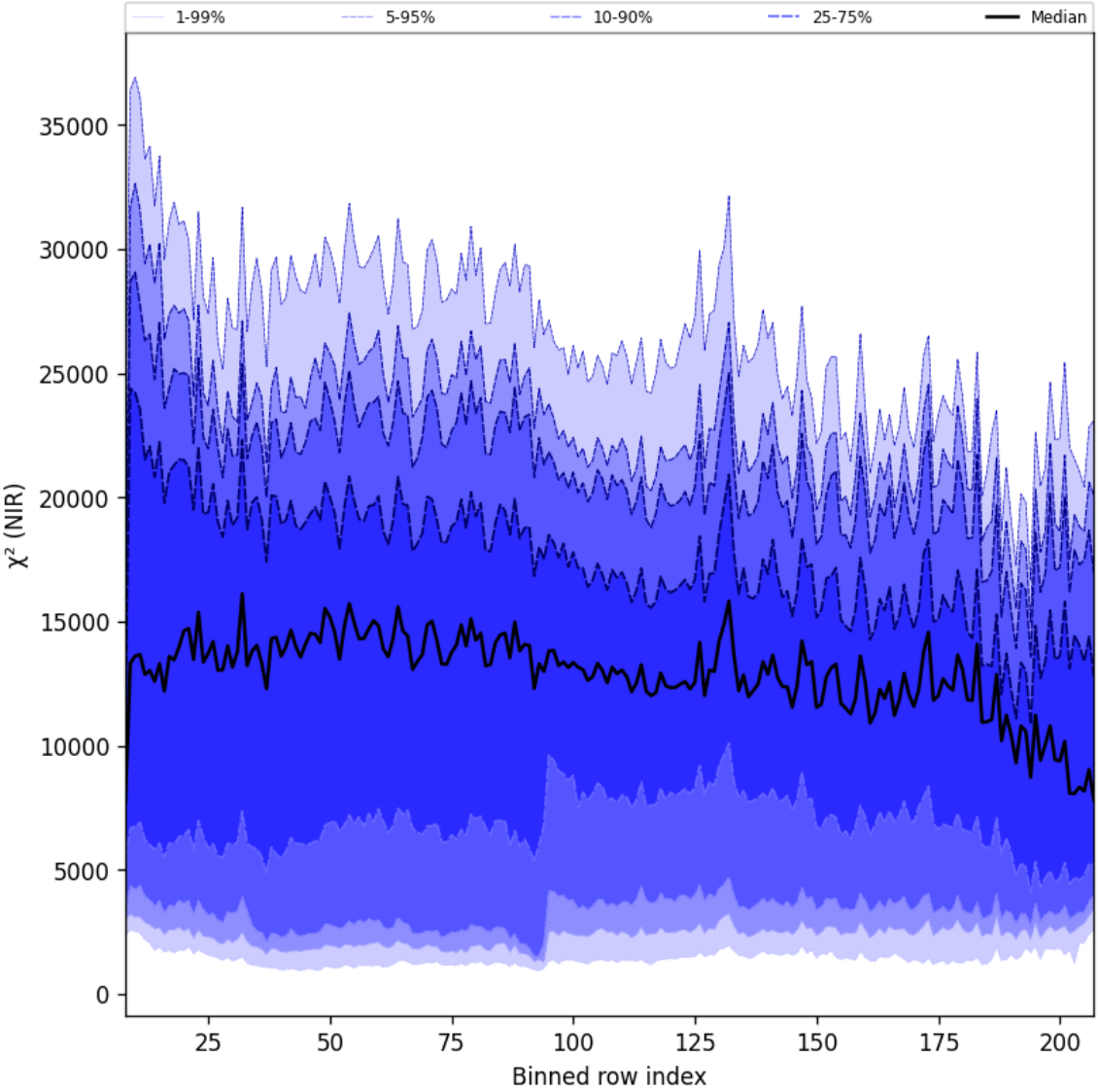

Figure 43: Along track statistics of "χ^2 (NIR)" for 2025-11-26 to 2025-11-28

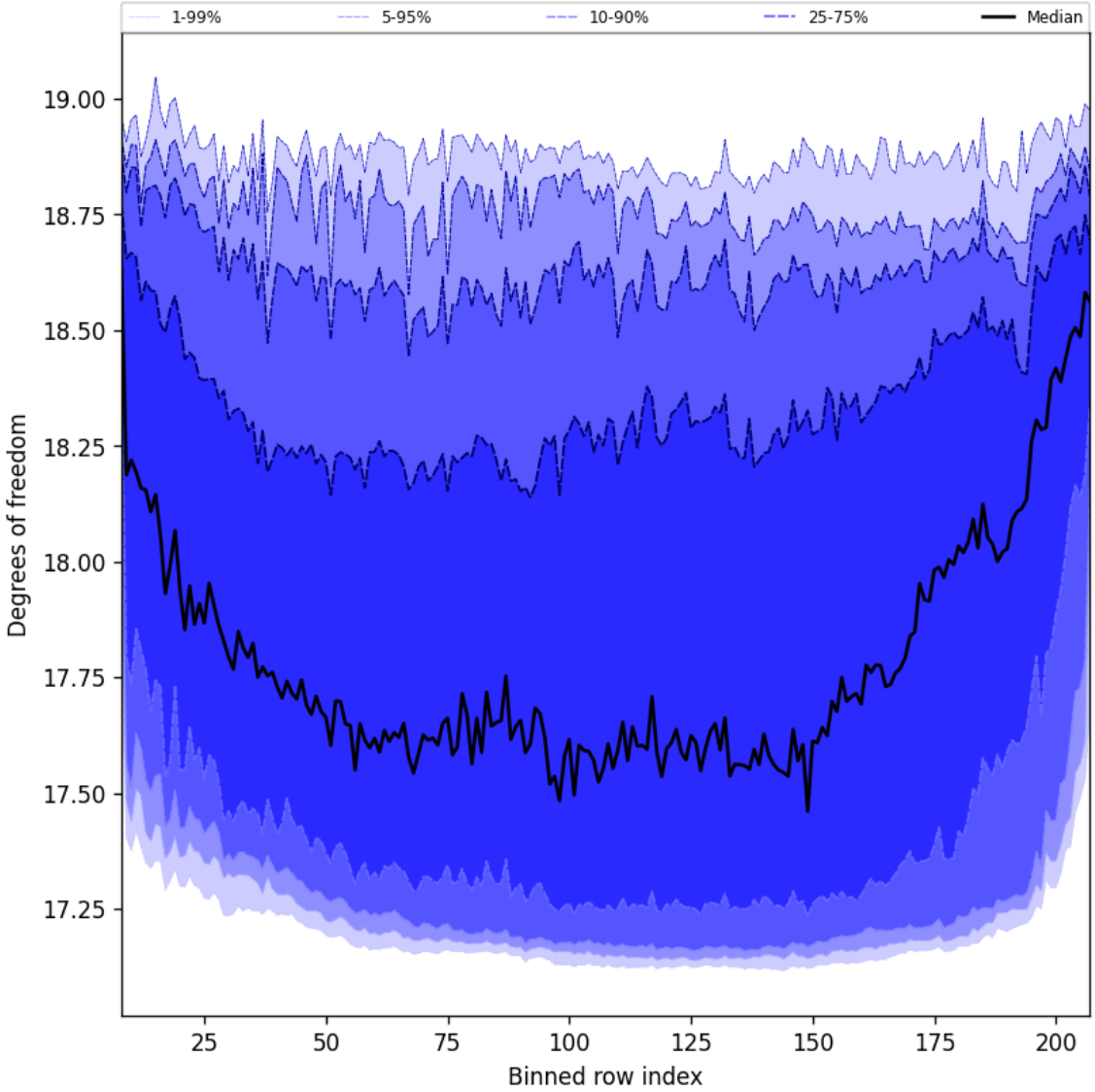

Figure 44: Along track statistics of “Degrees of freedom” for 2025-11-26 to 2025-11-28

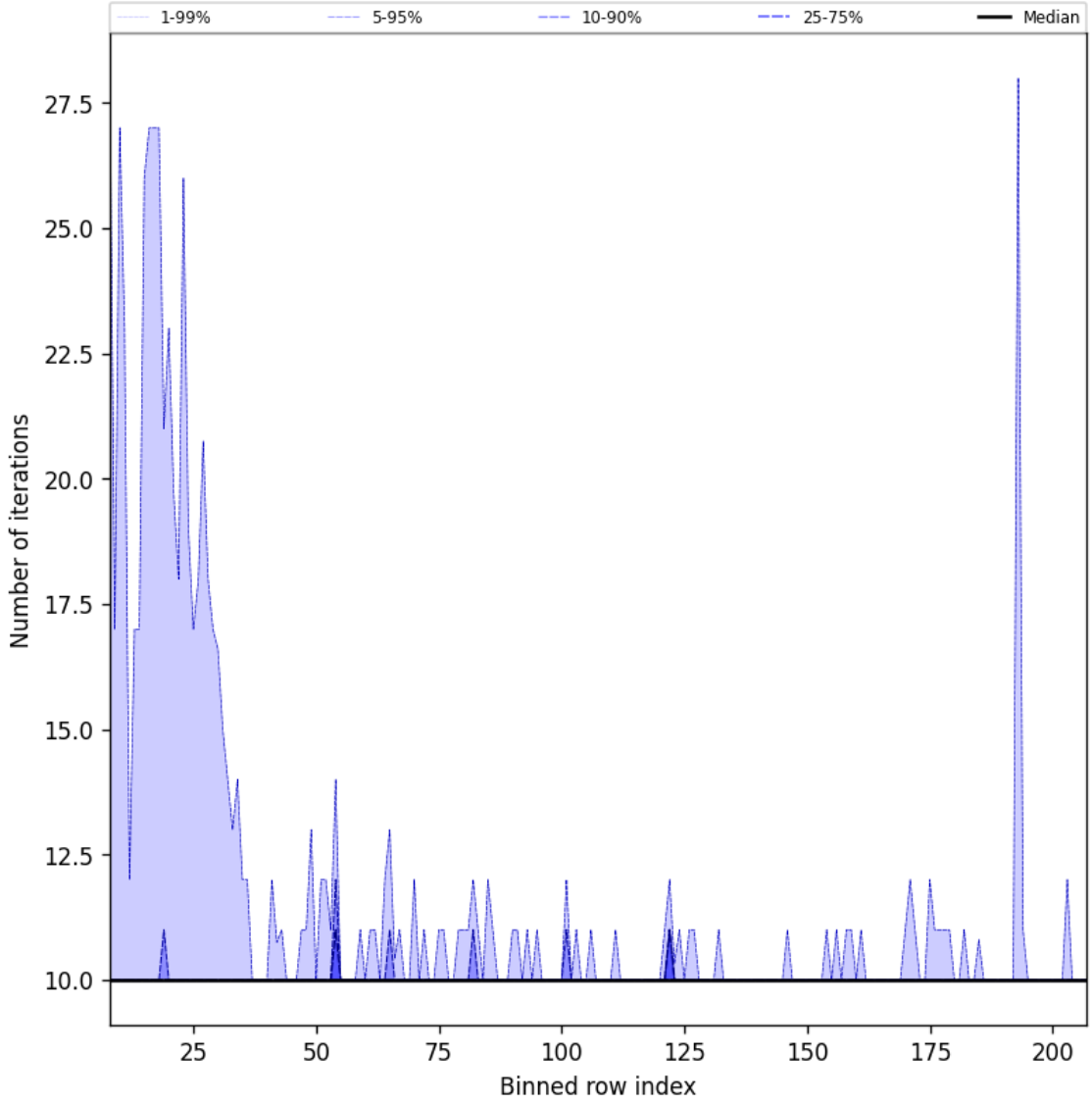

Figure 45: Along track statistics of “Number of iterations” for 2025-11-26 to 2025-11-28

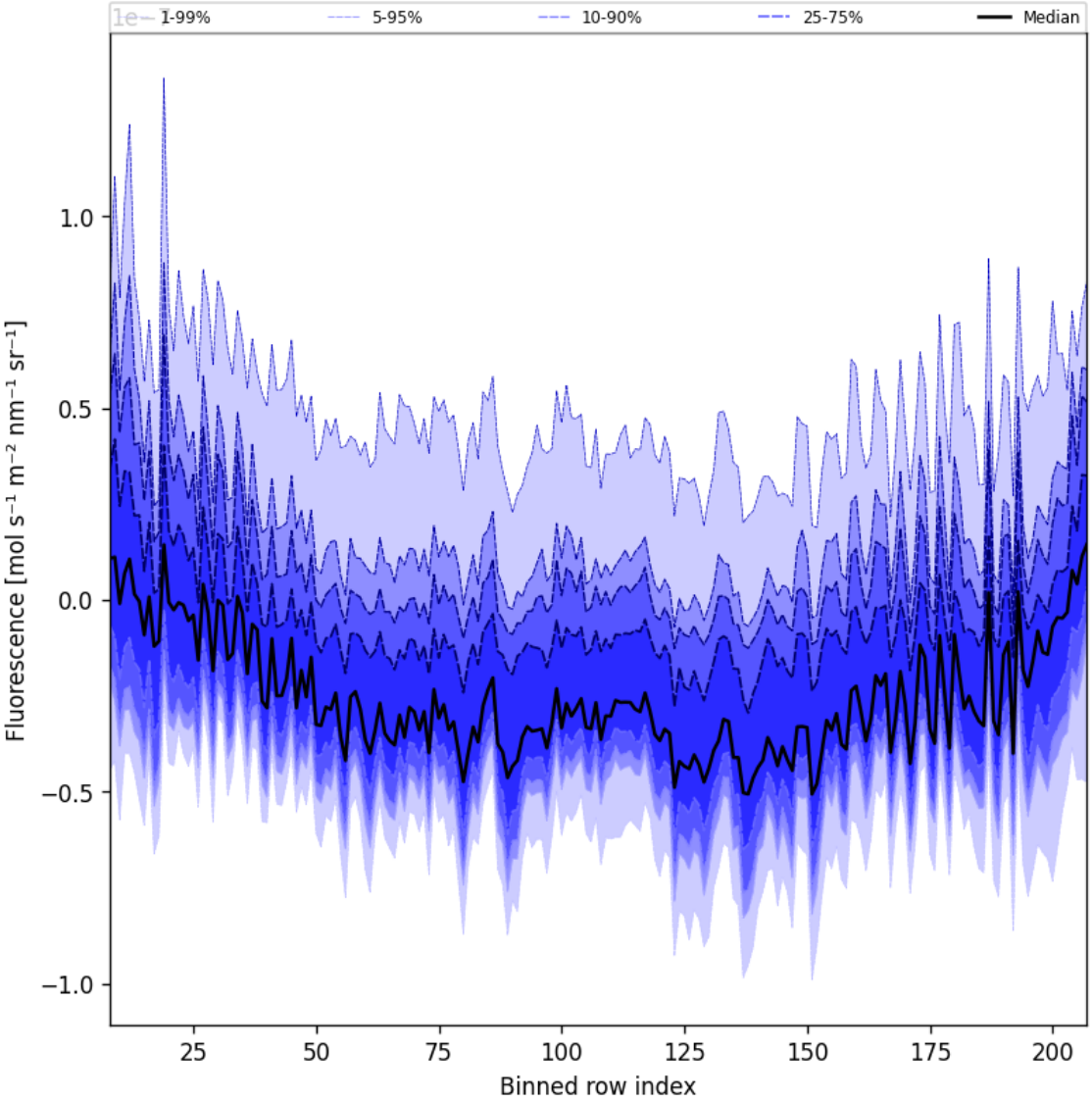

Figure 46: Along track statistics of “Fluorescence” for 2025-11-26 to 2025-11-28

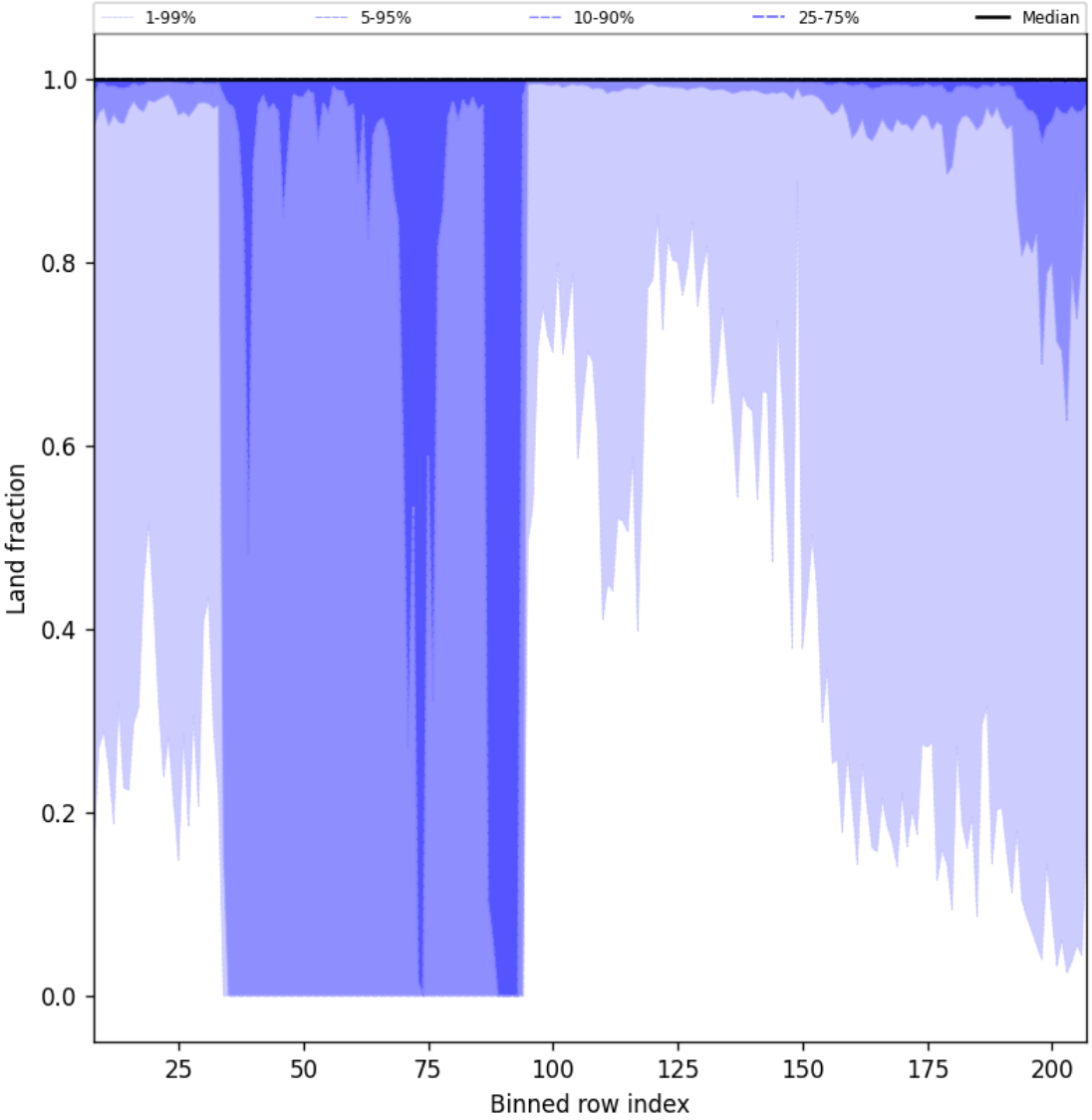

Figure 47: Along track statistics of “Land fraction” for 2025-11-26 to 2025-11-28

10 Coincidence density

To investigate the relation between parameters scatter density plots are produced. These include some 'hidden' parameters, latitude and the solar- and viewing geometries, in addition to all configured parameters. All combinations of pairs of parameters are included *once*, in one direction alone.

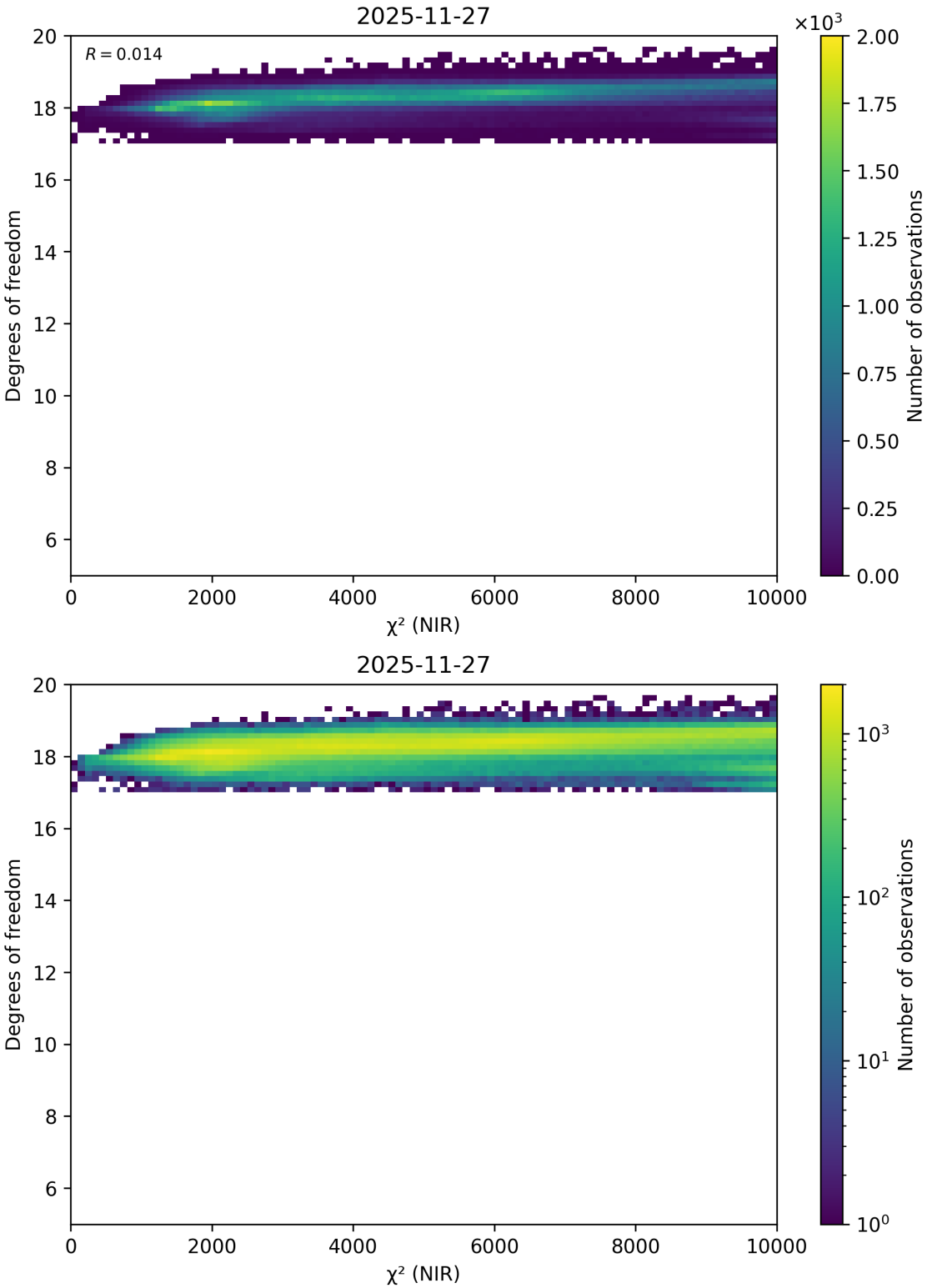

Figure 48: Scatter density plot of "χ^2 (NIR)" against "Degrees of freedom" for 2025-11-26 to 2025-11-28.

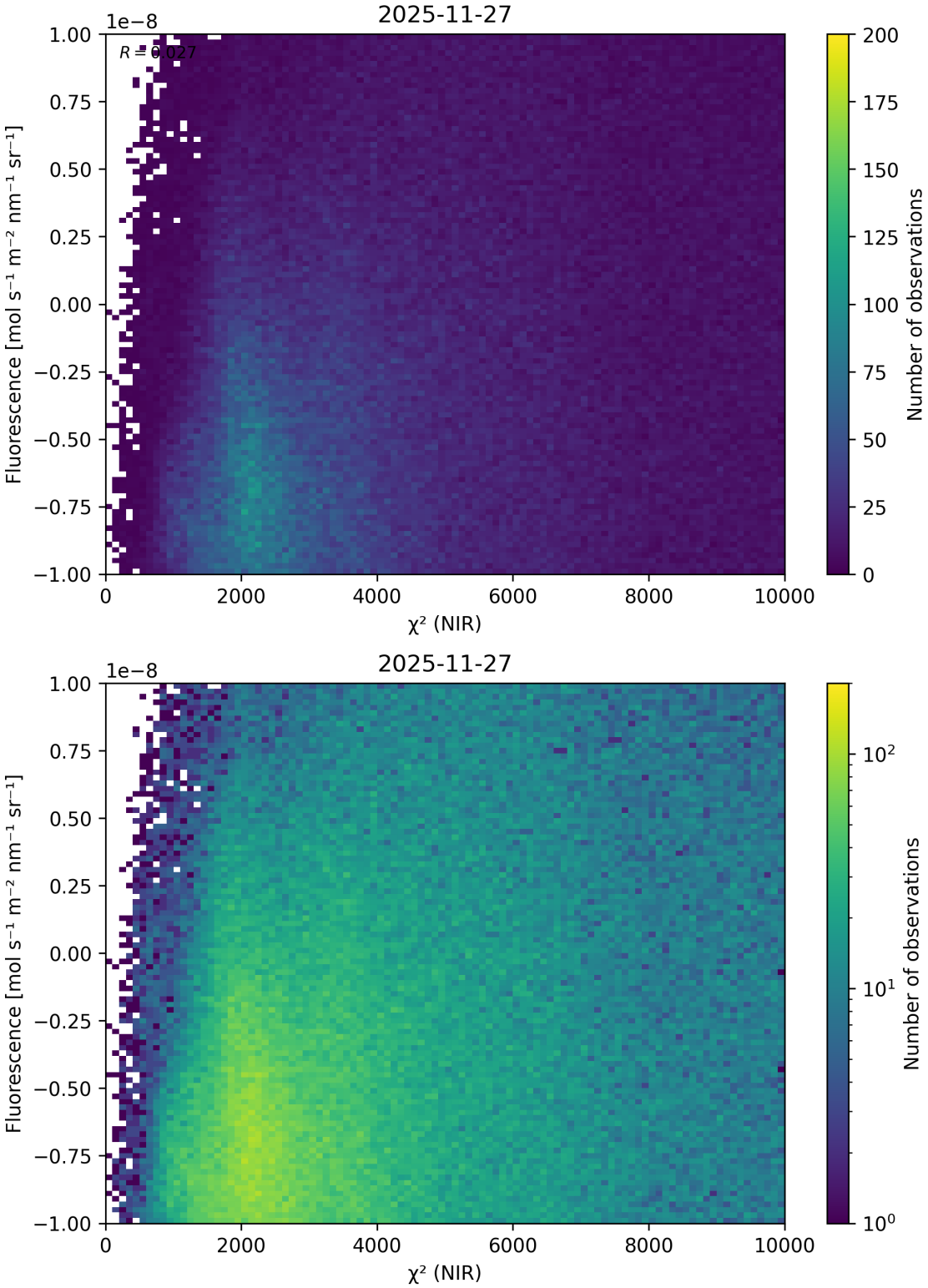

Figure 49: Scatter density plot of "χ^2 (NIR)" against "Fluorescence" for 2025-11-26 to 2025-11-28.

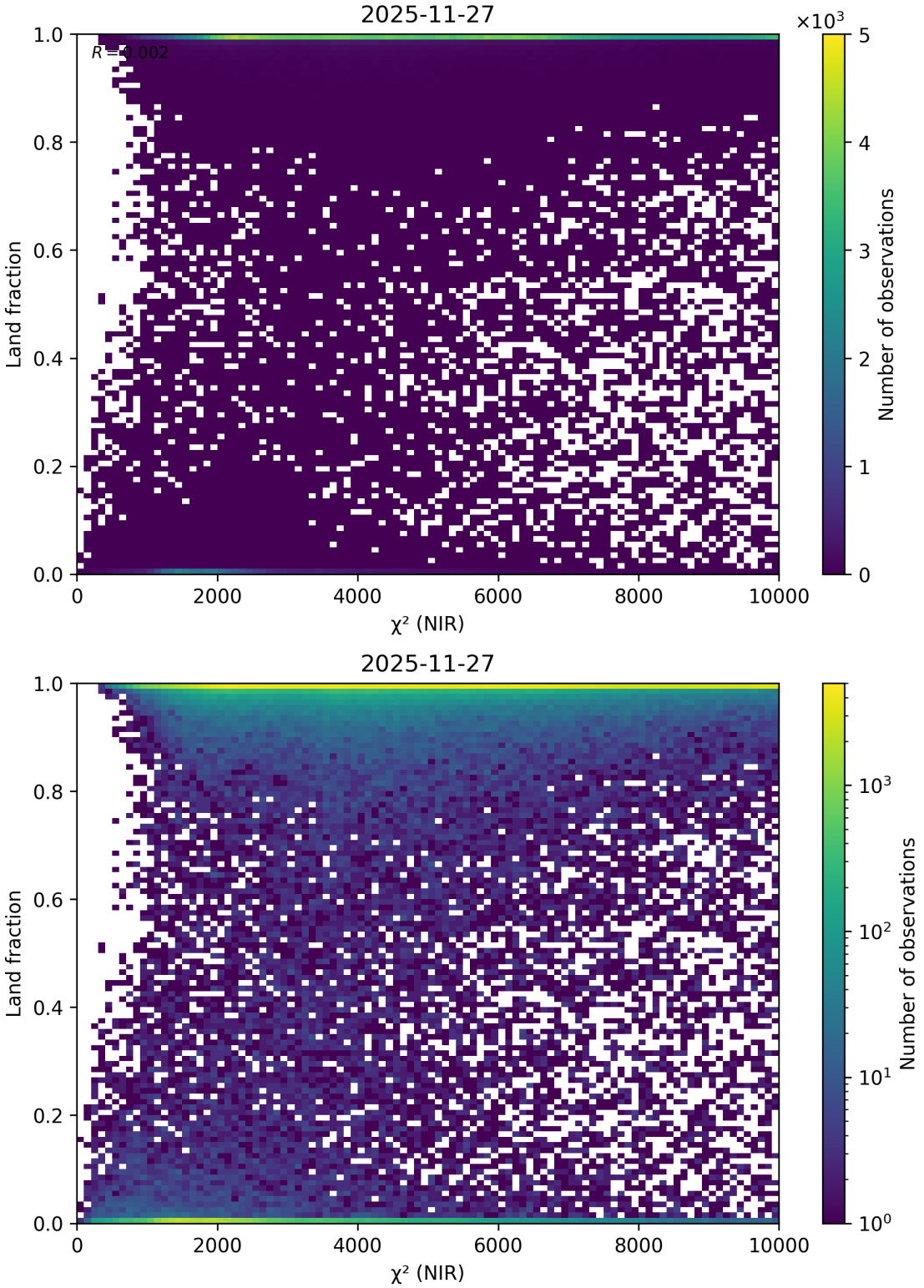

Figure 50: Scatter density plot of "χ^2 (NIR)" against "Land fraction" for 2025-11-26 to 2025-11-28.

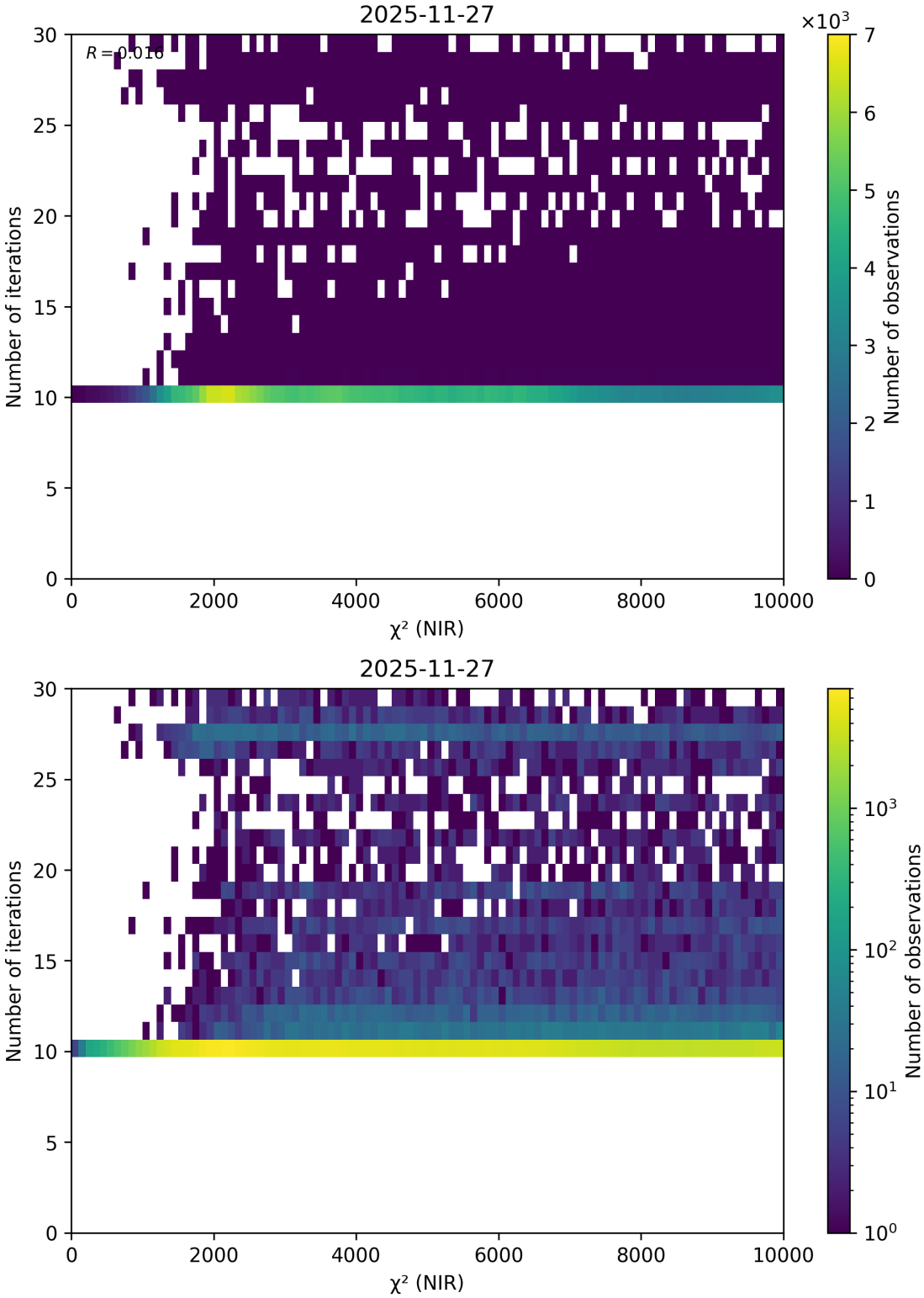

Figure 51: Scatter density plot of "χ^2 (NIR)" against "Number of iterations" for 2025-11-26 to 2025-11-28.

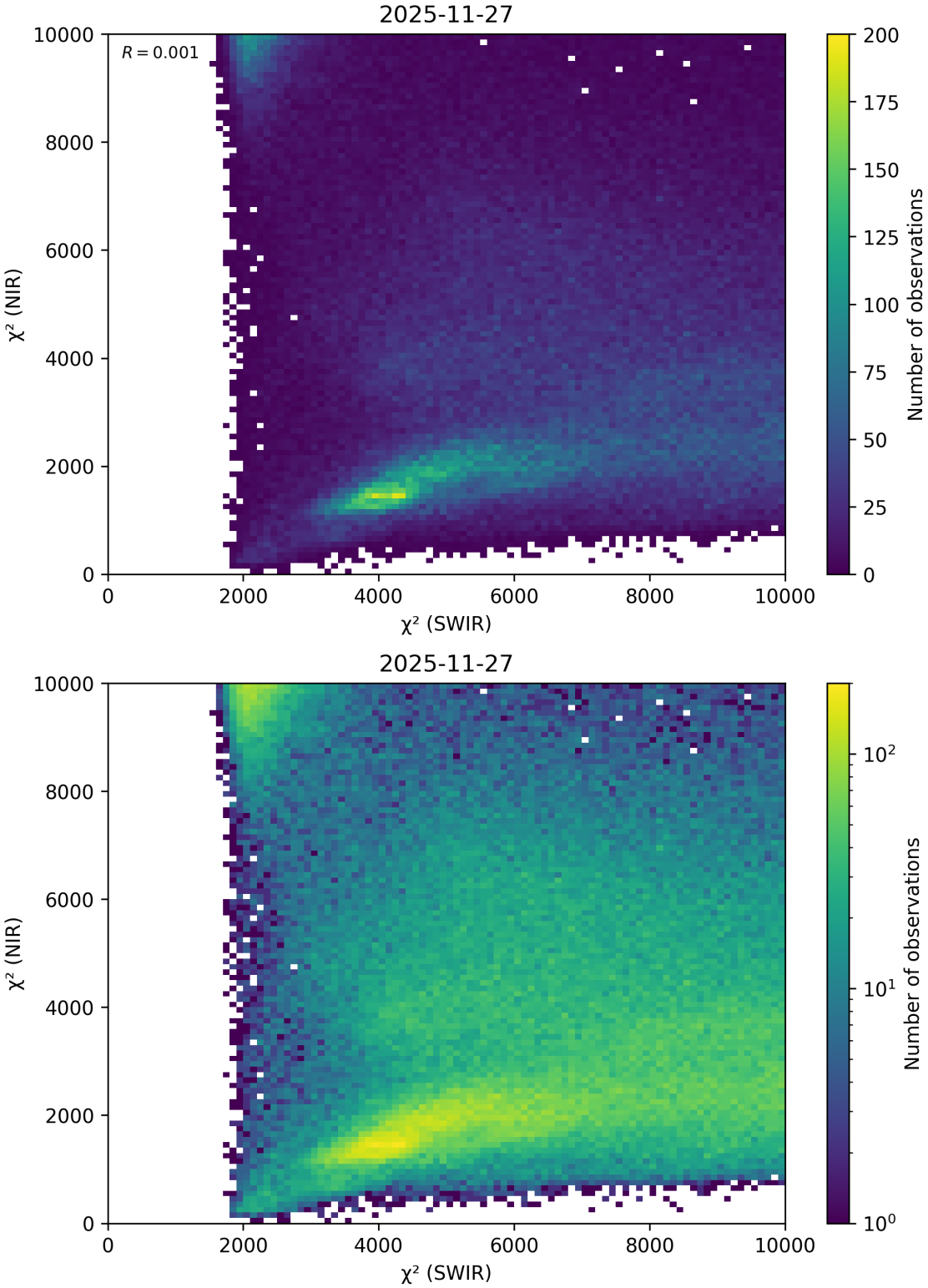

Figure 52: Scatter density plot of "χ^2 (SWIR)" against "χ^2 (NIR)" for 2025-11-26 to 2025-11-28.

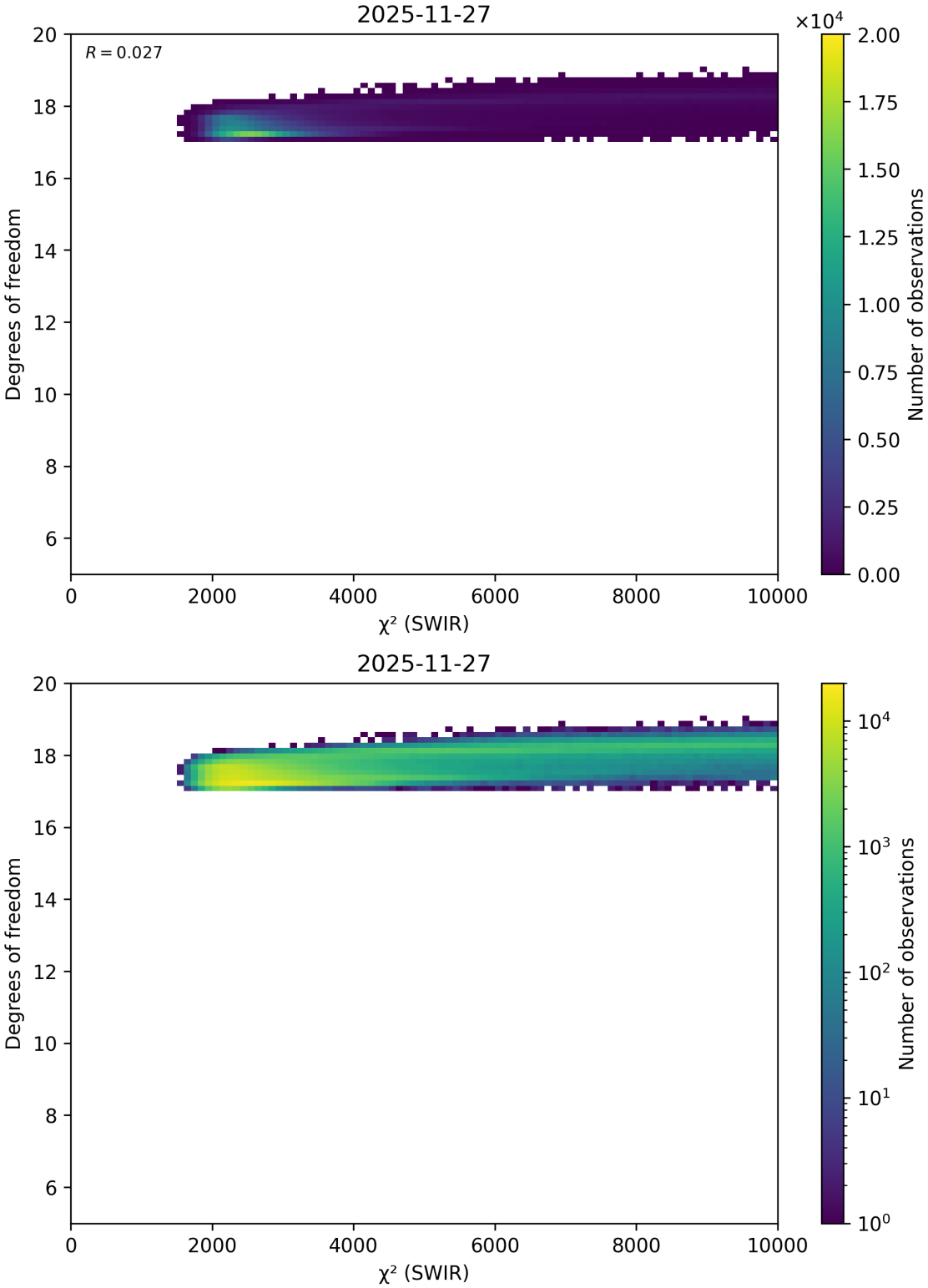

Figure 53: Scatter density plot of "χ^2 (SWIR)" against "Degrees of freedom" for 2025-11-26 to 2025-11-28.

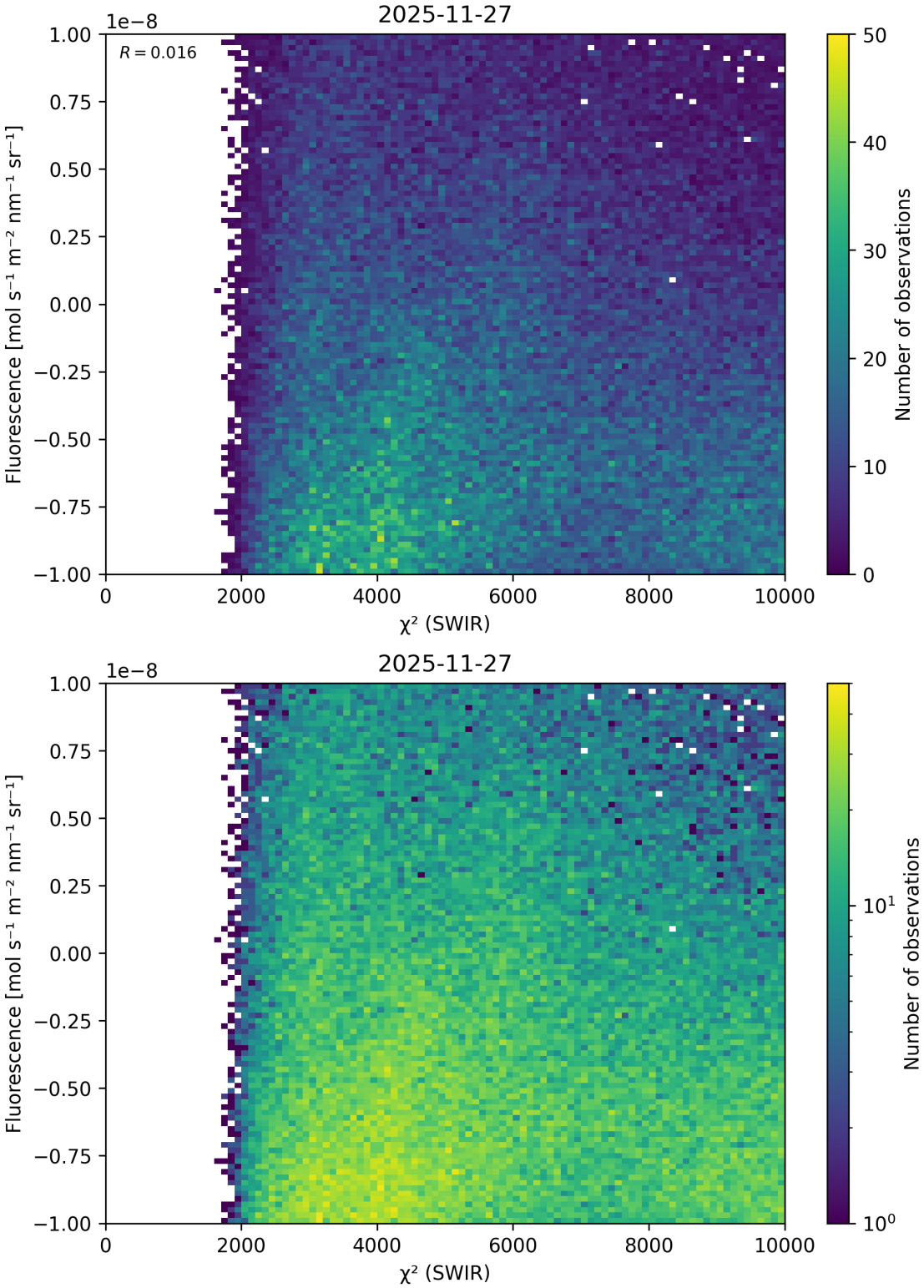

Figure 54: Scatter density plot of "χ^2 (SWIR)" against "Fluorescence" for 2025-11-26 to 2025-11-28.

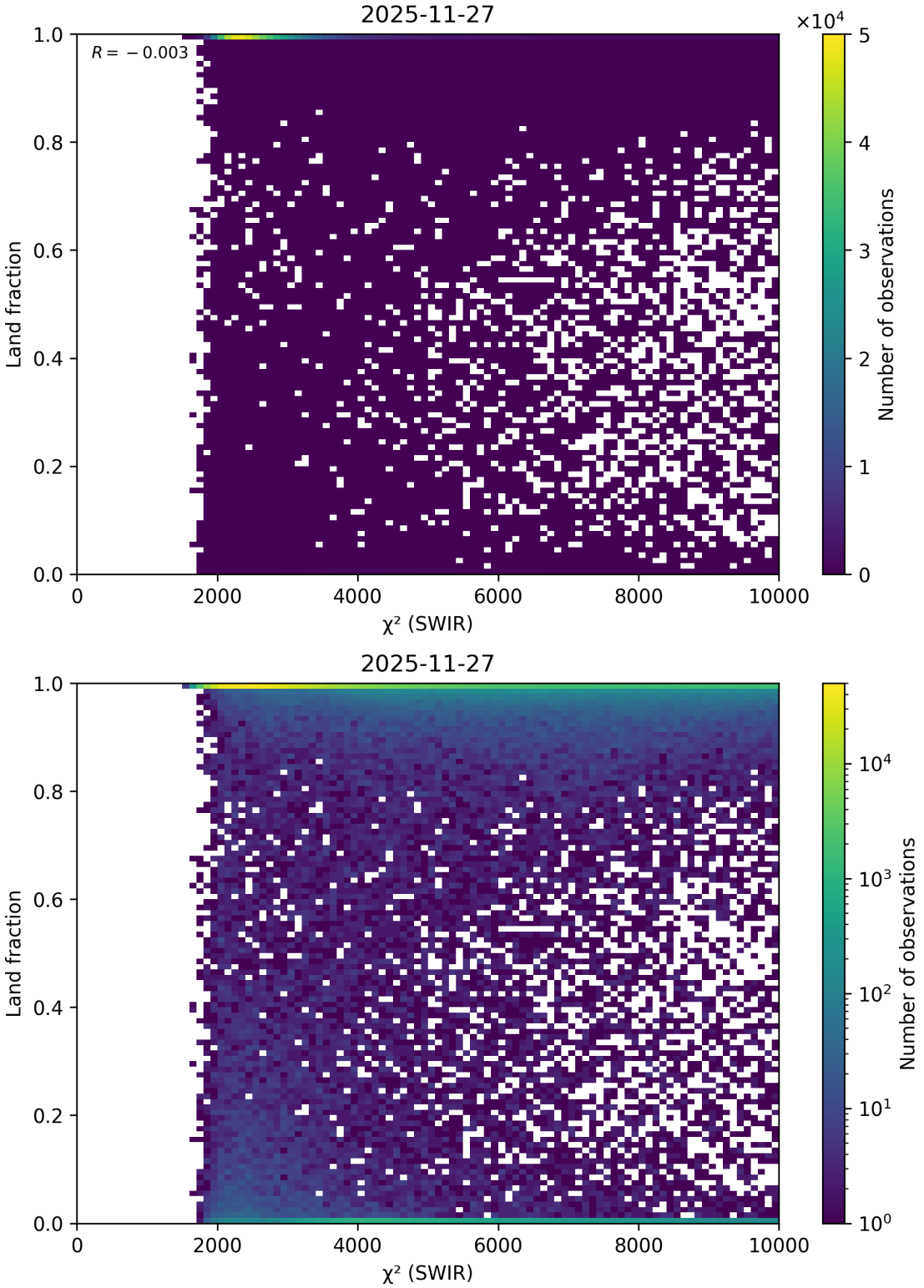

Figure 55: Scatter density plot of "χ^2 (SWIR)" against "Land fraction" for 2025-11-26 to 2025-11-28.

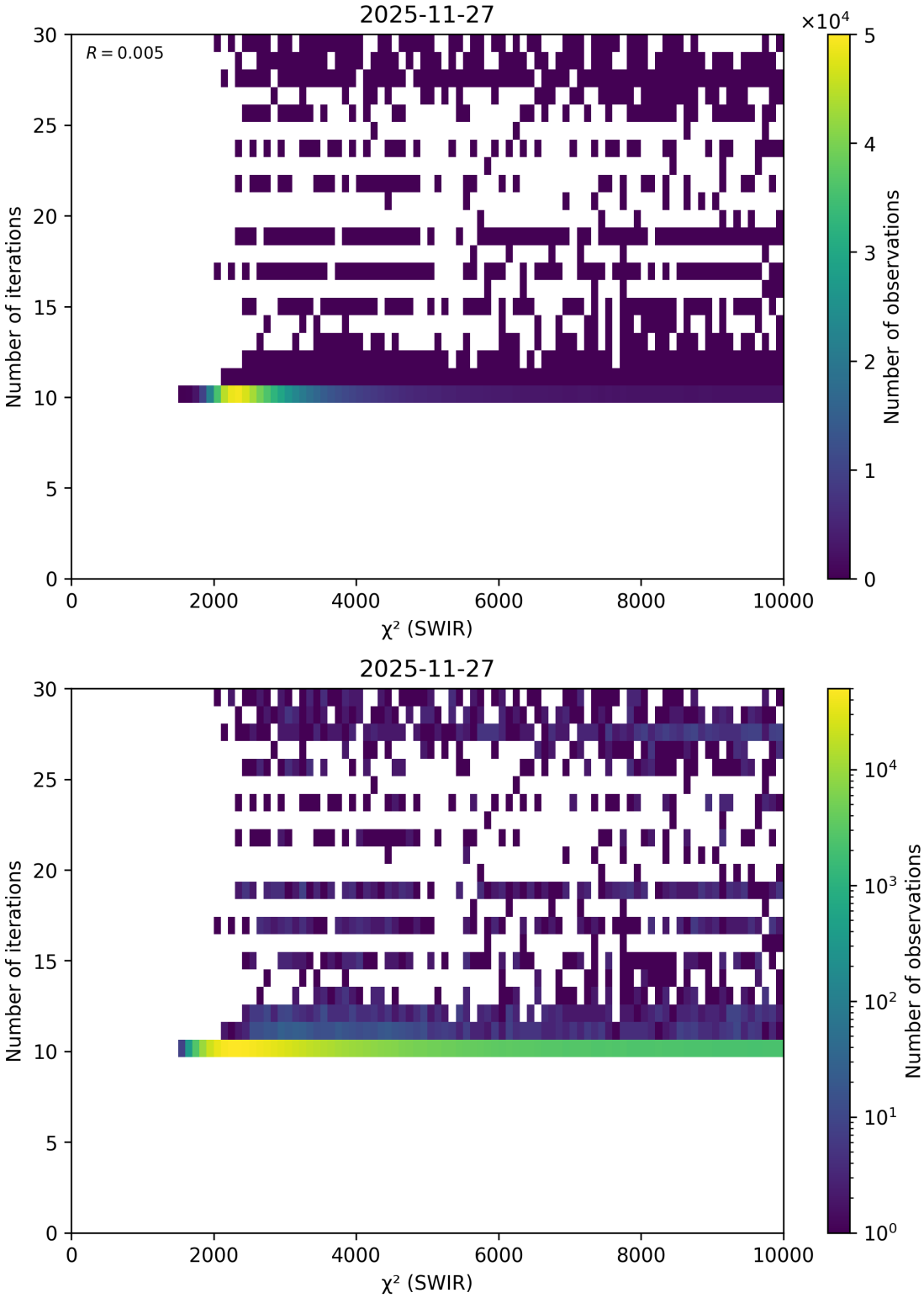

Figure 56: Scatter density plot of "χ^2 (SWIR)" against "Number of iterations" for 2025-11-26 to 2025-11-28.

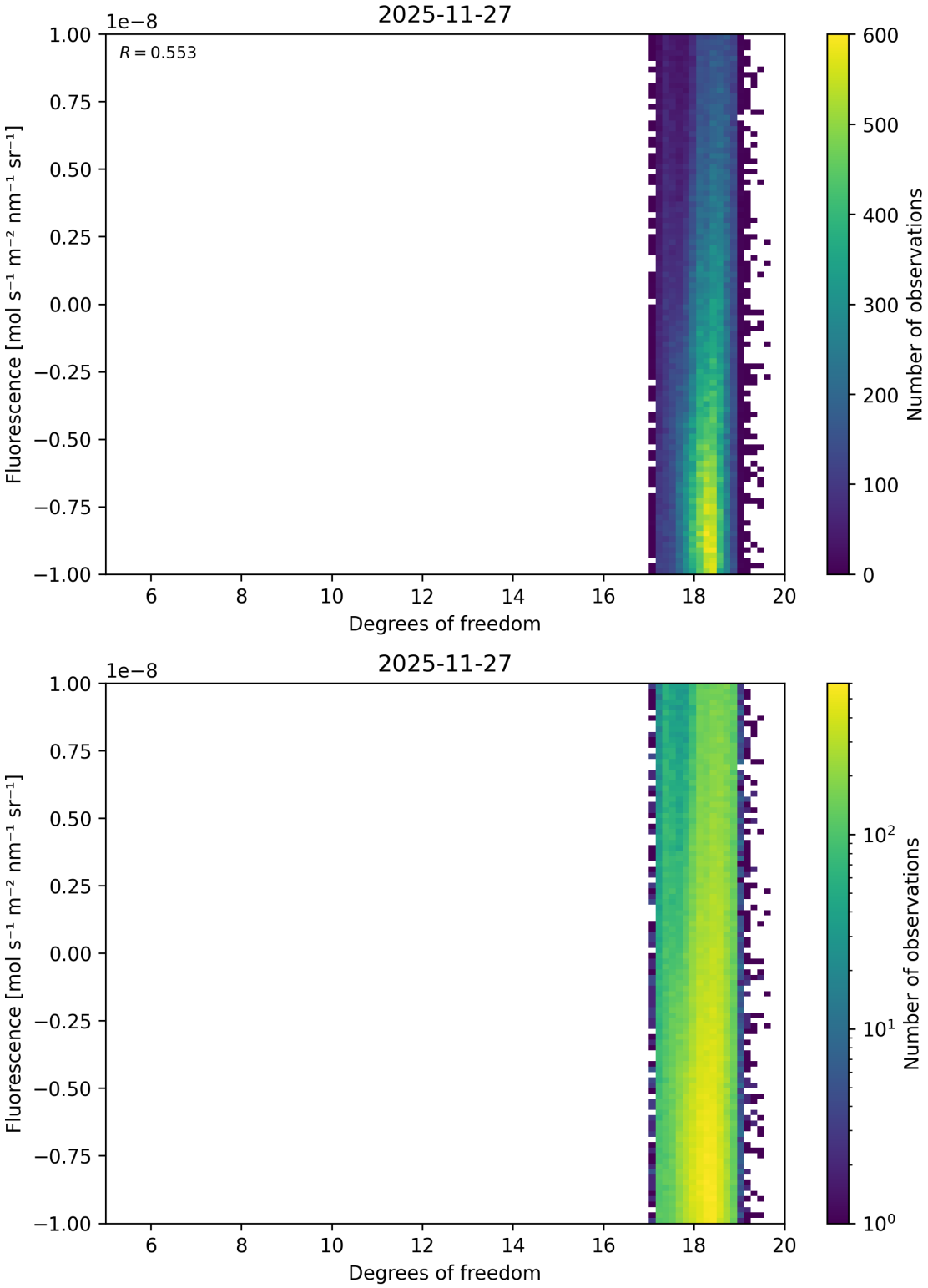

Figure 57: Scatter density plot of “Degrees of freedom” against “Fluorescence” for 2025-11-26 to 2025-11-28.

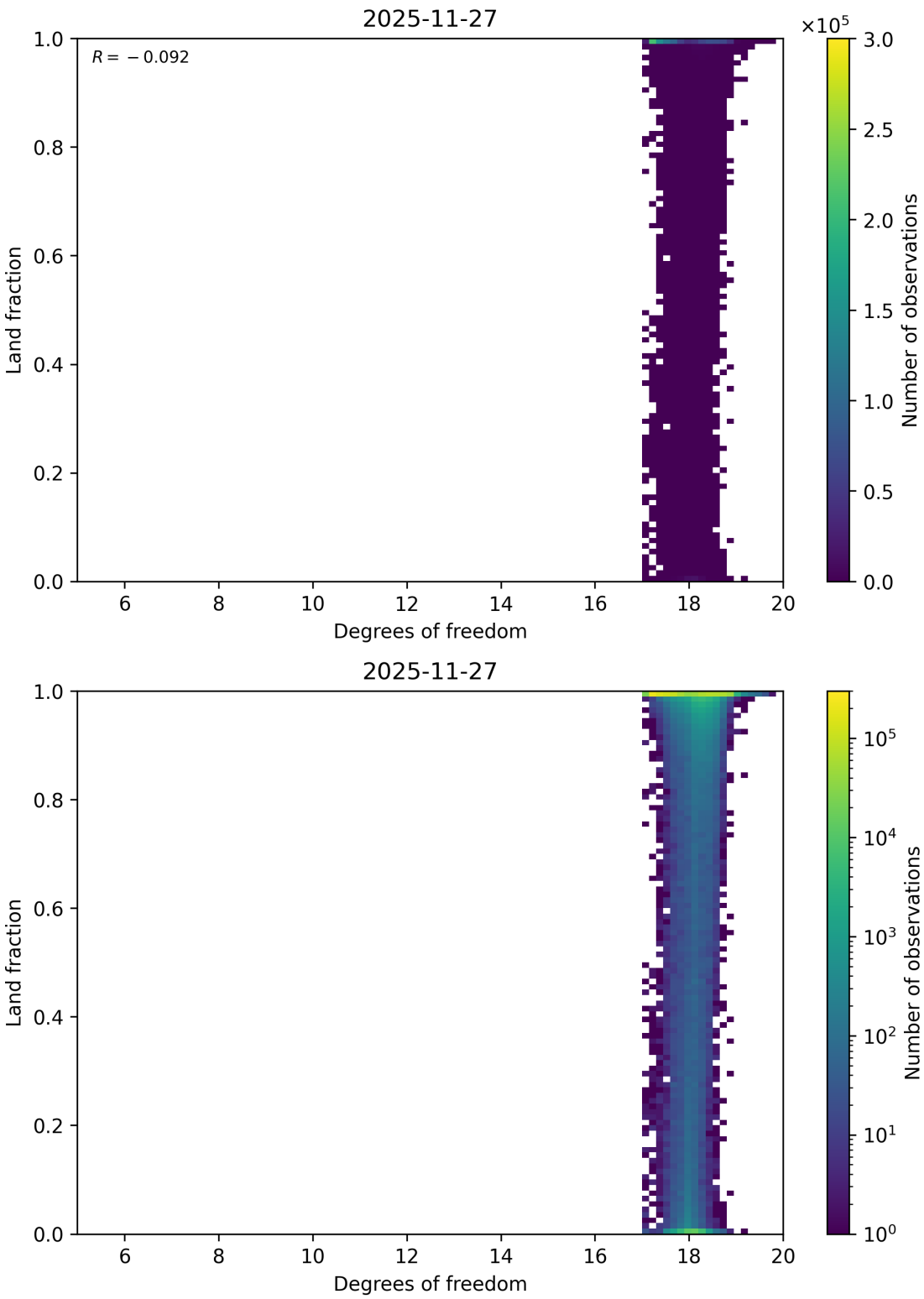

Figure 58: Scatter density plot of “Degrees of freedom” against “Land fraction” for 2025-11-26 to 2025-11-28.

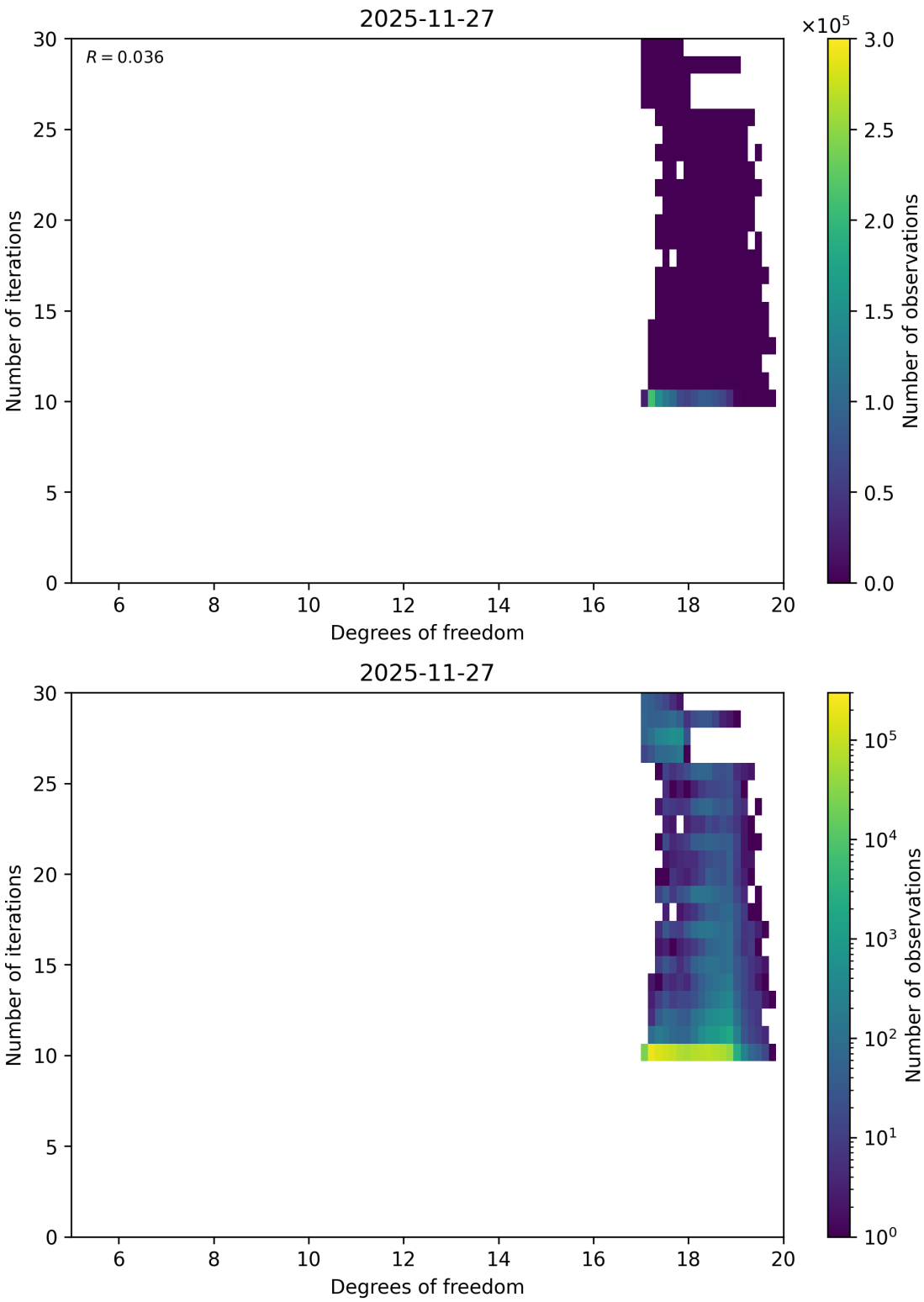

Figure 59: Scatter density plot of “Degrees of freedom” against “Number of iterations” for 2025-11-26 to 2025-11-28.

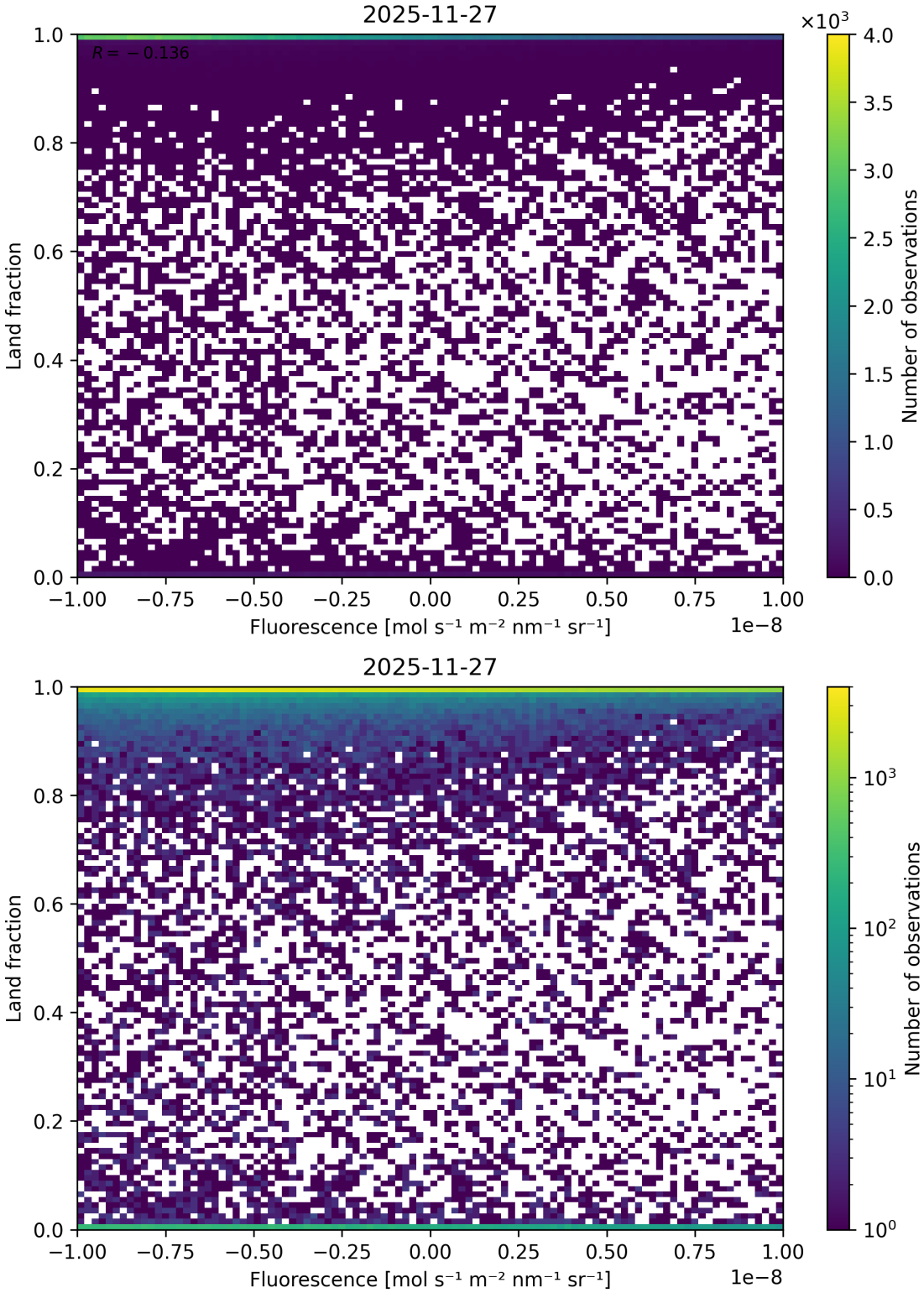

Figure 60: Scatter density plot of “Fluorescence” against “Land fraction” for 2025-11-26 to 2025-11-28.

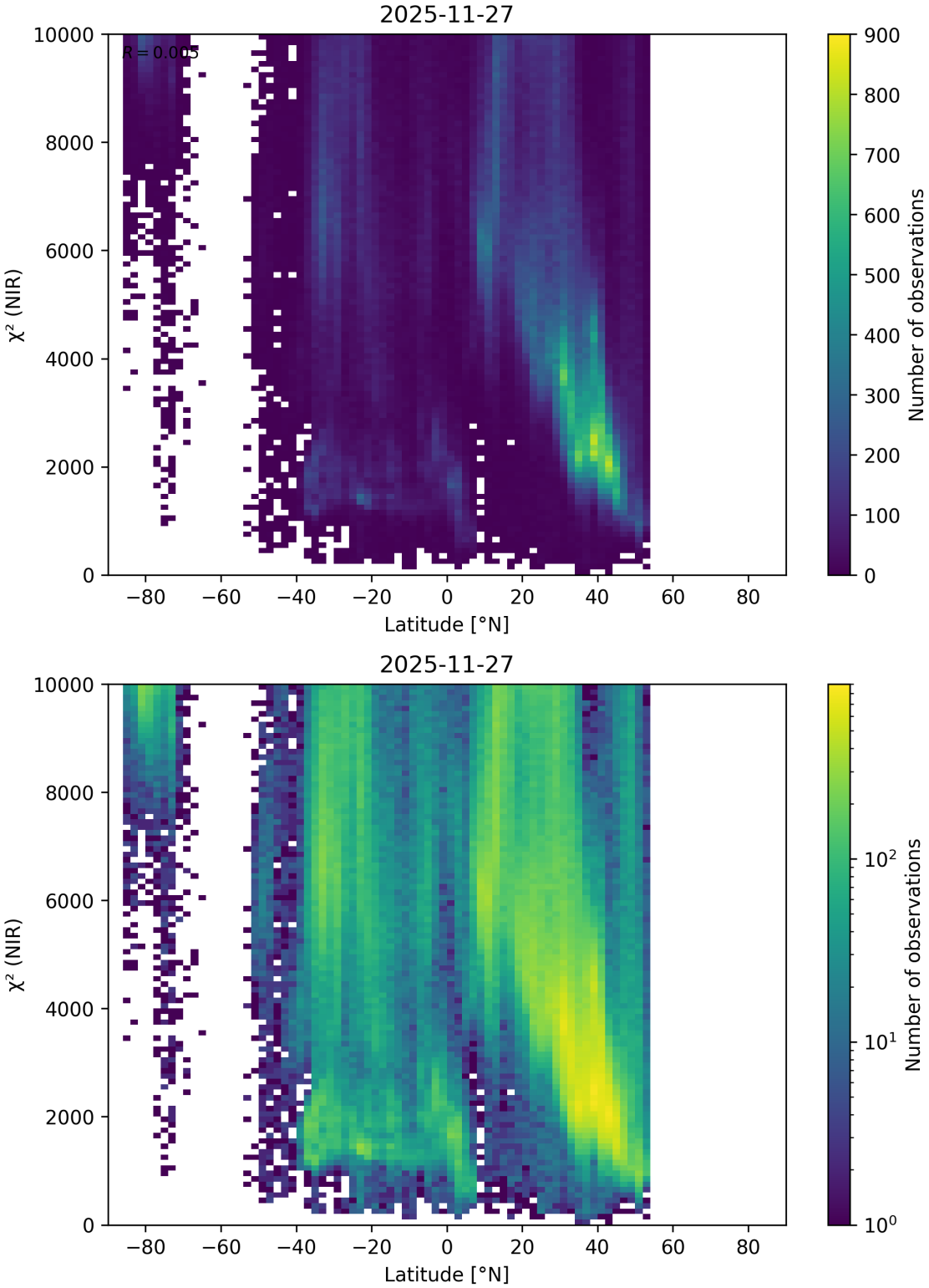

Figure 61: Scatter density plot of “Latitude” against “χ^2 (NIR)” for 2025-11-26 to 2025-11-28.

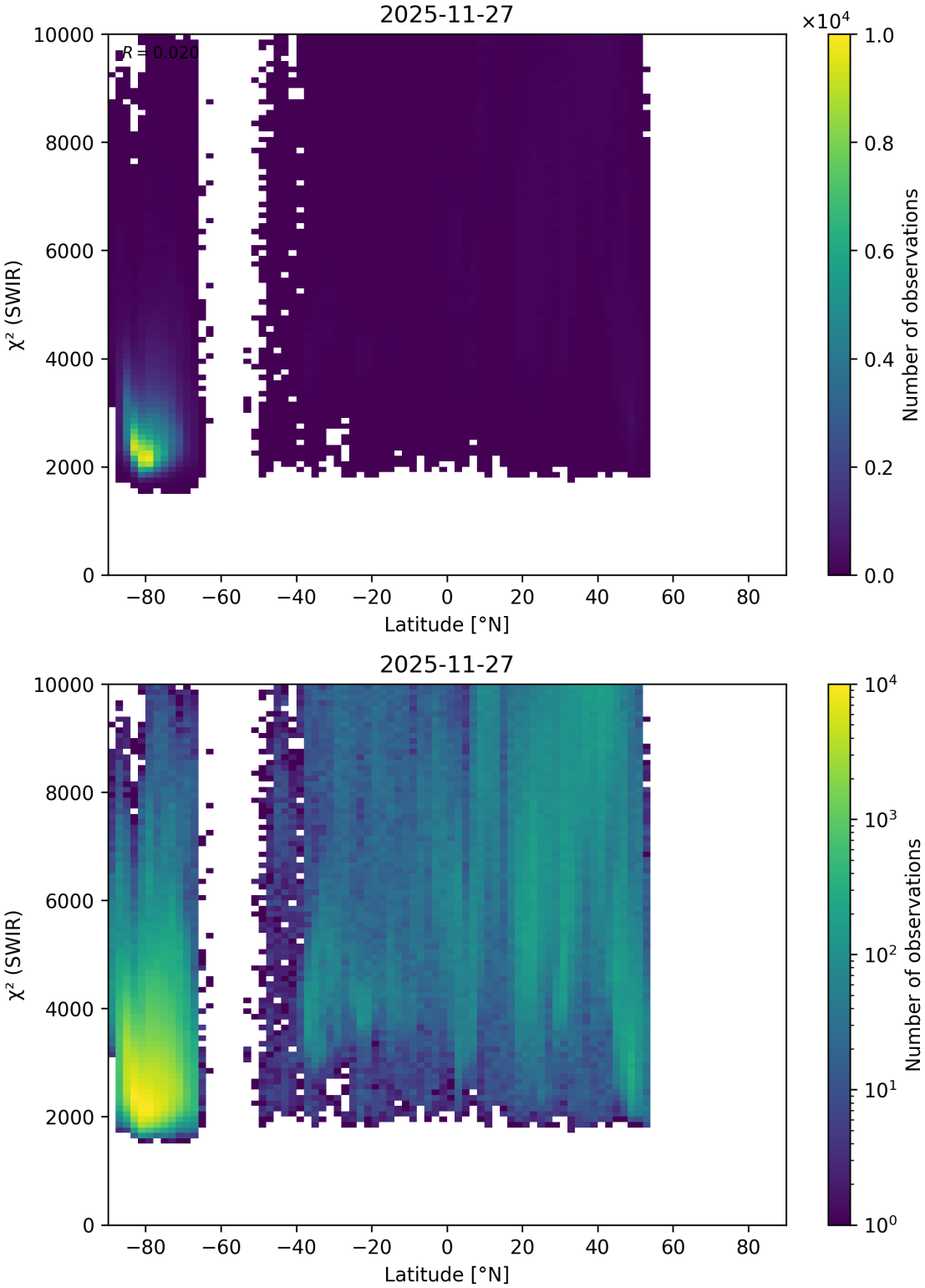

Figure 62: Scatter density plot of "Latitude" against "χ^2 (SWIR)" for 2025-11-26 to 2025-11-28.

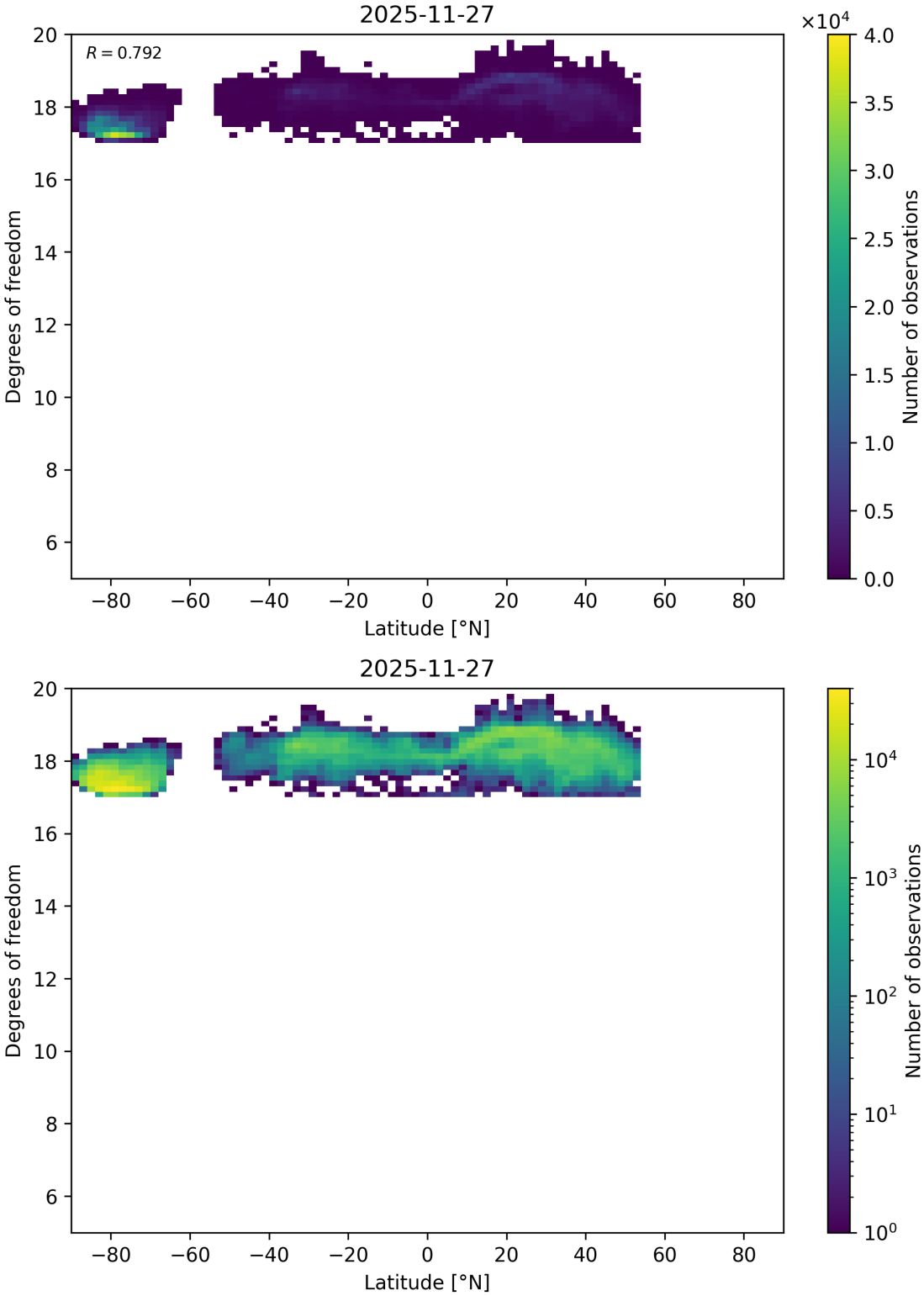

Figure 63: Scatter density plot of “Latitude” against “Degrees of freedom” for 2025-11-26 to 2025-11-28.

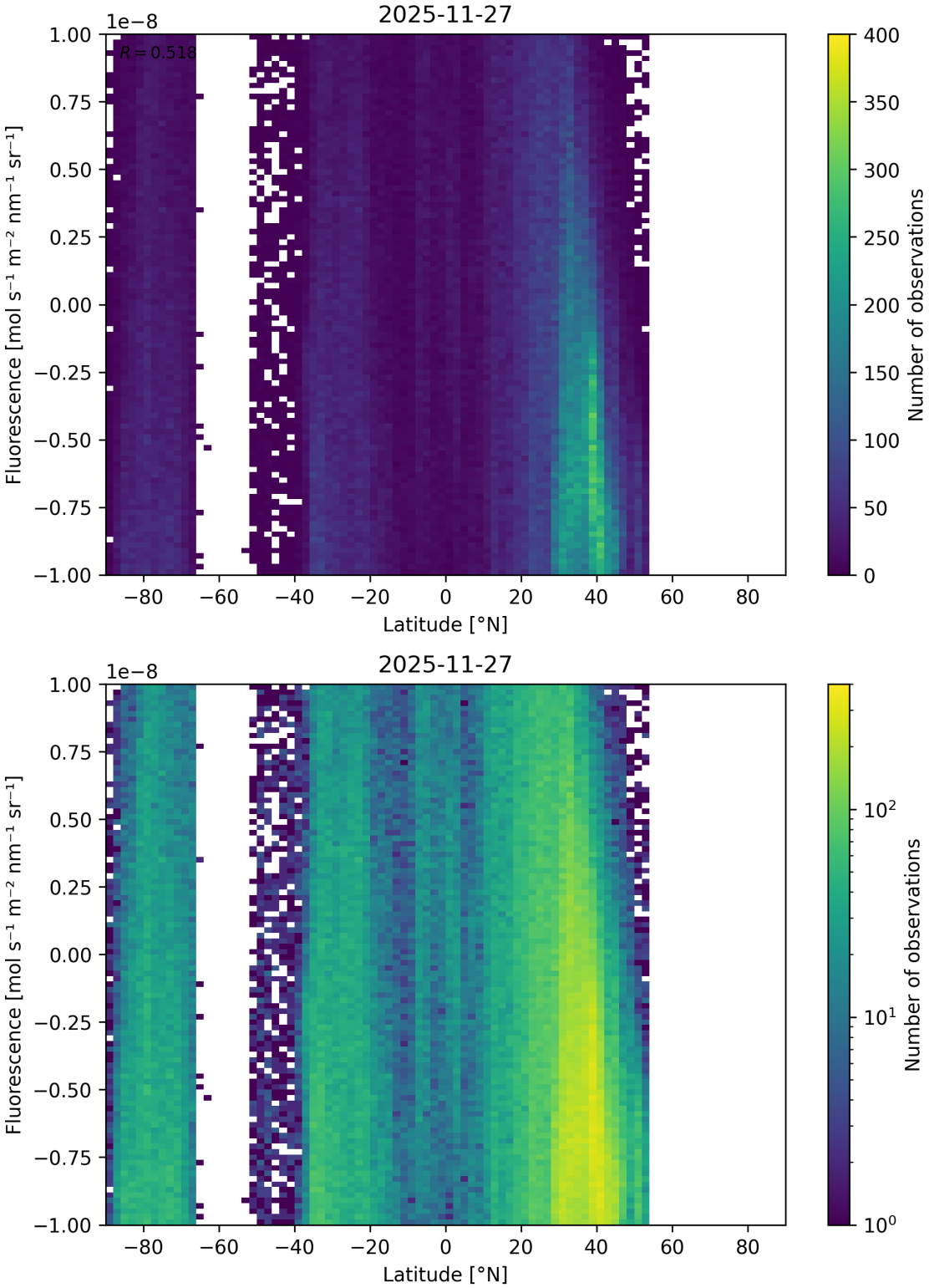

Figure 64: Scatter density plot of “Latitude” against “Fluorescence” for 2025-11-26 to 2025-11-28.

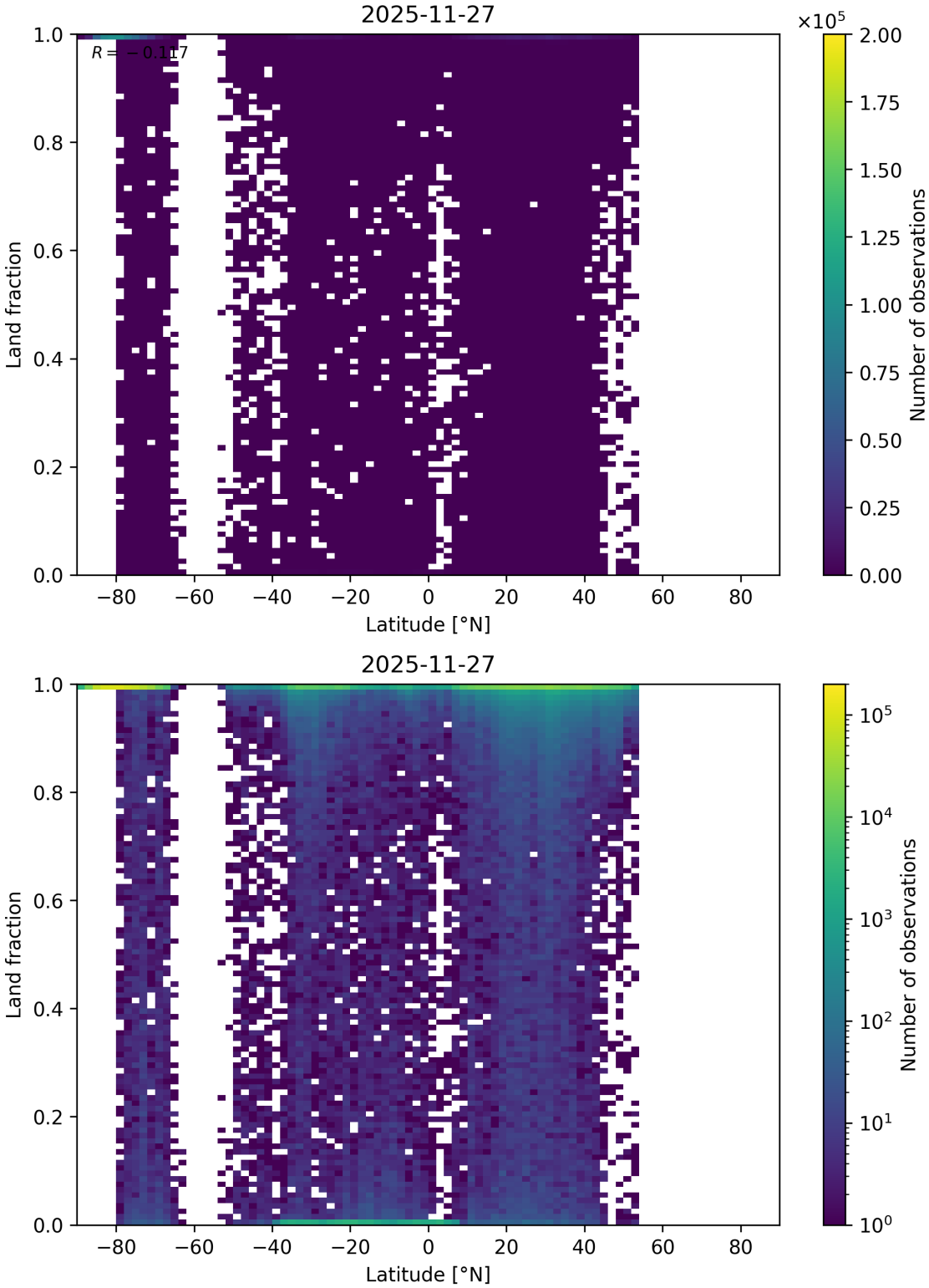

Figure 65: Scatter density plot of “Latitude” against “Land fraction” for 2025-11-26 to 2025-11-28.

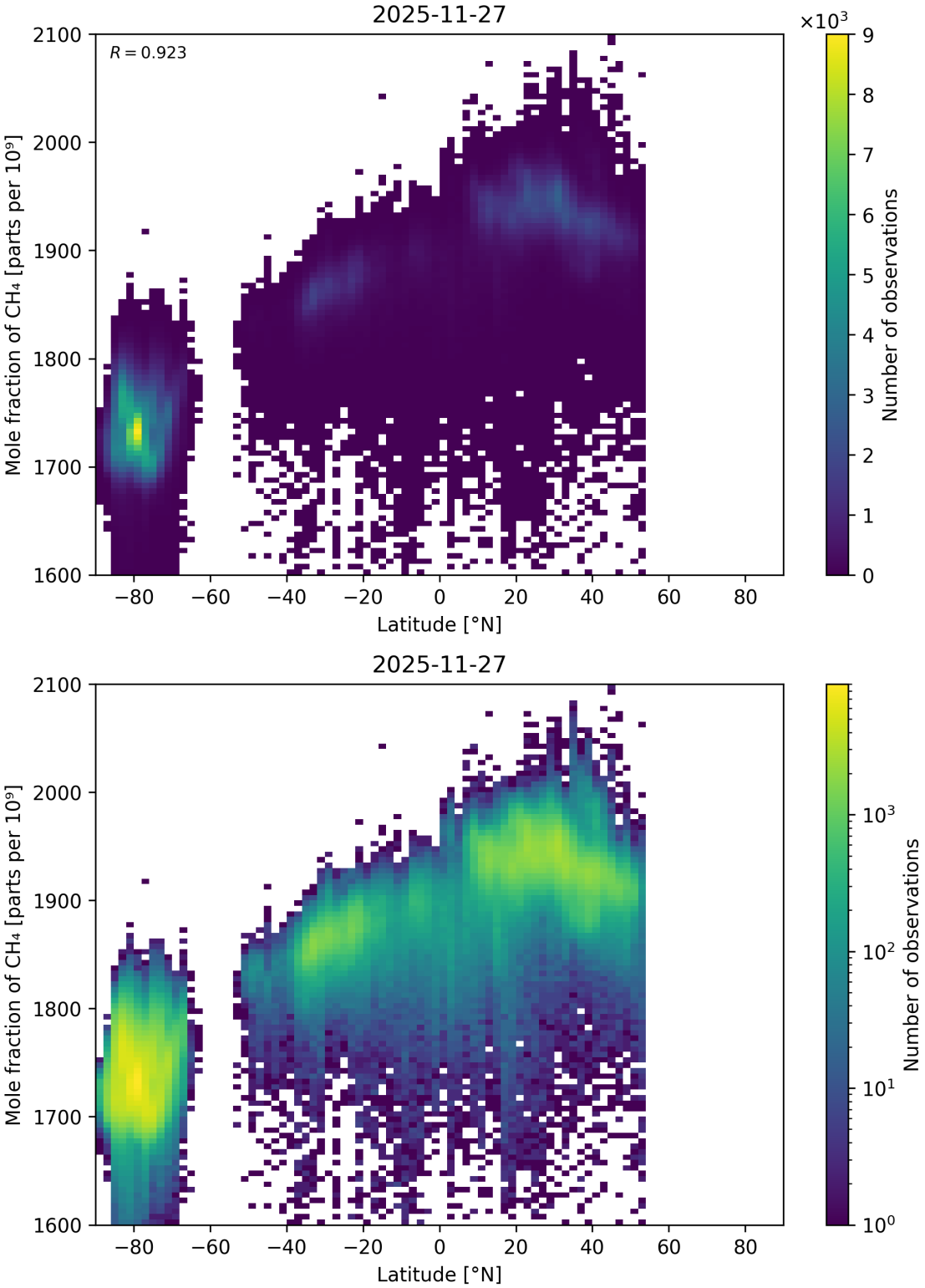

Figure 66: Scatter density plot of "Latitude" against "Mole fraction of CH_4" for 2025-11-26 to 2025-11-28.

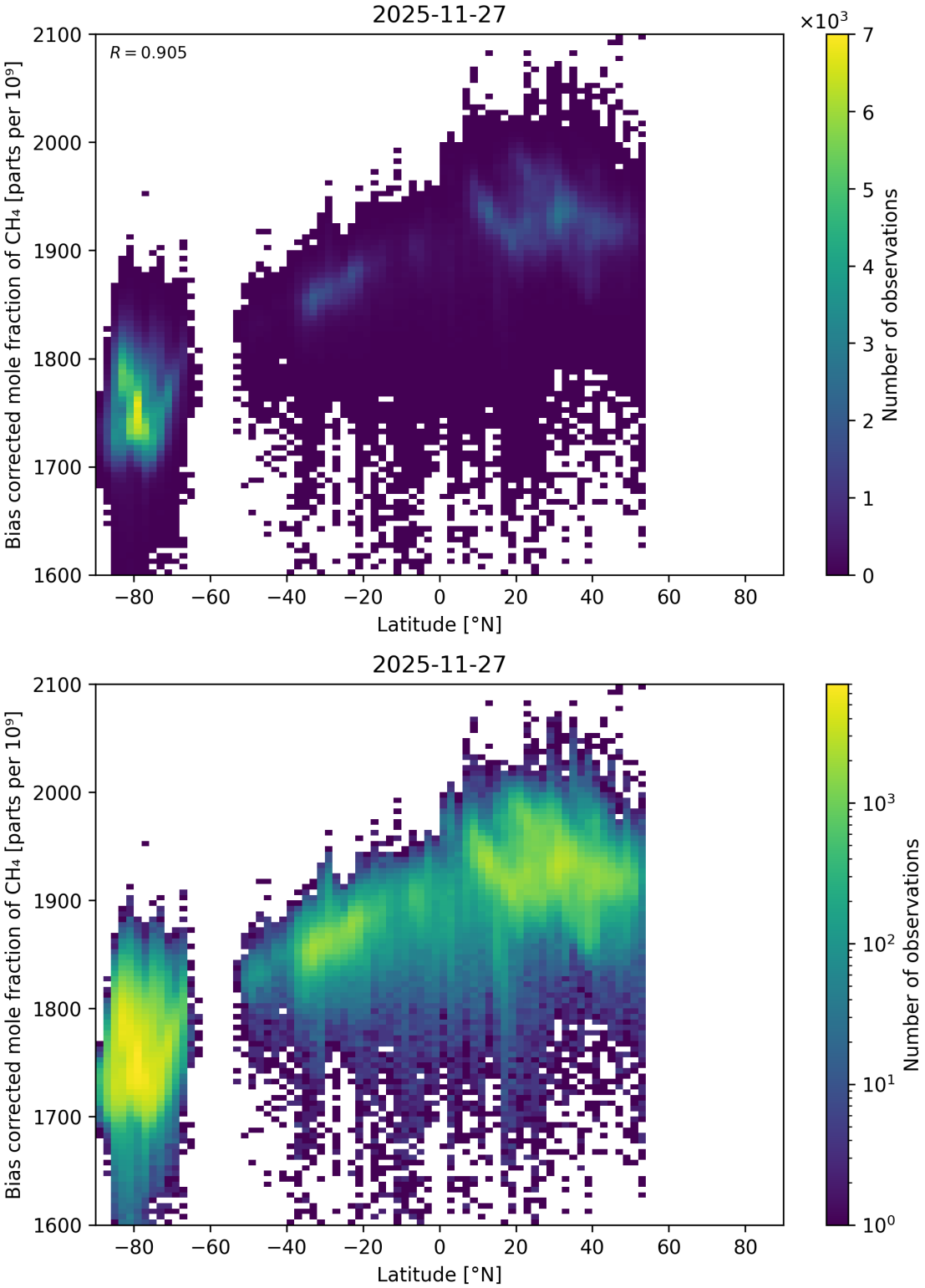

Figure 67: Scatter density plot of "Latitude" against "Bias corrected mole fraction of CH_4" for 2025-11-26 to 2025-11-28.

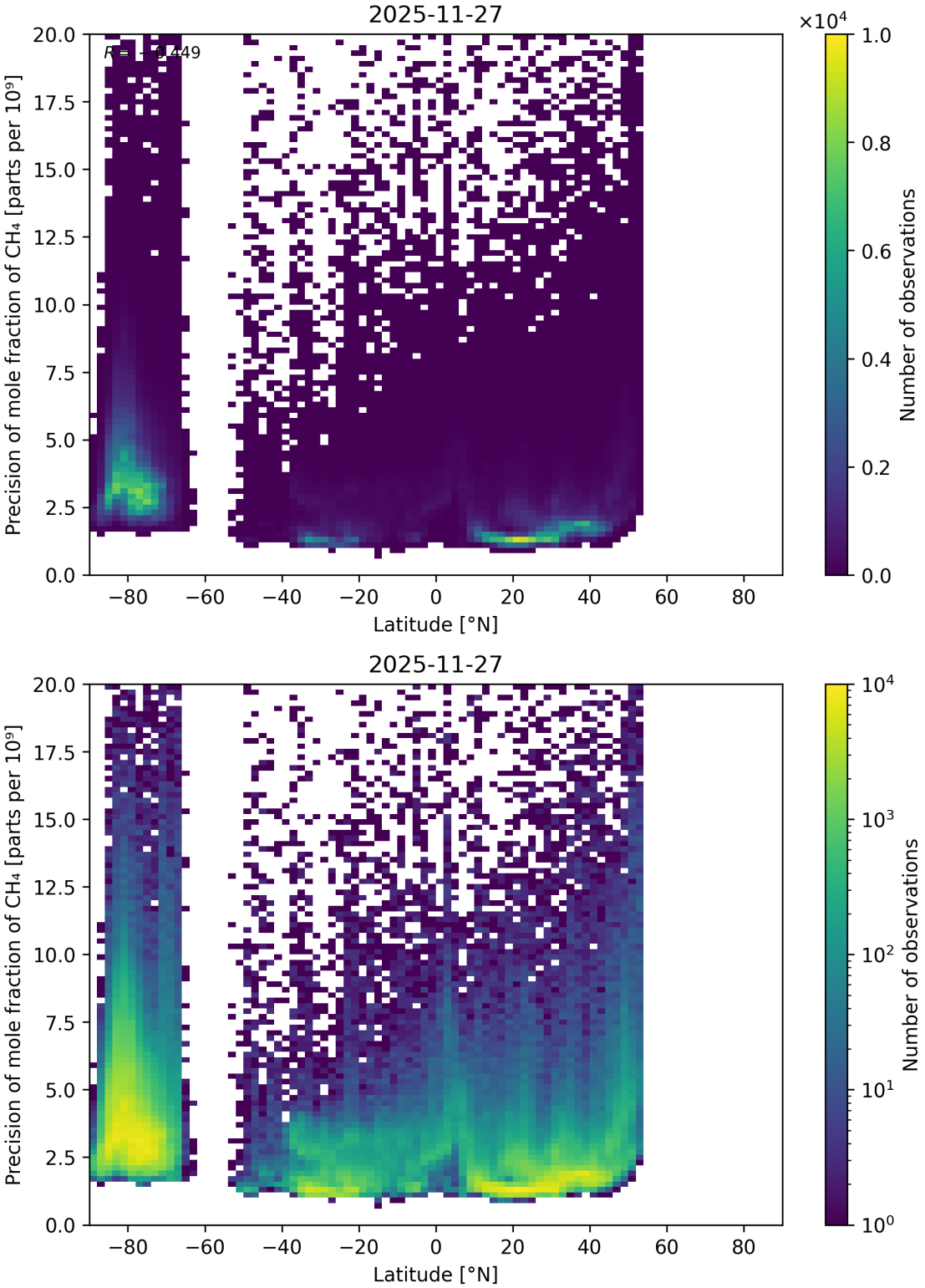

Figure 68: Scatter density plot of “Latitude” against “Precision of mole fraction of CH_4” for 2025-11-26 to 2025-11-28.

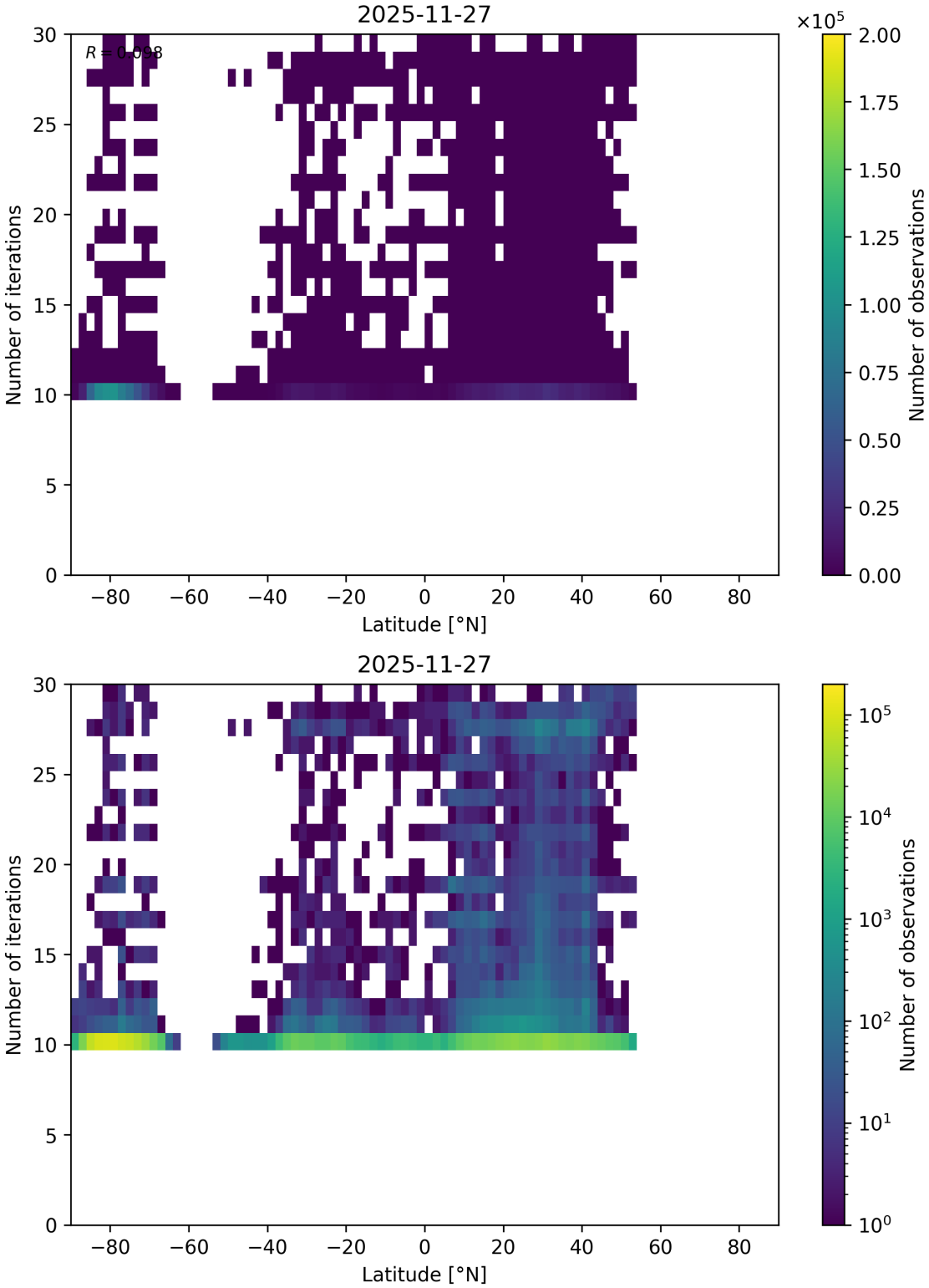

Figure 69: Scatter density plot of “Latitude” against “Number of iterations” for 2025-11-26 to 2025-11-28.

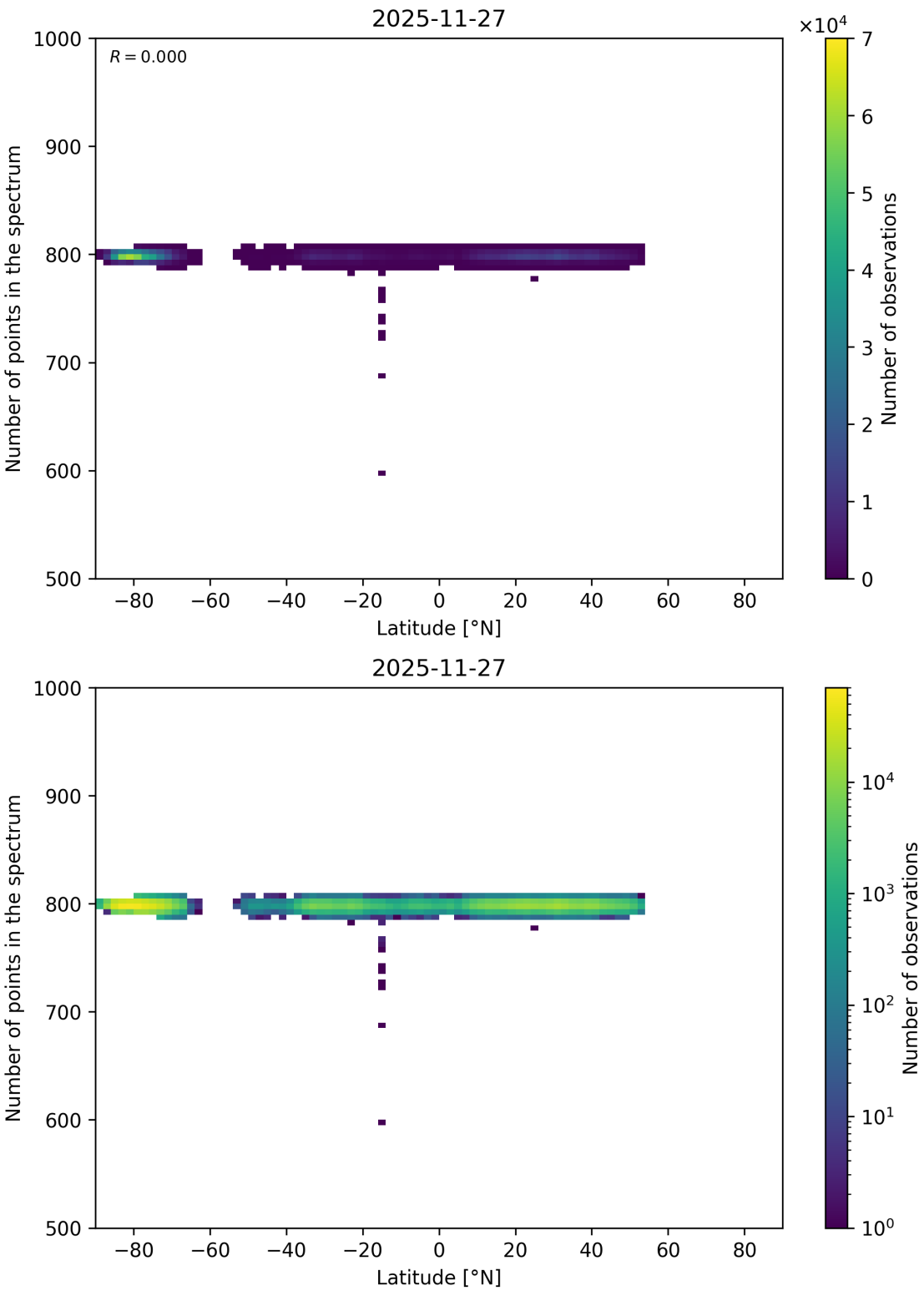

Figure 70: Scatter density plot of “Latitude” against “Number of points in the spectrum” for 2025-11-26 to 2025-11-28.

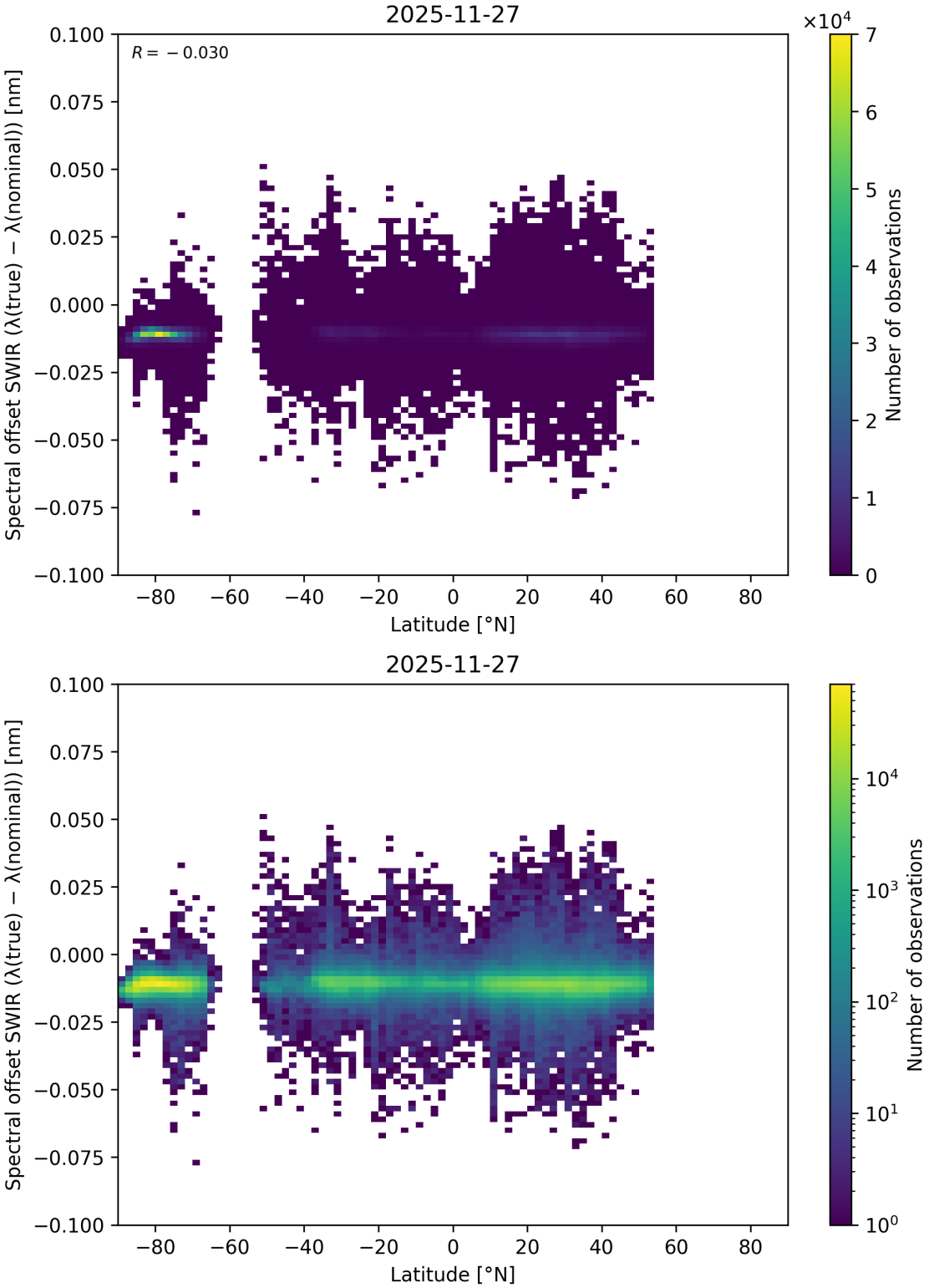

Figure 71: Scatter density plot of "Latitude" against "Spectral offset SWIR ($\lambda_{\text{true}} - \lambda_{\text{nominal}}$)" for 2025-11-26 to 2025-11-28.

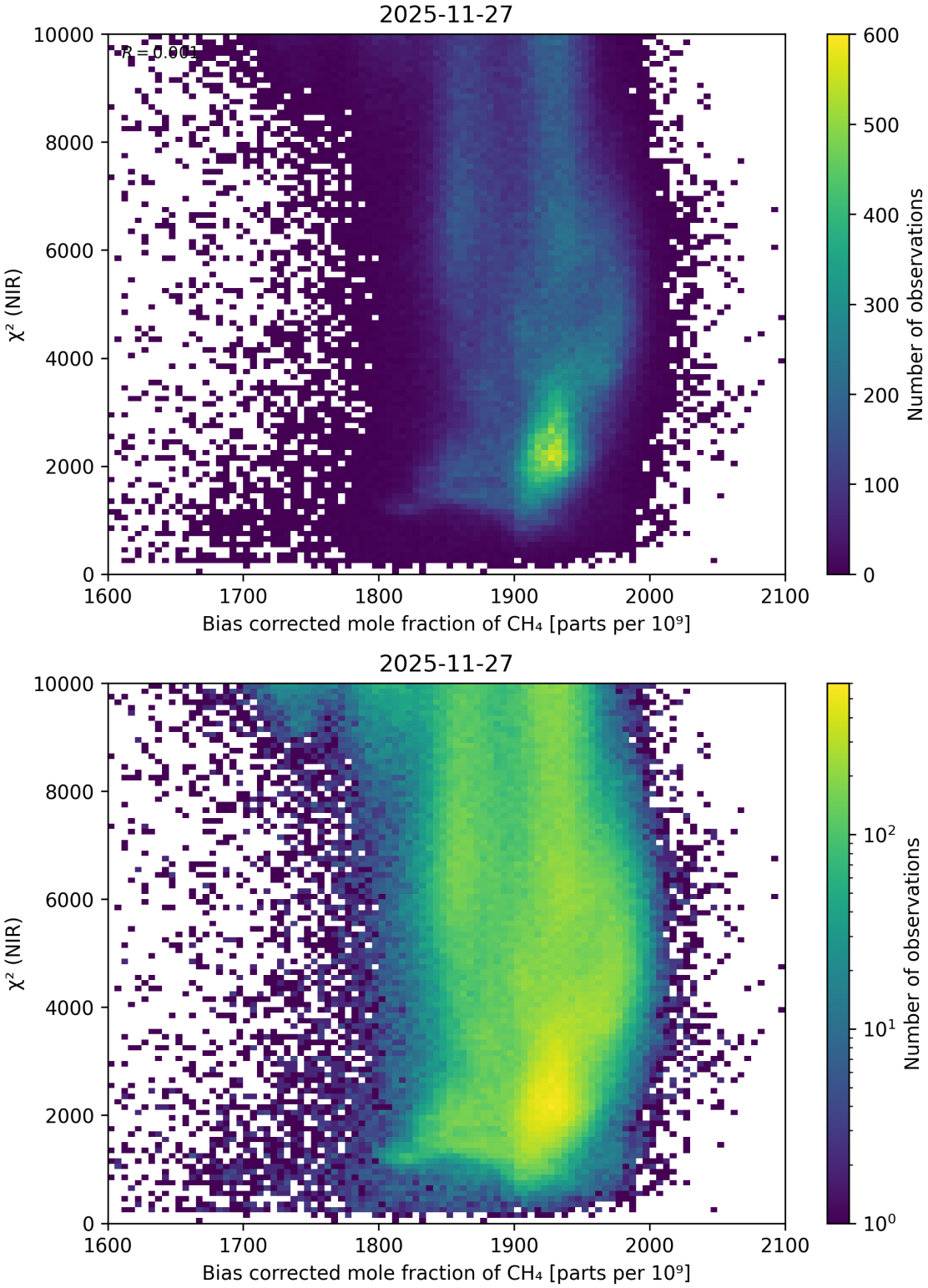

Figure 72: Scatter density plot of "Bias corrected mole fraction of CH_4" against "χ^2 (NIR)" for 2025-11-26 to 2025-11-28.

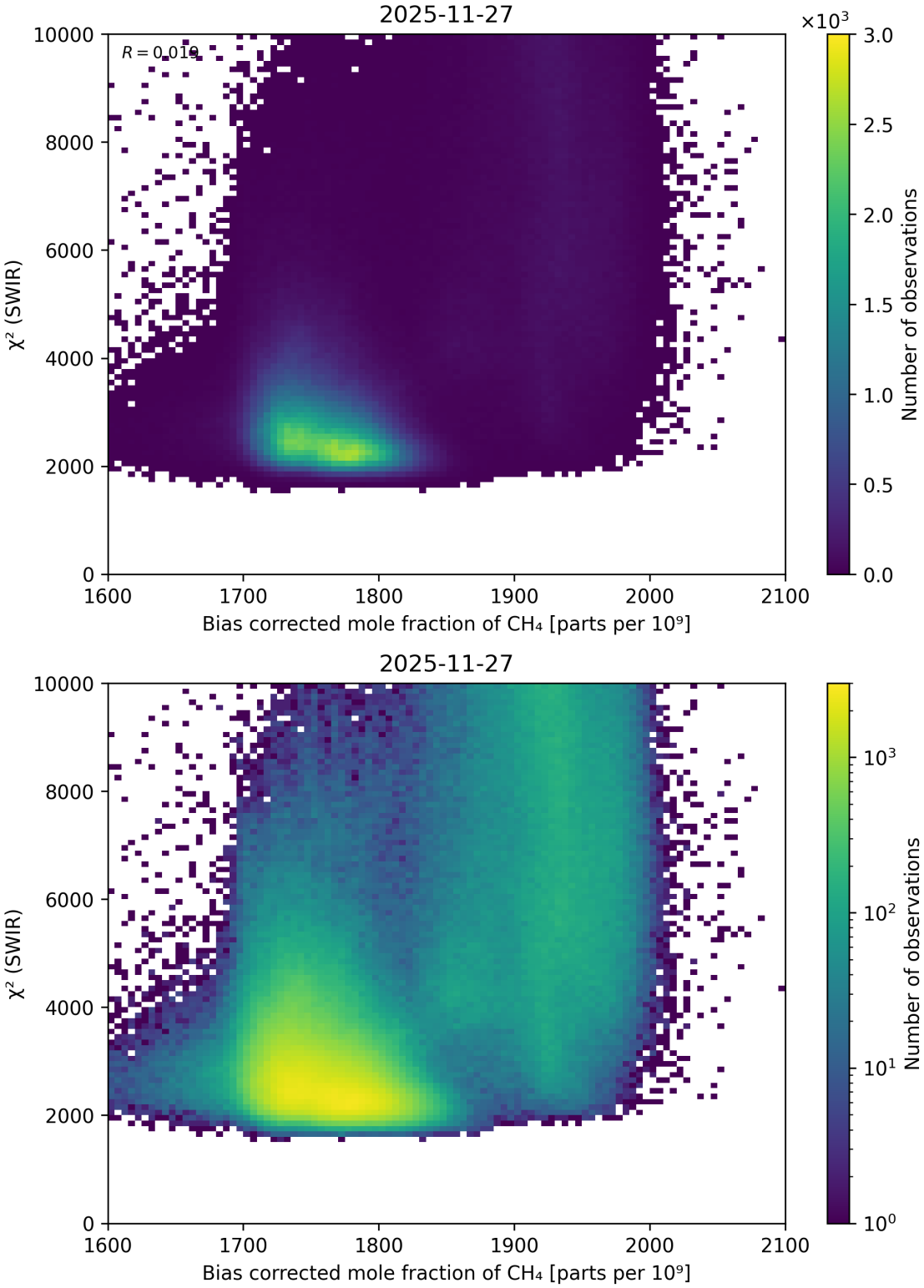

Figure 73: Scatter density plot of "Bias corrected mole fraction of CH_4" against "χ^2 (SWIR)" for 2025-11-26 to 2025-11-28.

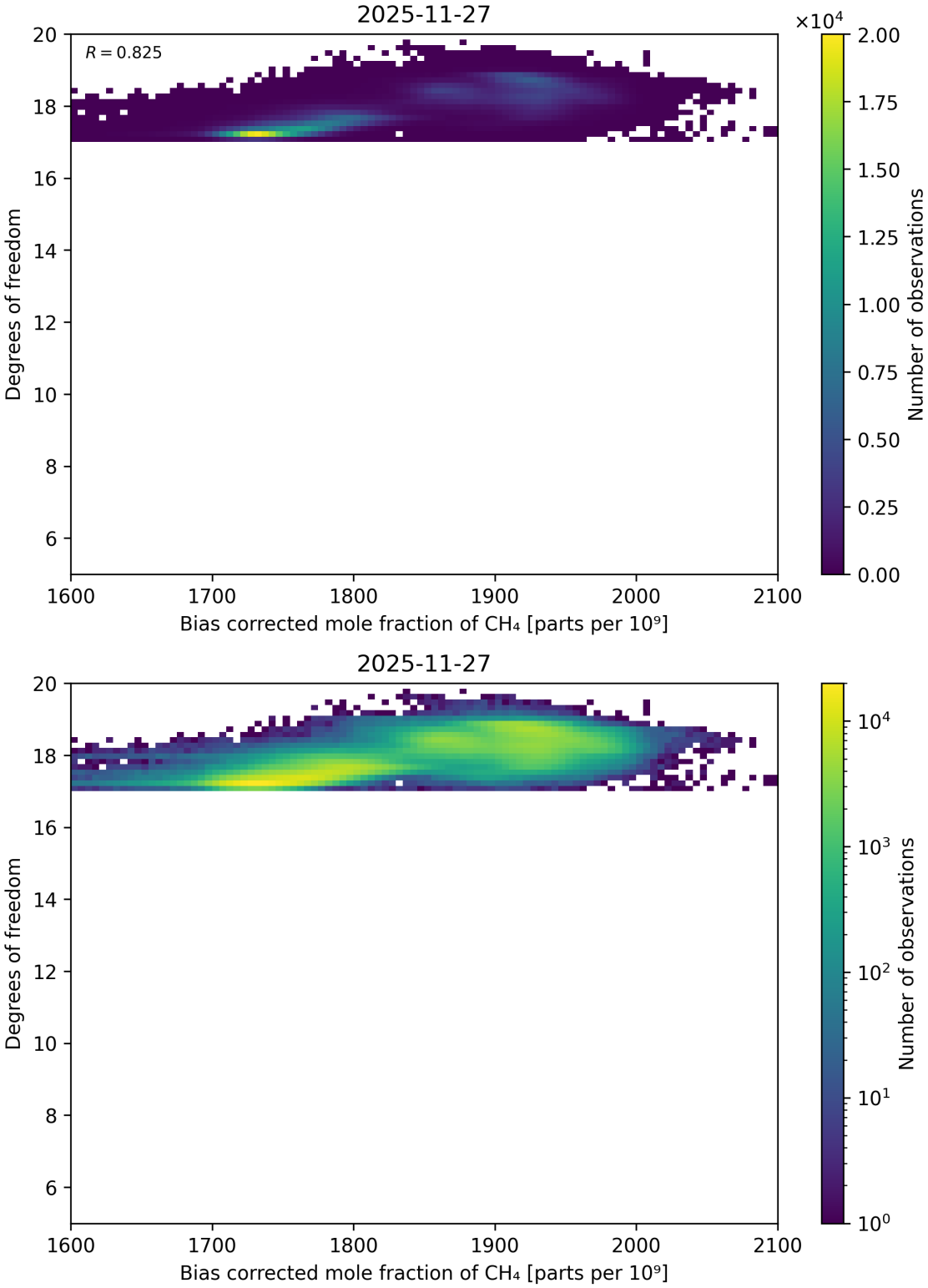

Figure 74: Scatter density plot of "Bias corrected mole fraction of CH_4" against "Degrees of freedom" for 2025-11-26 to 2025-11-28.

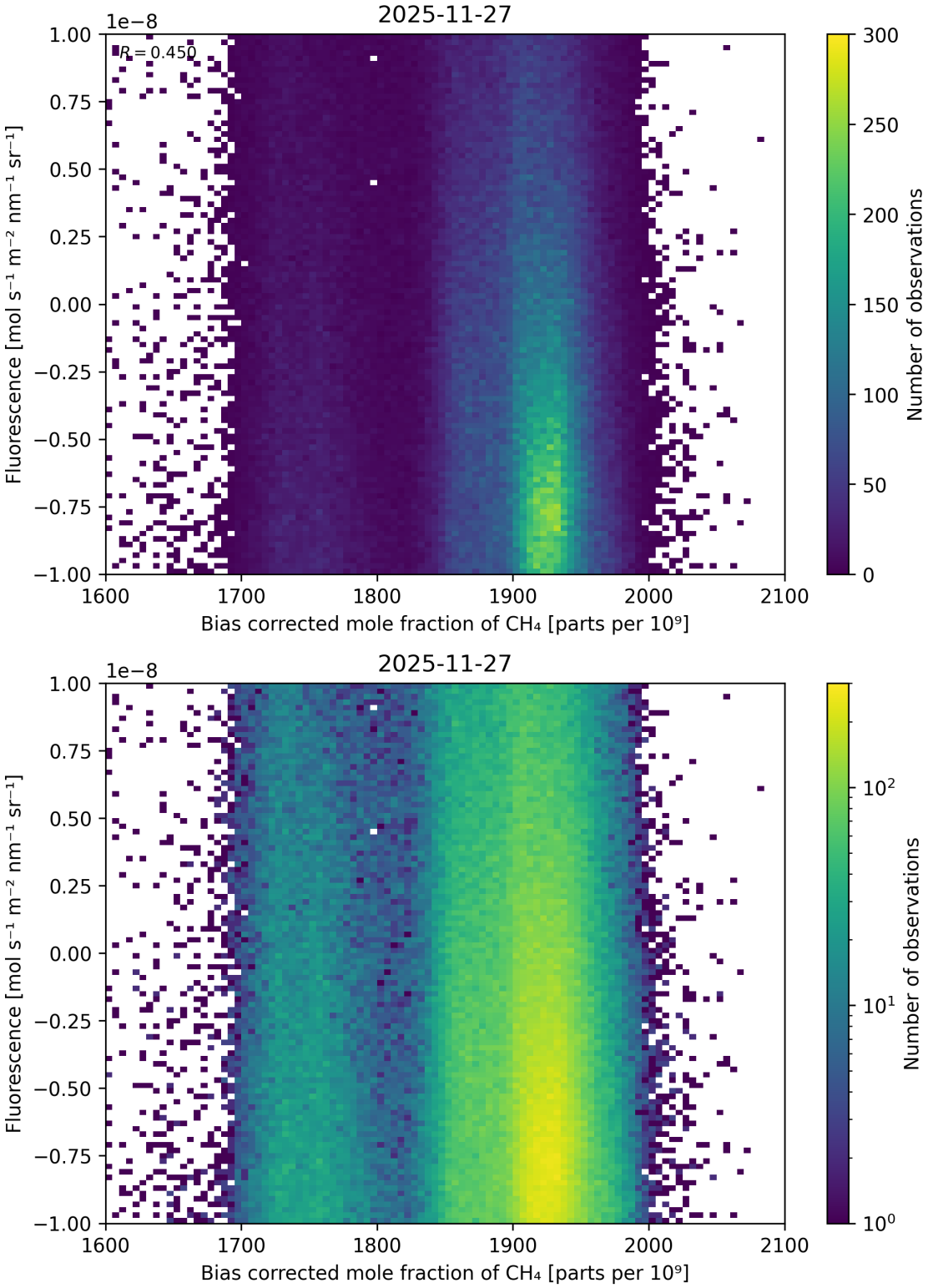

Figure 75: Scatter density plot of "Bias corrected mole fraction of CH_4" against "Fluorescence" for 2025-11-26 to 2025-11-28.

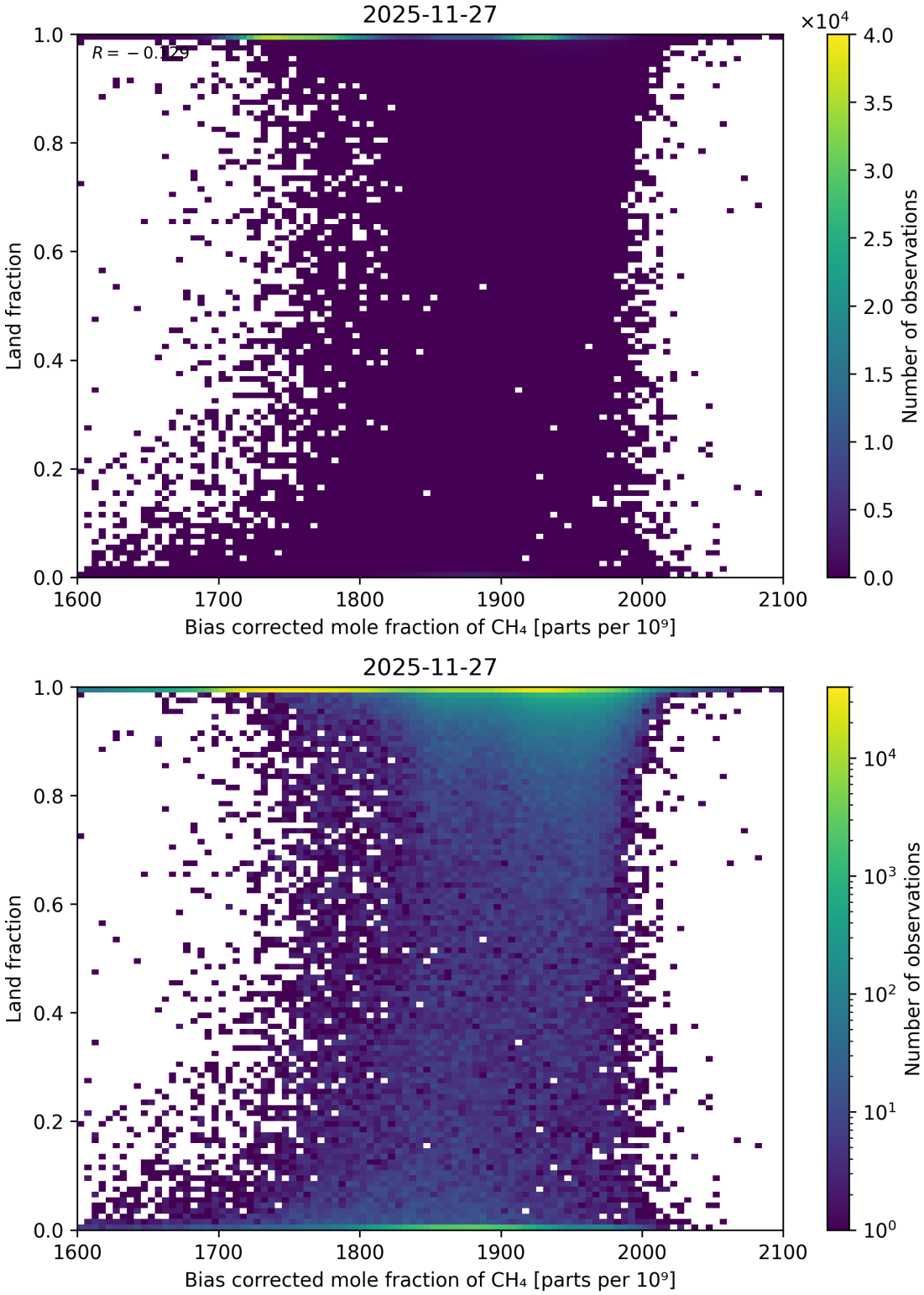

Figure 76: Scatter density plot of "Bias corrected mole fraction of CH_4" against "Land fraction" for 2025-11-26 to 2025-11-28.

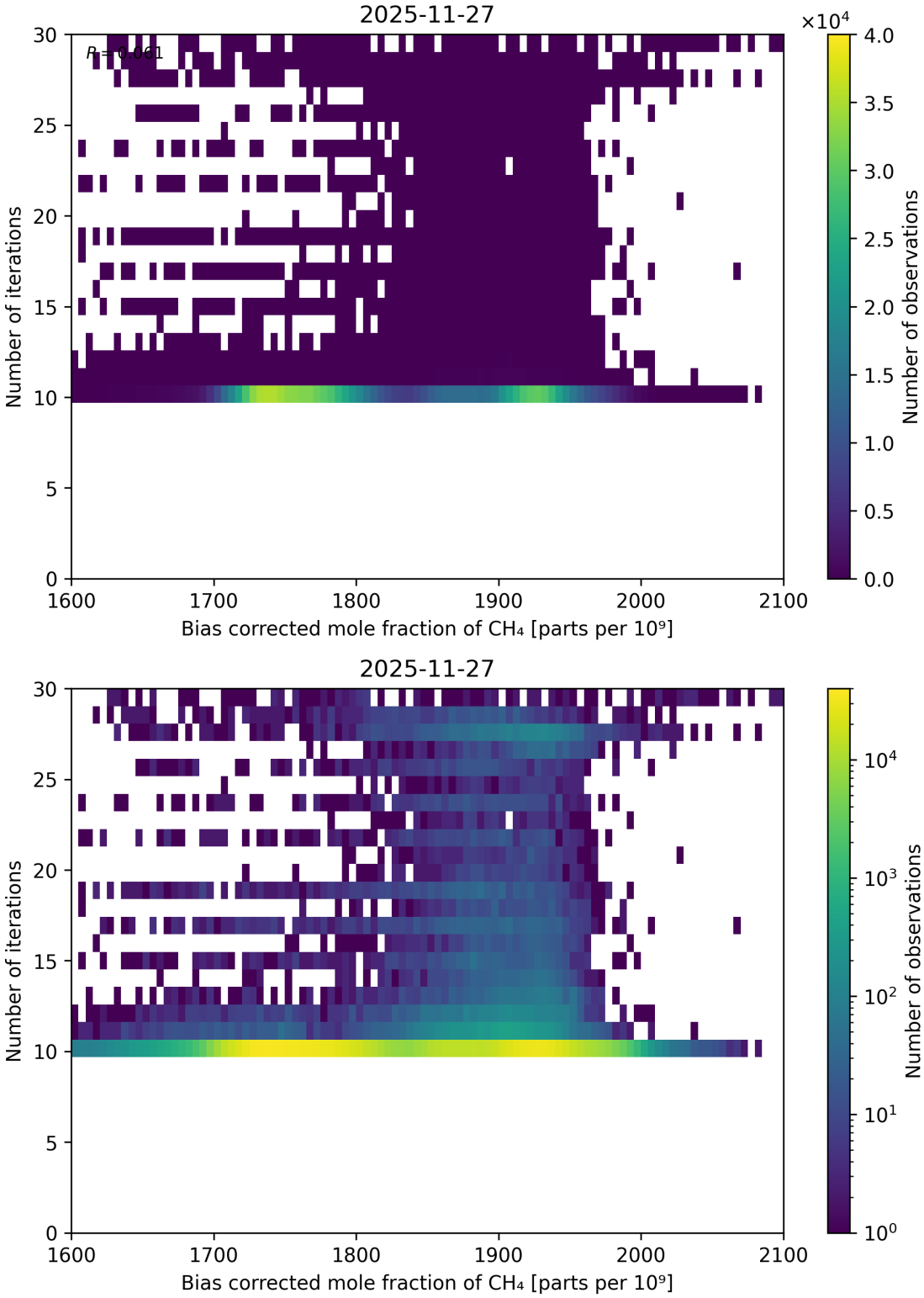

Figure 77: Scatter density plot of "Bias corrected mole fraction of CH_4" against "Number of iterations" for 2025-11-26 to 2025-11-28.

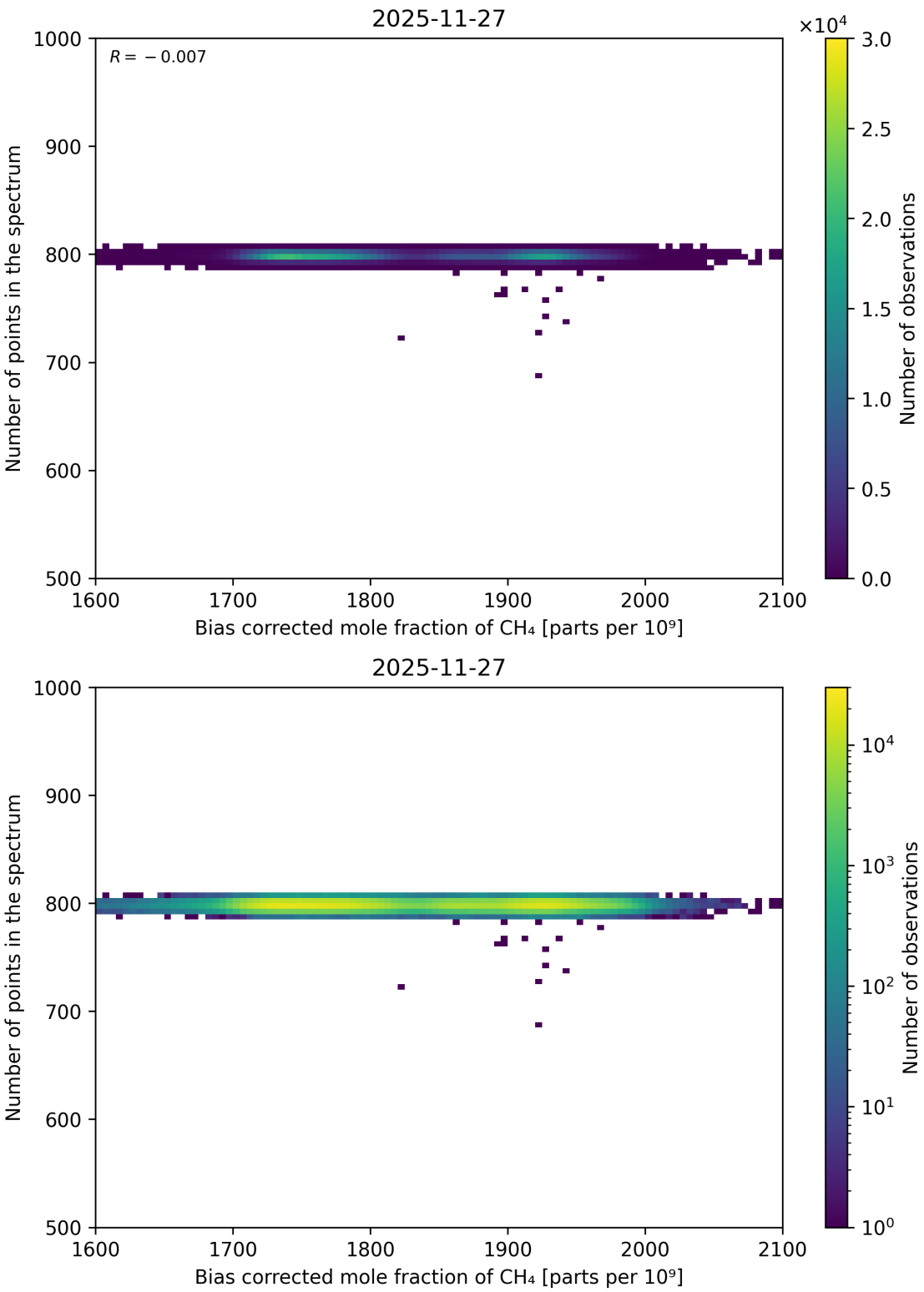

Figure 78: Scatter density plot of "Bias corrected mole fraction of CH_4" against "Number of points in the spectrum" for 2025-11-26 to 2025-11-28.

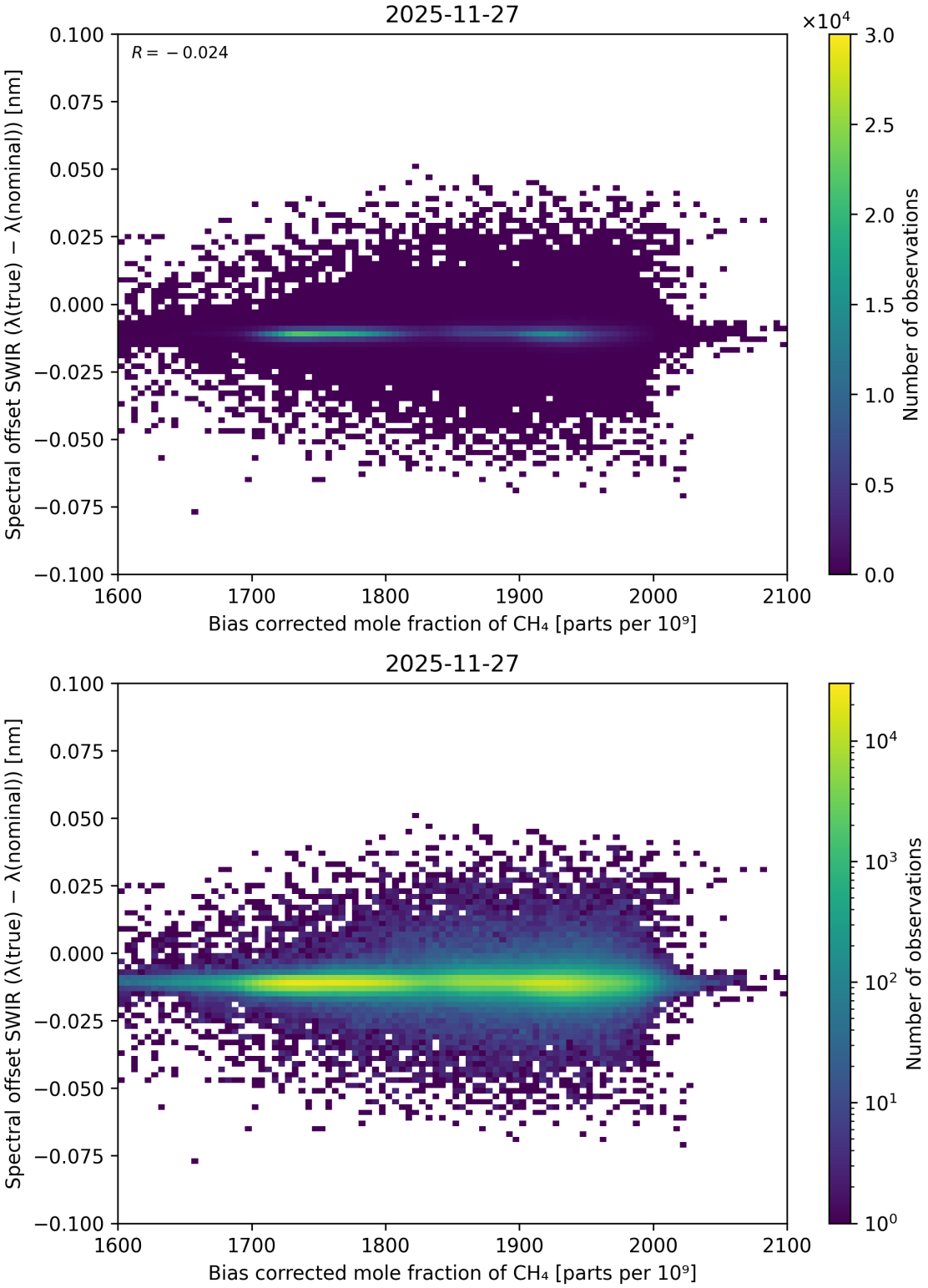

Figure 79: Scatter density plot of "Bias corrected mole fraction of CH_4" against "Spectral offset SWIR ($\lambda_{\text{true}} - \lambda_{\text{nominal}}$)" for 2025-11-26 to 2025-11-28.

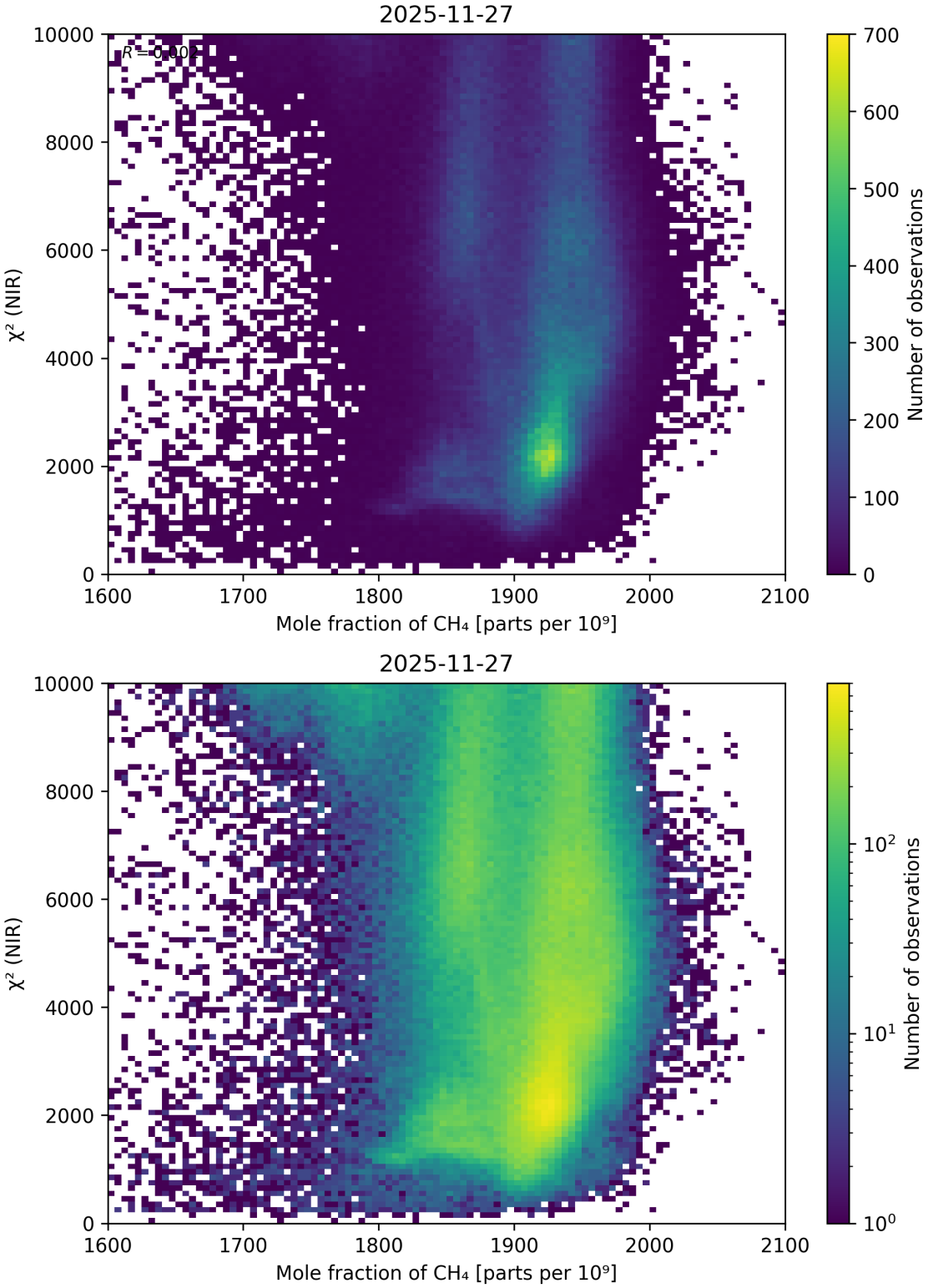

Figure 80: Scatter density plot of "Mole fraction of CH_4" against "χ^2 (NIR)" for 2025-11-26 to 2025-11-28.

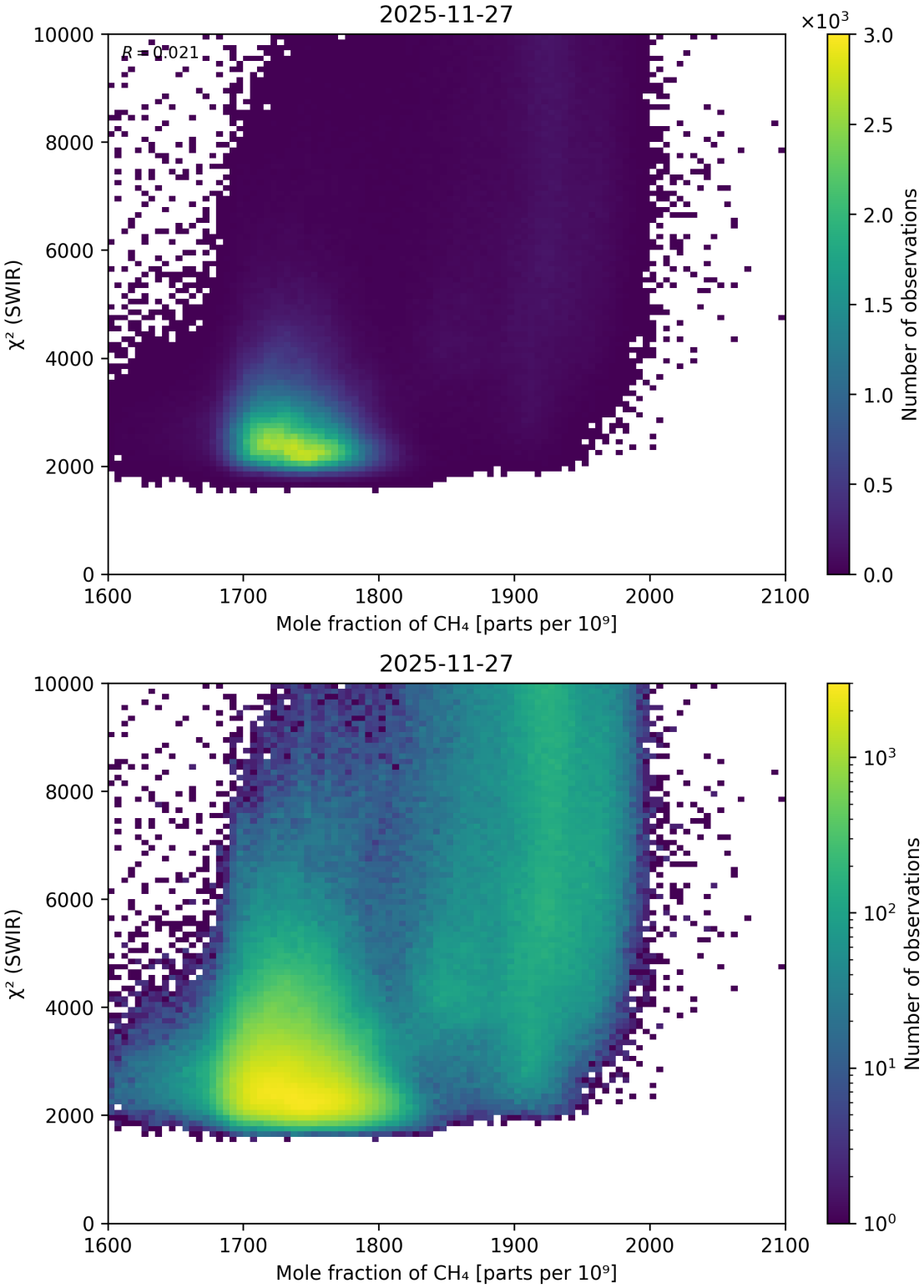

Figure 81: Scatter density plot of "Mole fraction of CH_4" against "χ^2 (SWIR)" for 2025-11-26 to 2025-11-28.

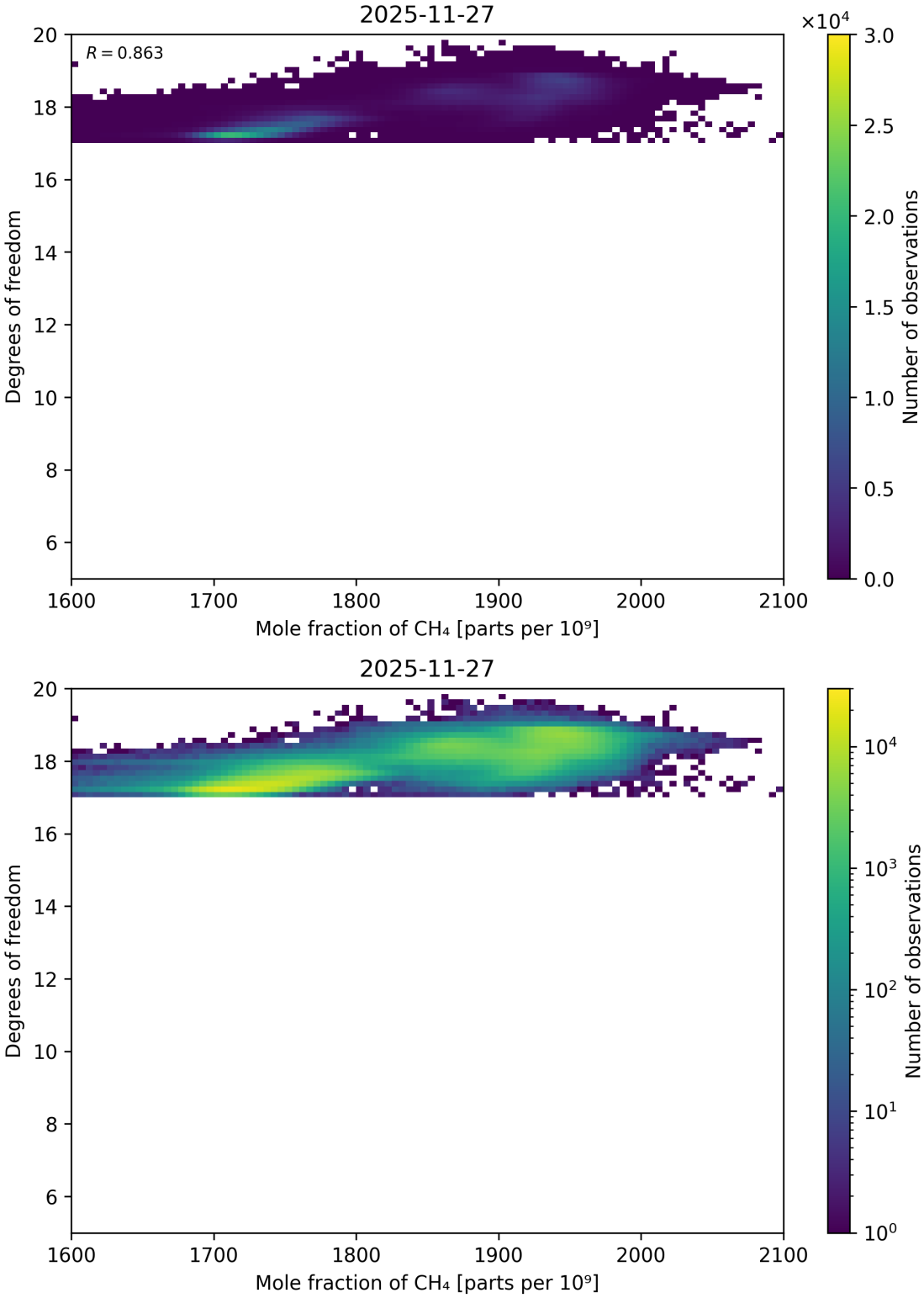

Figure 82: Scatter density plot of "Mole fraction of CH_4" against "Degrees of freedom" for 2025-11-26 to 2025-11-28.

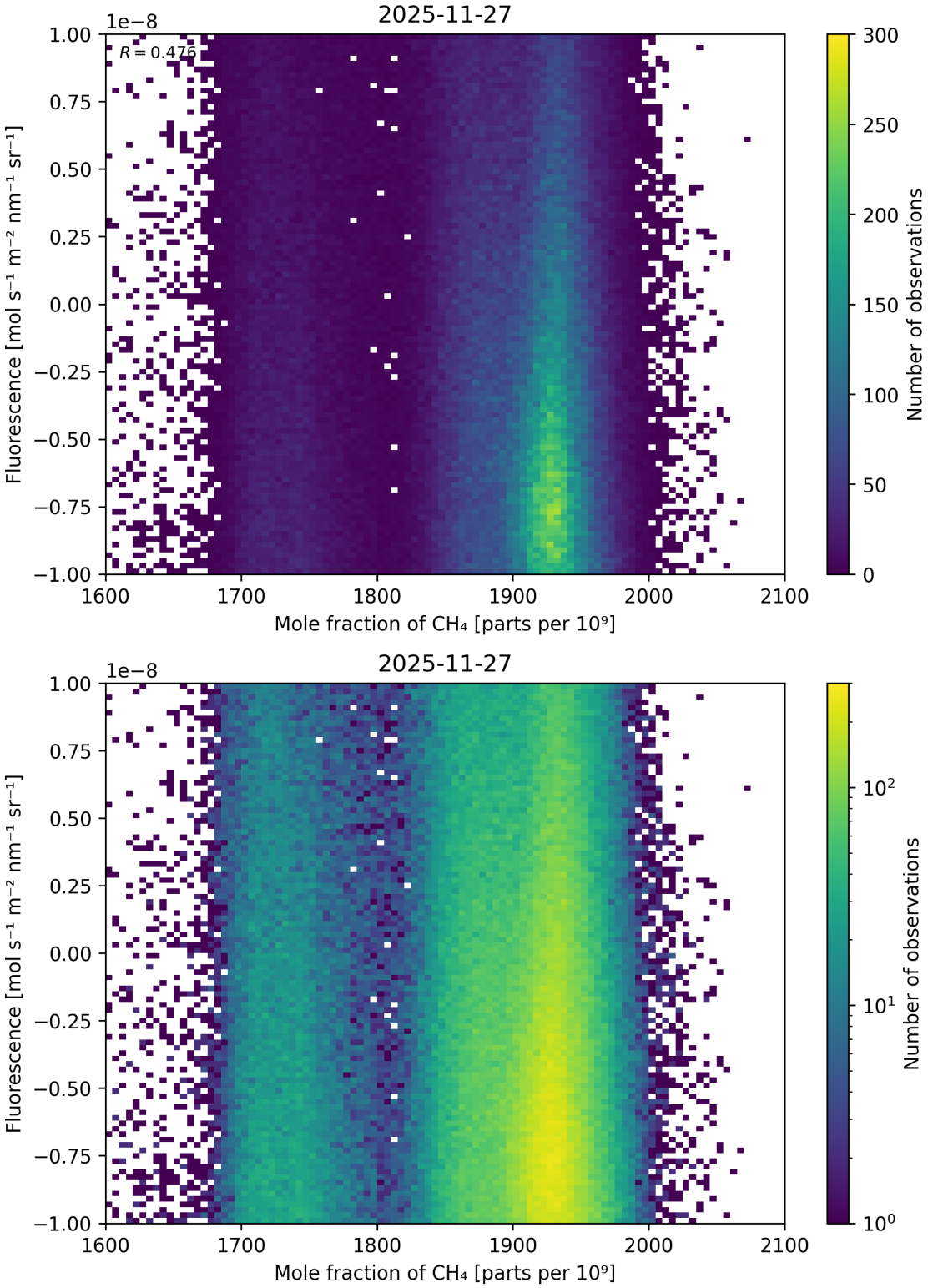

Figure 83: Scatter density plot of "Mole fraction of CH_4" against "Fluorescence" for 2025-11-26 to 2025-11-28.

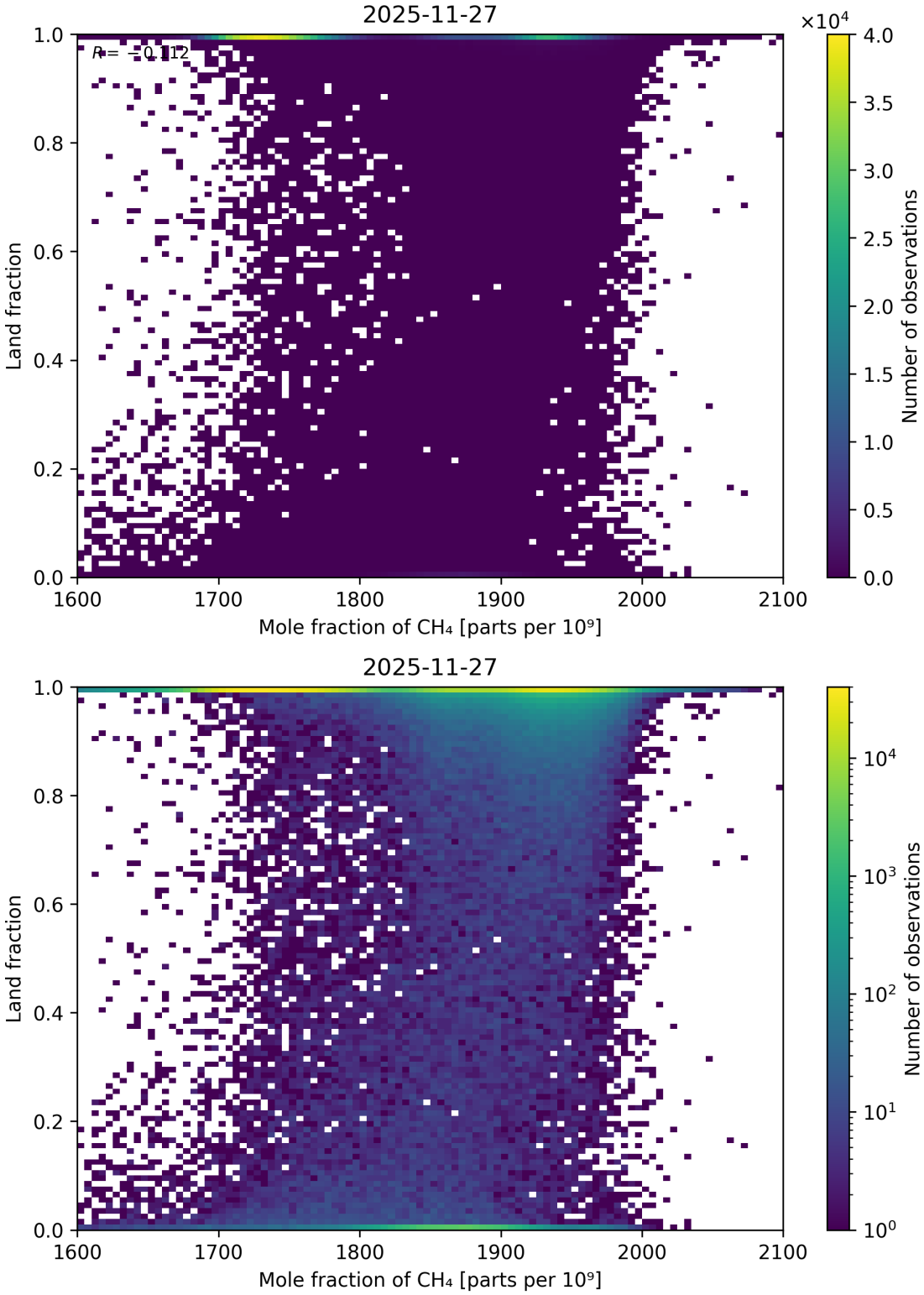

Figure 84: Scatter density plot of "Mole fraction of CH_4" against "Land fraction" for 2025-11-26 to 2025-11-28.

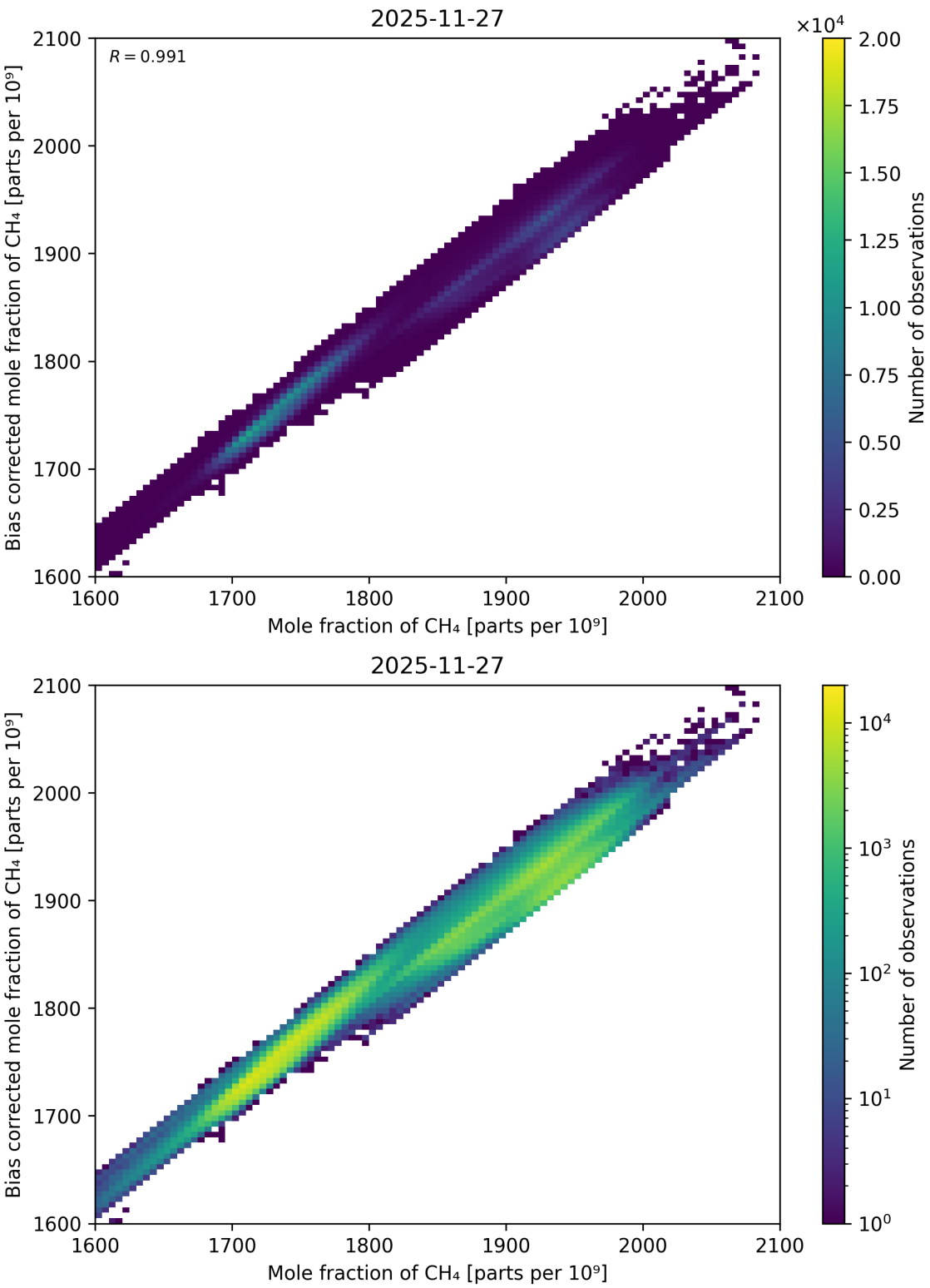

Figure 85: Scatter density plot of "Mole fraction of CH_4" against "Bias corrected mole fraction of CH_4" for 2025-11-26 to 2025-11-28.

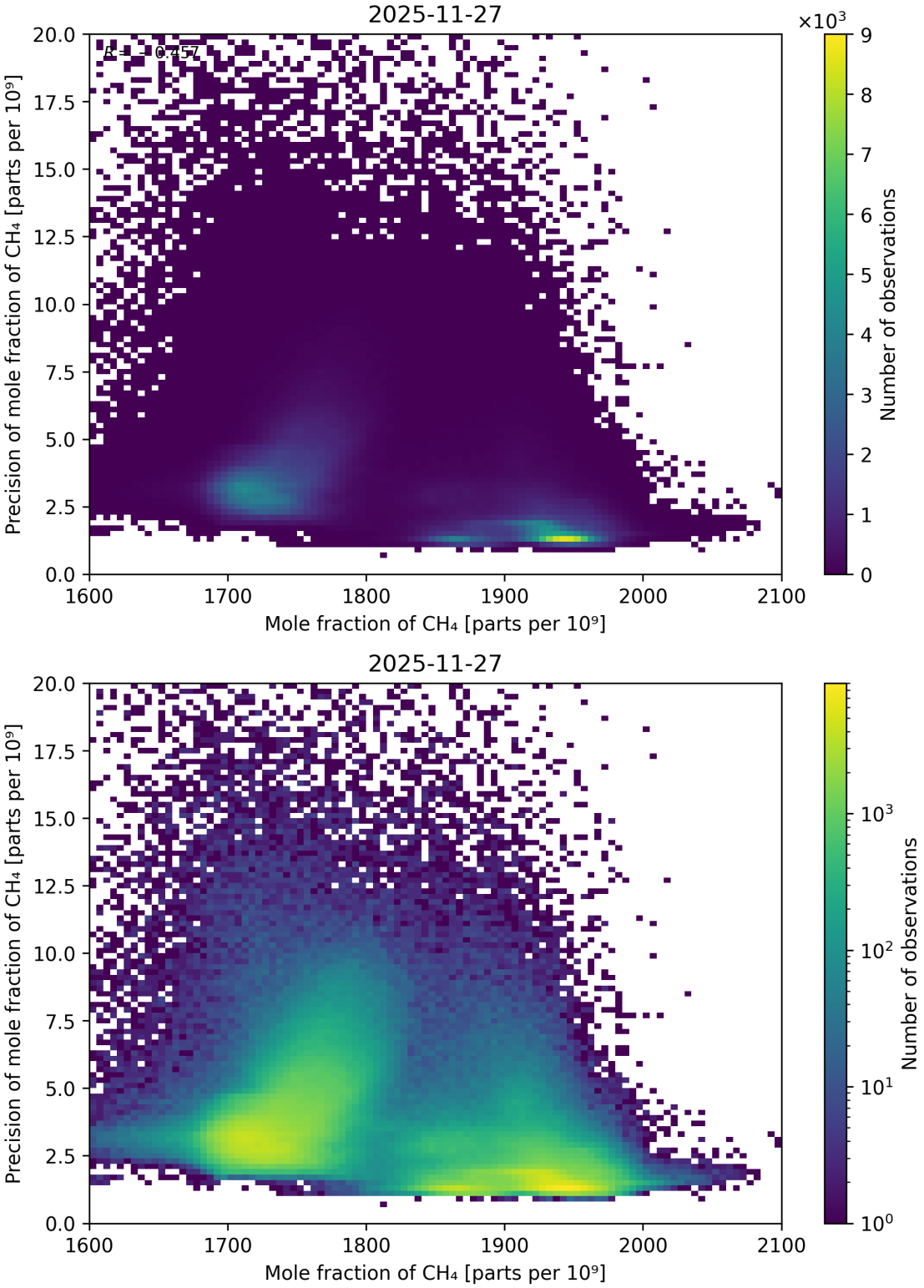

Figure 86: Scatter density plot of "Mole fraction of CH_4" against "Precision of mole fraction of CH_4" for 2025-11-26 to 2025-11-28.

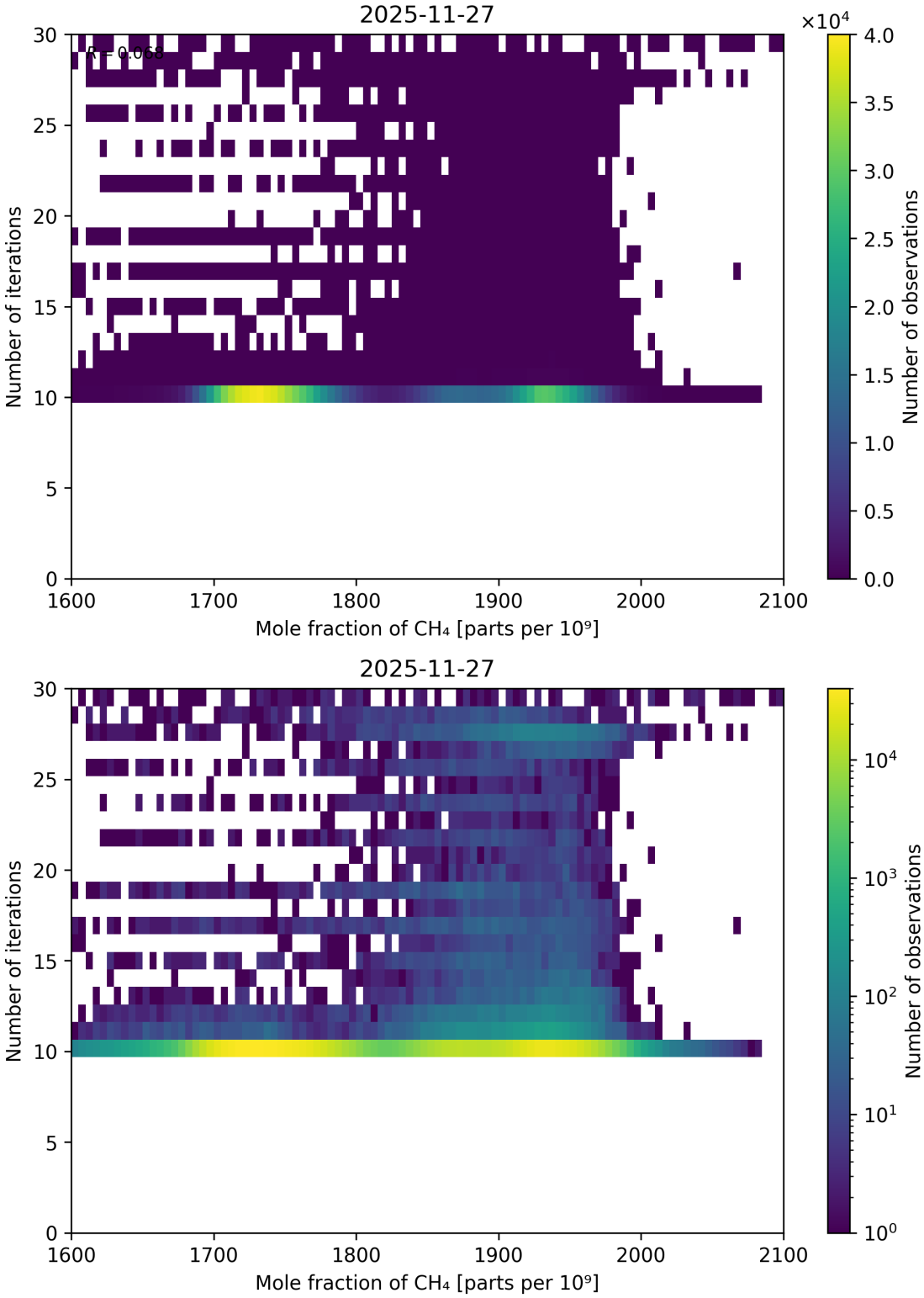

Figure 87: Scatter density plot of "Mole fraction of CH_4" against "Number of iterations" for 2025-11-26 to 2025-11-28.

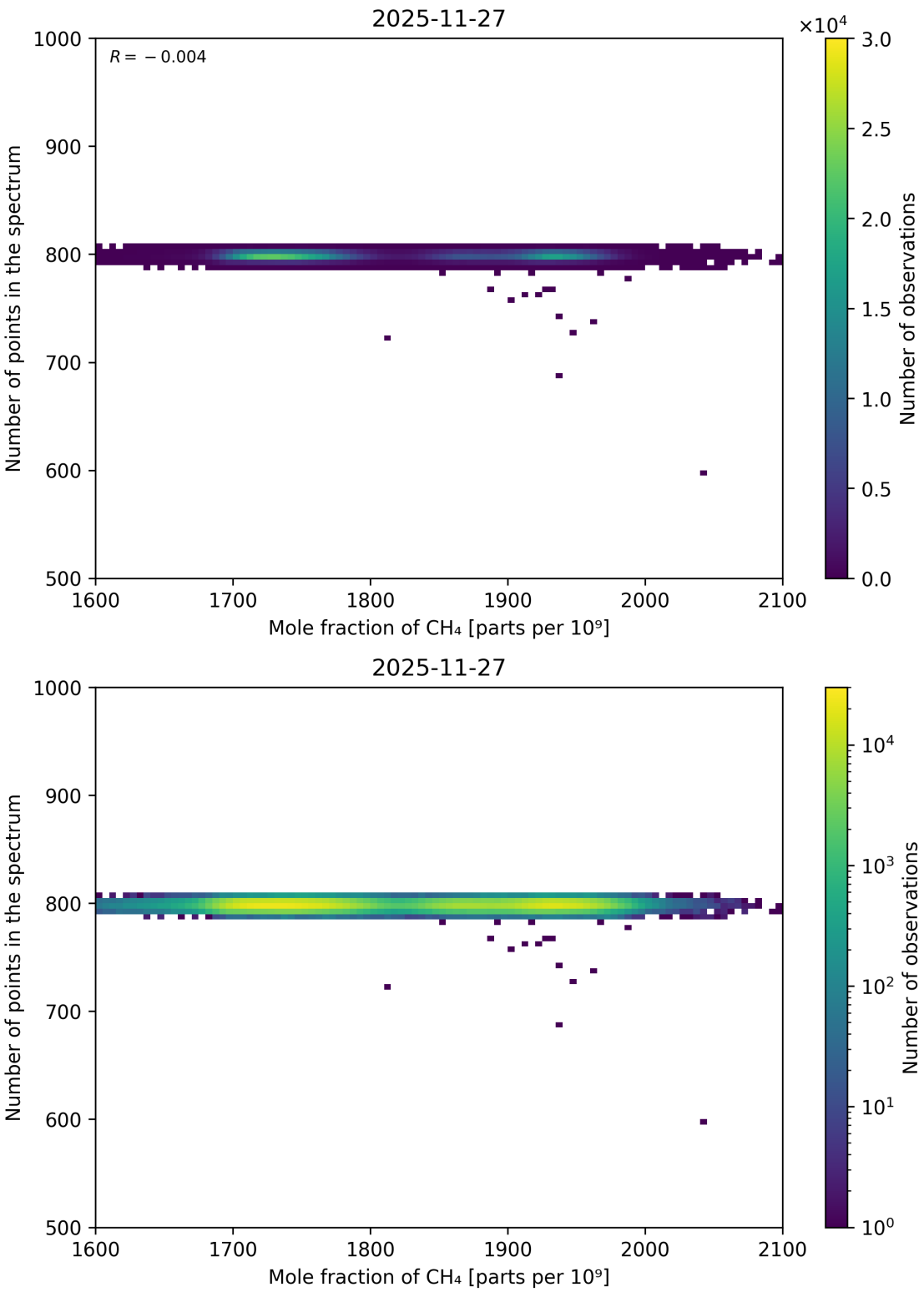

Figure 88: Scatter density plot of "Mole fraction of CH_4" against "Number of points in the spectrum" for 2025-11-26 to 2025-11-28.

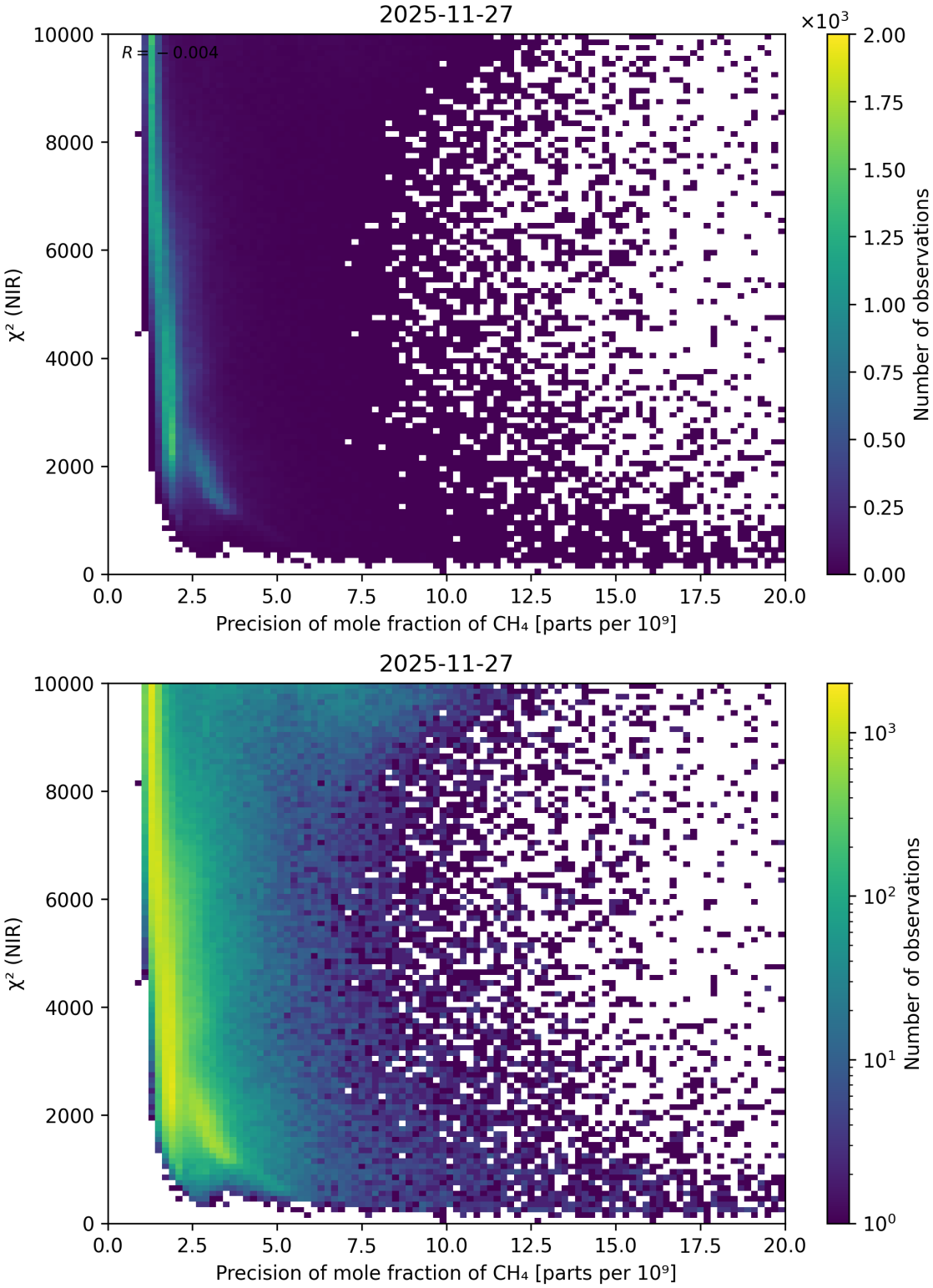

Figure 89: Scatter density plot of "Precision of mole fraction of CH_4" against "χ^2 (NIR)" for 2025-11-26 to 2025-11-28.

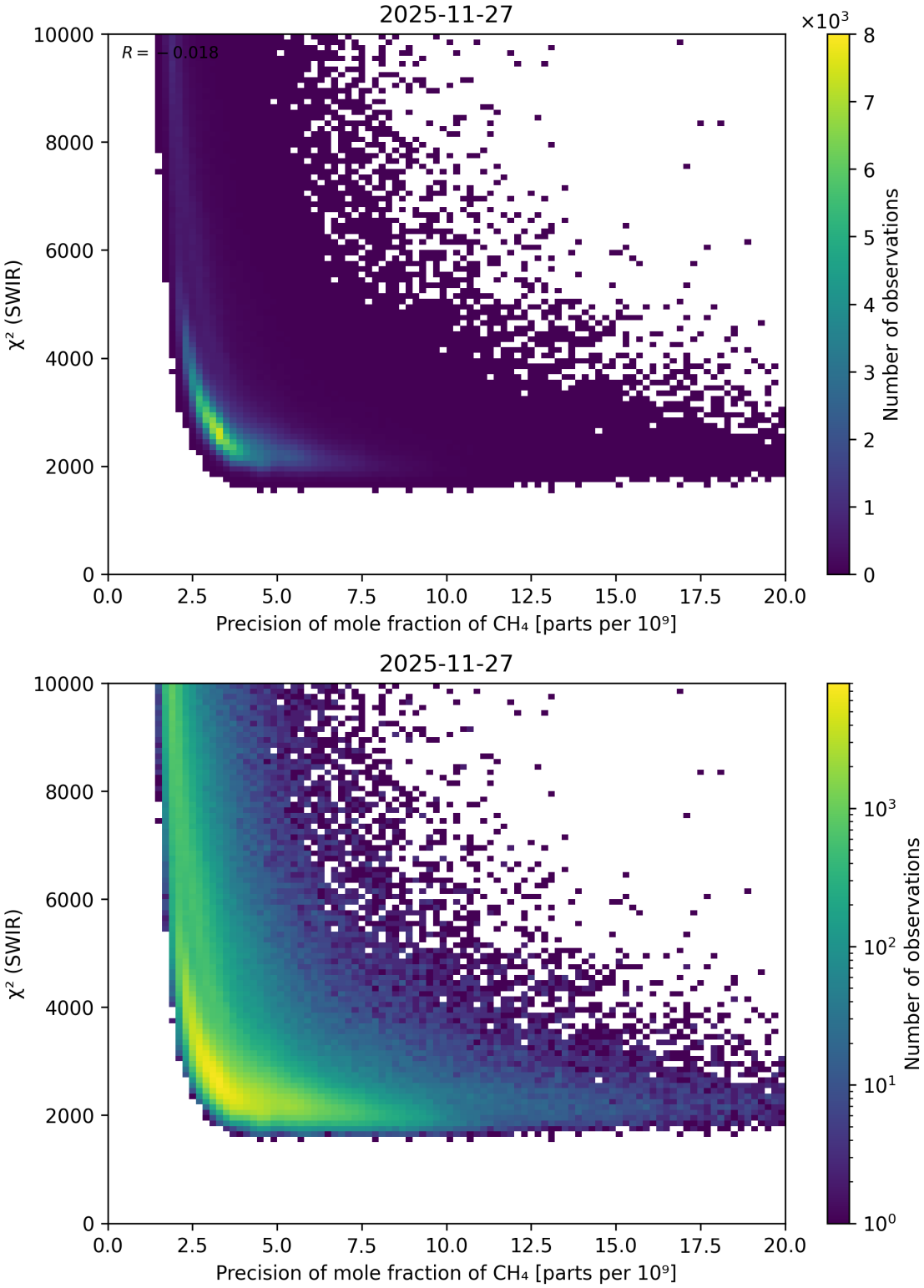

Figure 90: Scatter density plot of "Precision of mole fraction of CH_4" against "χ^2 (SWIR)" for 2025-11-26 to 2025-11-28.

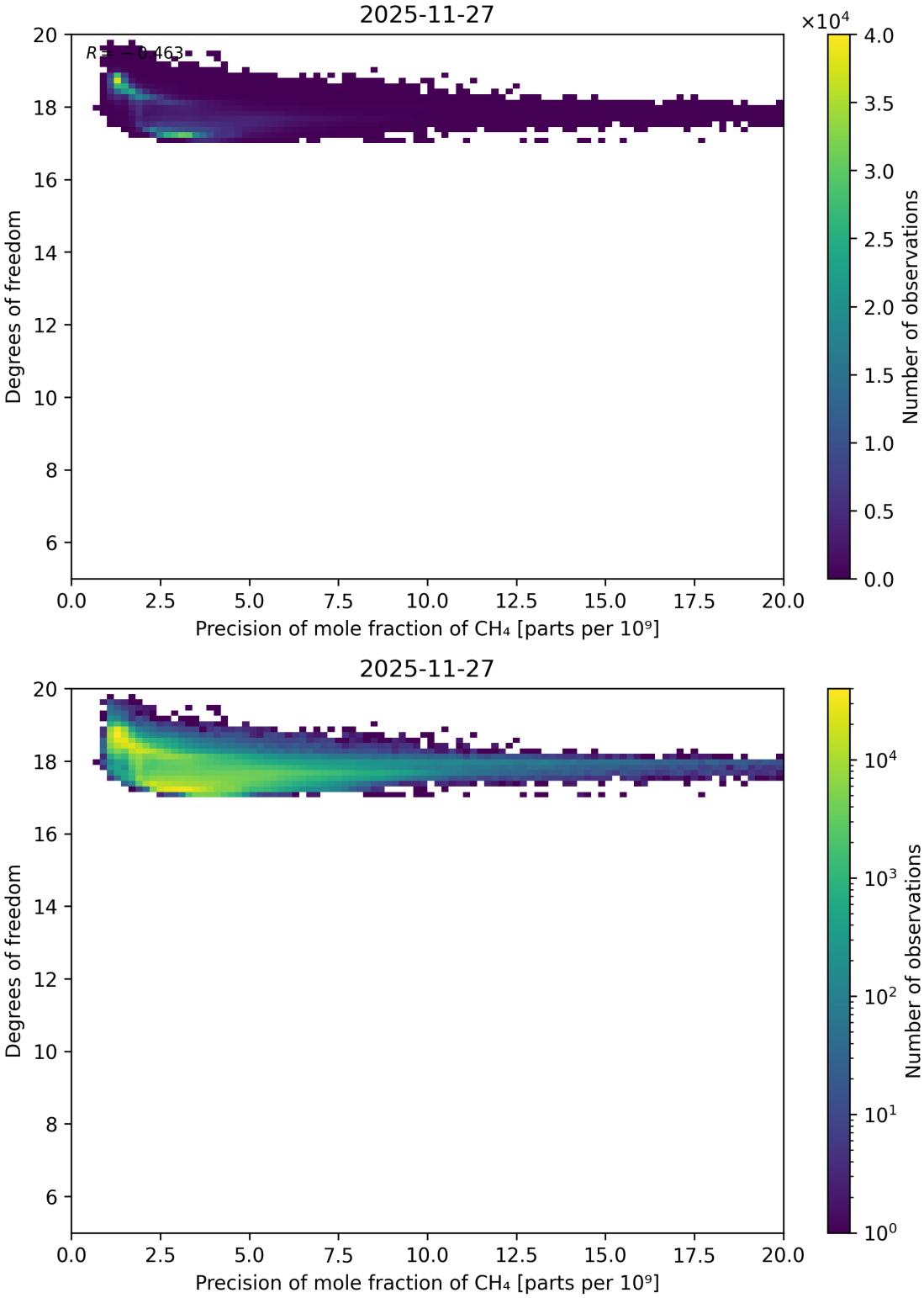

Figure 91: Scatter density plot of "Precision of mole fraction of CH_4" against "Degrees of freedom" for 2025-11-26 to 2025-11-28.

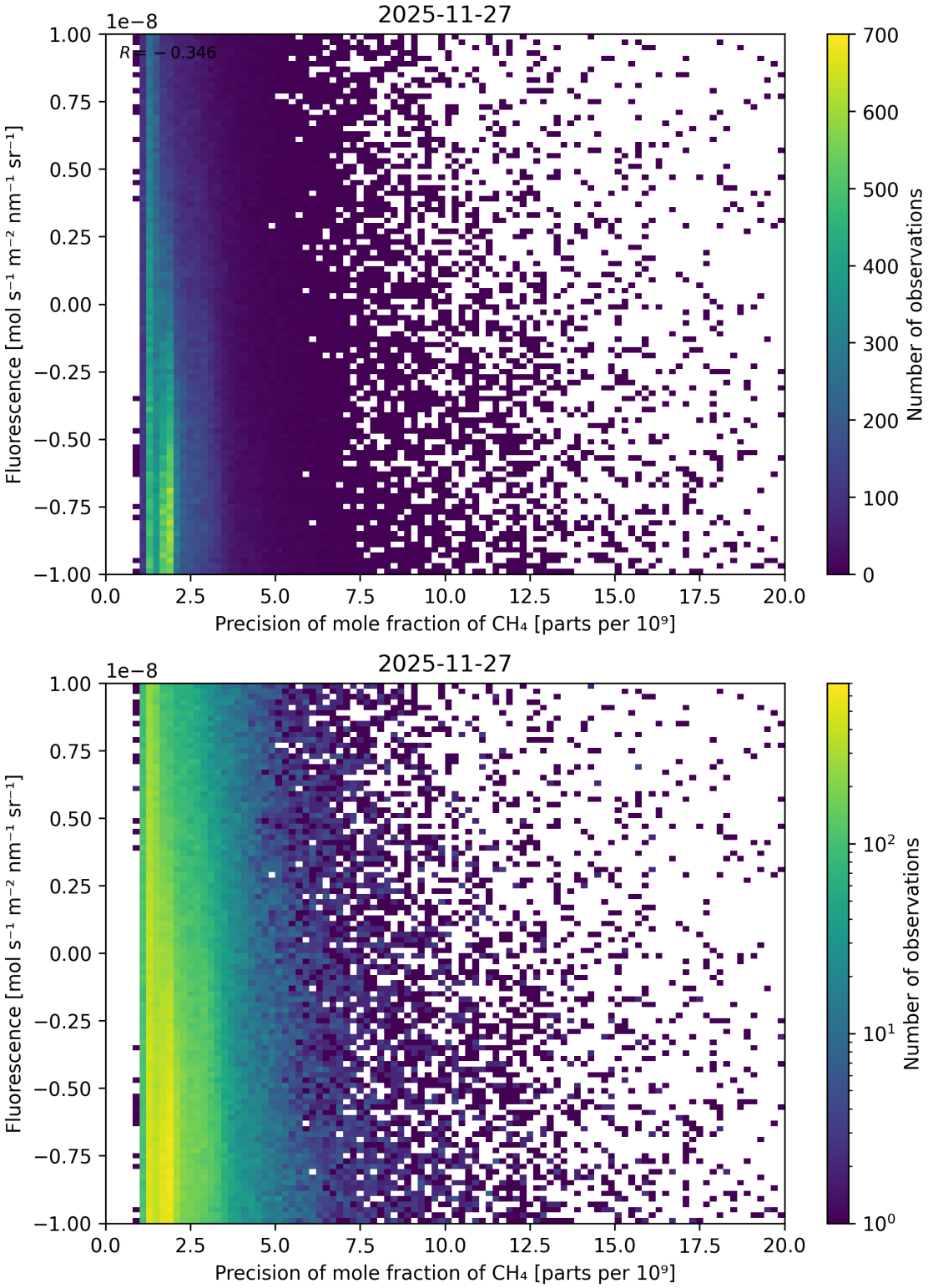

Figure 92: Scatter density plot of "Precision of mole fraction of CH_4" against "Fluorescence" for 2025-11-26 to 2025-11-28.

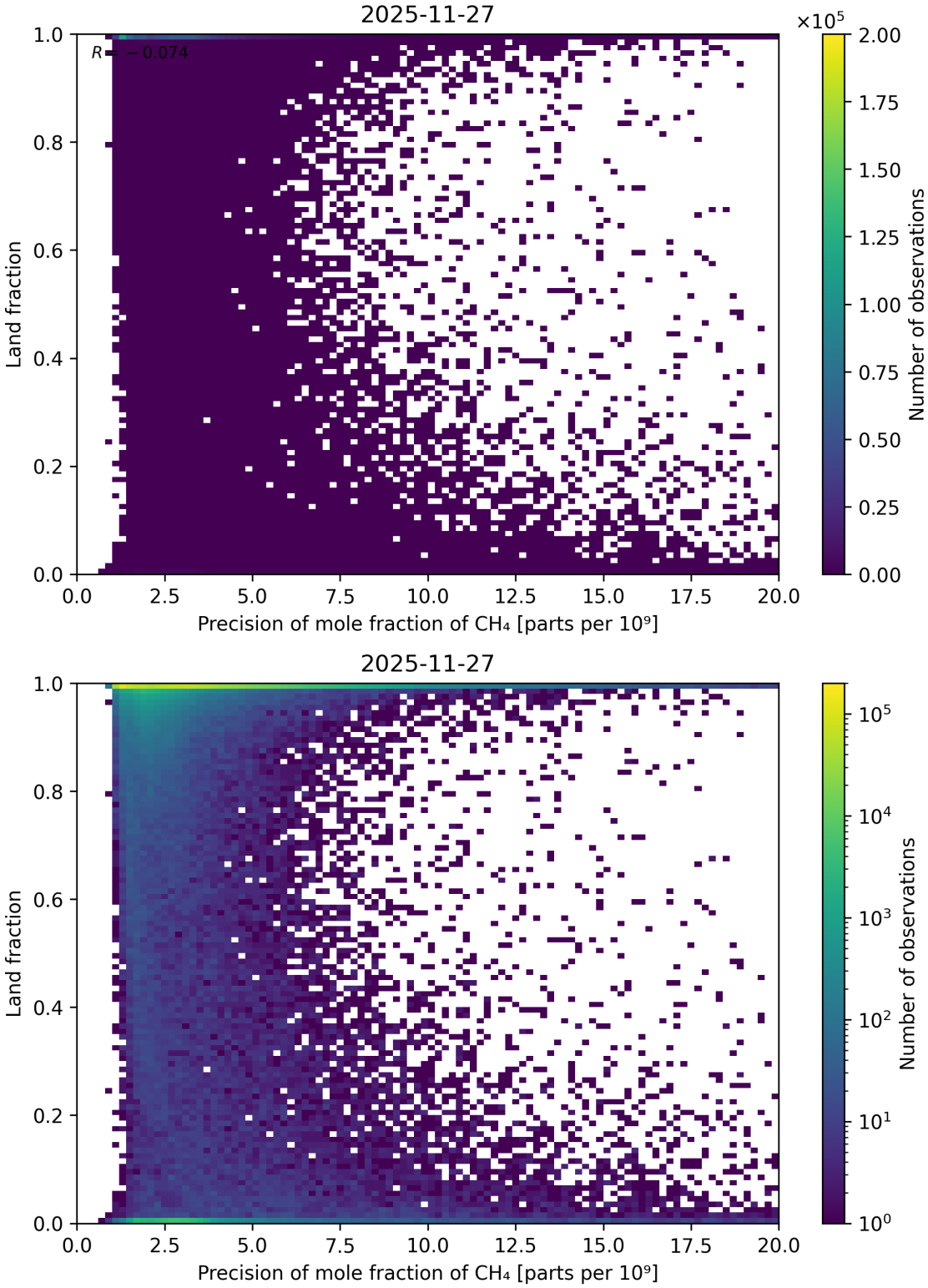

Figure 93: Scatter density plot of "Precision of mole fraction of CH_4" against "Land fraction" for 2025-11-26 to 2025-11-28.

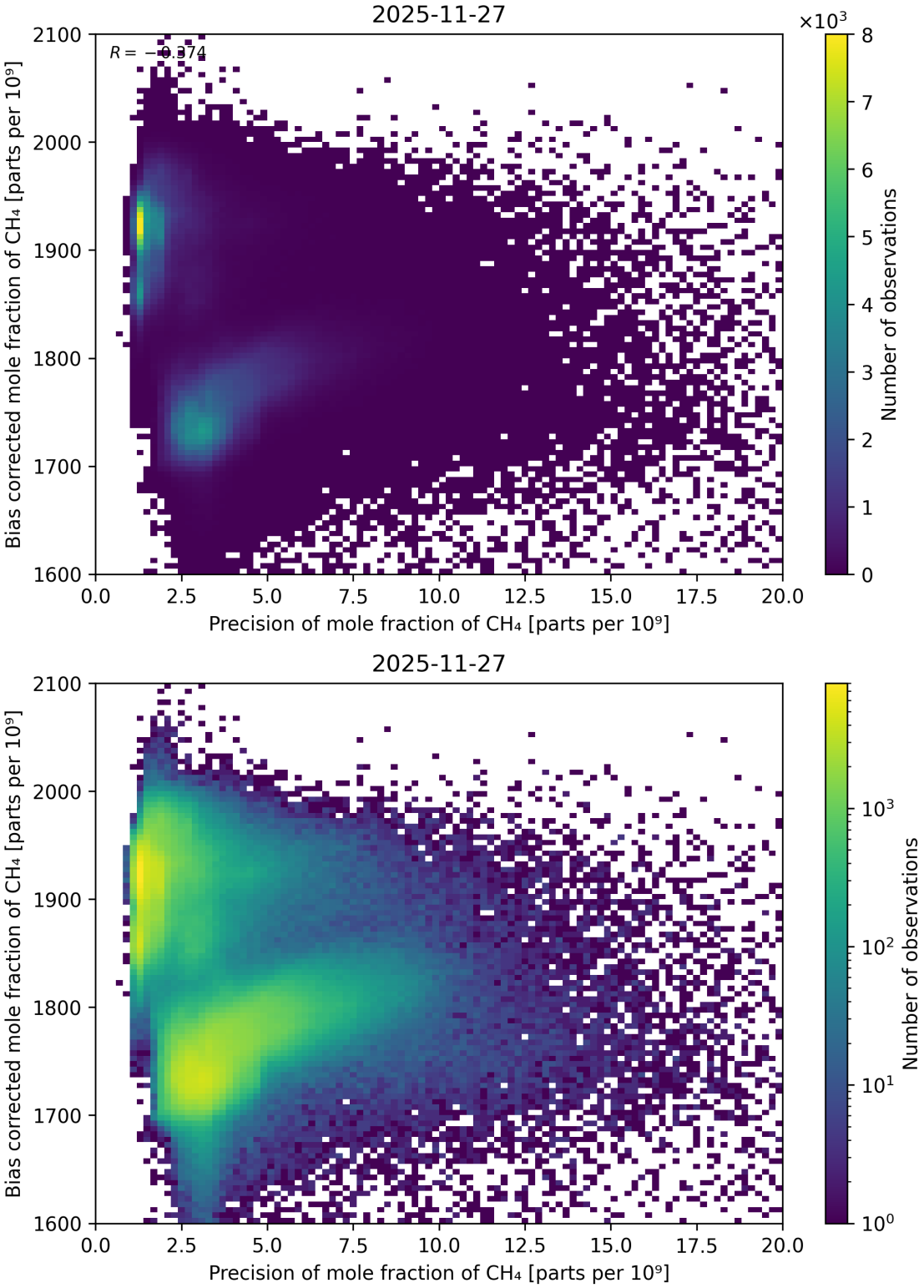

Figure 94: Scatter density plot of "Precision of mole fraction of CH_4" against "Bias corrected mole fraction of CH_4" for 2025-11-26 to 2025-11-28.

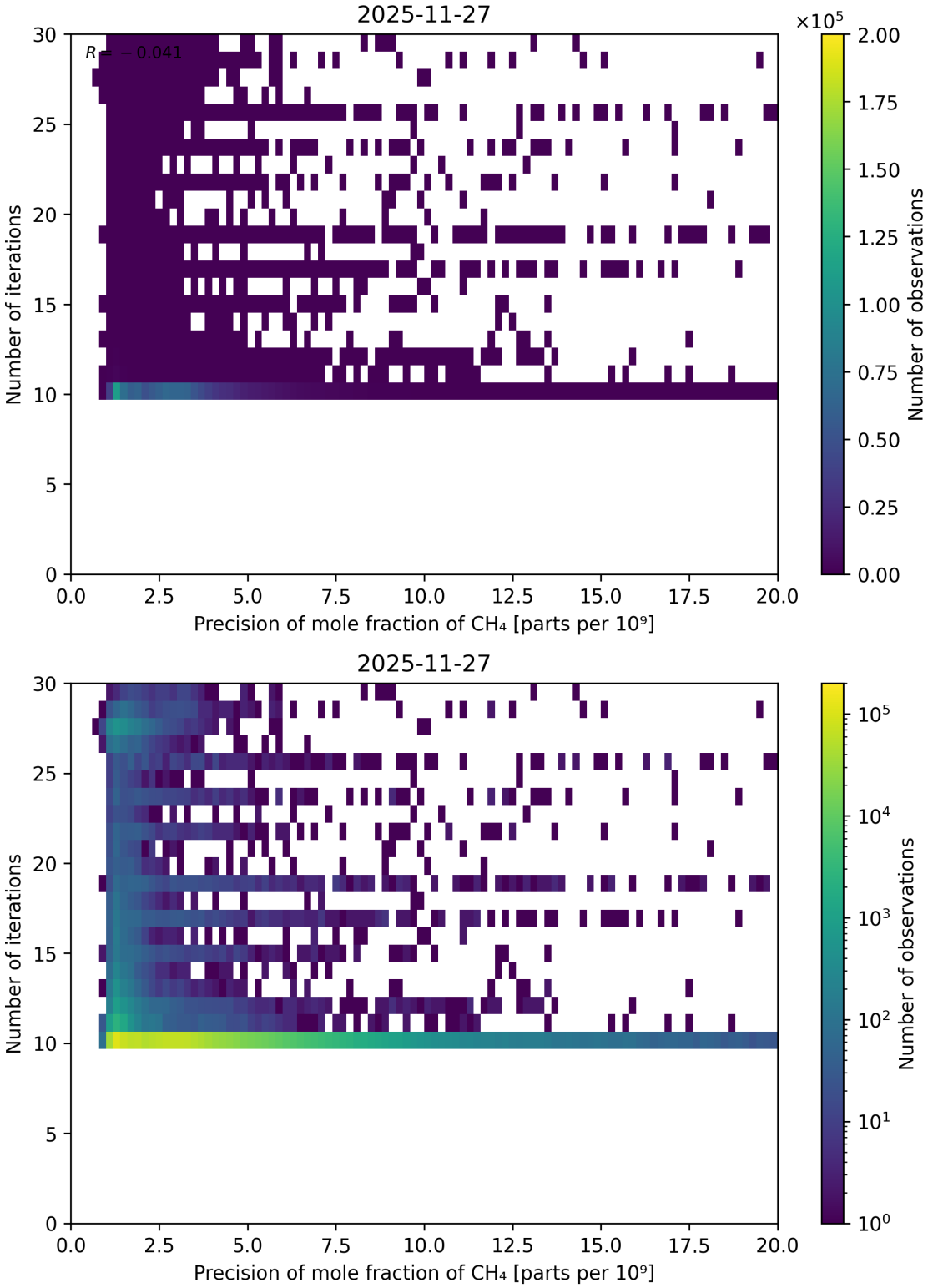

Figure 95: Scatter density plot of "Precision of mole fraction of CH_4" against "Number of iterations" for 2025-11-26 to 2025-11-28.

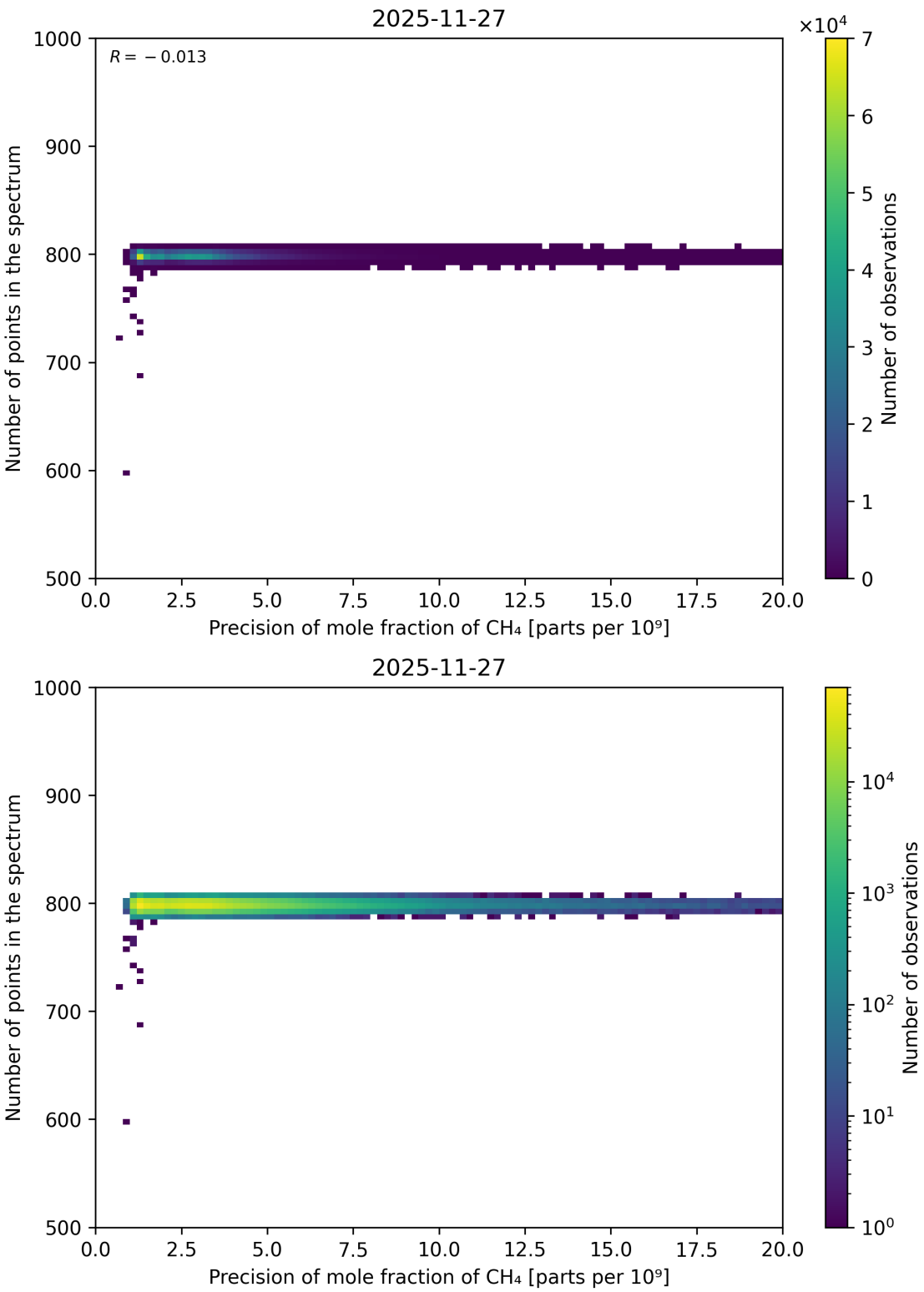

Figure 96: Scatter density plot of "Precision of mole fraction of CH_4" against "Number of points in the spectrum" for 2025-11-26 to 2025-11-28.

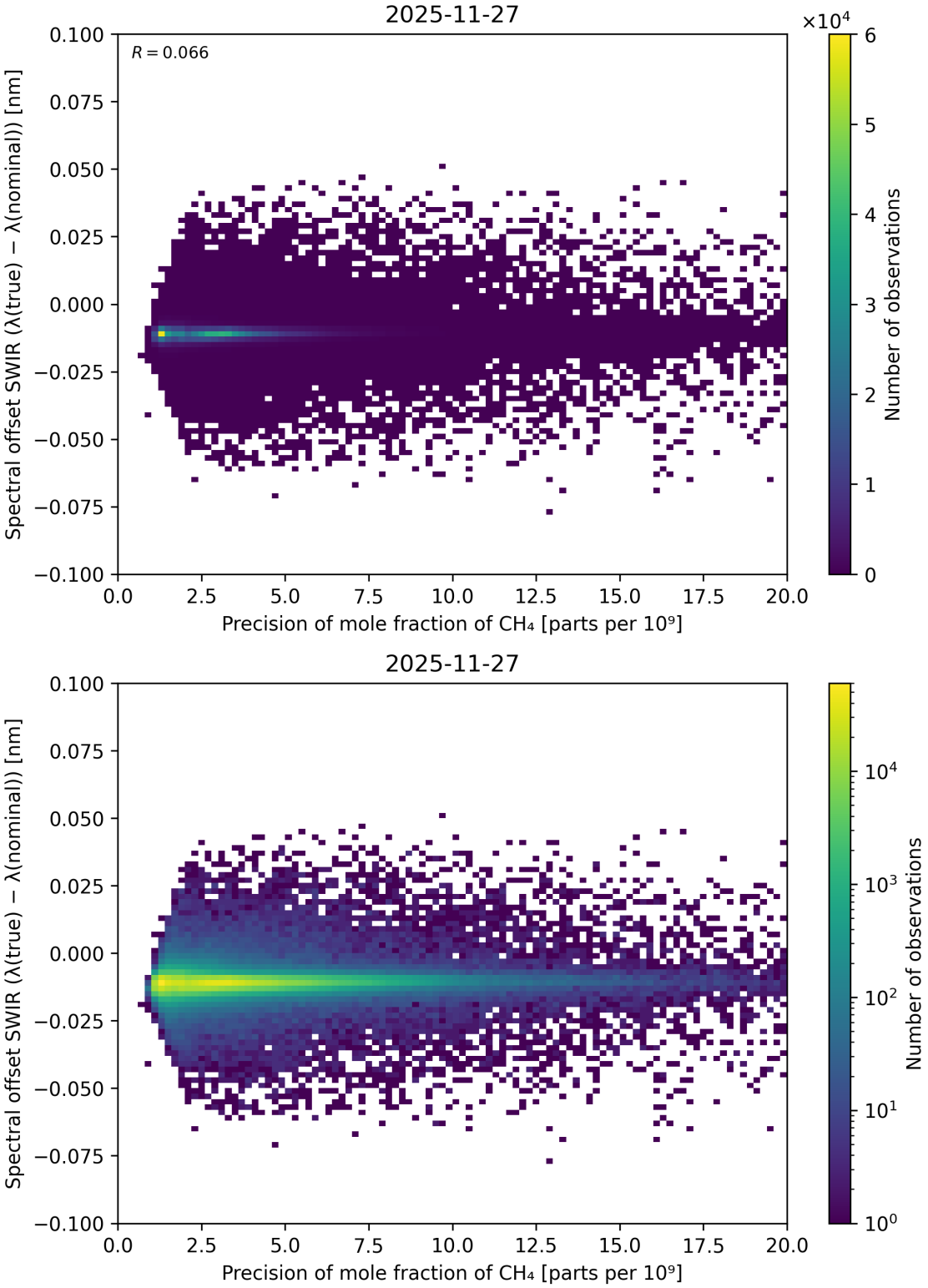

Figure 97: Scatter density plot of "Precision of mole fraction of CH_4" against "Spectral offset SWIR ($\lambda_{\text{true}} - \lambda_{\text{nominal}}$)" for 2025-11-26 to 2025-11-28.

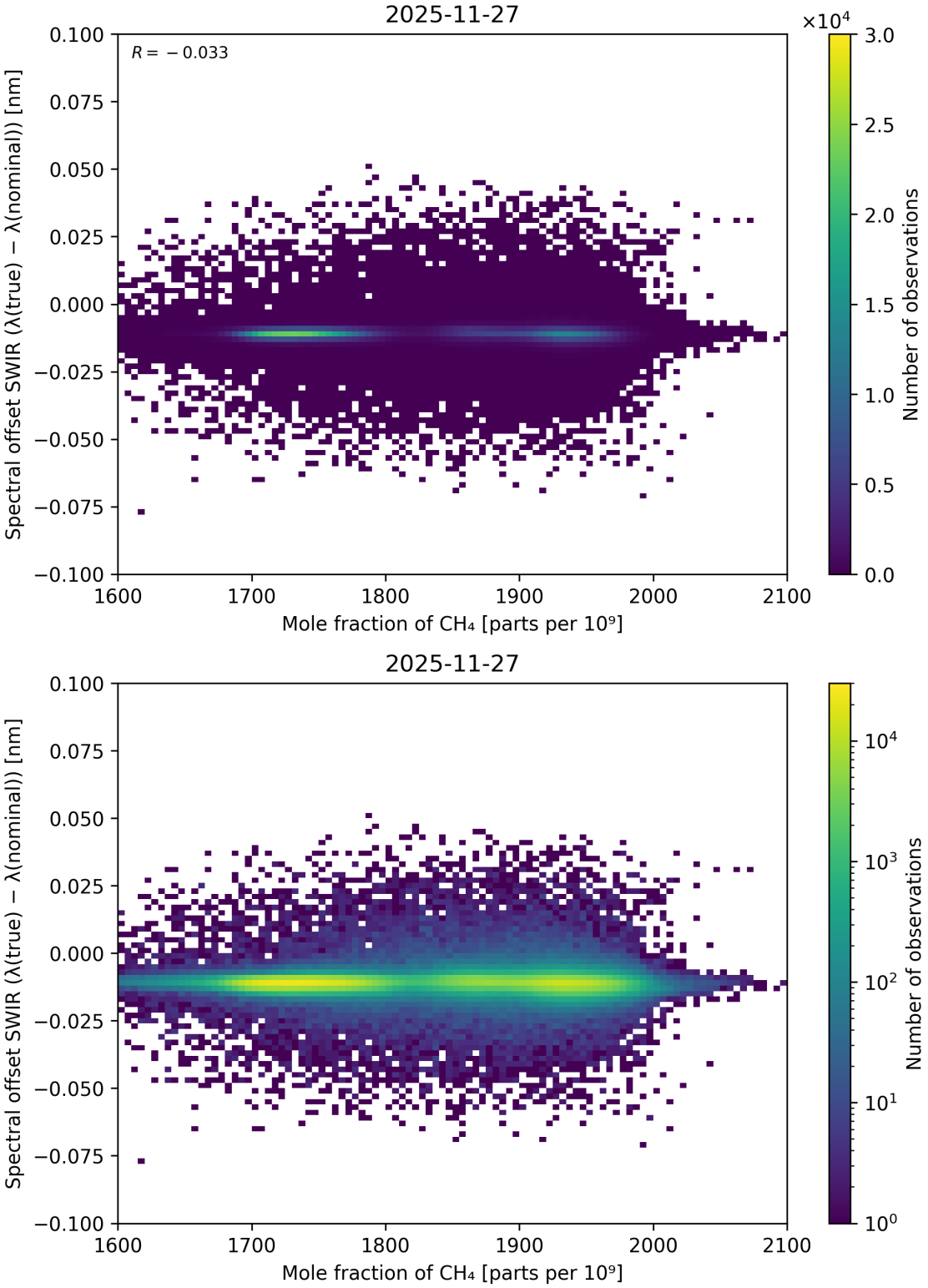

Figure 98: Scatter density plot of "Mole fraction of CH_4" against "Spectral offset SWIR ($\lambda_{\text{true}} - \lambda_{\text{nominal}}$)" for 2025-11-26 to 2025-11-28.

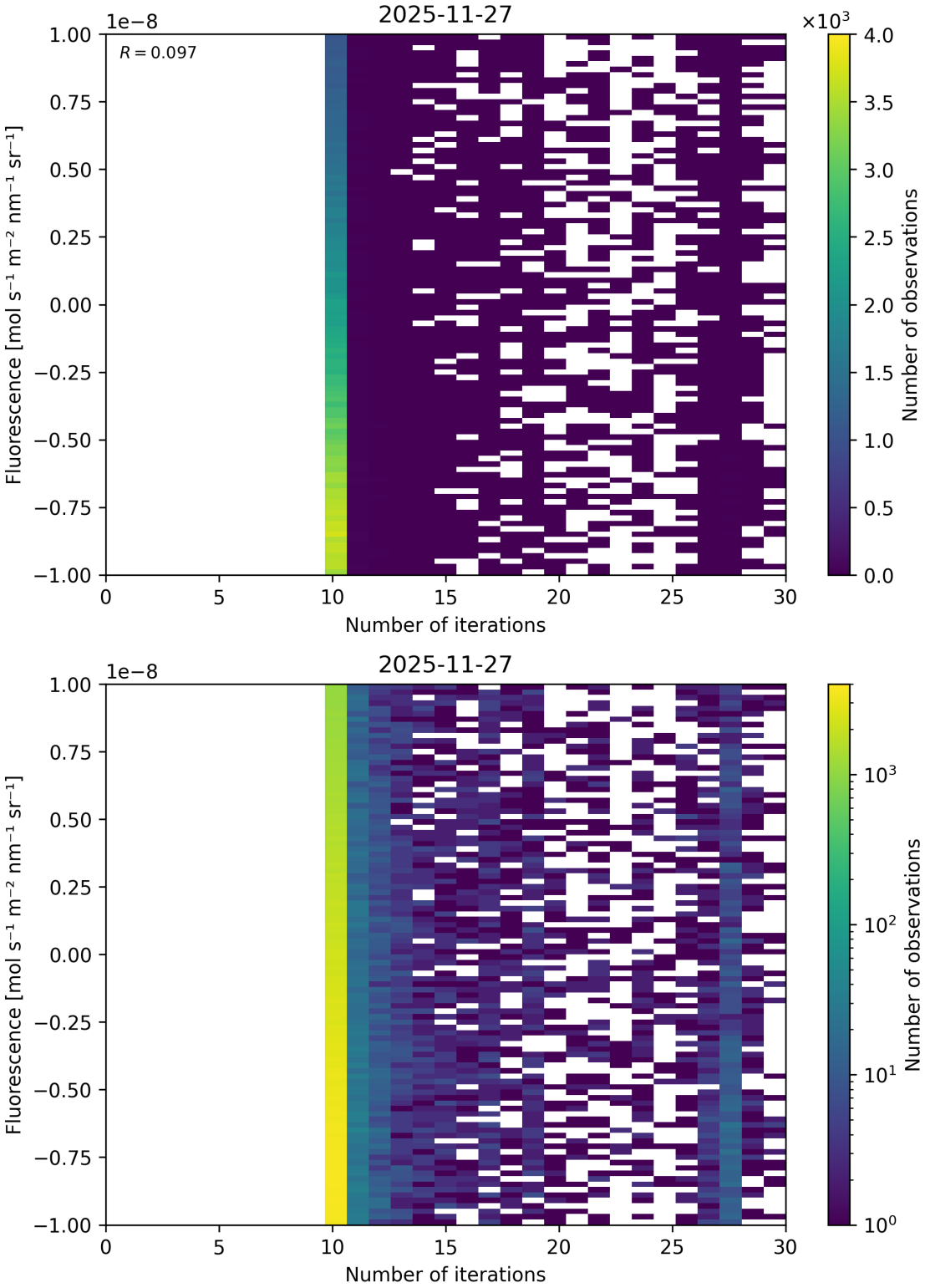

Figure 99: Scatter density plot of “Number of iterations” against “Fluorescence” for 2025-11-26 to 2025-11-28.

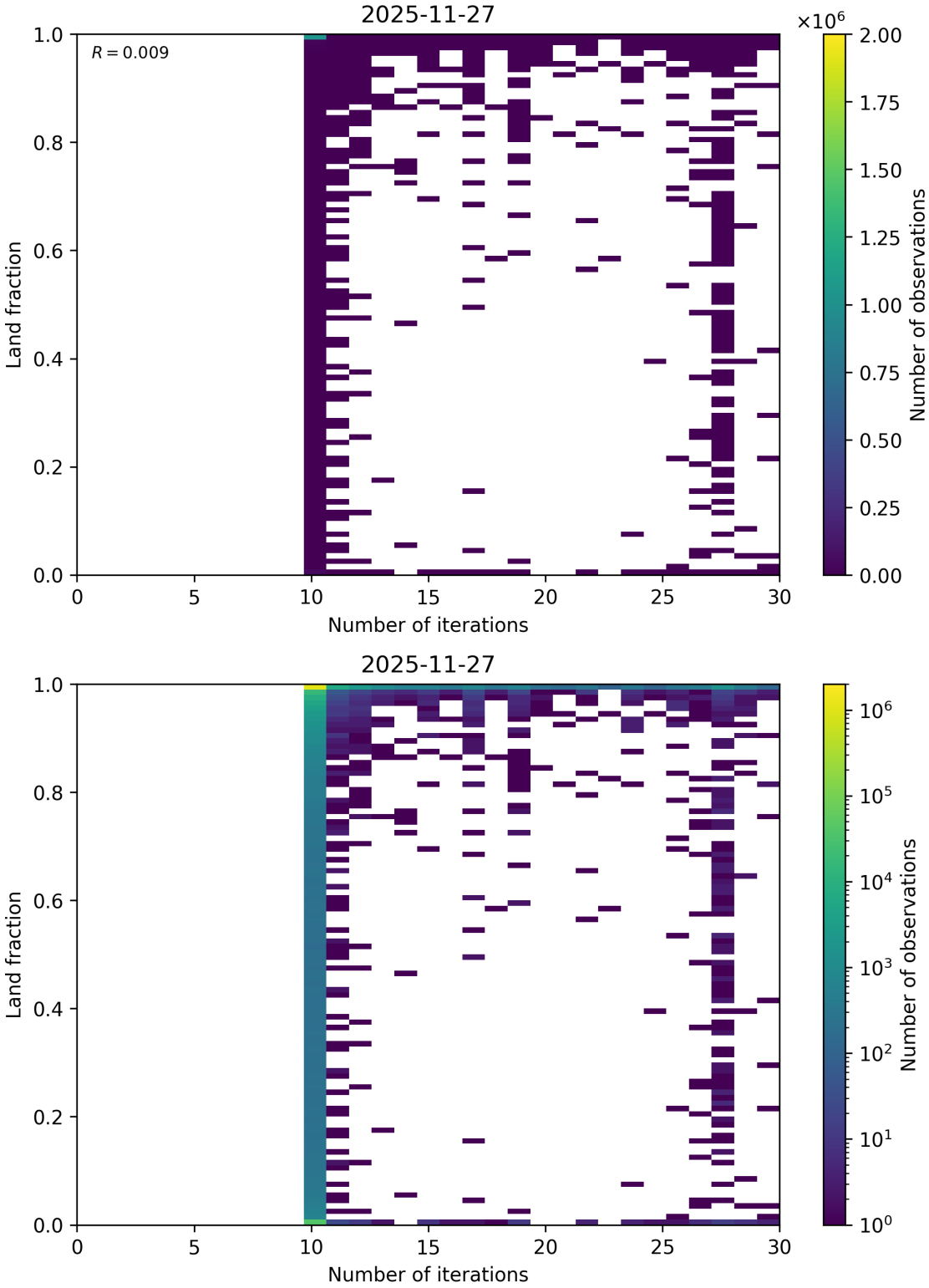

Figure 100: Scatter density plot of “Number of iterations” against “Land fraction” for 2025-11-26 to 2025-11-28.

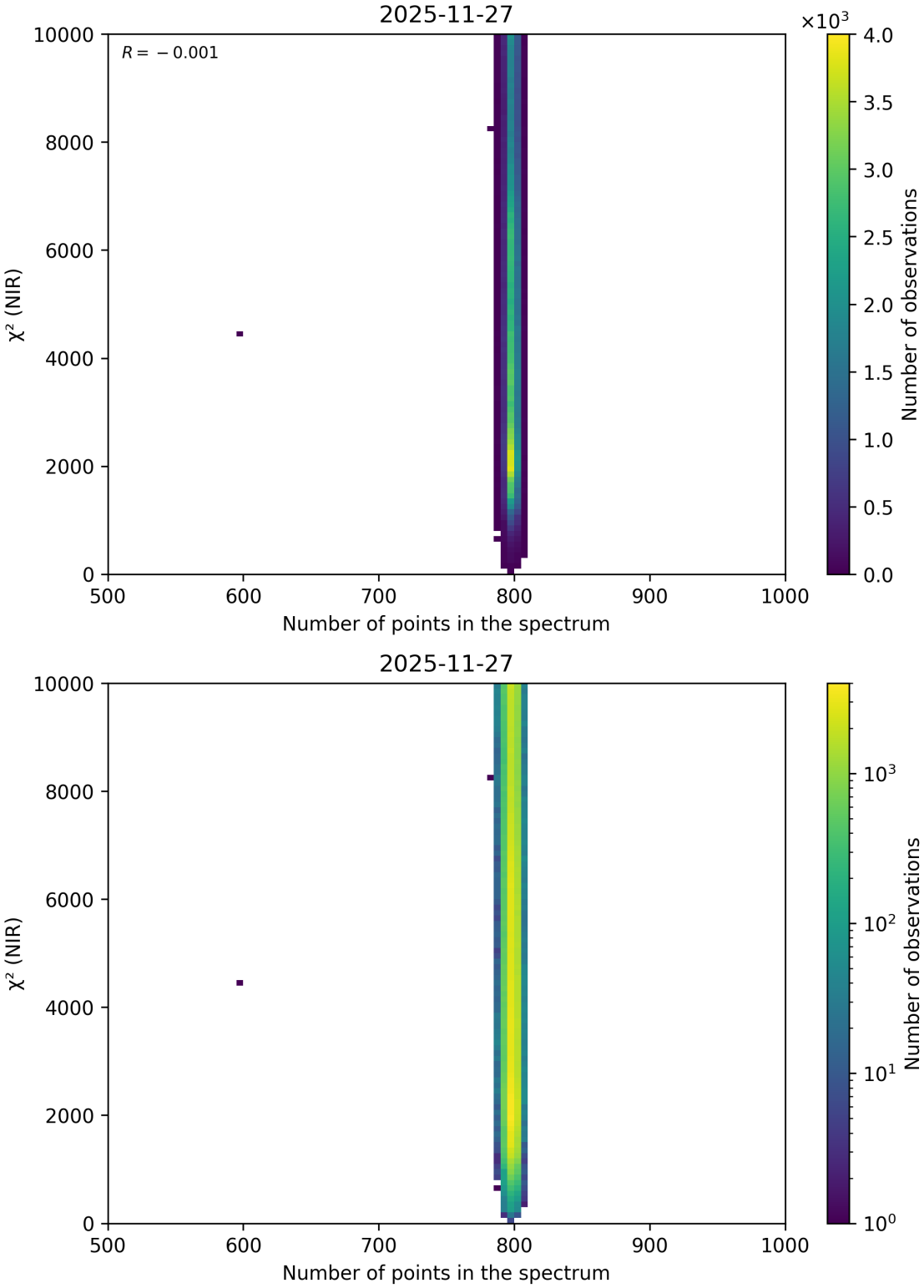

Figure 101: Scatter density plot of "Number of points in the spectrum" against "χ^2 (NIR)" for 2025-11-26 to 2025-11-28.

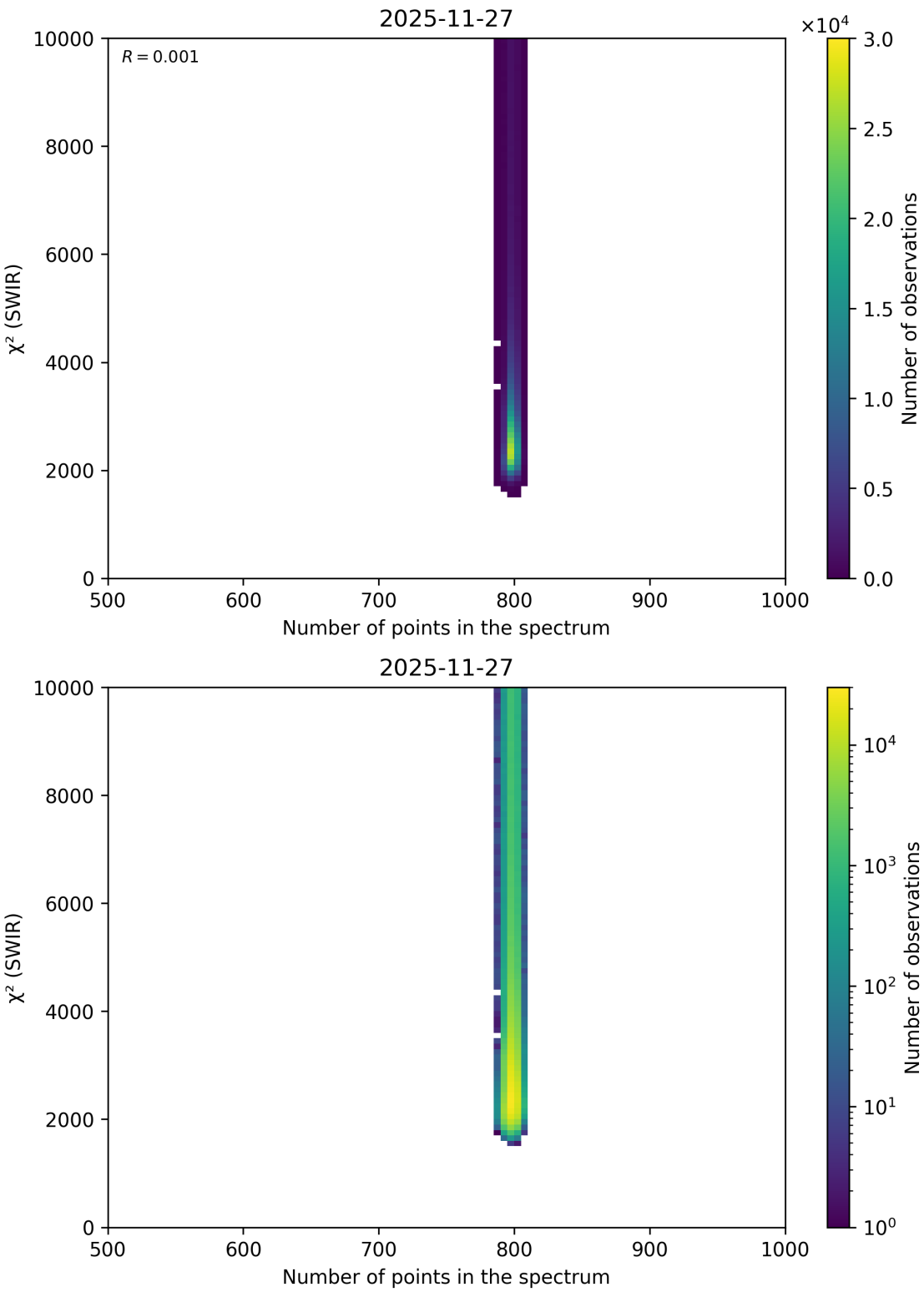

Figure 102: Scatter density plot of "Number of points in the spectrum" against "χ^2 (SWIR)" for 2025-11-26 to 2025-11-28.

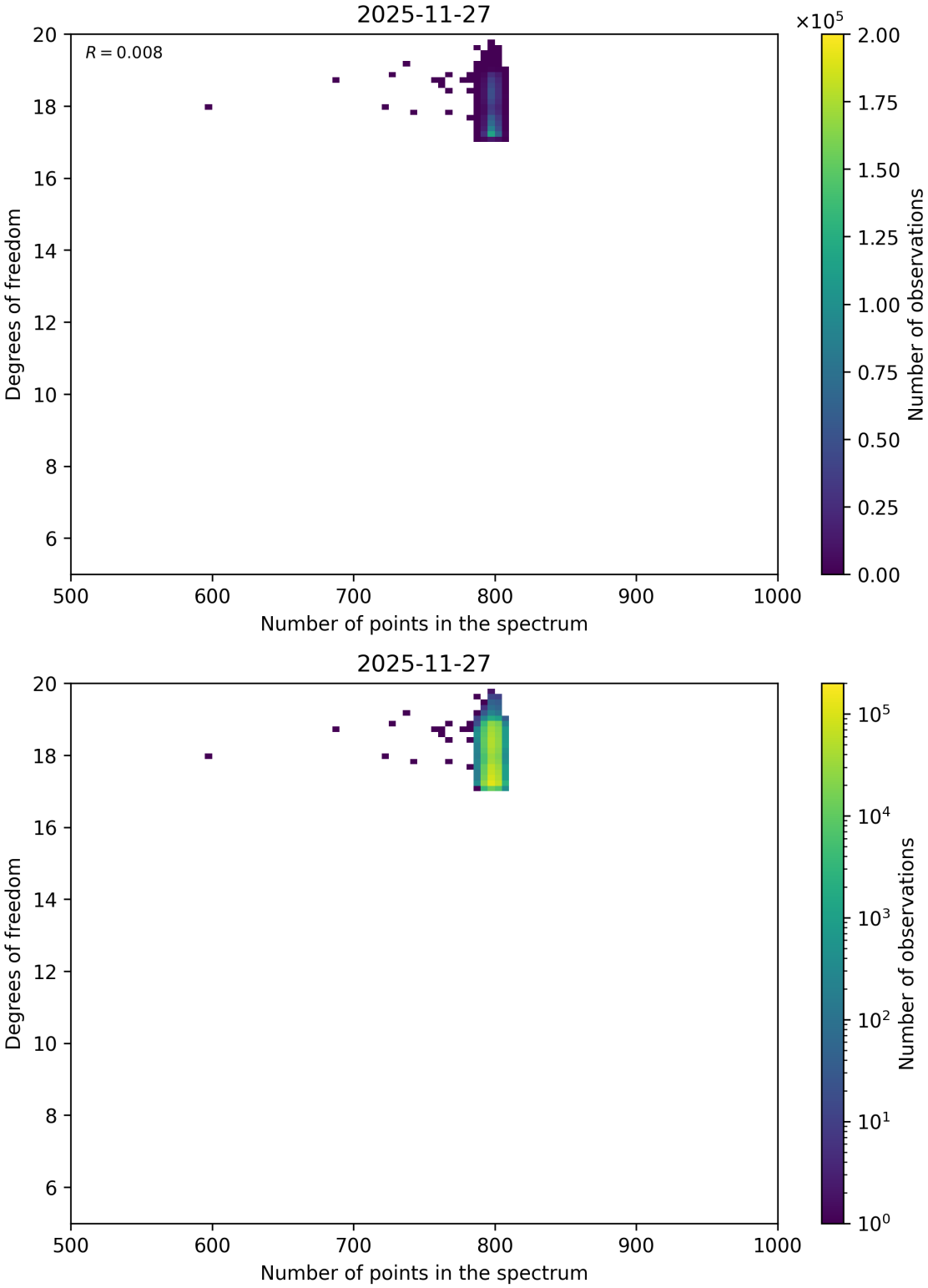

Figure 103: Scatter density plot of "Number of points in the spectrum" against "Degrees of freedom" for 2025-11-26 to 2025-11-28.

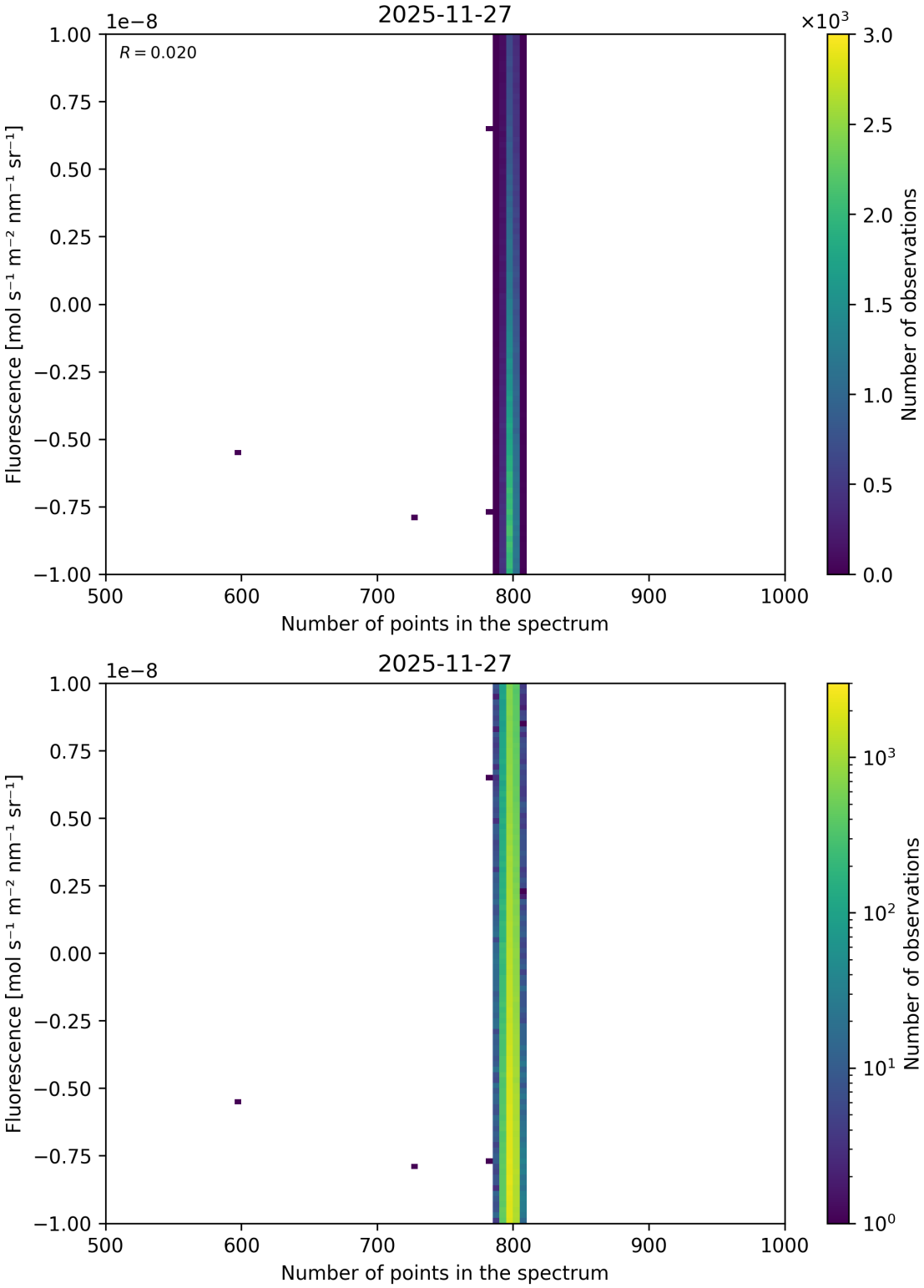

Figure 104: Scatter density plot of “Number of points in the spectrum” against “Fluorescence” for 2025-11-26 to 2025-11-28.

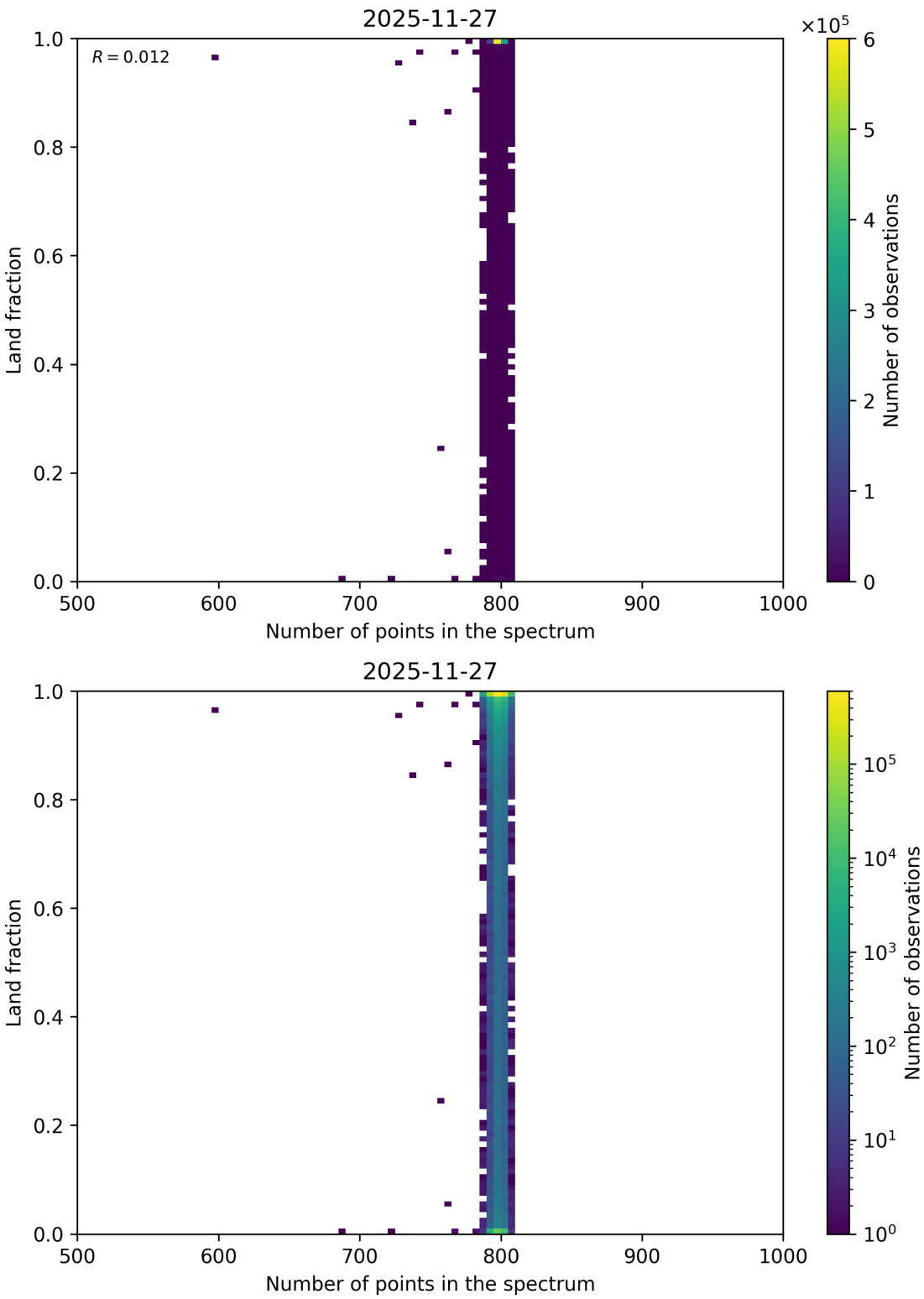

Figure 105: Scatter density plot of "Number of points in the spectrum" against "Land fraction" for 2025-11-26 to 2025-11-28.

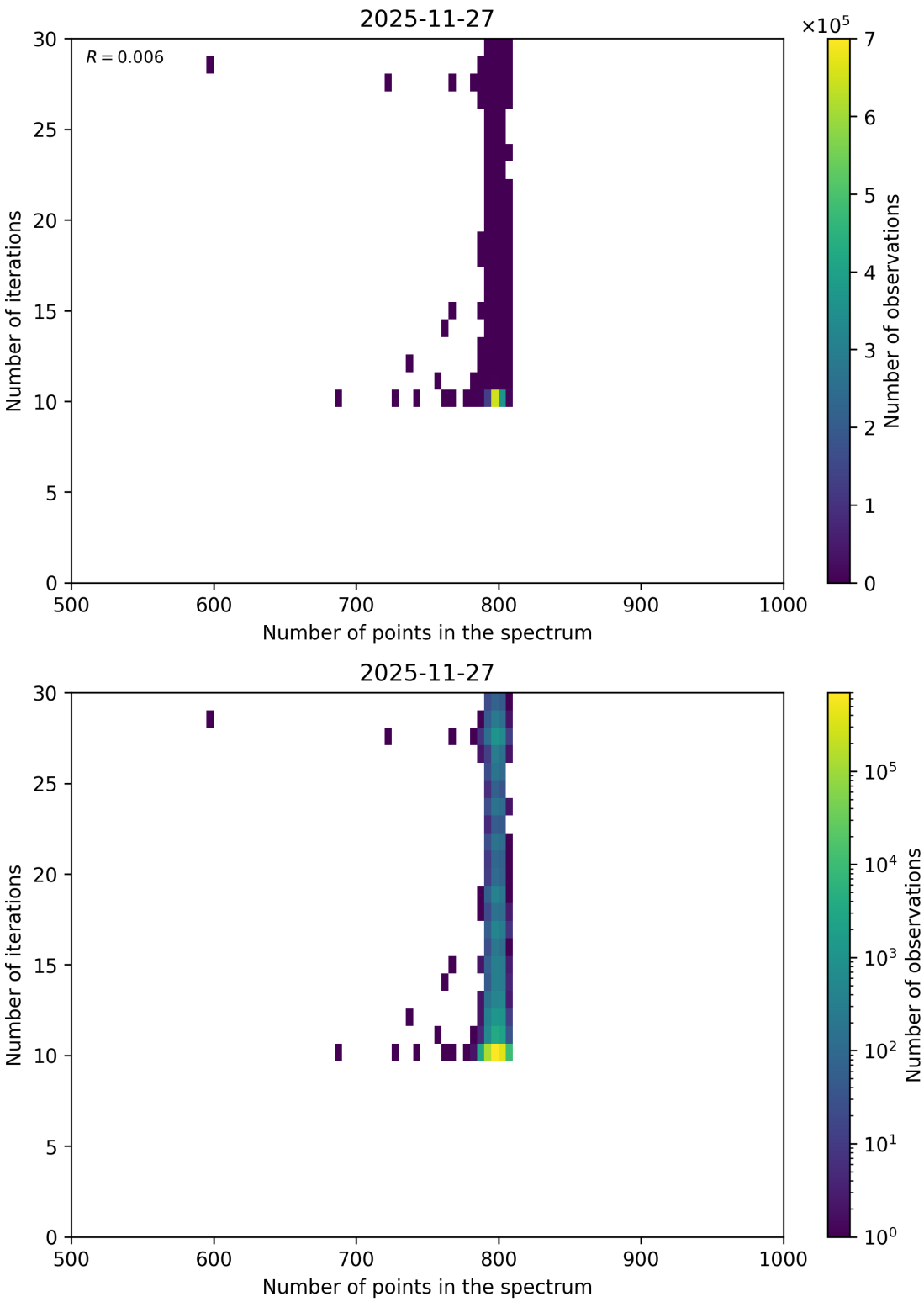

Figure 106: Scatter density plot of "Number of points in the spectrum" against "Number of iterations" for 2025-11-26 to 2025-11-28.

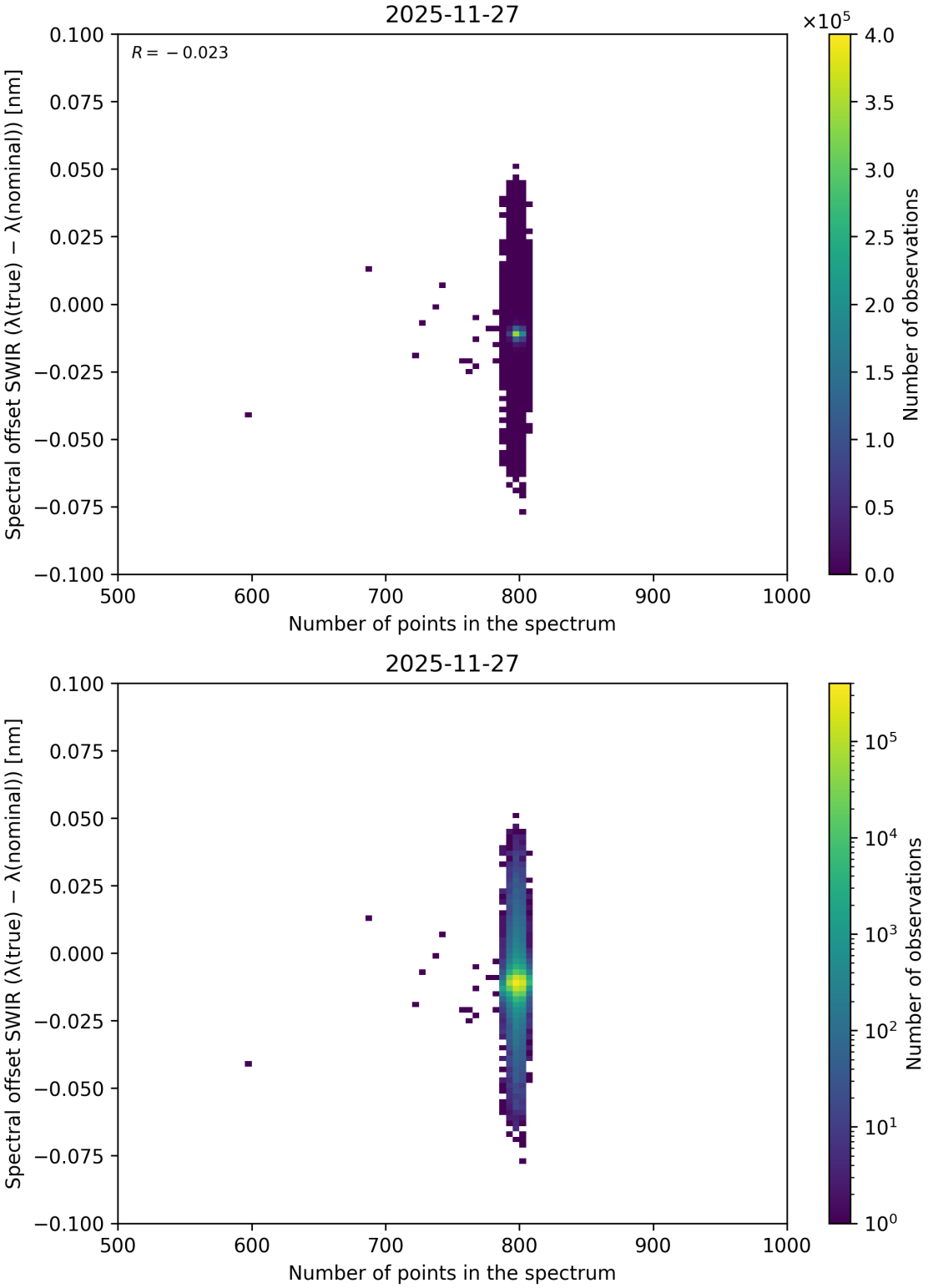

Figure 107: Scatter density plot of "Number of points in the spectrum" against "Spectral offset SWIR ($\lambda_{\text{true}} - \lambda_{\text{nominal}}$)" for 2025-11-26 to 2025-11-28.

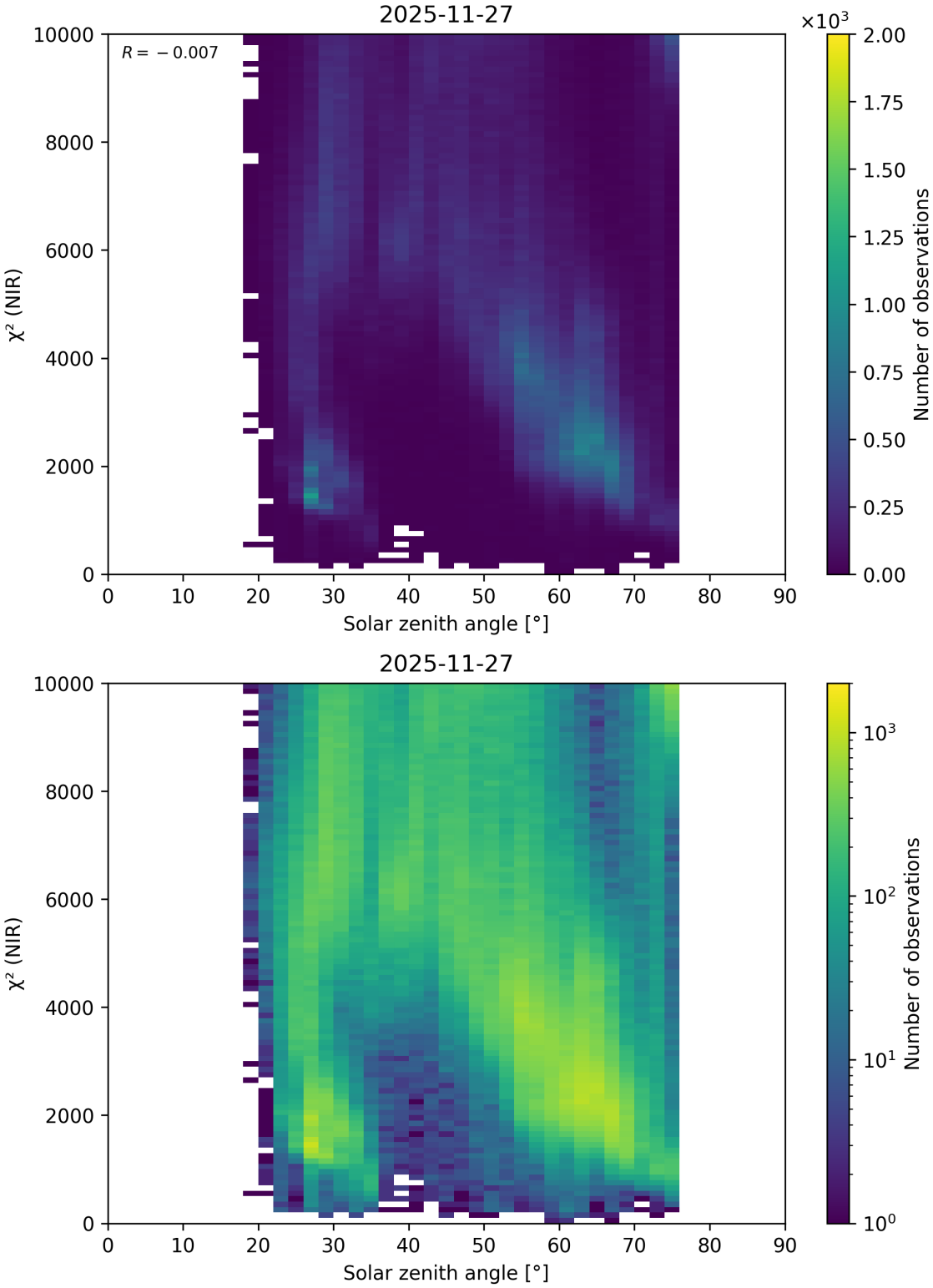

Figure 108: Scatter density plot of “Solar zenith angle” against “χ^2 (NIR)” for 2025-11-26 to 2025-11-28.

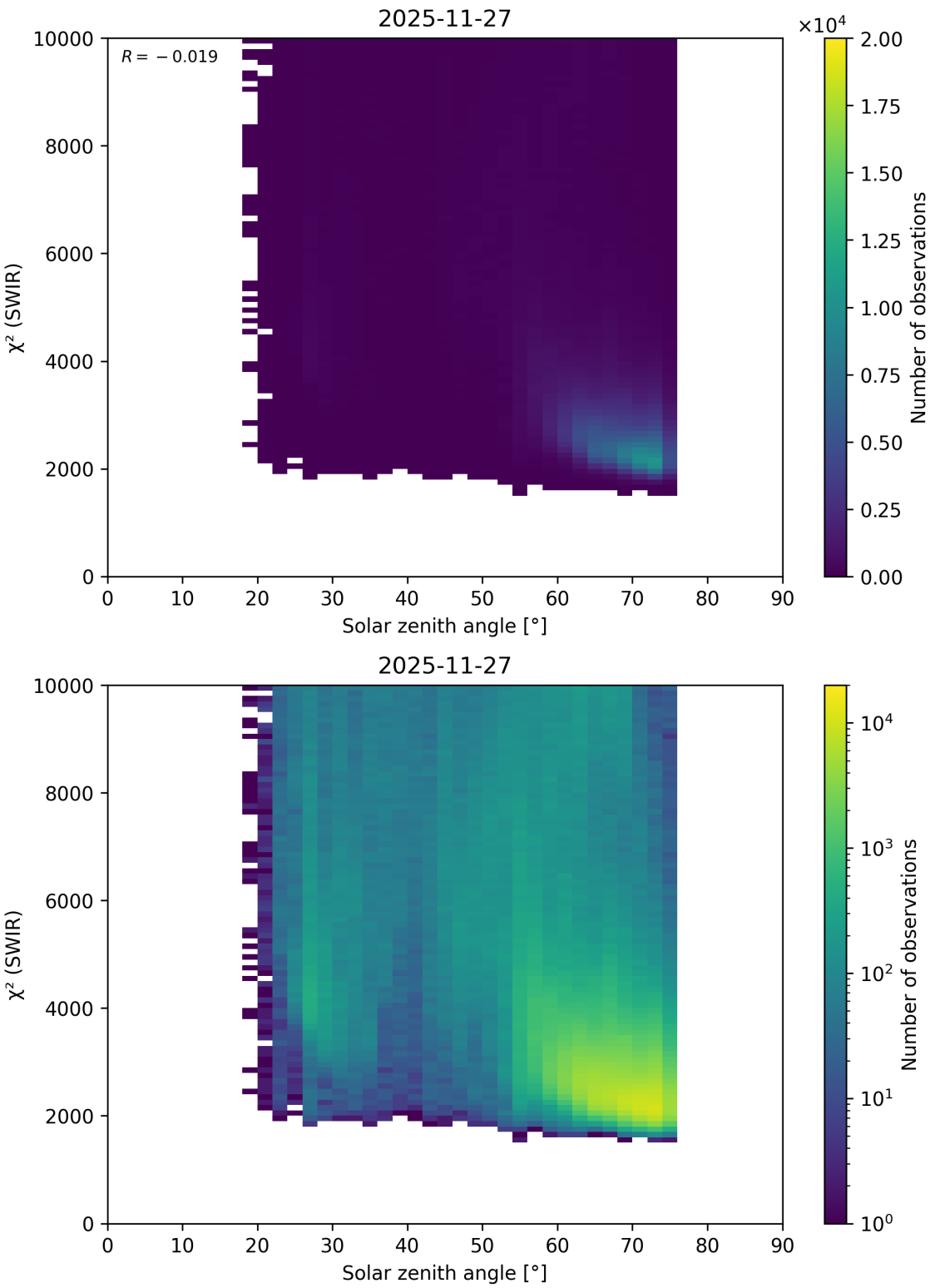

Figure 109: Scatter density plot of "Solar zenith angle" against "χ^2 (SWIR)" for 2025-11-26 to 2025-11-28.

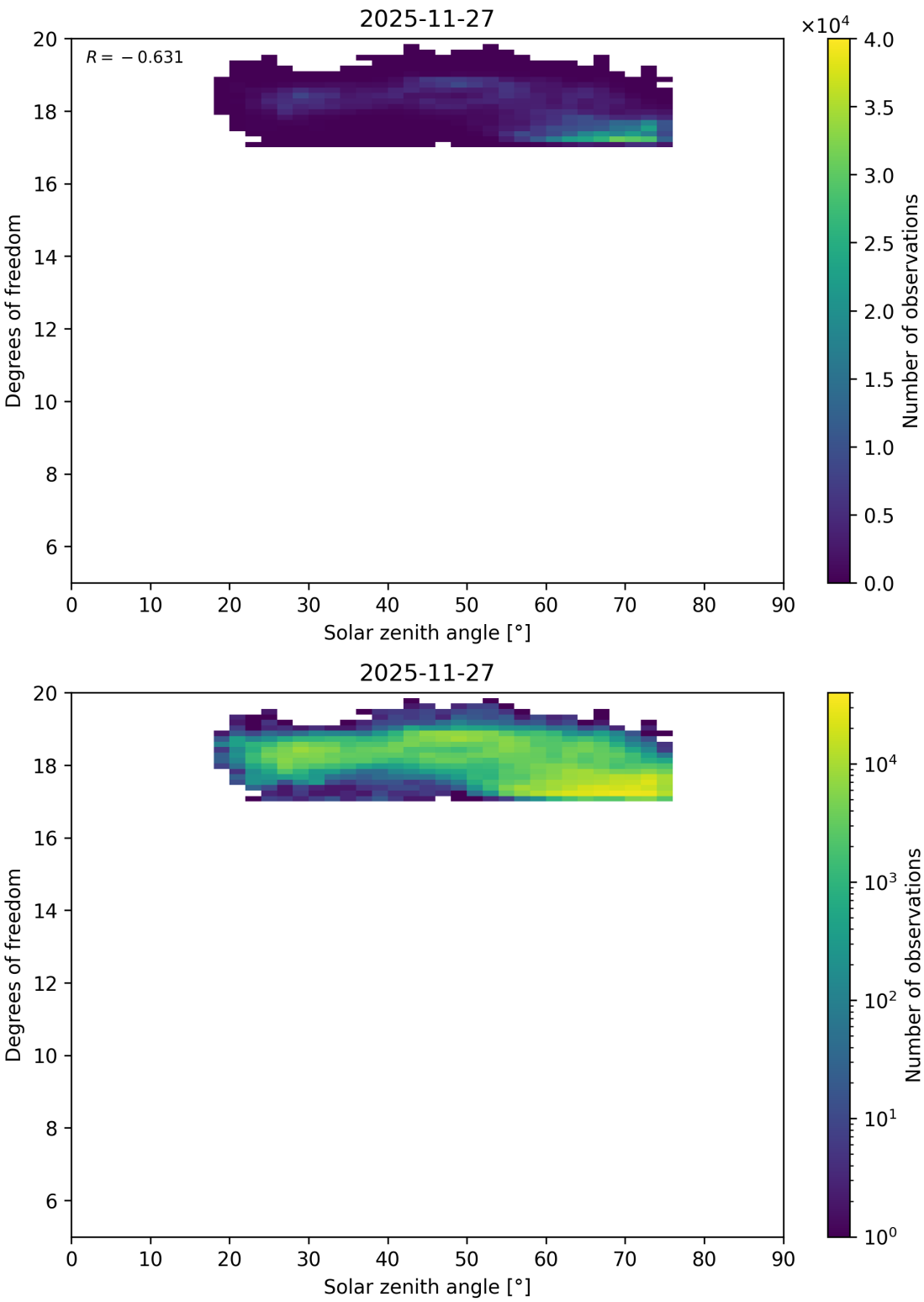

Figure 110: Scatter density plot of “Solar zenith angle” against “Degrees of freedom” for 2025-11-26 to 2025-11-28.

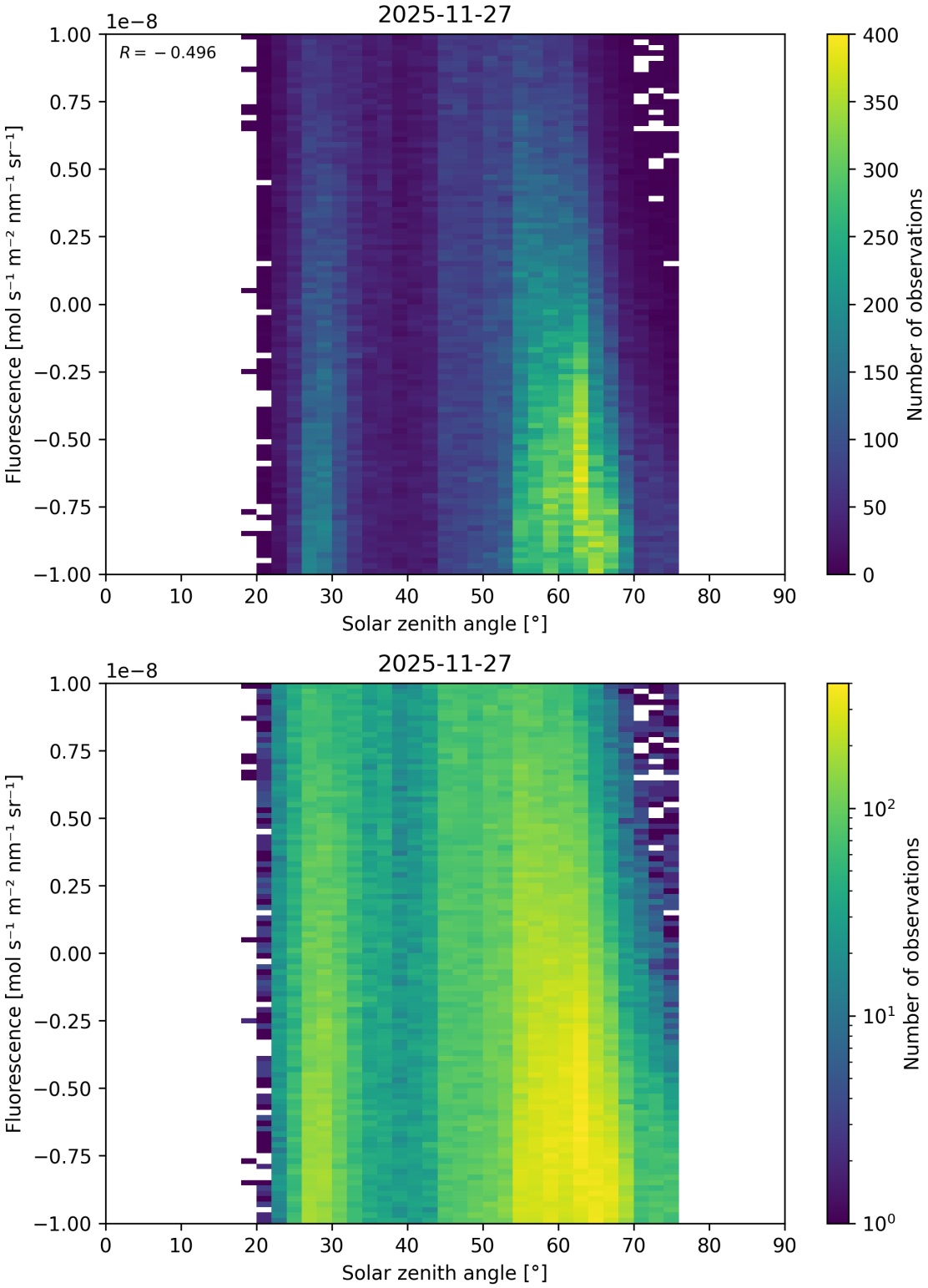

Figure 111: Scatter density plot of “Solar zenith angle” against “Fluorescence” for 2025-11-26 to 2025-11-28.

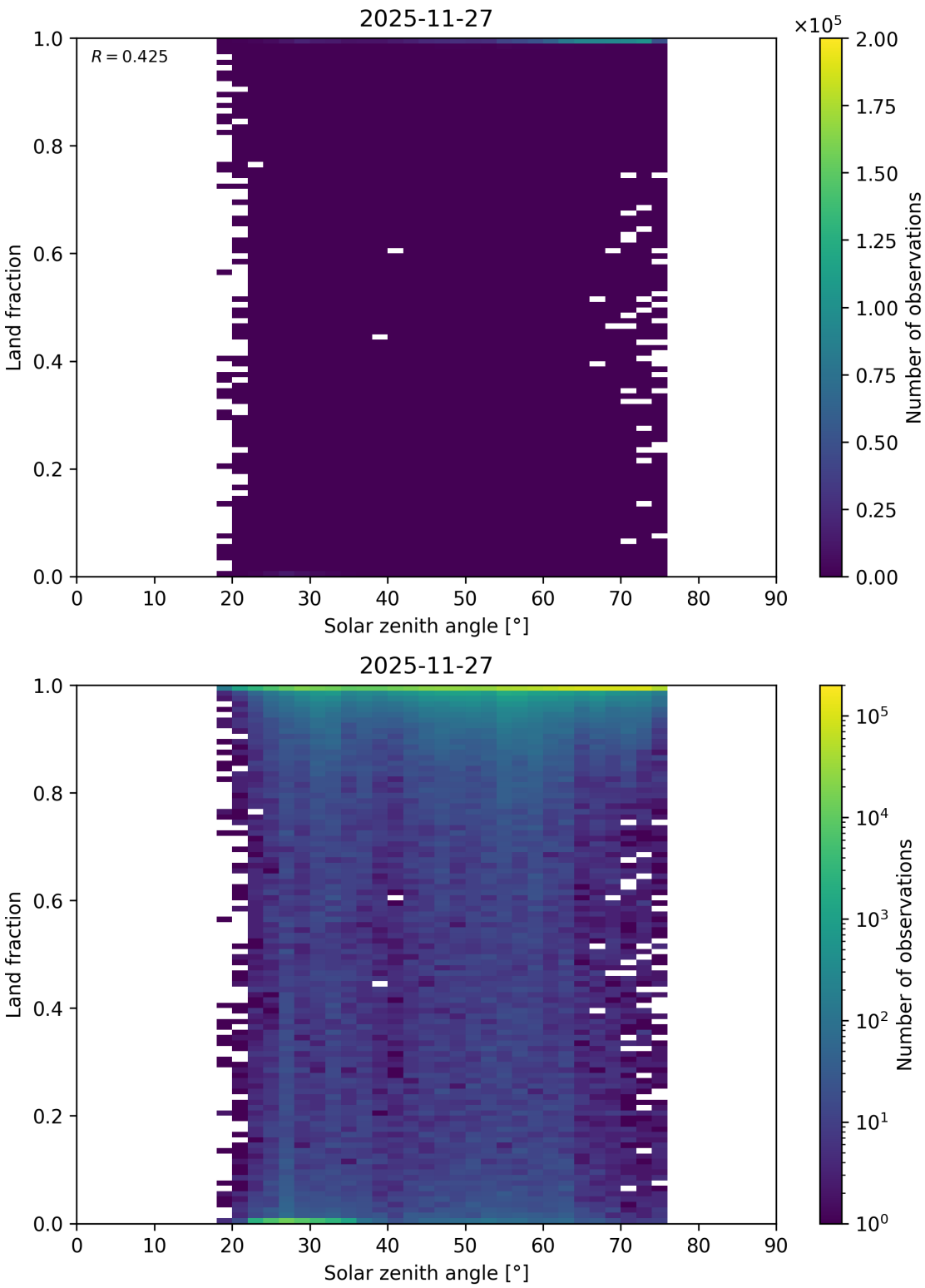

Figure 112: Scatter density plot of “Solar zenith angle” against “Land fraction” for 2025-11-26 to 2025-11-28.

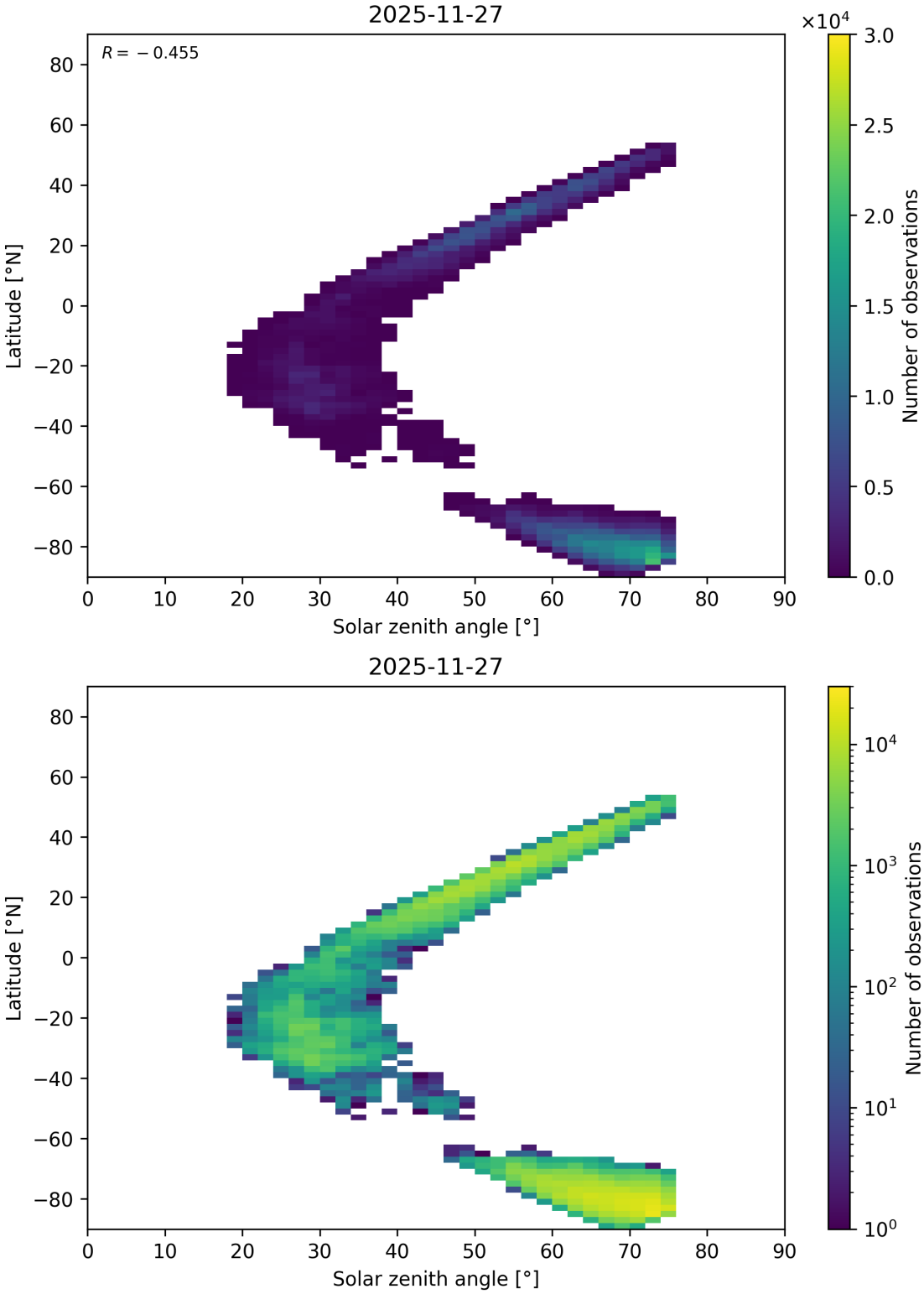

Figure 113: Scatter density plot of “Solar zenith angle” against “Latitude” for 2025-11-26 to 2025-11-28.

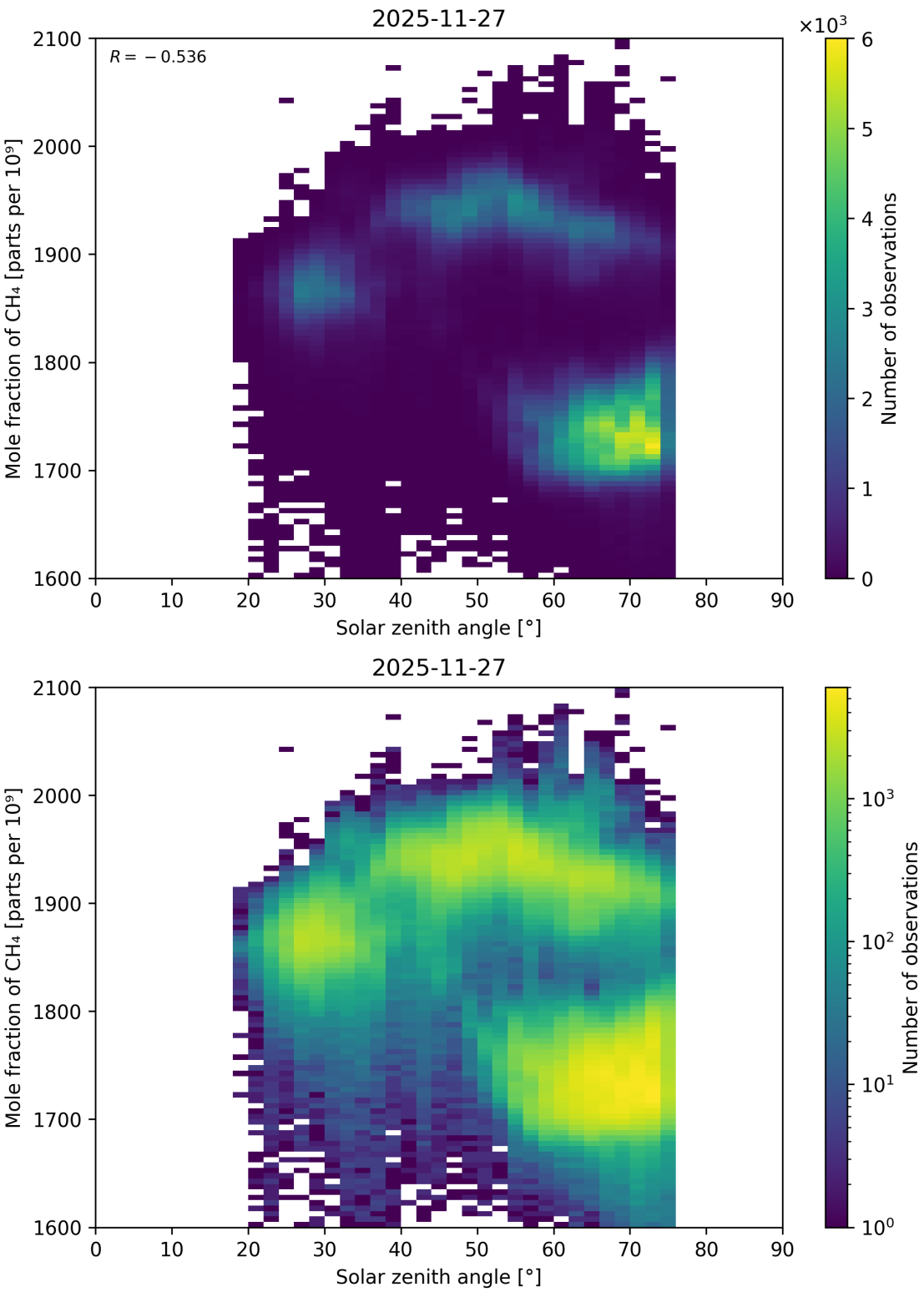

Figure 114: Scatter density plot of “Solar zenith angle” against “Mole fraction of CH_4” for 2025-11-26 to 2025-11-28.

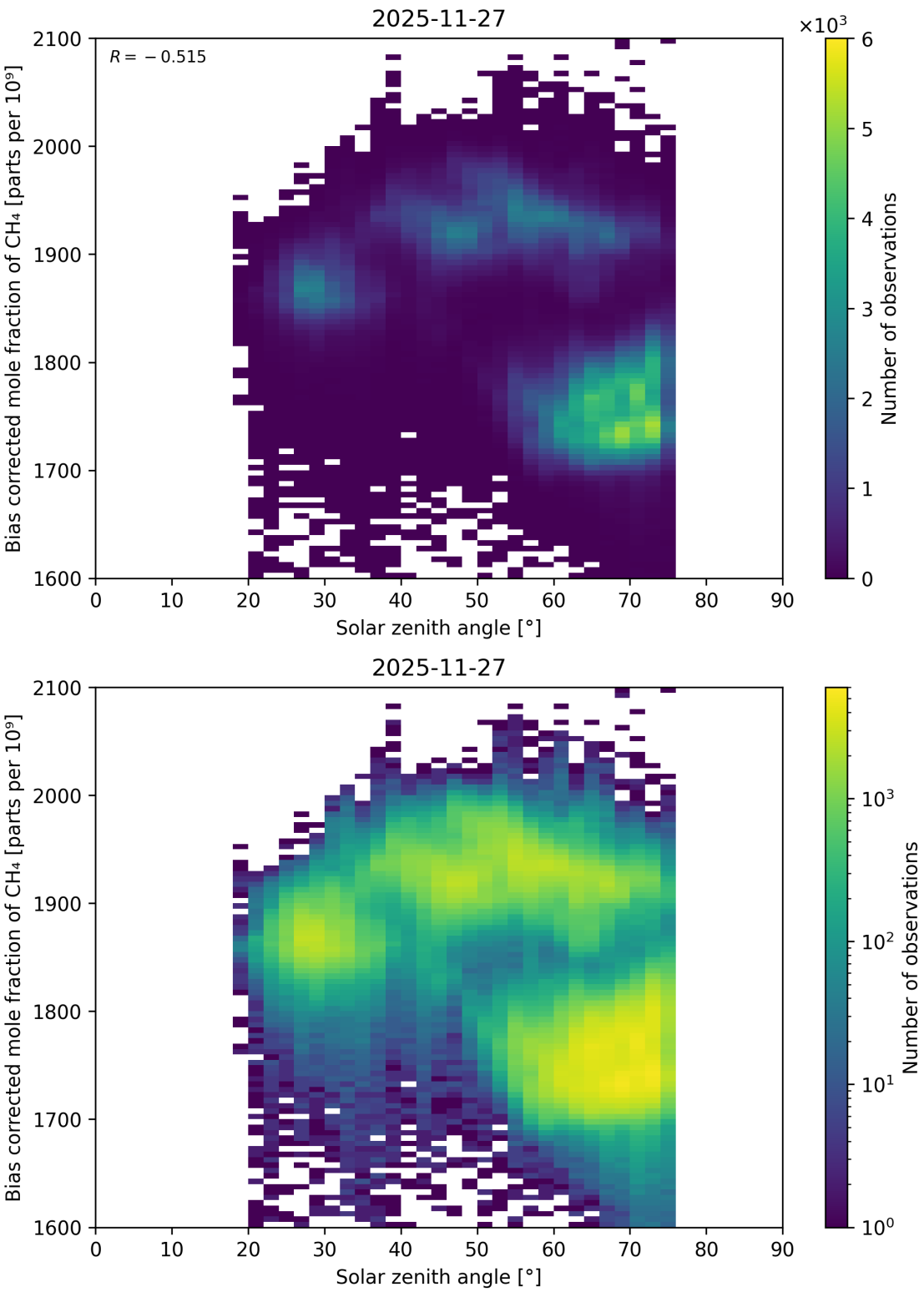

Figure 115: Scatter density plot of "Solar zenith angle" against "Bias corrected mole fraction of CH_4" for 2025-11-26 to 2025-11-28.

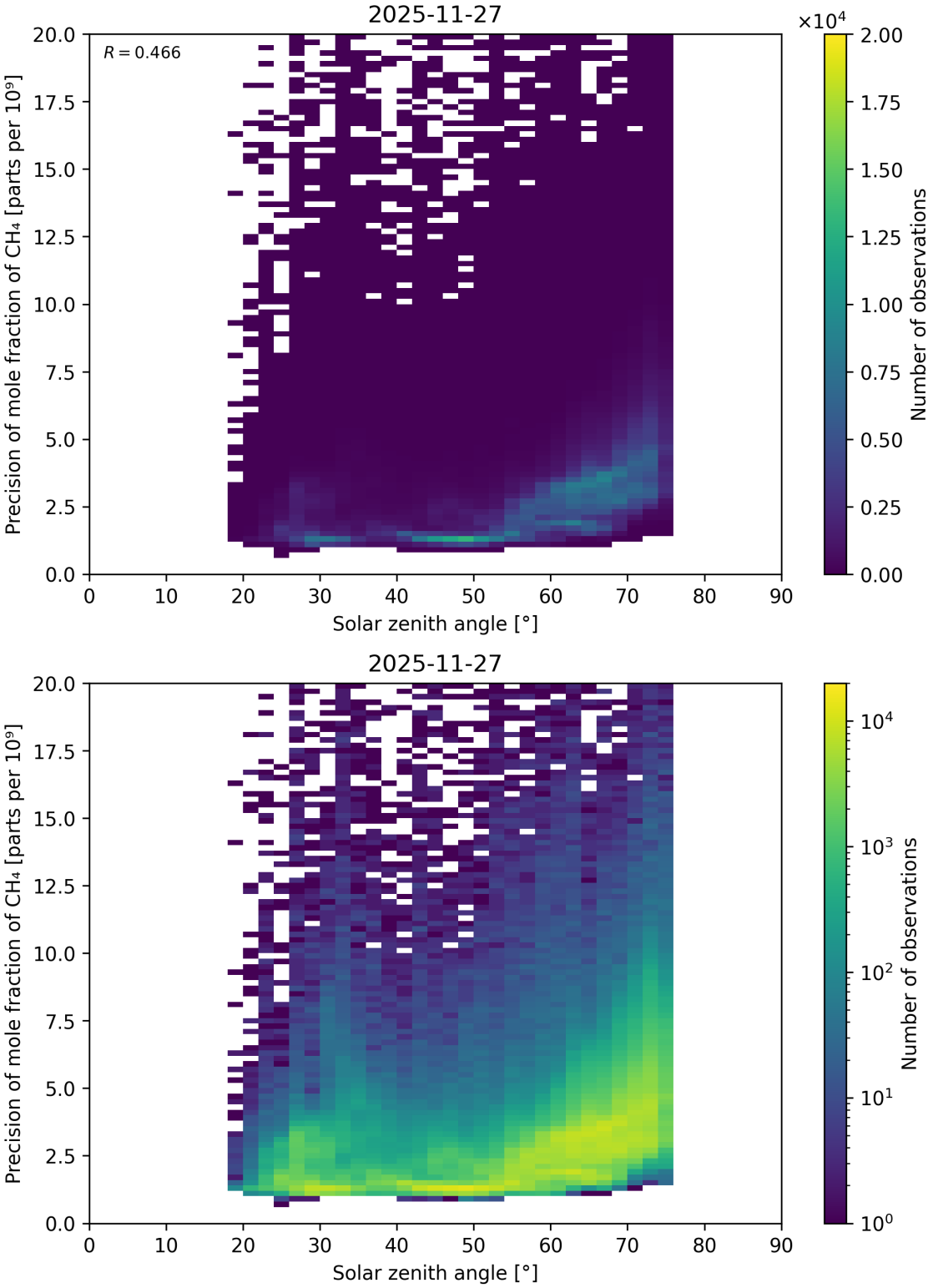

Figure 116: Scatter density plot of "Solar zenith angle" against "Precision of mole fraction of CH_4" for 2025-11-26 to 2025-11-28.

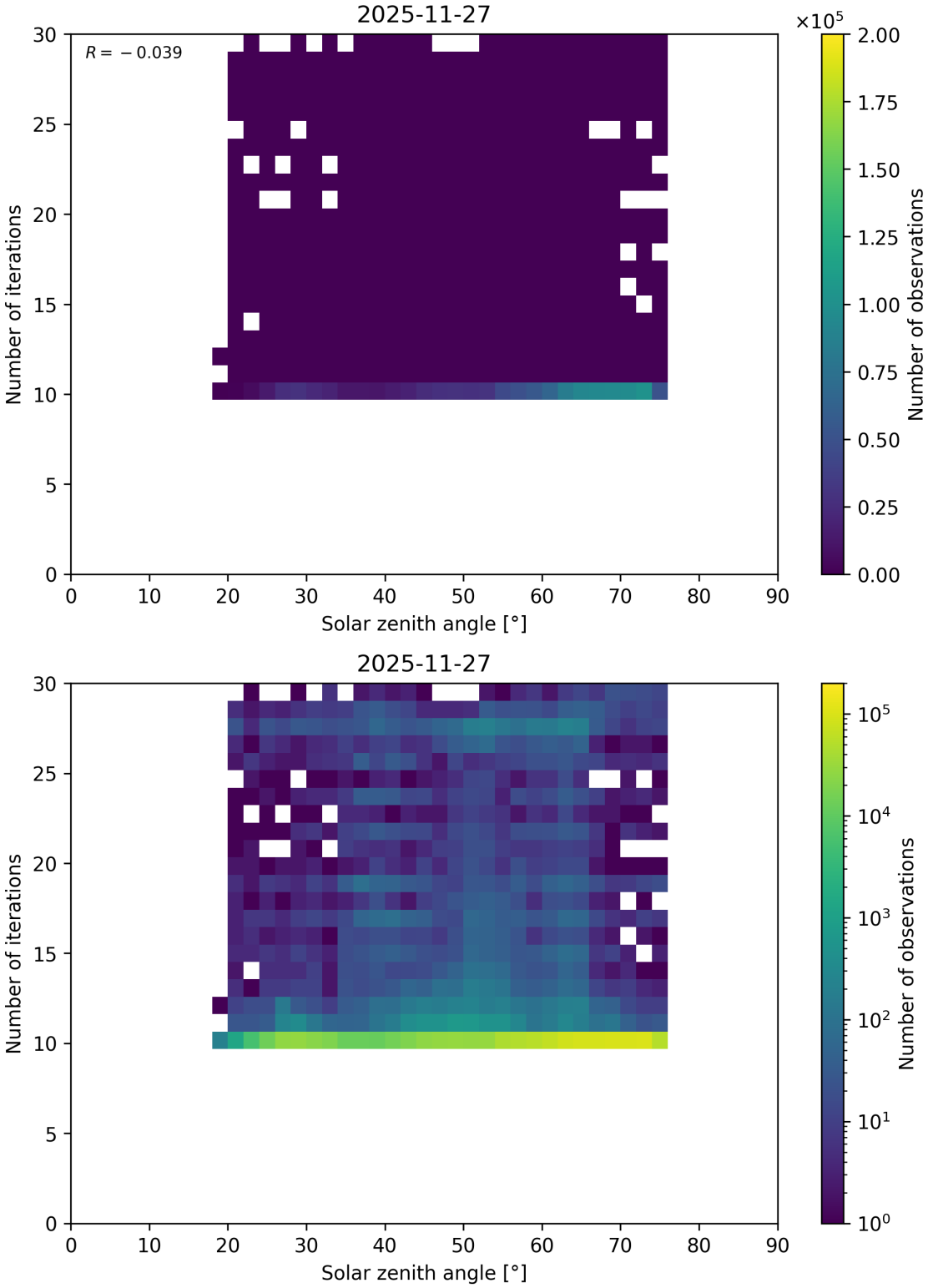

Figure 117: Scatter density plot of “Solar zenith angle” against “Number of iterations” for 2025-11-26 to 2025-11-28.

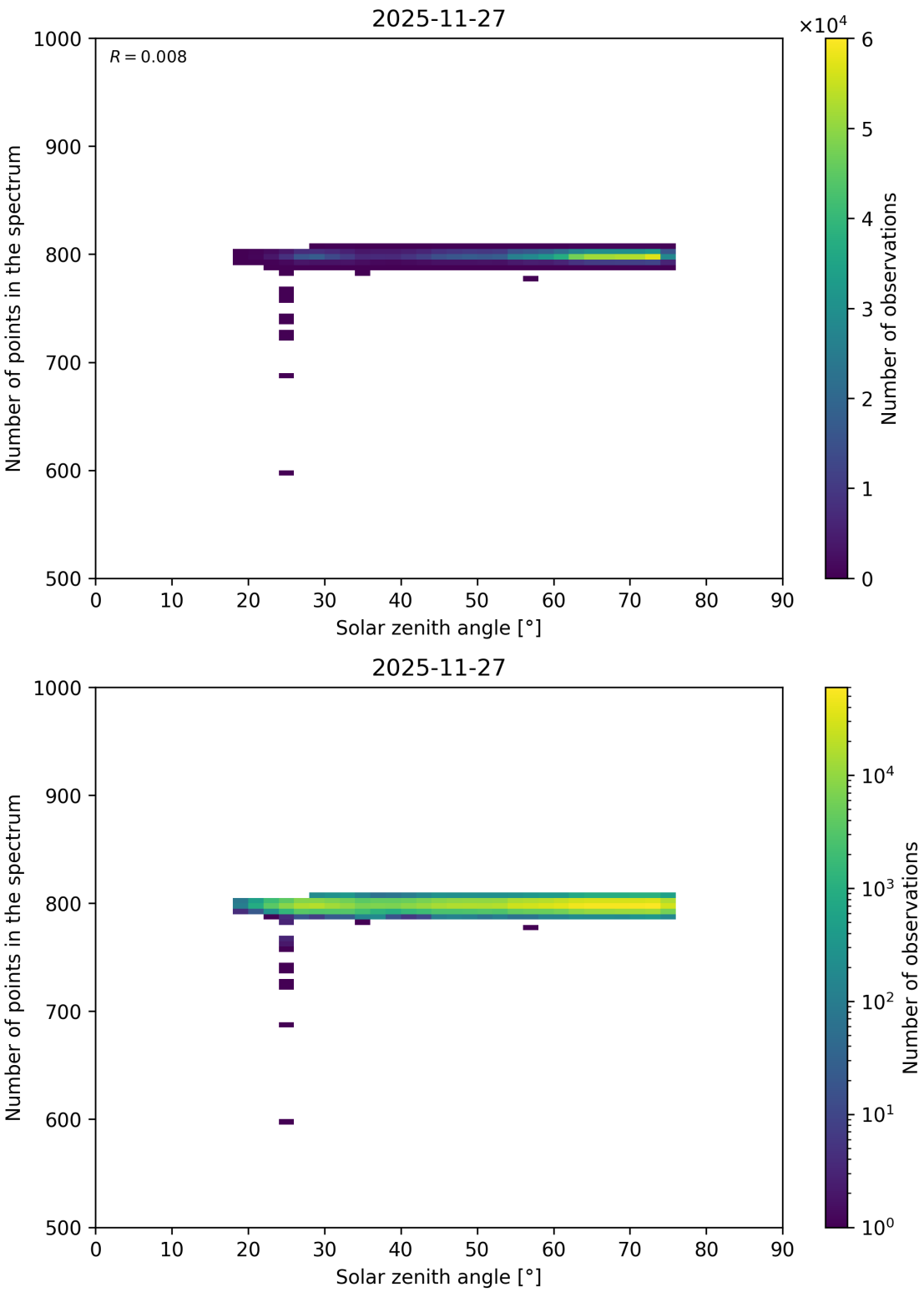

Figure 118: Scatter density plot of “Solar zenith angle” against “Number of points in the spectrum” for 2025-11-26 to 2025-11-28.

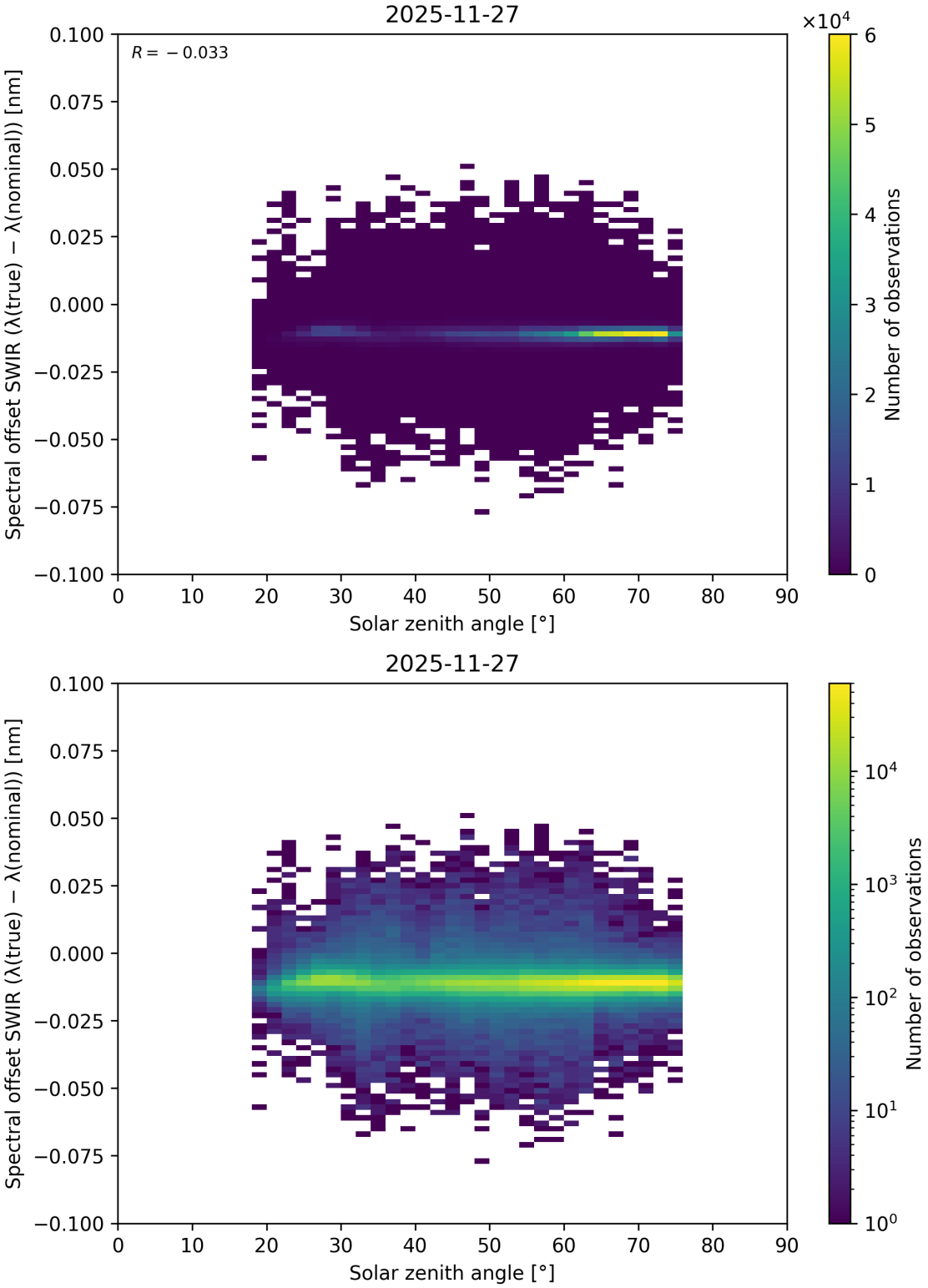

Figure 119: Scatter density plot of "Solar zenith angle" against "Spectral offset SWIR ($\lambda_{\text{true}} - \lambda_{\text{nominal}}$)" for 2025-11-26 to 2025-11-28.

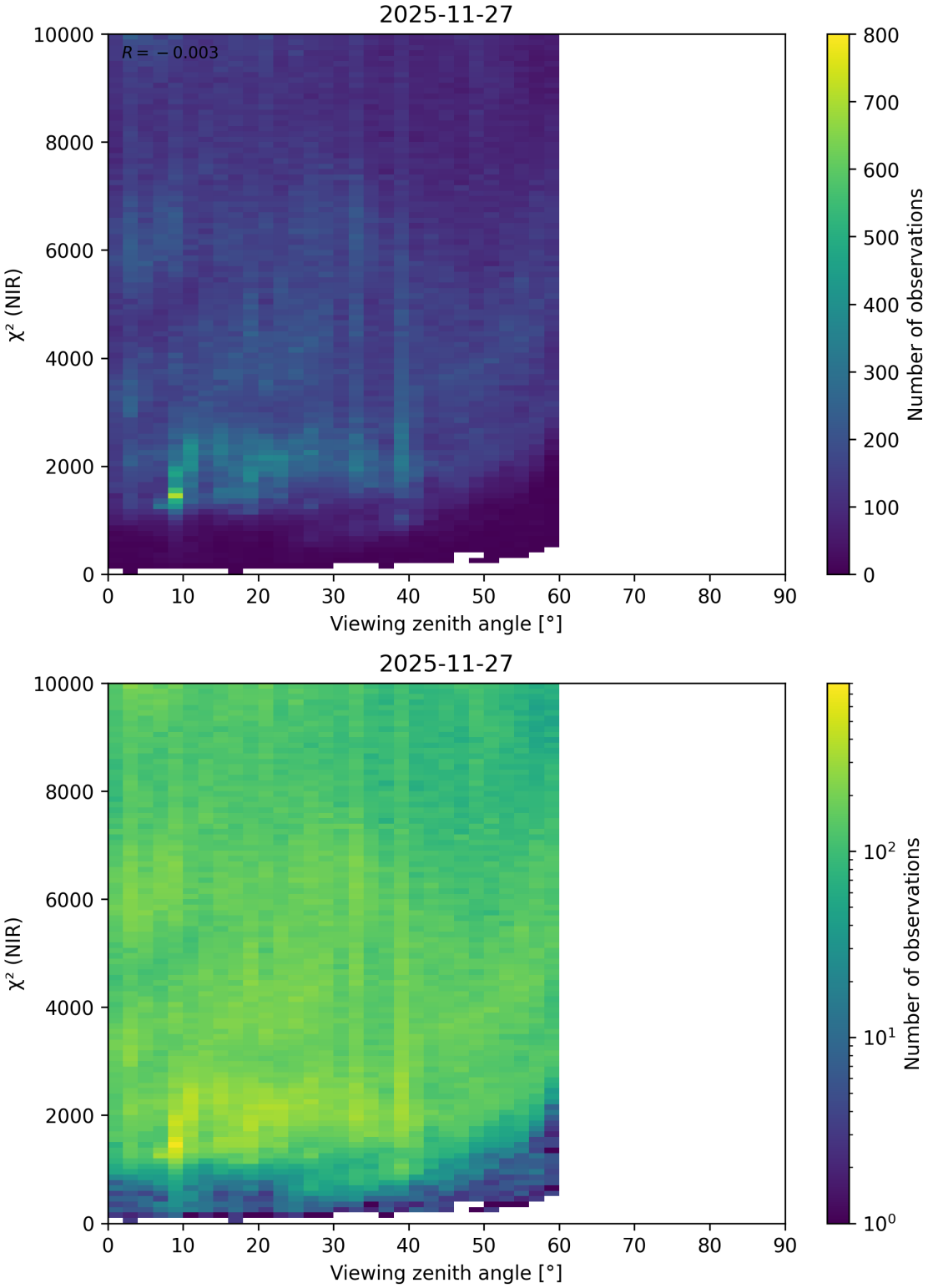

Figure 120: Scatter density plot of “Viewing zenith angle” against “χ^2 (NIR)” for 2025-11-26 to 2025-11-28.

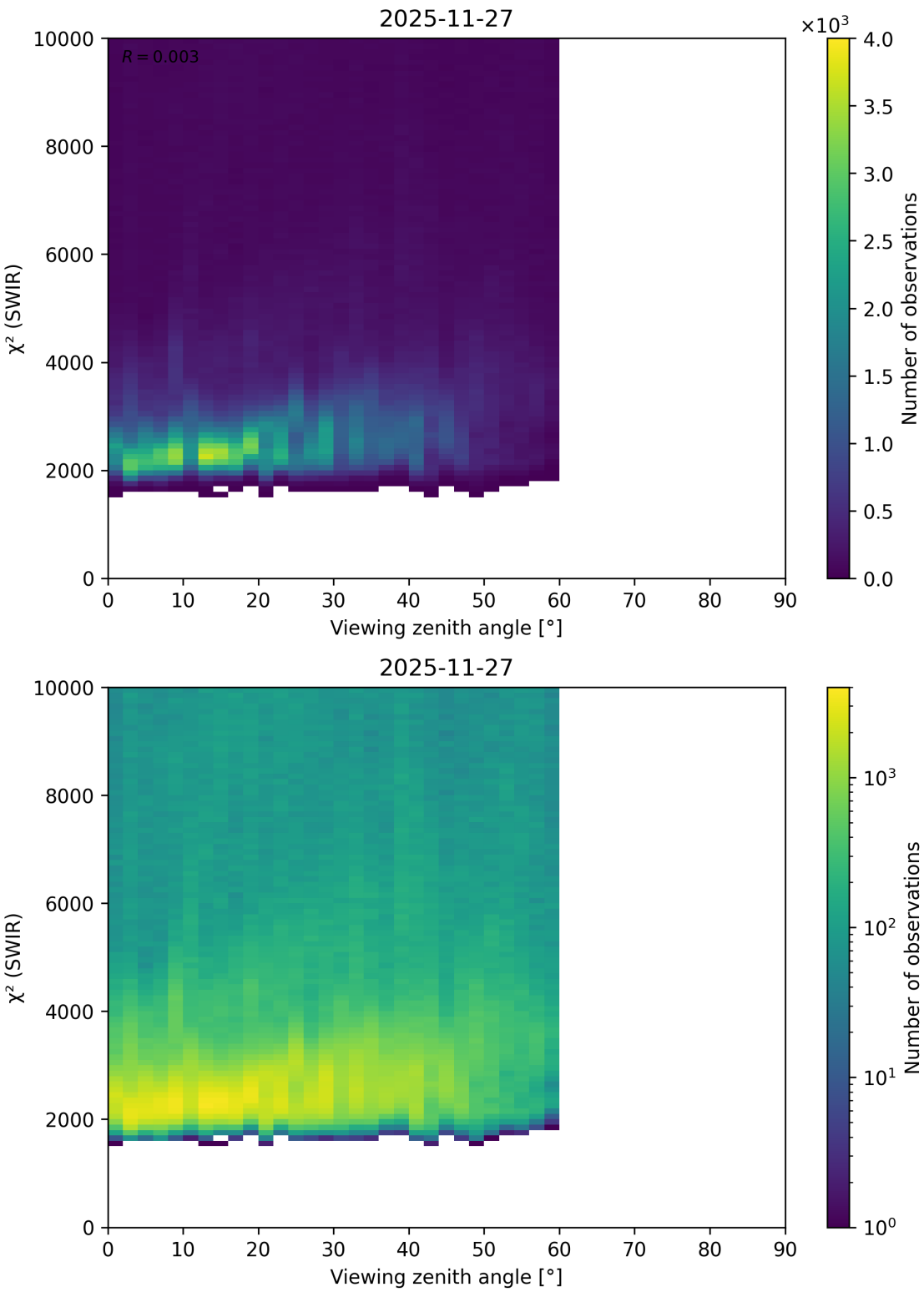

Figure 121: Scatter density plot of "Viewing zenith angle" against "χ^2 (SWIR)" for 2025-11-26 to 2025-11-28.

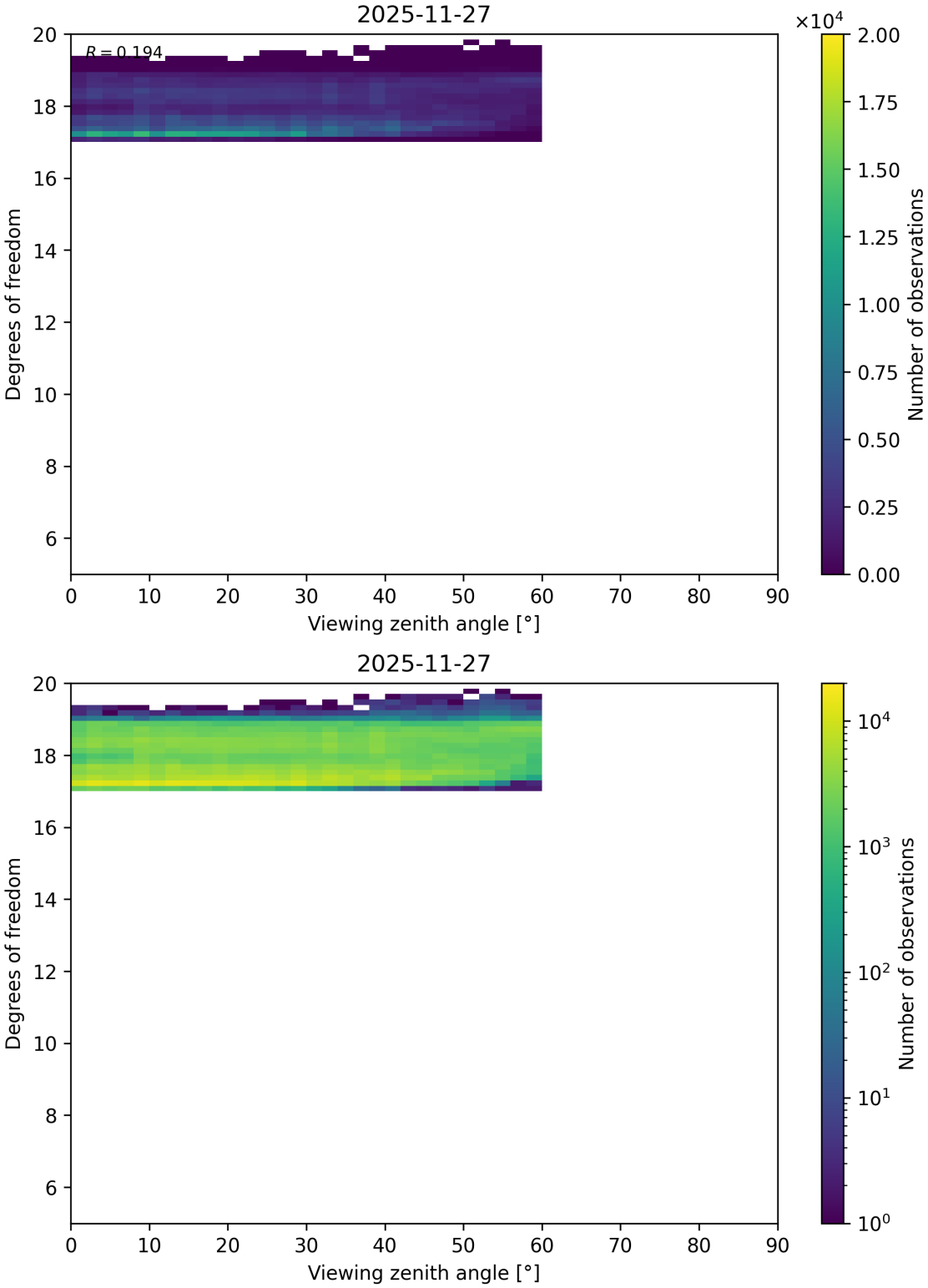

Figure 122: Scatter density plot of “Viewing zenith angle” against “Degrees of freedom” for 2025-11-26 to 2025-11-28.

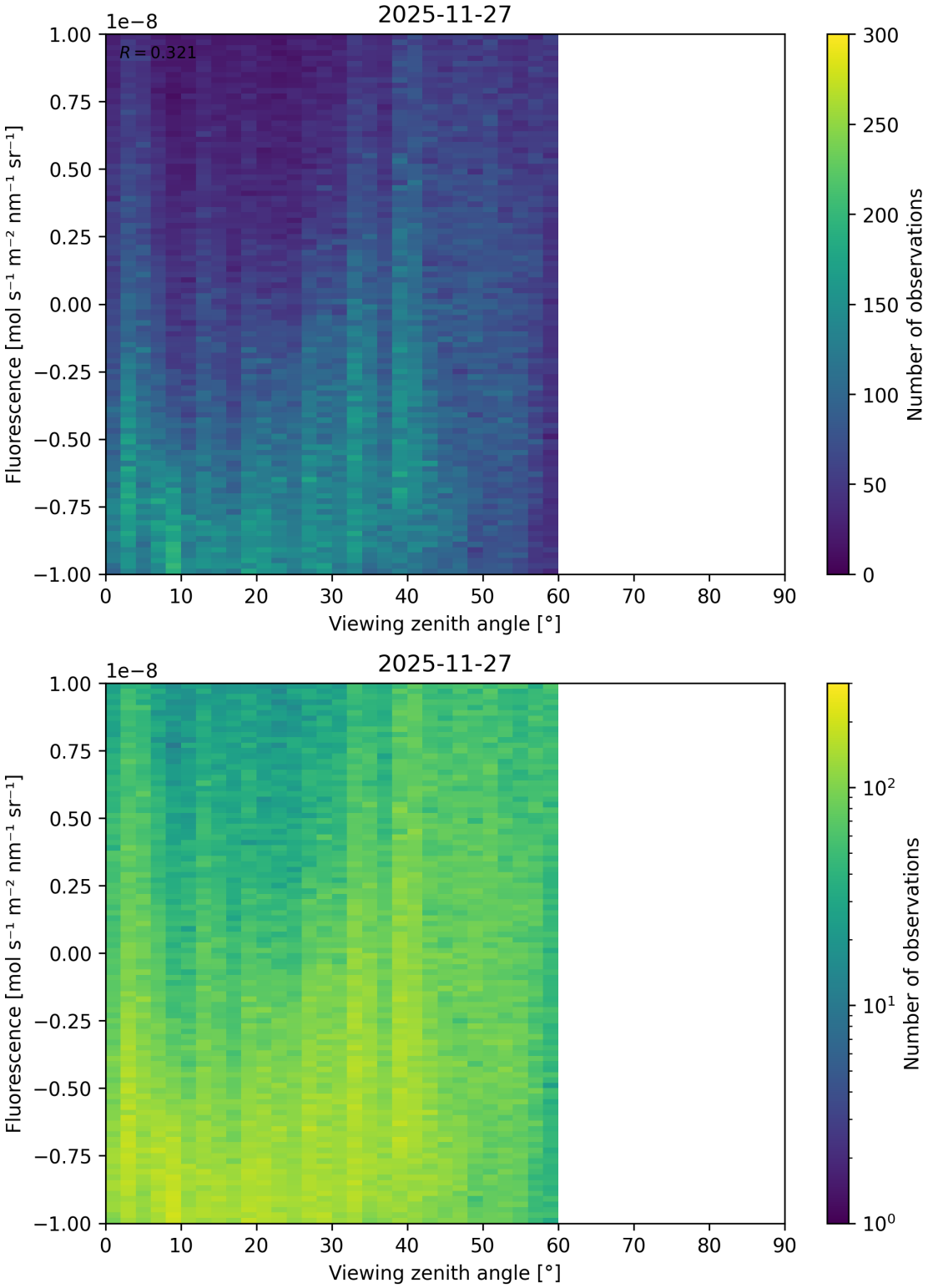

Figure 123: Scatter density plot of “Viewing zenith angle” against “Fluorescence” for 2025-11-26 to 2025-11-28.

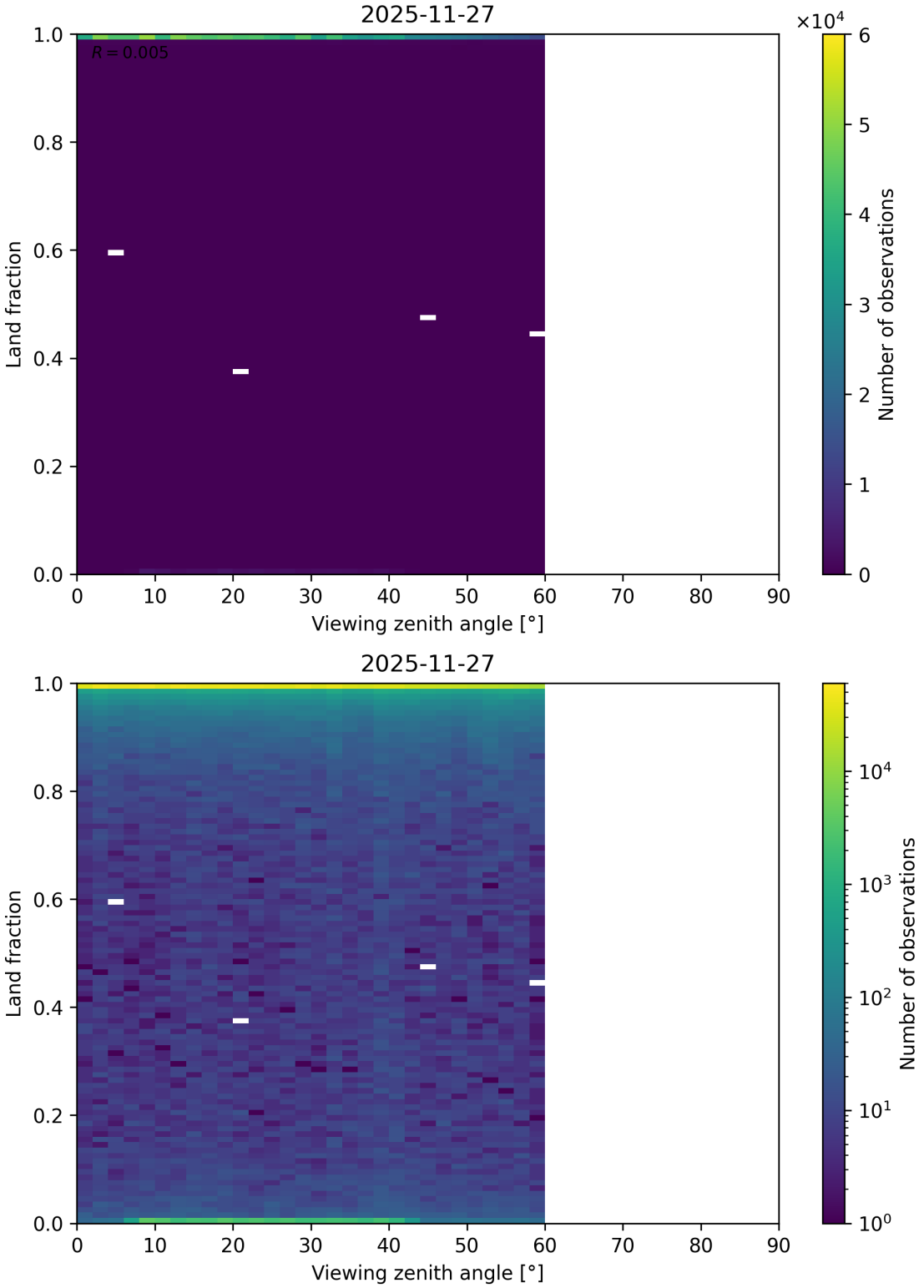

Figure 124: Scatter density plot of “Viewing zenith angle” against “Land fraction” for 2025-11-26 to 2025-11-28.

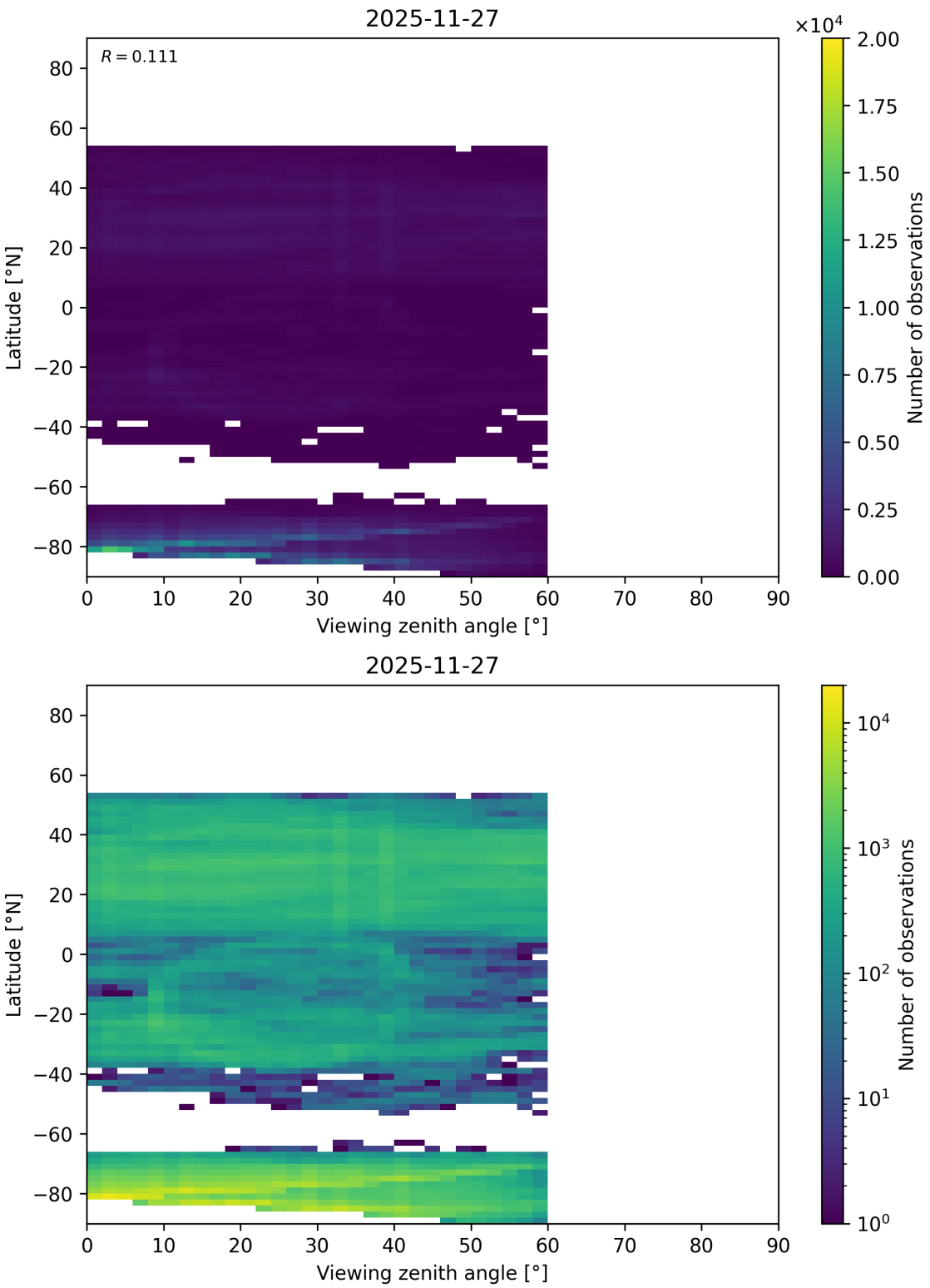

Figure 125: Scatter density plot of “Viewing zenith angle” against “Latitude” for 2025-11-26 to 2025-11-28.

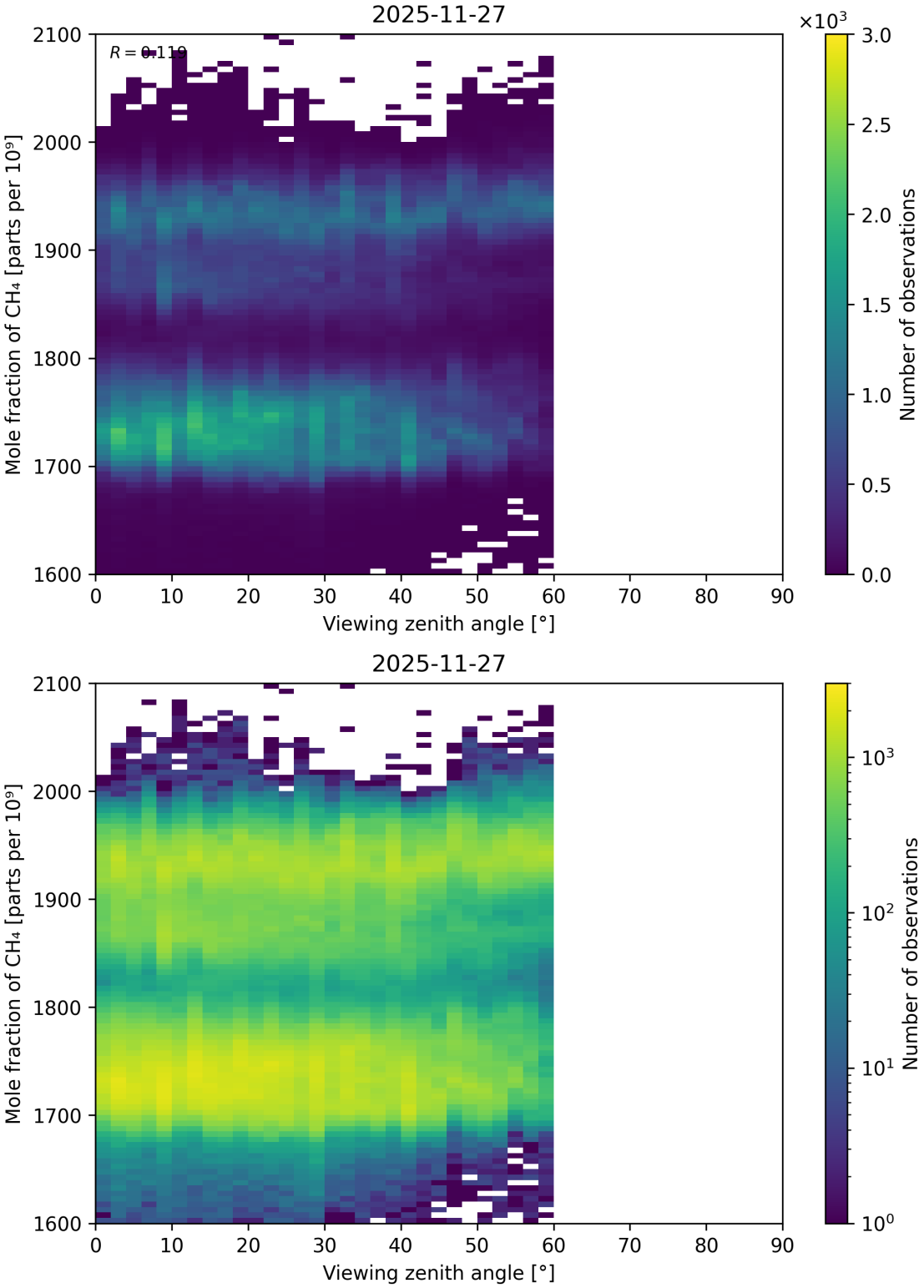

Figure 126: Scatter density plot of "Viewing zenith angle" against "Mole fraction of CH_4" for 2025-11-26 to 2025-11-28.

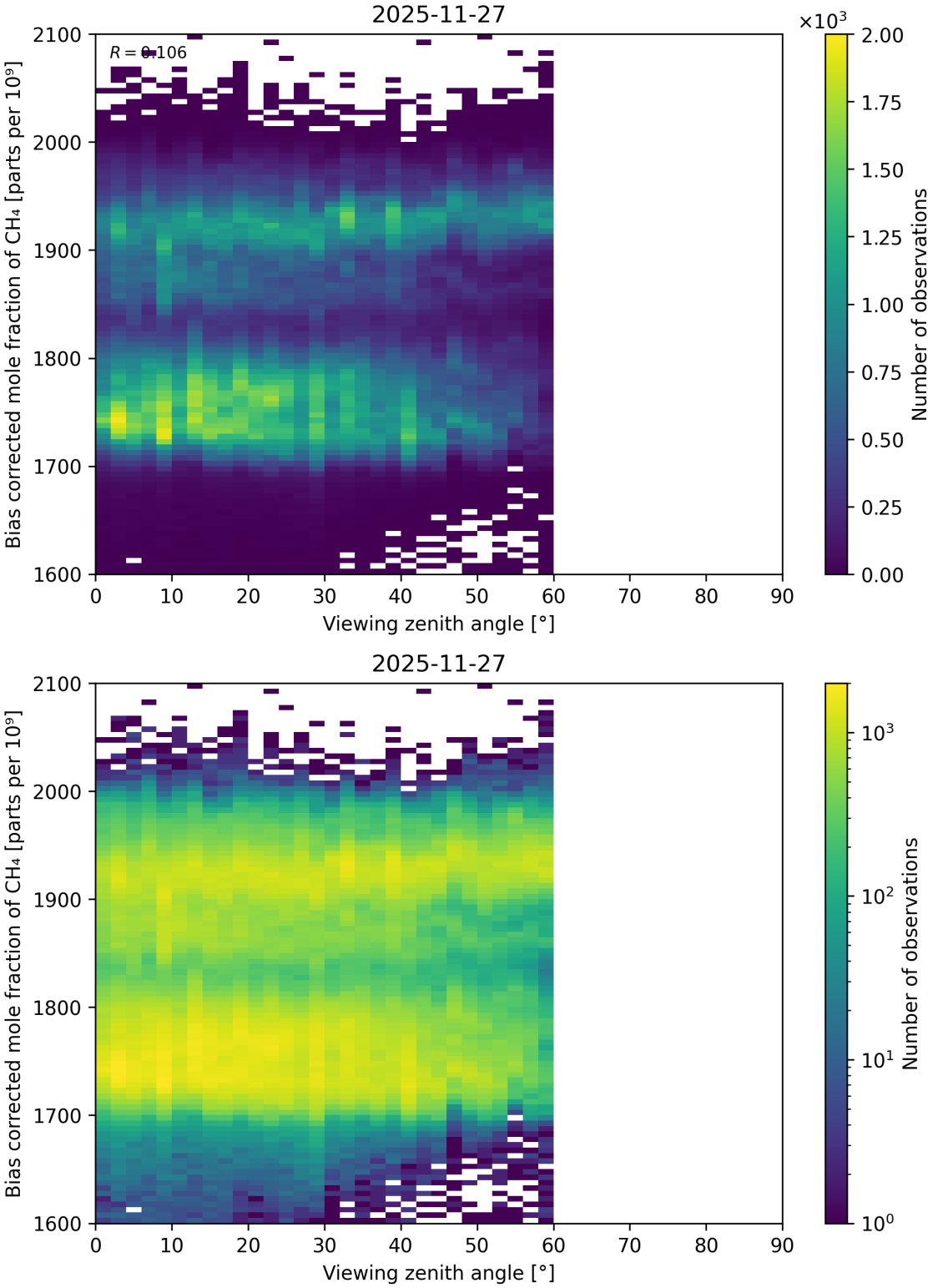

Figure 127: Scatter density plot of "Viewing zenith angle" against "Bias corrected mole fraction of CH_4" for 2025-11-26 to 2025-11-28.

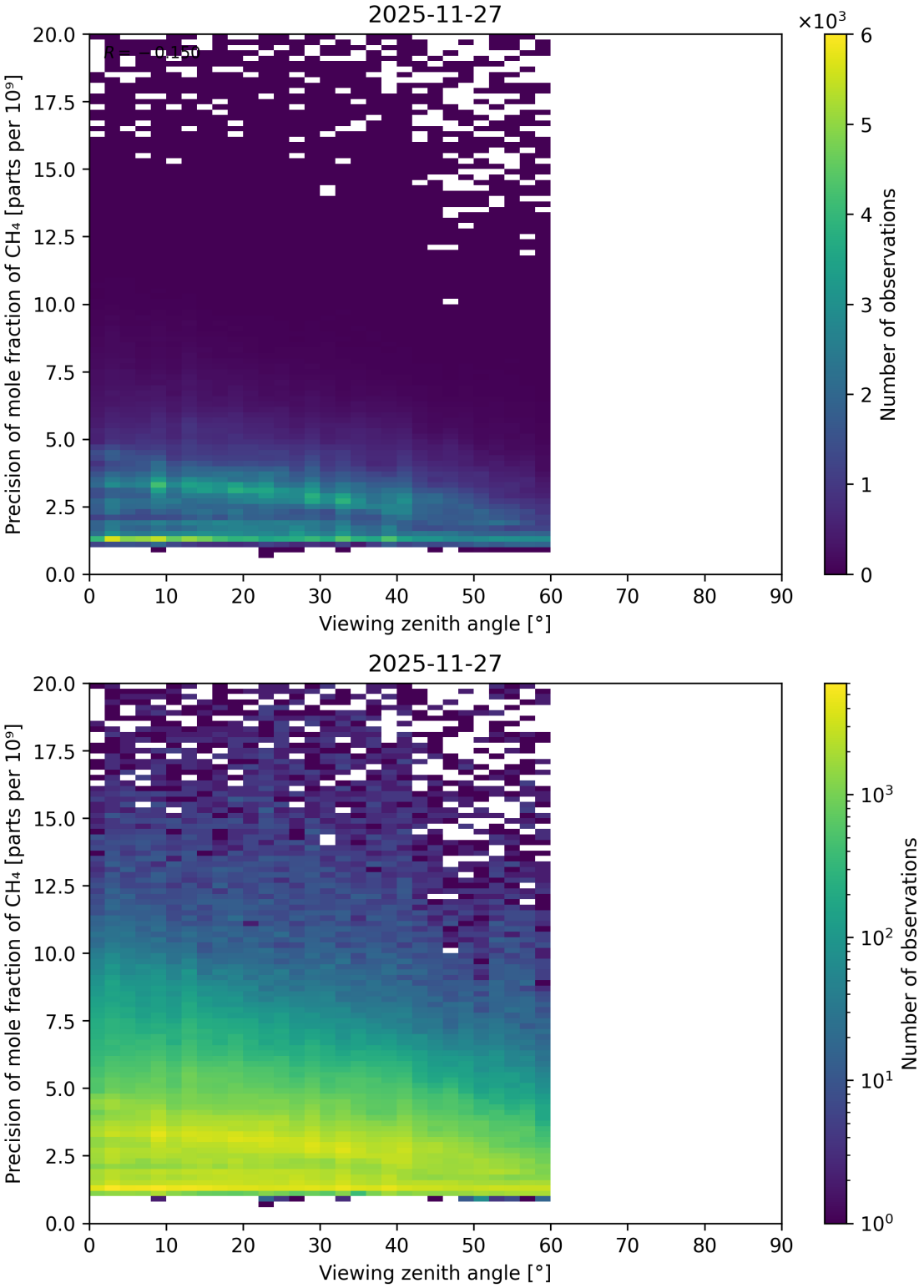

Figure 128: Scatter density plot of “Viewing zenith angle” against “Precision of mole fraction of CH_4” for 2025-11-26 to 2025-11-28.

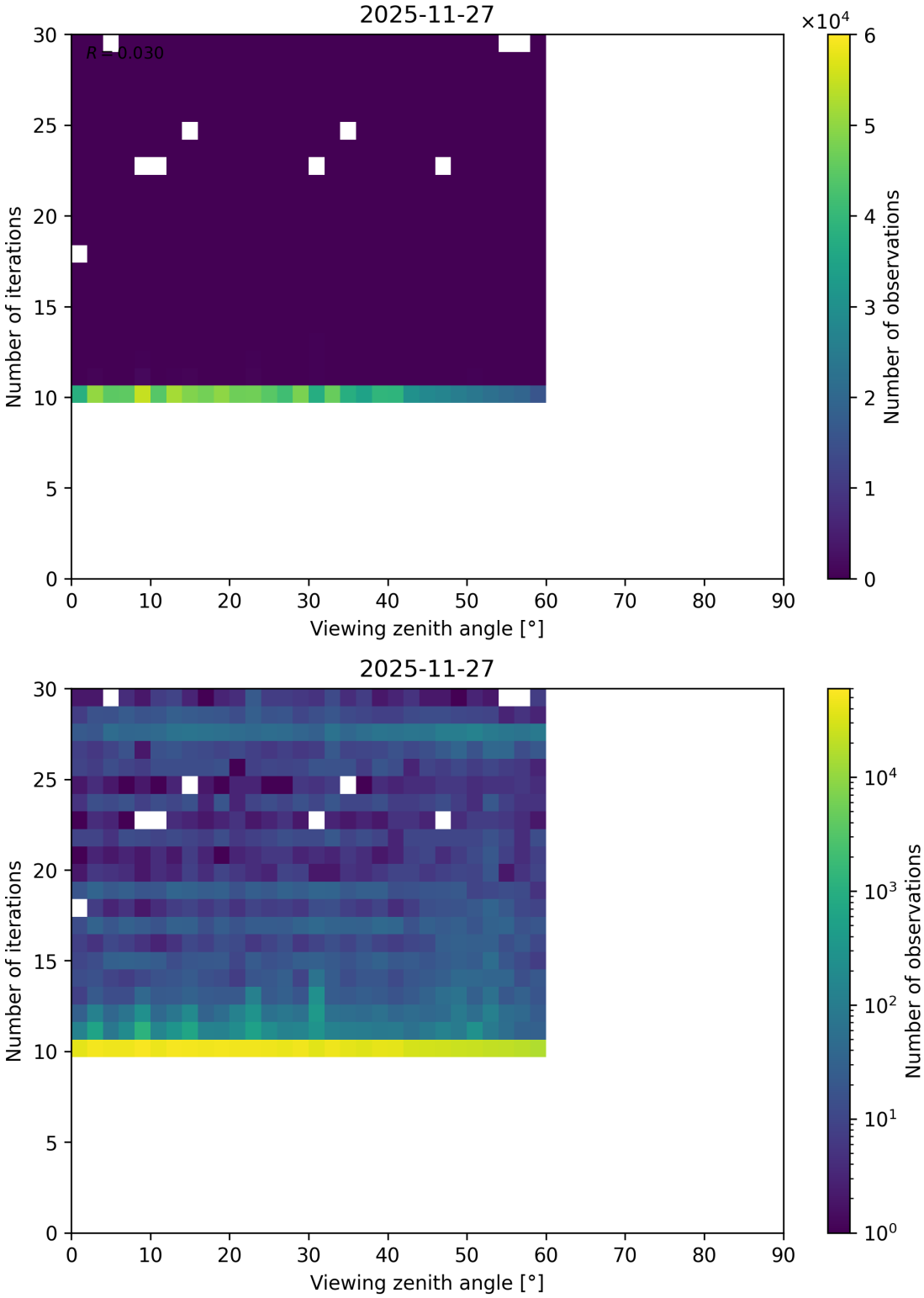

Figure 129: Scatter density plot of “Viewing zenith angle” against “Number of iterations” for 2025-11-26 to 2025-11-28.

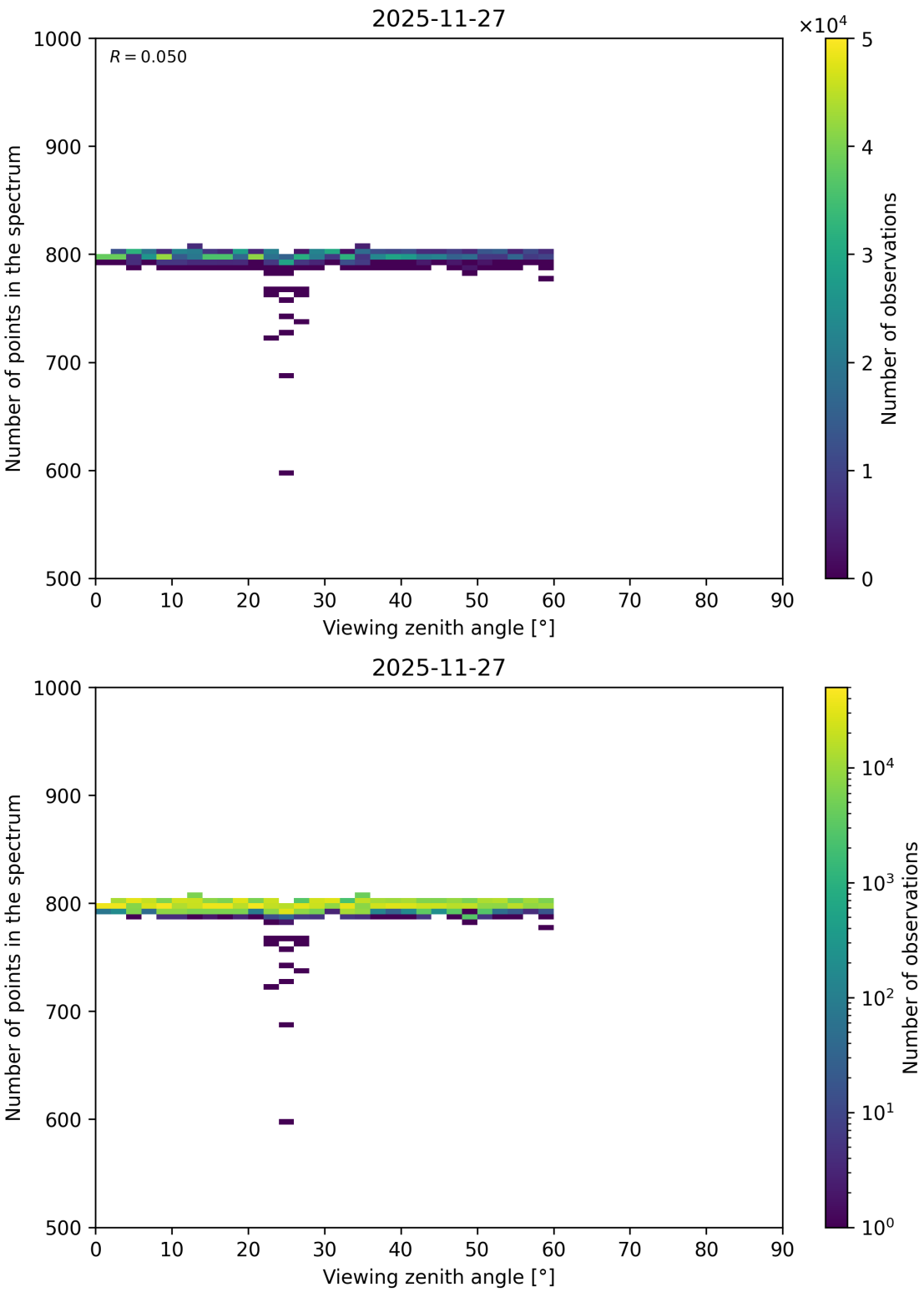

Figure 130: Scatter density plot of “Viewing zenith angle” against “Number of points in the spectrum” for 2025-11-26 to 2025-11-28.

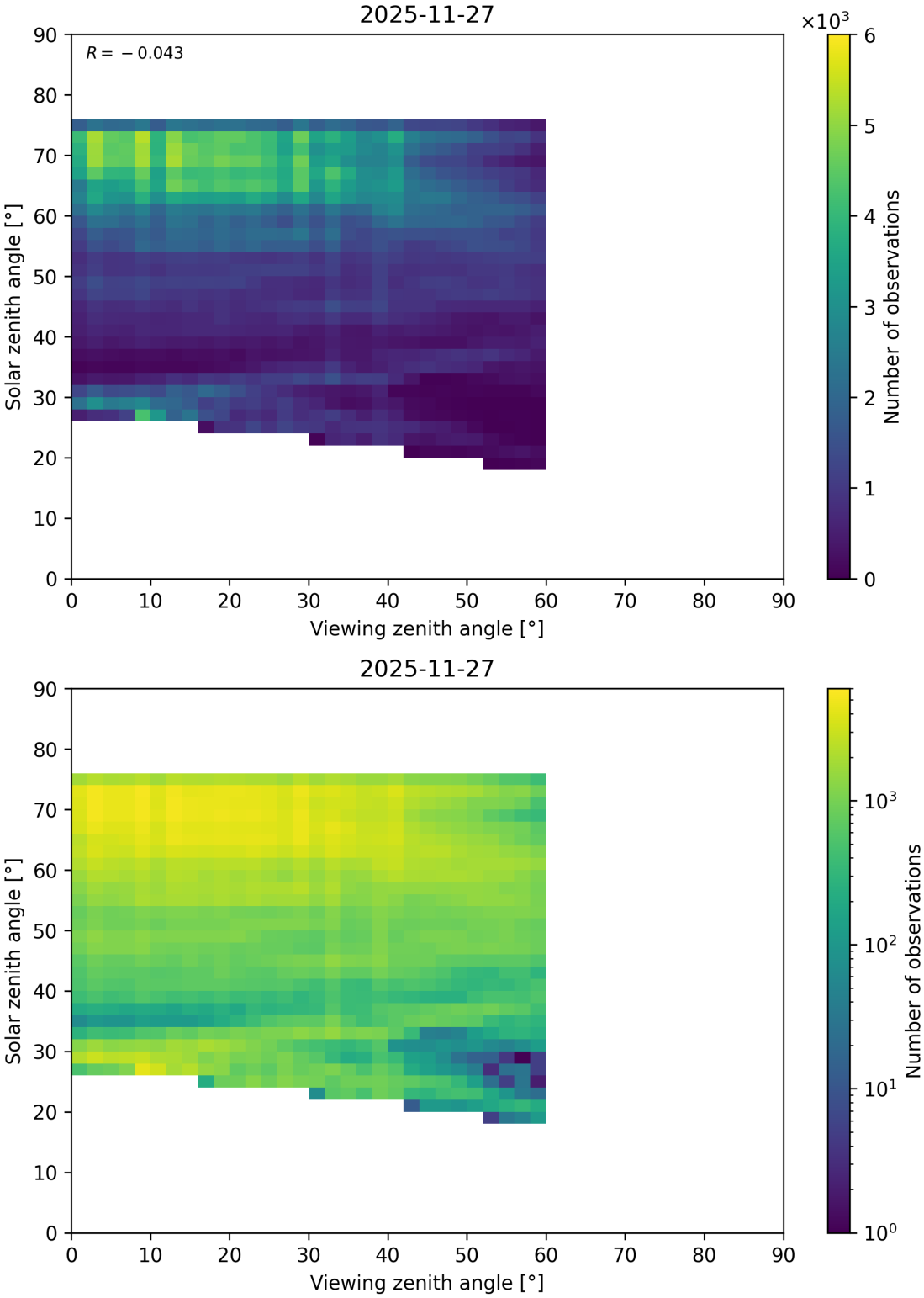

Figure 131: Scatter density plot of “Viewing zenith angle” against “Solar zenith angle” for 2025-11-26 to 2025-11-28.

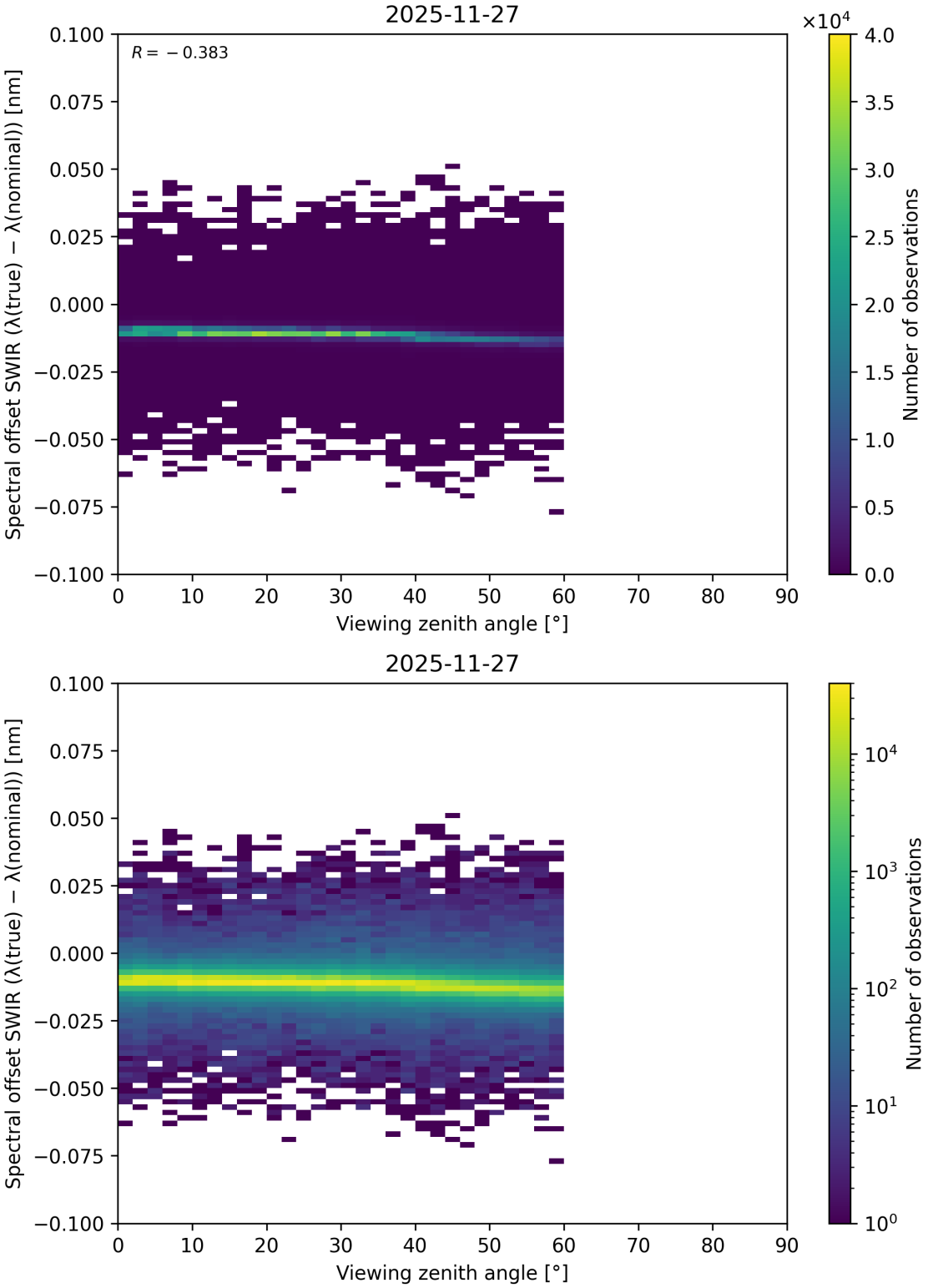

Figure 132: Scatter density plot of "Viewing zenith angle" against "Spectral offset SWIR ($\lambda_{\text{true}} - \lambda_{\text{nominal}}$)" for 2025-11-26 to 2025-11-28.

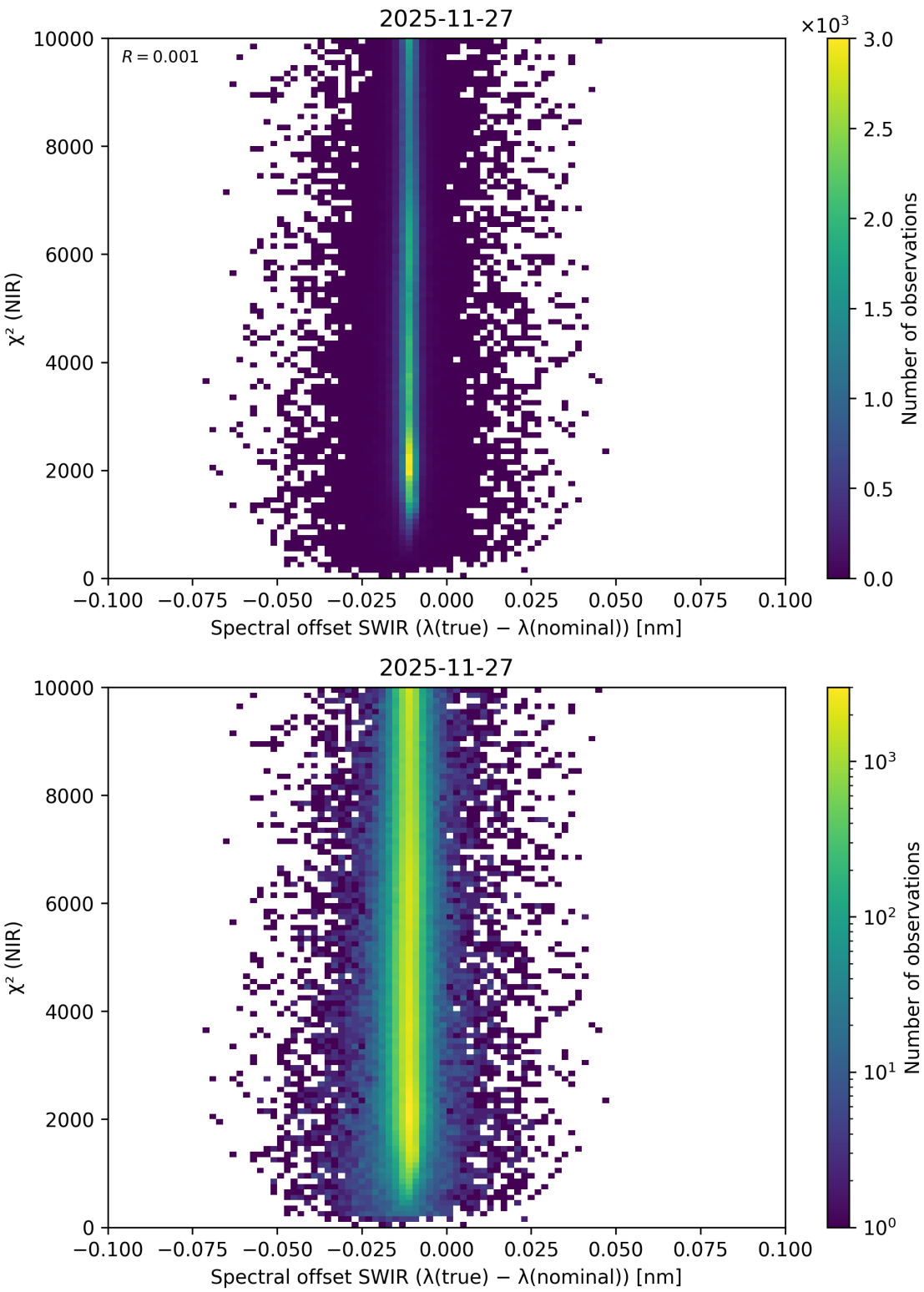

Figure 133: Scatter density plot of "Spectral offset SWIR ($\lambda_{\text{true}} - \lambda_{\text{nominal}}$)" against "$\chi^2$ (NIR)" for 2025-11-26 to 2025-11-28.

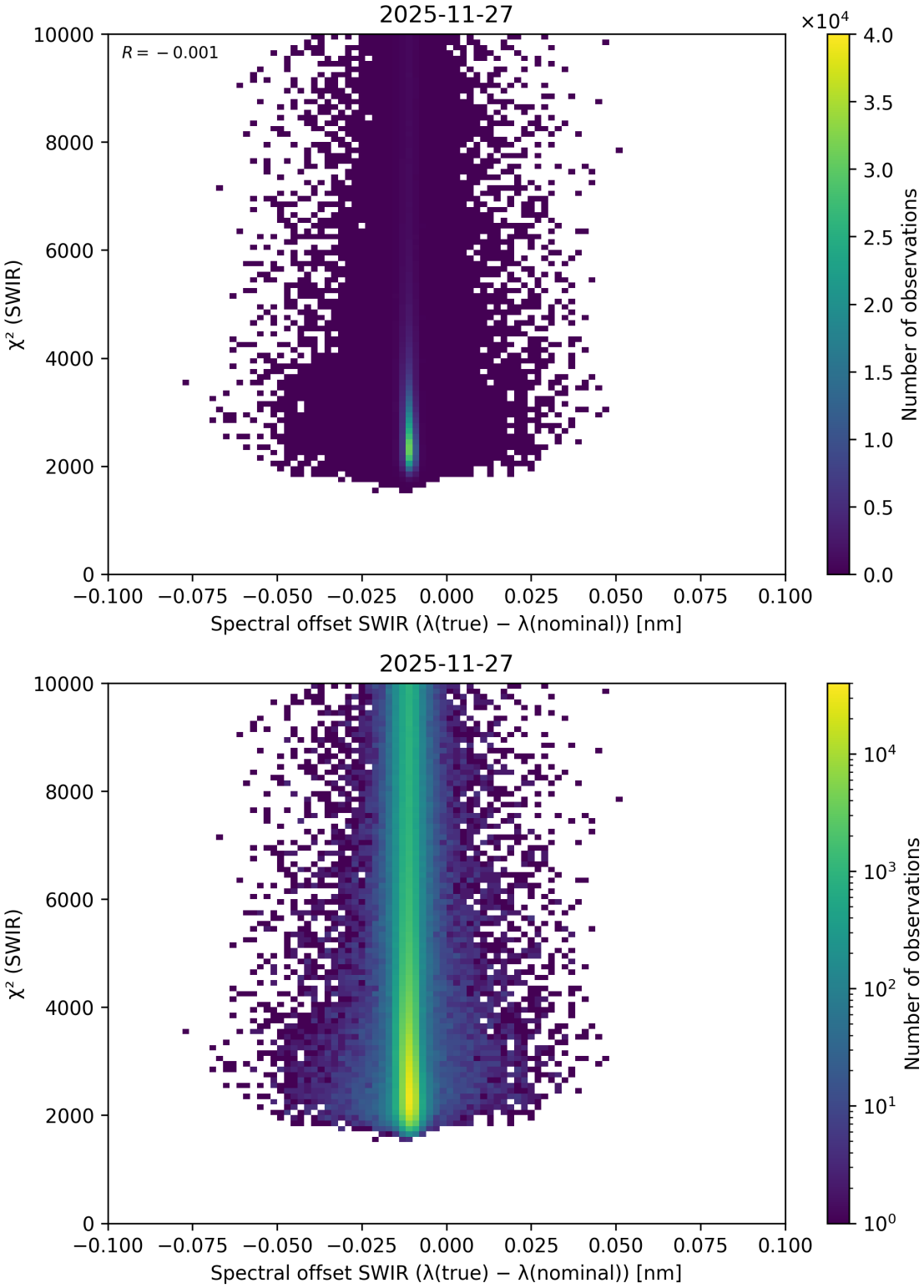

Figure 134: Scatter density plot of "Spectral offset SWIR ($\lambda_{\text{true}} - \lambda_{\text{nominal}}$)" against "$\chi^2$ (SWIR)" for 2025-11-26 to 2025-11-28.

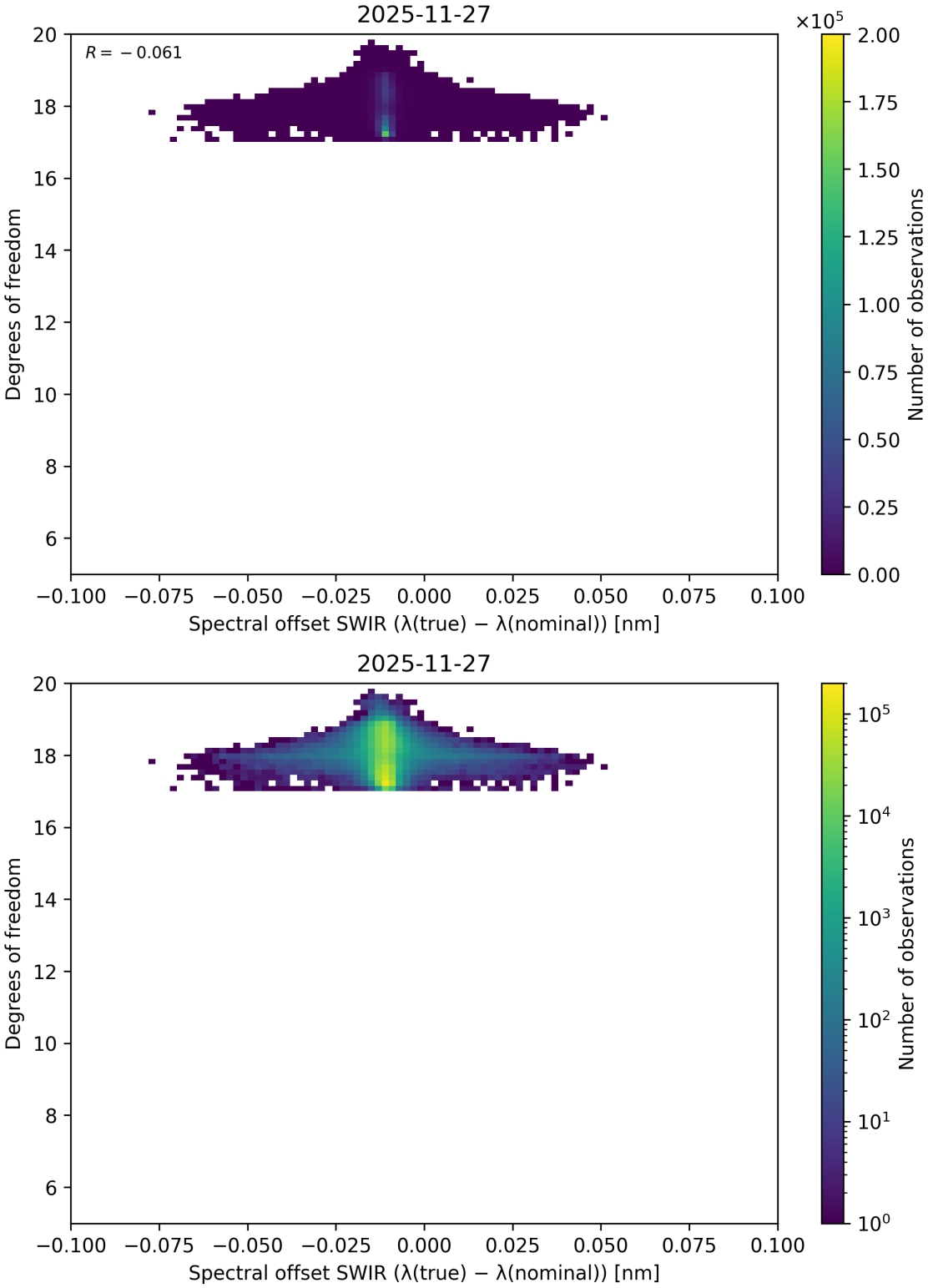

Figure 135: Scatter density plot of "Spectral offset SWIR ($\lambda_{\text{true}} - \lambda_{\text{nominal}}$)" against "Degrees of freedom" for 2025-11-26 to 2025-11-28.

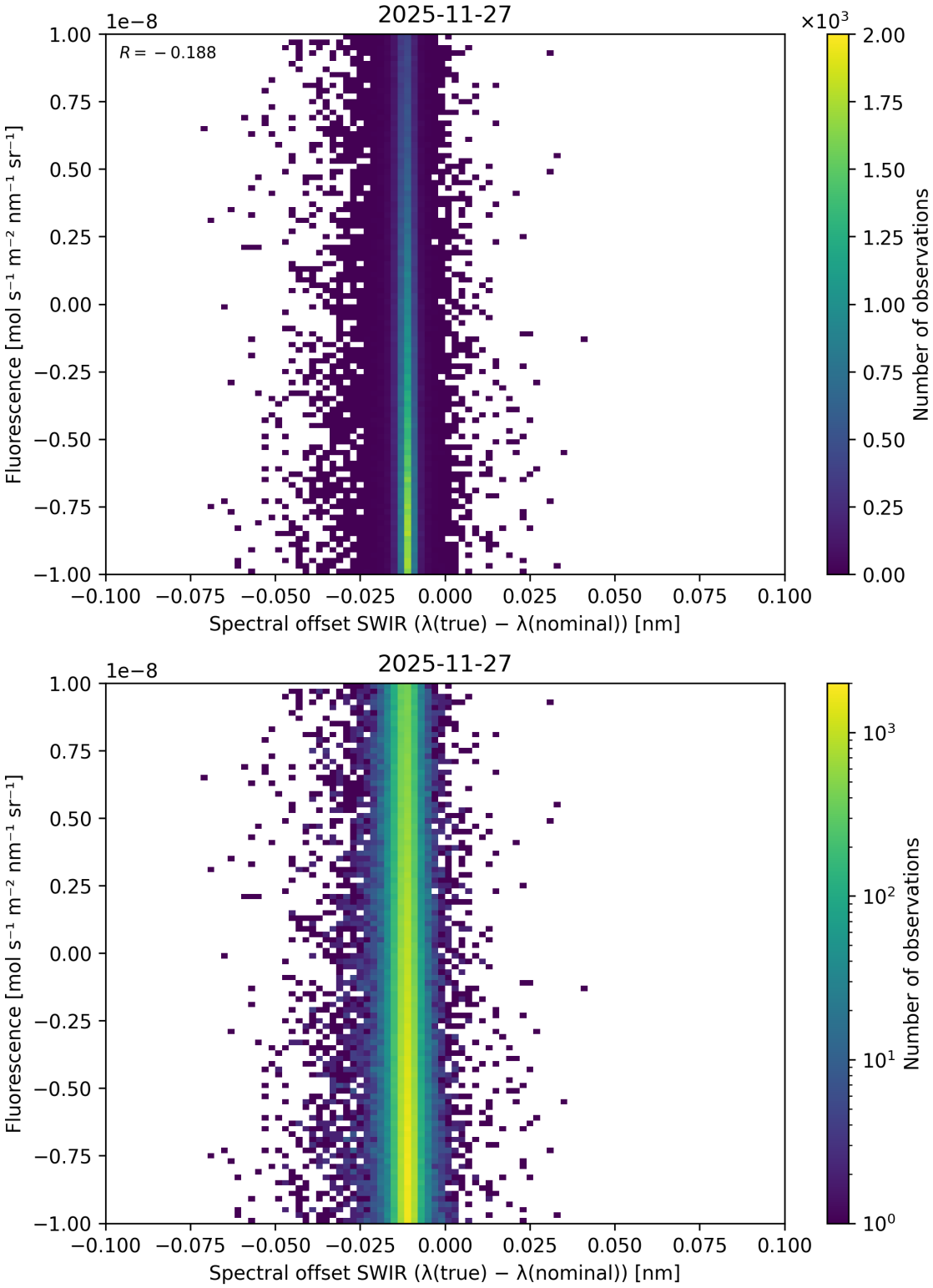

Figure 136: Scatter density plot of "Spectral offset SWIR ($\lambda_{\text{true}} - \lambda_{\text{nominal}}$)" against "Fluorescence" for 2025-11-26 to 2025-11-28.

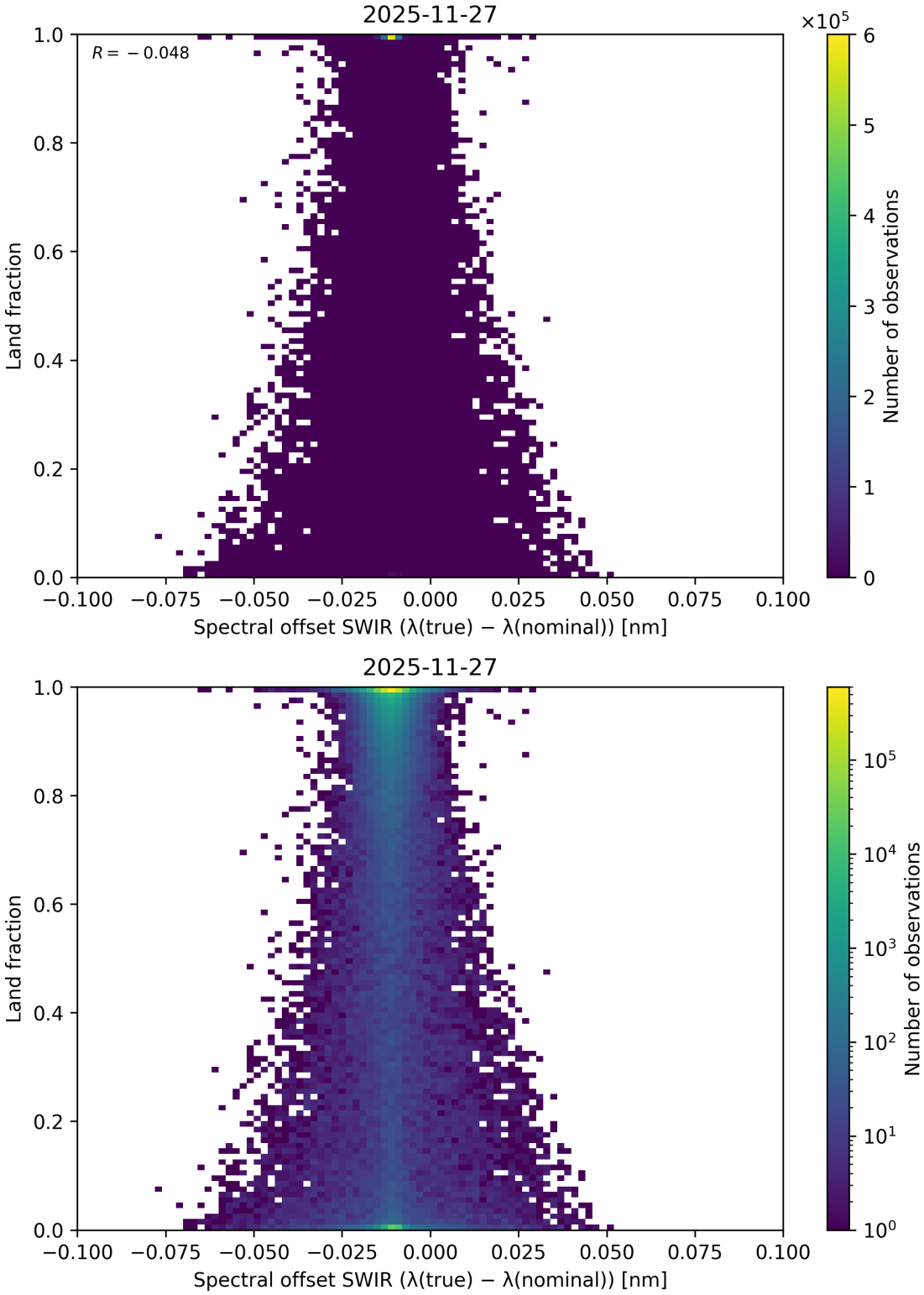

Figure 137: Scatter density plot of "Spectral offset SWIR ($\lambda_{\text{true}} - \lambda_{\text{nominal}}$)" against "Land fraction" for 2025-11-26 to 2025-11-28.

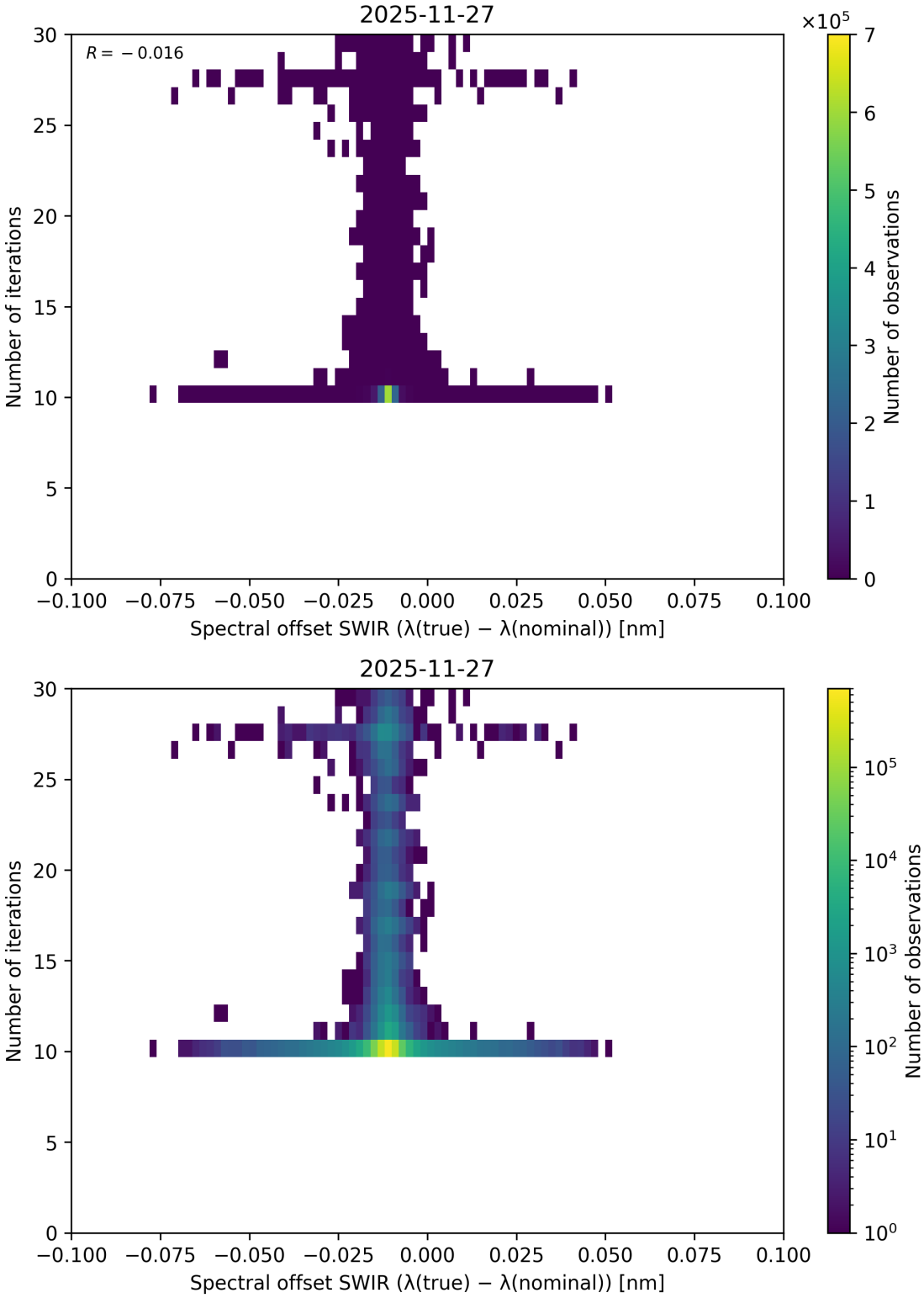

Figure 138: Scatter density plot of "Spectral offset SWIR ($\lambda_{\text{true}} - \lambda_{\text{nominal}}$)" against "Number of iterations" for 2025-11-26 to 2025-11-28.

Contents

List of Figures

List of Tables

11 Copyright information of ‘PyCAMA’

Maarten Sneep (maarten.sneep@knmi.nl).